Distributed Uncertainty Analysis Techniques for Conceptual Launch Vehicle Design

A Thesis
Presented to
The Academic Faculty

by

David Jeremy McCormick

In Partial Fulfillment
Of the Requirements for the Degree of
Doctor of Philosophy in Aerospace Engineering

Georgia Institute of Technology

July 2001

For My Family

Acknowledgements

I would like to thank everyone who helped with this work. First, I would like to thank my advisor Dr. John Olds. Your clear insights and excellent guidance have helped me through my entire graduate career, but never more than while working on this thesis. I would also like to thank my committee, namely Drs. Mavris, Schrage, Johnson and Shonkwiler. Without their help, this work would not have been complete. I would also like to thank soon-to-be Dr. David Way for the many valuable exchanges on probabilistic techniques. They were a great help. I would also like to thank those organizations that have hosted me during my summers in graduate school, namely the Kaiser-Marquardt Corporation, NASA Langley Research Center and the Lockheed-Martin Corporation.

After spending five years seeing people come and go, there are a lot of people out to which I must give a shout. First, a hi to all the guys from the GLC. It looks like my thesis is concluded. A sincere thank you to all the members of the SSDL, especially John, Dave, Laura, Irene, Brad and well, everybody for all their help. Beunos ding dong diddley dias to some past lab guys, namely Pete and Dave, for the fun out in Denver, especially to Pete for hooking me up with Lockheed. Tooley, thanks for bringing the Bimese to the world. It is entirely your responsibility. To Leland thanks for the cans of soup and all the bets you lost in the name of Texas. I love Bass. Wegs, thanks for the candy and doughnuts. Finally I would like to deliver ridiculous thanks to my peeps… ridiculously awesome thanks. To Beaver, Roundhead, Drago, Reuben (sorry, can't do R^3), Doug, and Neo, I'm going to miss adventure team. I'd especially like to thank Drago

and Neo for keeping me from being homeless. For Roundhead, a thanks to all the “laaadies”. And Beaver, you’re the Beaver, not Tim Diesel, because the Beaver is the Beaver. To Karim, go Gators. I’d also like to thank Dirty Dave and his CD collection. It’s bigger than my car and sounds better, too.

Finally, I’d like to thank my family, Mom, Dad, Molly and Trouble. Through all this stuff, you are always there.

Table of Contents

LIST OF TABLES

LIST OF ILLUSTRATIONS

NOMENCLATURE

Abbreviations

°R	degrees Rankine
abs.	absolute
atm.	atmospheres
C. I.	confidence interval
cu. ft.	cubic feet
deg.	degrees
Eqn.	equation
fps.	feet per second
ft.	feet
ft3.	feet cubed
hrs.	hours
inc.	inclination
klb.	thousand pounds
lb.	pounds
min.	minutes
Mlb.	million pounds
MW	megawatt
nmi.	nautical miles
psf.	pounds per square feet

rel.	relative
sec.	seconds
sq. ft.	square feet
std. dev.	standard deviation
T/W	Thrust to Weight
U.S.	United States

Acronyms

3DOF	Three Degree of Freedom
ACC	Advanced Carbon-Carbon Composite
AMV	Advanced Mean Value
ANOVA	Analysis of Variance
APAS	Aerodynamic Preliminary Analysis System
ARC	Ames Research Center
CCD	Central Composite Design
CDF	Cumulative Distribution Function
CO	Collaborative Optimization
DOE	Design of Experiments
DOT	Design Optimization Tool
DPD	Discrete Probability Distribution
DPOMD	Discrete Probability Optimal Matching Distribution
DS	Descriptive Sampling
DSM	Design Structure Matrix
FPI	Fast Probability Integration
GCE	Geocentric-Equatorial

GLOW	Gross Liftoff Weight
GRAM99	Global Reference Atmospheric Model – 1999 Version
ISE	Integrated Systems Engineering
KSC	Kennedy Space Center
LaRC	Langley Research Center
LEO	Low Earth Orbit
LeRC	Lewis Research Center
MC	Monte Carlo
MDO	Multidisciplinary Design Optimization
MER	Mass Estimating Relationship
MPP	Most Probable Point
MPPL	Most Probable Point Locus
MR	Mass Ratio
NASA	National Aeronautics and Space Administration
OBD	Optimization Based Decomposition
OEC	Overall Evaluation Criteria
OML	Outer Mold Line
POST	Program to Optimize Simulated Trajectories
PSAM	Probabilistic Structural Analysis Methods
RLV	Reusable Launch Vehicle
RSE	Response Surface Equation
RSM	Response Surface Methodology
RSTS LSA	Reusable Space Transportation System Large Scale Architecture
SCORES	Spacecraft Object-Oriented Rocket Engine Simulation
SGI	Silicon Graphics, Inc.
SiC	Silicon Carbide

SLI	Space Launch Initiative
SSDL	Space Systems Design Lab
SSME	Space Shuttle Main Engine
SSTO	Single Stage to Orbit
STS	Shuttle Transportation System
SwRI	Southwest Research Institute
TiAl	Titanium Aluminide
TPS	Thermal Protection System
TUFI	Toughened Uniform Fibrous Insulation
UCAV	Unmanned Combat Aerial Vehicle
VAB	Vehicle Analysis Branch
VB	Visual Basic
WBS	Weight Breakdown Structure

Symbols

ρ	Density
μ	Gravitational parameter
ϕ	Gravitational potential function
θ	Local inclination angle
γ	Ratio of specific heats
β	Reliability index
σ	Standard deviation
σ_{sb}	Stefan-Boltzmann constant
$\Im$	Thrust
μ_c	Control variable expectation value

$\chi^2_{\alpha/2}$	Inverse cdf of chi-square distribution at $\alpha/2$
ε_{jk}	Sample from a uniform [0,1) distribution
$\%\varepsilon$	Percent error
ε	Black body emissivity
A^*	Throat area
A1	First vector of outputs from contributing analysis A
A2	Second vector of outputs from contributing analysis A
$\vec{a}$	Acceleration vector
A_e	Nozzle exit area
AR	Area ratio
b	Control variate parameter
B	Vector of outputs from contributing analysis B
C	Control variable estimate
C	Vector of outputs from contributing analysis C
C_σ	Covariance Matrix
C_v	Material heat capacity
C_d	Coefficient of drag
C_l	Coefficient of lift
Cp	Coefficient of pressure
f	Probability density function
f’	Surrogate probability density function
g	Constraint function
g_c	Acceleration due to gravity at the surface of the Earth
h_v	Heat of vaporization
I	Identity matrix

I_{sp}	Specific impulse
J_n	Nth gravitational harmonic term.
m	Mass
N	Number of trials
O	Vector containing system objective
p_0	Stagnation pressure
p_a	Ambient pressure
P_{ch}	Chamber pressure
P_{constr}	Probability of constraint satisfaction
p_e	Nozzle exit pressure
p_{jk}	Element of a matrix of independent permutations
P_n	Nth Legendre polynomial
$\bar{x}$	Points in the analysis space
$\bar{x}_{sns}$	Points in standard normal space
Q	Integrated heat load
$\dot{Q}$	Heat rate
R	Design resolution
r	Distance from the center of mass of the earth
R	Estimator for correlation coefficient
R_N	Nose radius
s	Estimator for standard deviation
S_{ref}	Vehicle aerodynamic reference area
T	Temperature
$t_{\alpha/2}$	Inverse cdf of student's t-distribution at $\alpha/2$
T_{trans}	Hasofer-Lind transformation matrix
V_A	Velocity in Chapman's equation

$\vec{E}$	Vector of expectation values
$\vec{P}$	Vector of probabilities
X	Design vector
X_{jk}	Sample location on a uniform [0,1) distribution for overall method
Y	Generic estimator
Y(b)	Generic control variate estimator
$z_{1-\alpha/2}$	Inverse cdf of standard normal distribution at $1-\alpha/2$

SUMMARY

Recent trends in aerospace conceptual design have lead to the use of distributed computational models covering multiple disciplines. Unfortunately at the level of conceptual design, many simplifying assumptions must be made because of the lack of design maturity. The problem with this lies in that current computational models are for the most part deterministic. They do not allow a designer to express uncertainties from such sources as user assumptions, computational model error and physical unknowns. Methods are therefore sought to use these distributed multidisciplinary deterministic models to generate probabilistic designs that can more accurately express the future performance of a concept.

To this end, a new multidisciplinary probabilistic sizing algorithm for launch vehicles utilizing distributed iterative uncertainty simulations has been created. A distinguishing feature of this new algorithm is that it performs uncertainty calculations at the contributing analysis level. By reducing the communications requirements and lowering the dimensionality of the local uncertainty analyses, the distributed method has many advantages for reusable launch vehicle conceptual design.

In addition to this, a new approximation method was tested against several existing variance reduction and metamodeling techniques for each of the contributing

analyses in the reusable launch vehicle design problem. Once a preferred approximation method was identified for each analysis on the basis of a balance of speed and accuracy, the iterative system was optimized using gradient search methods to find a probabilistic optimum across heterogeneous computer platforms.

This probabilistic optimization problem consisted of 84 noise variables and 4 design variables. This problem setup consistently found system optimums in 6-8 hours. It utilized several probability approximation methods run in an iterative manner to generate probabilistic vehicle sizing information. Once the probabilistic optimum was identified and confirmed using this process, a system-level Monte Carlo random simulation of the vehicle design was conducted around the optimum point to confirm the accuracy of the distributed approximation method. Because this simulation was prohibitively expensive, it was only conducted at the single optimum point. Following this accuracy confirmation, a comparison to a deterministic optimization of the same problem illustrated the difference between the probabilistic and deterministic optimums.

CHAPTER I

INTRODUCTION

Space access can be defined as mankind's ability to break free of the Earth's gravity and travel outside its atmosphere. Making space access routine requires breakthroughs in aerospace technology and physics that either have not been made or are not yet mature. To help bring this about, the National Aeronautics and Space Administration (NASA) and other government and industry organizations invest in key technologies that promise to make routine space access a reality. Through technologies, these organizations hope to improve the quality of life for the people footing the bill, the American taxpayer in the case of U.S. government efforts and the shareholder in the case of industry efforts.

Taxpayers and shareholders hope that routine space access will bring about changes in space activities with measurable benefits. The most direct benefits for both groups are related to potential commercial space activities. Currently, this consists mostly of communications applications, with some earth observation activities [1]. Despite the early promise of large low earth orbit satellites, the communications satellite industry still mostly consists of large, geostationary spacecraft that serve the telecommunications industry infrastructure [2]. However, direct to consumer marketing has recently made strong headway in the form of digital television and radio services using these satellites [2]. The time delay in communication has also turned out to have only a minor impact on wireless internet services [2] using geostationary satellites. It was previously thought that

large Low Earth Orbit (LEO) constellations would be required to service this market. These are potential growth areas for near term future launch market demand.

Future commercial activities may take advantage of beneficial characteristics of the space environment. Drug and exotic materials manufacturing research benefits from the low apparent gravity of orbit through a variety of mechanisms [3]. Also, the medical effects of weightlessness using test animals is of common interest to many researchers [4]. Many commercial experiments in these areas are currently under consideration for Space Station Alpha missions [5]. Research here could result in drugs and materials that are impossible to manufacture on Earth, yet that have a great benefit to humankind.

Far future commercial applications such as Space Solar Power [6, 7, 8] and Space Tourism [9, 10, 11] promise far more in terms of the scope of human activity in space. Space Solar Power takes advantage of higher solar energy conversion efficiency in space, as well as uninterrupted power generation to provide an environmentally-friendly method for generating large quantities of power. To do this would require a huge amount of cheap space lift capacity, something unavailable now. Space Tourism is a potential $50 billion [10] industry, directly relating to reusable human space flight. However, this revenue stream relies on a market for space lift capacity that is far cheaper and more reliable than anything that exists today [11].

The non-commercial benefits of routine access to space are just as appealing. Militarily, the taxpayer sees benefit in controlling the high ground of space for observation and potential defense from missile attacks [12, 13]. Taxpayers also benefit from human space exploration. While this may seem to be a tenuous connection, the human desire to explore can have a powerful effect. It may also be one of humanity's

most beneficial biological urges, given the growing evidence for regular mass-extinctions due to celestial body impacts [14]. Space colonization may provide the population redundancy needed for human life to survive such an impact. Another related benefit of routine access to space may be the ability to prevent such an impact altogether. Planetary defense is a benefit of space exploration that easily transcends economic concerns.

Figure 1 – Earth-Comet Impact Artist's Concept

A final, and in the past overriding, motivation for human space access was national pride. It may soon again be a motivating factor, as China has recently made significant progress in its manned space program with the flight of its prototype Shenzhou spacecraft [15]. These flights, combined with its plans for a new rocket, the Long March LM-2EA, designed specifically for lifting large payloads to low earth orbit [15] for the purpose of building a space station show that China is serious about manned spaceflight.

To reach the goal of routine space access, NASA must decide where to invest its limited resources. To do this, they need to compare optimized applications of the technologies to get an idea of where to put their money. The comparisons must be made using accurate forecasts of how these technologies affect vehicle concepts. All this requires advanced concept optimization incorporating new ideas and new combinations of technologies. At the same time, these optimizations should include all available information. Finally, all this must be ready at a moment's notice. This area of advanced concept optimization is where this thesis work is directed. Conceptual launch vehicle design exists to serve this technology investment community and provide direction for making cost-effective decisions.

Conceptual launch vehicle design as it exists today is a team-oriented effort. Often, multiple contractors with different corporate cultures must work together to create an integrated and optimized design. The distributed process tends to consist of separate analyses run by different disciplinary experts with a large deal of experience in analyzing their particular problem. These team-oriented environments are important to engaging engineers in a positive way to solve conceptual launch design problems. This method has been proven to work in the past and should be considered as a starting point for improvements in the design optimization process.

Also, conceptual launch vehicle design has been largely deterministic, causing errors due to simplifying assumptions, numerical imprecision, unknown external factors and the others. The only attempts at accounting for these uncertainties have been through the use of safety factors or margins. This is a weakness that should be addressed.

The demanding physics of launch vehicles [16] creates aggressive performance requirements and often creates a strong temptation to design to the edge of feasibility. Because this can often lead to an unacceptable probability of failure, launch vehicle design should have probabilistic information in its conceptual optimizations.

What is needed is a way to efficiently and accurately calculate the uncertainty contained in a distributed design analysis so that decisions can be made to minimize the impact of this uncertainty early in the launch vehicle design cycle, when such decisions are relatively cheap. This avoids the situation of a design surviving the simplifying assumptions of conceptual design, but then being revealed as infeasible in later, more committed stages of design. At the same time, the analysis techniques should retain their team-oriented approach. The current situation for many existing launch vehicle design organizations is that analyses exist on multiple platforms and have methods tailored to their individual disciplines. Given the inherent difficulties of probabilistic optimization in this situation, the temptation therefore exists to create monolithic models for the entire design problem, thus eliminating the difficulties of interfacing disciplinary codes. However, the retention of the team-oriented approach results in less institutional stress, and makes local maintenance of engineering analyses more practical.

There are advantages to distributed disciplinary codes. First, the owner of each code can be a disciplinary expert and therefore modify and run the code correctly. Second, there are very specialized methods for optimization as well as uncertainty analysis that have been or could be developed for these analyses that can be tested individually and be shown to work well on an individual analysis, without involving the entire multidisciplinary analysis organization in the verification process. The creation of

monolithic codes can be quite beneficial to design evaluation cycle times, but the loss in flexibility must be considered before that route is taken.

1.1 Design Evolution

In the life of an aerospace program, there are three traditionally acknowledged stages in the design process: conceptual, preliminary and detailed design [17]. Conceptual design deals with questions of feasibility, requirements, tradeoffs and the most basic factors of the product. Preliminary design takes these product parameters from conceptual design and begins design work on the various subsystems. Traditionally, sometime during preliminary design the details are frozen and a construction proposal can be made with confidence in the ability and cost of the project [17]. Detailed design is the step where individual machined parts are then designed so that they can be manufactured for the actual production of the aircraft.

The conceptual design phase is the focus of this research. The traditional purpose of this phase is to determine whether or not an idea has any chance of meeting the requirements for success. This is usually done using a very top-level analysis, not only for reasons of computational and setup time, but also because many of the design details required for more in depth analysis have yet to be determined by human designers. The nature of conceptual design is therefore very uncertain, as unknown quantities must be analyzed to determine the objective functions in a probabilistic sense. Several techniques for extracting a single deterministic objective value from probability distribution information have been advanced [18, 19, 20, 21, 22, 23, 24]. The focus of this research is to find new ways of generating probabilistic information in an inherently

multidisciplinary design optimization environment while maintaining the advantages of this environment.

Because this research concentrates on the multidisciplinary aspects of probabilistic design optimization, it has applications that go beyond launch vehicle conceptual design. Any engineering system that requires multiple analyses to work together in a coordinated fashion, while incorporating uncertainty in the analysis could find this research useful. The ability to scale into larger and more complex problems is also a primary advantage of distributed multidisciplinary analysis techniques.

CHAPTER II

MOTIVATION

2.1 Conceptual Launch Vehicle Design Motivation

NASA's top priority is now the Space Launch Initiative (SLI) [25]. Its stated goal is to reduce the cost per pound to low earth orbit to $1,000. The primary reason this is the agency's priority is the fact that half of the energy to get to the outer planets is tied up in escaping the gravity well of Earth. This gravity well is the fundamental boundary to human activity in space as identified by the U.S. Congress. It therefore affects all space programs under consideration and is therefore a high return investment for the government.

The current situation is that U.S. space access is primitive, expensive and risky. The nation's current commercial space launchers rely on 1950's technology (Figure 2), while at the same time newer foreign competitors control the majority of the launch market. This situation is unlikely to improve without systems designed for higher operability, higher reliability and lower cost. Reliability is a key cost driver as insurance can be a large percentage of the costs of a commercial launch as well as a mission barrier if it cannot be found. Also, more often than not, the cost of the payload far exceeds its launch cost, making its loss even more difficult to insure. This all combines to create the situation that the current commercial (and presumably lowest-cost) path to space does not go through this country.

Figure 2 – Atlas Then and Now

At the same time the commercial launch industry is stagnant, the government launch sector is relying on nearly as old technology to perform increasingly numerous and difficult tasks. The Shuttle Transportation System (STS) was built on 1970's technology and is nearly as primitive as current U.S. commercial launchers. It requires an army of thousands to operate, some say rebuild, after every flight and by its very design is limited in its commercial applicability. This is due to the fact that it is required to be flown as a manned system, and after the Challenger disaster it was not deemed worth the risk to the lives of astronauts to launch commercial payloads. In spite of these drawbacks,

neglect of space access development means that the STS is expected to continue service into 2012 and possibly beyond.

The goal of SLI is to reverse the current situation in commercial and government space access by systematically searching for new transportation architecture that can be implemented before the STS becomes unusable. It is hoped that the low cost of this new system will also allow the U.S. to retake its position as the leader in commercial space access. Through capital development, NASA hopes to eventually get more for less.

Unfortunately, NASA has a less than perfect track record when it comes to getting more for less. Its faster, better, cheaper philosophy has lowered the probability of success of its exploration projects to an unacceptable level [26]. While all of these sound good, they require a fundamental change in the way engineering is done. Even with this change, the rewards will most certainly be limited when all three of these metrics are considered simultaneously. The problem is that this change has not yet taken place. The methods chosen to date for the realization of this philosophy have consisted mostly of skipping costly, but necessary error prevention and testing measures. The elimination of systems engineering positions and verification processes has been blamed for the loss of Mars Climate Orbiter [27]. As if to emphasize the point, the very next Mars mission, Mars Polar Lander failed due to what was later determined to be a critical underfunding of all the Mars programs [28]. This underfunding caused the elimination of testing programs and experienced personnel, creating an unworkable situation of limited engineering resources and experience. To illustrate the this aggressive budget trend, the both of the failed Mars missions combined cost less than the single successful Mars Pathfinder mission [28]. While Pathfinder was also a faster, better, cheaper mission, it was obviously not taken to the extreme of the two failures.

This philosophy of taking on additional risk to save money [29] has also lead to extremely aggressive performance and budget predictions that have recently caused cutbacks or the death of several manned space flight programs. An example of a recently cancelled program is the X-33. Because of its philosophy of increased risk tolerance [28], NASA adopted a baseline Reusable Launch Vehicle (RLV) design with too many new technologies and construction techniques. Dramatic testing failures and overruns due to this risk have now killed this program [30]. Underestimated budgets have also claimed other victims, namely the X-34 and a good portion of the International Space Station [30]. Both relied on the introduction of entirely new primary systems without the money to pay for them. In the end, this has cost these programs dearly.

All of these trends in the space exploration arm of NASA show that the idea of doing more with less requires a real shift in engineering methods and practices, not just the elimination of activities and personnel. Because NASA has seemingly not backed off its aggressive cost goal promises [25], new methods must be adopted quickly to prevent the types of disasters cost cutting activities have caused to date.

Part of doing more with less involves accurate forecasting and design optimization with more information about future systems during early stages of development. This enables more programmatically robust systems to be generated that will not fall victim to changes late in the design cycle, when such changes are the most expensive to make. This is a potential systems engineering improvement that could help NASA meet the cost goals it has already promised, without incurring more program risk. This all needs to be done while retaining disciplinary experience.

For this thesis, these factors translate to a desire to have a formal method for optimization that ensures a true optimum in the face of uncertainty while at the same time retaining traditionally distributed analyses. This will allow disciplinary experts to retain an integral role in all aspects of model creation. Therefore, the experience of the expert in probabilistic simulation of a particular discipline can be fully utilized to generate accurate and efficient estimates, addressing a key concern in many editorials [26, 27, 28, 29, 30] about recent failures.

By introducing flexible probabilistic optimization into the design cycle, decisions on certain design variables can be made with a maximized amount of information, while leaving others to float. This process can be repeated throughout the design process, ensuring a vehicle with a consistent optimum while still allowing work to go forward, with a reduced possbility of changes later in the design cycle.

2.2 Paradigm Shift in Conceptual Design

According to the National Science Foundation [31] there should be three simultaneous goals for any engineering project [31, 32]:

- The committed and incurred costs should be pushed as far forward in time as is possible. This minimizes the possibility of expensive changes later in the program.
- Knowledge about the design should be obtained earlier, so that when decisions are made about the design, these can benefit from as much information as is possible.
- Lastly, design freedom must be retained later into the design process so that more information about the design can be obtained before decisions are locked down.

This research is intended to push committed cost into the future by allowing certain decisions to be made on the basis of probabilistic outputs, as opposed to making decisions by using information from more expensive design work and hardware construction. Probability information will be obtained at the earliest stages of design, thus satisfying the second condition of the desired paradigm shift. Thirdly, the techniques for conceptual design presented in this research allow the conceptual designer to set certain variables while letting others be set at some later date. This leaves exactly the desired amount of design freedom to be left in the design, while reducing the cost committed as described in the first shift. Ideally, this characteristic can be used to set variables that directly affect a large number of disciplines early on, while leaving variables with limited system-wide impact to later definition. This should reduce the number of system-wide changes that need to be made late in the design cycle, while allowing system design to proceed.

2.2.1 Application to Reusable Launch Vehicle Design

Much of current RLV conceptual multi-disciplinary design is typified by deterministic design methods. Methods such as these ignore uncertainty information that can be important to a design. Because of this designers are required to make “best guess” estimates of key design parameters, losing critical knowledge of the range of uncertainty that might be associated with that guess.

In addition to the above stated uncertainty due to design maturity, there is uncertainty related to the computational methods used to analyze concepts [23, 32-43]. This means that quantification of this fidelity error used in combination with simulation-based design uncertainty techniques is required for truly accurate conceptual design.

This unexpressed information in traditional optimization can result in a deterministically constrained optimum that will often lead to a high probability of an infeasible design [44, 45, 46]. This is due to the tendency of constrained optimums to lie directly on constraint boundaries. When uncertainty is added to these results, the probability will spread around the deterministic point. As a result, much of the probability will extend beyond the feasible frontier. This is shown in Figure 3. Aerospace conceptual design therefore requires fast and accurate methods for determining system uncertainty.

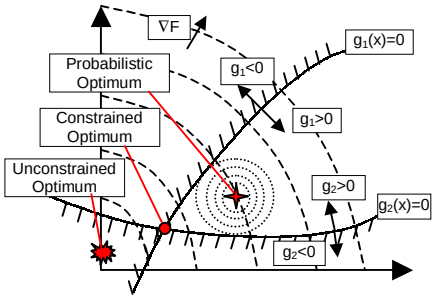

Figure 3 – Comparison of Constrained Optimums

Another advantage of probabilistic optimization is that it may be possible to create designs that are insensitive to sources of uncertainty. This is the idea of robust design, first introduced by Taguchi [47, 48, 49, 50, 51]. The intent of robust design is to use those factors over which the designer has control to achieve a result with low uncertainty in a response of interest. A great deal of work has been done recently to bring this idea into conceptual design using a variety of techniques. [22, 24, 38-42, 52-59] Through this work, the usefulness of this type of conceptual information has been shown using practical engineering approaches. It has laid the groundwork for

probabilistic conceptual design and generated a great deal of interest in the subject among those in the aerospace industry.

By including uncertainty in the design process, decisions can be made earlier in the life cycle of a product, when changes are inexpensive. This shift should enable faster development cycles resulting in higher quality products.

Also, because current uncertainty analysis is typified by single analysis techniques, there is a motivation to extend this to the area of distributed multidisciplinary design optimization, with several contributing analyses acting in a loosely integrated framework. Currently, design optimization in many organizations reflects this type of framework, so integrating probabilistic analysis into this could take the idea of probabilistic optimization to new engineering organizations.

Beyond just containing multiple disciplines, distributed implies that there are separate codes at varying locations that are "owned" by different people. This is illustrated by Figure 4. This distributed situation allows the individual engineer to monitor his/her own analysis and make sure that the results are both valid and correctly interpreted. Probabilistic methods to date have focused on creating a highly integrated top-level analysis that can be used to generate point designs. Then, a distribution estimation technique like Monte Carlo or response surface methodology is used around the outside of the entire analysis. The disadvantage of this is that it requires tight coupling of the analyses if Monte Carlo analysis is to be used. If an alternative fast approximation method is used, then these methods may be overwhelmed by the dimensionality of the entire system problem [60]. This is because as the entire system is considered, all the noise variables present in all of the contributing analyses must be handled by the system-

level probability analysis. If the problem could be decomposed into several, parallel lower level analyses, this dimensionality problem should be reduced.

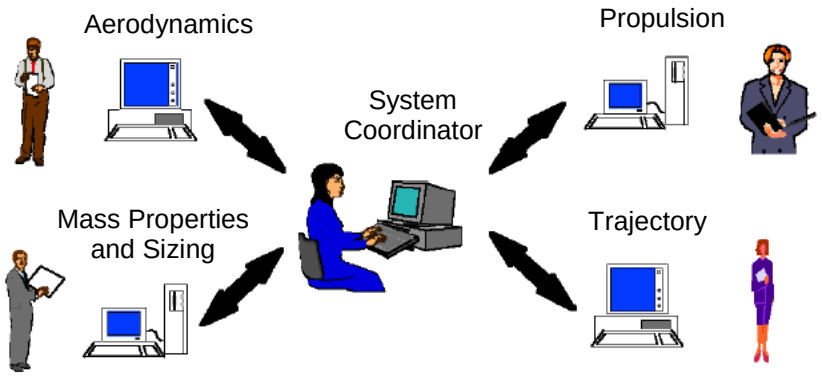

Figure 4 – Distributed Computational Framework

By breaking the probabilistic analysis into separate simulations, the type of probabilistic simulation used can be tailored to the specific sub-problem. In addition, the dimensionality of the sub-problem will likely be lower than that of the full problem, increasing the effectiveness and efficiency of alternatives to Monte Carlo simulation. A method is therefore sought to allow disciplinary experts to choose the most efficient means of probabilistic analysis while at the same time ensuring an optimum vehicle as result of their efforts.

The overall motivation of this research is to combine multidisciplinary design optimization with uncertainty analysis in a way that retains the positive attributes of each while hopefully reducing some of the negative aspects of design techniques that utilize each separately.

The next section sets the goals for this research and provides objectives for measuring their attainment. There are several goals here, as the research covers a fairly large spectrum of multidisciplinary design. Primarily, this research is designed to test the effectiveness of multidisciplinary design optimization methods to reduce the computational expense of accounting for uncertainty in launch vehicle conceptual design. Beginning with Monte Carlo methods as a baseline, this research will identify the most useful uncertainty analysis methods for inclusion in this multidisciplinary analysis. It will then attempt to use uncertainty calculations undertaken at the contributing analysis level to reduce the expense of probabilistic multidisciplinary analysis for launch vehicles.

CHAPTER III

RESEARCH APPROACH

3.1 Goals and Objectives

The overriding goal for this activity is to introduce a new formal method for distributed, probabilistic conceptual launch vehicle design. An important aspect of this framework demonstration is that the probabilistic analysis take place at the contributing analysis level, therefore reducing the dimensionality of each of the analyses. This will also show how the methods can be tailored to the particular problems, according to the experience and knowledge of disciplinary experts. The following list of goals and corresponding objectives was the guide for this research:

- Demonstrate a distributed probabilistic multidisciplinary framework.

This distributed philosophy of multidisciplinary design optimization has many advantages [61, 62, 63, 64]. Among these are local ownership of analyses, compatibility with existing analysis infrastructure and distributed computational effort. If the goal of demonstration of a distributed probabilistic framework for conceptual launch vehicle design optimization is met, then all of these advantages will be enjoyed. At the same time, probabilistic information, which is crucial at the conceptual design phase will be brought into conceptual launch vehicle optimization.

The demonstration of the conceptual launch vehicle design framework will include a detailed account of the procedure to construct it. It will include any problems or hazards encountered and assist those who wish to create similar problem setups for other conceptual design problems. In this light, ease of setup is a high priority. Problem setup should be on the order of or less than two man-weeks. Anything longer than this amount of time represents a significant investment and is unlikely to be implemented by industry.

Another objective used to measure the success of this demonstration will be the amount of probabilistic analysis able to be undertaken at the contributing analysis level. The degree to which probabilistic analysis can be done at this lower level will indicate how distributed the computational effort and responsibility has become. The objective for success was the creation of design framework that performed all significant calculations at the contributing analysis level.

- In this framework, multiple heterogeneous computer platforms will be utilized on a conceptual launch vehicle design problem.

By utilizing analysis integration software packages, a repeatable framework for analysis across heterogeneous platforms will show that application of this method is possible in established engineering environments with several, discrete analyses running on separate platforms.

This demonstration will show that a heterogeneous platform approach is feasible in combination with this probabilistic framework. Success will be measured here by

utilizing more than one computing platform in the conceptual launch vehicle example problem.

- This distributed probabilistic framework should have a significant computational expense savings when compared to Monte Carlo simulation.

To make this method competitive with other options for system-level probabilistic analysis, a two or greater order of magnitude improvement in speed when compared to a Monte Carlo simulation is required. This will ensure that the analysis method is competitive in terms of other options.

- Optimization should be able to be completed in a reasonable amount of time.

To ensure that this method is applicable in real engineering situations, an entire optimization should be able to be completed overnight. This should simplify manpower tasking while waiting for results, as another task does not need to be found for the engineer if the optimization can be run during off hours.

- Optimization using this method should be repeatable.

To measure the success of this goal, several confirmation optimizations of the primary optimization beginning with different initial guesses must find the same optimum point. Success here is all of the confirmation optimizations finding the same answer.

- The distributed probability approximations should arrive at accurate values.

This objective will be measured against a confirmation Monte Carlo simulation. The approximate framework should be no more than 5% off on the important problem constraints and objective function evaluation. The other secondary output parameters should also have errors within the calculated error bound for the Monte Carlo simulation.

- Uncertainty sources for conceptual launch vehicle design will be identified and reasonable distribution assumptions will be made.

The goal of uncertainty identification is crucial to an accurate representation of the conceptual launch vehicle design problem. This will involve identification of the sources of uncertainty, both environment and human based. Therefore, this research should identify and quantify as many open-source launch vehicle uncertainty parameters as is possible. These sources can then be represented by appropriate input distributions and included in the conceptual launch vehicle example problem. This work should be helpful to future launch vehicle designers who wish to include a formal mechanism to account for modeling uncertainties. However, most practicing organizations should be able to better quantify these uncertainties than this research given the competitive nature of many of the quantities of interest and the experience of most manufacturers.

- A new family of promising techniques, Discrete Probability Optimal Matching Distributions (DPOMD) for the probability prediction of a single analysis should be demonstrated.

The goal is to demonstrate the application of these new techniques to launch vehicle conceptual design contributing analyses. This way, if the accuracies of the methods are good, they can easily be used in later launch vehicle conceptual studies. This application will also show the relative ease of setup for these methods. The demonstrated ease of setup should reduce the opportunities for user error in application of the methods

when compared to some other fast approximation techniques. It will increase the real-world accuracy and decrease the overall expense of the methods as they are applied after this research. This is due to the fact that human interface time is often the most expensive aspect of any engineering enterprise.

To measure the success of the research with respect to the goal of demonstrating the new method, a detailed discussion of the setup of these methods will be included. This should indicate how much effort and how many user assumptions were required for the methods. The objective here is that these new methods be run in a very "black-box" manner, using information easily obtained by the user to generate quality uncertainty information for many types of problems.

- Several competing methods should be tested on the contributing analyses of the optimization problem to find methods best suited for those analyses.

The objective for measuring the success or failure here will be the identification of a method for each of the analyses that is both fast and accurate. The knowledge gained by these tests should show the strengths and weaknesses of the probability analysis methods in terms of the contributing analysis being tested. More specifically, the goal for computational speed relates to its effect on the users ability to optimize the problem. Therefore, the goal here is for reduced computational expense expressed in actual function calls, not in metamodel building cost for techniques that utilize these. A secondary goal related to these tests will be to gauge the accuracy and expense of the new DPOMD methods for uncertainty analysis. This goal will be accomplished during the course of the primary goal.

The uncertainty methods will be compared on the basis of their accuracy and their computational expense. Accuracy will be measured by the relative error of the relevant

inputs and outputs when compared to a Monte Carlo simulation. Whether or not an input or output is considered relevant will be determined by the requirements made on the contributing analysis by other contributing analyses in the proposed launch vehicle conceptual design framework. The accuracies of these variables are the key to successful integration into a potential design framework of the contributing analyses being tested. The goal of selecting preferred methods for each of these contributing analyses will be measured by the decision of which distribution analysis technique is used in the design framework test, the goals of which will follow in this chapter. This decision will go to the analysis method that shows the best overall performance on all the required coupling variables.

The second objective for this comparison will be to measure the computational expense of the differing methods. This will be measured by the time it takes to execute a single probabilistic analysis call. At least a two order of magnitude improvement in computational expense is expected when the approximation methods are compared to a typical Monte Carlo analysis. This goal is essential to enabling optimization, since this process can entail hundreds of function calls to the overall system. Some methods included a great deal of up front computation to generate a metamodel, but then the metamodel was inexpensive to execute. For the sake of a simple comparison, the computational expense of the metamodel generation was excluded from the expense totals.

The final objective for this comparison is related to the hypothesis that each contributing analysis benefits differently from each approximation method. This will be measured by the diversity of the methods chosen for uncertainty analysis in each of the contributing analyses.

3.2 Thesis Organization

To meet the goals and objectives set in this chapter, a series of tests were planned on various aspects of the proposed RLV probabilistic optimization method. These tests were designed to find the best methods for disciplines having characteristics common to a certain class of analysis. Then these methods were utilized in a distributed, heterogeneous computing environment to optimize a reusable launch vehicle concept. A Monte Carlo simulation then verified the results of the optimization. Finally, the difference between the probabilistic and deterministic optimums was found by a more traditional deterministic optimization.

The first step in finding appropriate contributing analysis probabilistic methods was to conduct a background search. This helped determine which methods were available and appropriate for the task they would eventually be required to perform. The search concentrated on promising variance reduction techniques, most probable point reliability methods and new design of experiments methods from the author. Because variance reduction techniques and the new methods had the best chance of being useful in the desired situation, these were the primary focus of the background section. The Most Probable Point (MPP) methods background consisted of an overview of the terminology and assumptions made by different methods based on MPP. A smaller search was conducted on MDO methods. The background on MDO methods was designed to show the current state of research in this area and indicate where there is room for work on these methods.

Once a group of preferred group methods was found, these were tested on the contributing analyses proposed for the overall system design. At that point, they were compared to Monte Carlo simulation and eventually each other on the basis of relative

error and speed. Based on these criteria, a method was selected for each of the contributing analyses to be used in the overall system design problem.

Once the preferred contributing analysis methods were defined, the overall system problem was constructed using the ModelCenter© analysis integration software package and the fixed-point iteration method. The probabilistic analyses were then executed iteratively to optimize an all-rocket single stage to orbit reusable launch vehicle (SSTO RLV) based on the NASA-Langley Vehicle Analysis Branch (VAB) wing-body shape. The process optimized the 95% confidence level dry weight. This confidence level was selected to reflect the desired risk level of the dry weight result.

To determine the accuracy of the probabilistic design process after the optimization, a Monte Carlo simulation on the entire vehicle was conducted. The major probabilistic constraints and objective function values were compared to the estimates, keeping in mind the error bands on the Monte Carlo simulation results. These comparisons give a good idea of the accuracy that can be expected from this distributed design method.

To illustrate some advantages of probabilistic optimization, a deterministic optimization of the same design problem was undertaken using more traditional deterministic methods. For this simulation, all of the uncertainty assumptions were set to their most likely values and a traditional 15% dry weight margin was added to defend against vehicle growth. The 15% margin was selected because it is a widely used value in conceptual launch vehicle design. The results of this analysis were compared using two criteria. The first criterion was the difference between the optimal variable settings for the probabilistically optimized RLV and traditionally optimized RLV. The second was to

examine the difference between the reported vehicle result for the two problems. This would show to what confidence level the traditional 15% dry weight margin vehicle corresponds. Once all the tests were completed, conclusions were drawn relating to the goals and objectives set in this chapter.

CHAPTER IV

RLV DESIGN PROCESS

Reusable Launch Vehicle (RLV) design is a constantly changing process. Given the lack of consensus on a single design or core technology base, the methods by which conceptual designs are brought about must be continuously modified to account for new ideas. This constant flux has hindered the creation of a standardized monolithic tool that can be used for RLV design and has meant often times that very ad hoc methods were applied for each design situation.

A good example of current state of practice in RLV design is the ISAT project underway at NASA Marshall Space Flight Center [65]. The center of this project is an integrated team room where the members analyses can be run and interfaced while everyone is in the ISAT room on the local network of computers, utilizing the interface software RECIPE© [66]. This allows for design ideas to be tested in real time in a team environment. This is a step improvement over traditional design meetings for the reason that the concept space can be explored by the team while they meet. The disadvantages of this current state of practice is that it hinders collaboration with remote partners, it does not allow for automated exploration of the design space and there is no systematic method for finding the optimum vehicle for the considered requirements. However, as current state of practice, this method of design could be easily implemented anywhere, with little institutional change.

Going to the state-of-the-art in conceptual RLV design involves a more automated framework for analysis. Recent efforts in the ISE project at NASA Ames and Langely Research Centers (ARC and LaRC) have successfully demonstrated this automated remote network capability in the Reusable Space Transportation System Large Scale Architecture (RSTS LSA) facet of the program. Here advanced networking methods have been applied to create a virtual network of engineering analyses that are able to coordinate multiple partners in remote locations. Also, many commercial frameworks packages have been applied to the RLV problem, most notably ModelCenter© [61]. These prototypes have demonstrated the creation of autonomously executable design processes for RLV's to which any number of top-level optimization and/or probabilistic methods could be applied. The one thing that the current state of the art has in common with state of practice methods is that the analyses for both have remained on widely distributed computing platforms. This distributed approach has several advantages related to flexibility [67] and should be a requirement for RLV design.

Research into more advanced RLV design processes has included several tests of decomposition methods [68-76]. These are methods designed to reduce the iteration between the analyses by either optimal ordering or central control of the analyses through a system-level optimizer. Most notable in the field in terms of its application to RLV design has been Collaborative Optimization (CO) [62, 63, 64, 77, 78, 79]. This is a technique for distributing the optimization burden across the local contributing analyses in such a way that a single system optimum can be found. This technique has been applied to the RLV design problem in a deterministic manner on multiple occasions, with varying success [61, 79]. Chief among the disadvantages of this method are that the problem setup for the contributing analyses must be changed to use a very unintuitive objective function. Also, the claimed advantage of using well-known optimization

methods for the contributing analyses is also questionable, since the topology of the objective function formulation for the contributing analyses seldom resembles the original problem setup for that discipline. This fundamentally changes the optimization problem and can make it difficult for optimization methods currently existing in that analysis to work.

Research into the RLV design problem to date has for the most part concentrated on finding deterministic optimums. Applications of advanced decomposition methods have ignored, except through the use of safety margins, the possibility of uncertainty in the problem assumptions. Probabilistic analysis in the RLV field has been limited to offline analysis for generating weight growth data [37] and economic forecasts [80, 7, 11]. These offline analyses have all been single-discipline problems, with no forecasting done on how these result impact other disciplines. Those methods that have been applied to RLV design online have utilized system sensitivities [81] as surrogates for probability estimates. In addition, these sensitivities were applied from the top level, not generated by the local analyses in distributed manner.

To date, probabilistic analysis has been focused on single-level problems. This means that in a multidisciplinary design environment, these techniques must be applied at the top level, around the combined system of contributing analyses. An exception to this would be the work on the System Uncertainty Analysis Method by Du and Chen [51], which used contributing analysis sensitivities to generate system level probability distribution estimates. However, it did not allow for local control of the probability analysis and did not accommodate more sophisticated methods for uncertainty analysis other than a simple gradient-based, normal assumption approximation. It also does not

allow for heterogeneous methods to interact in a constructive manner. In addition to these issues, it has not been applied to RLV design.

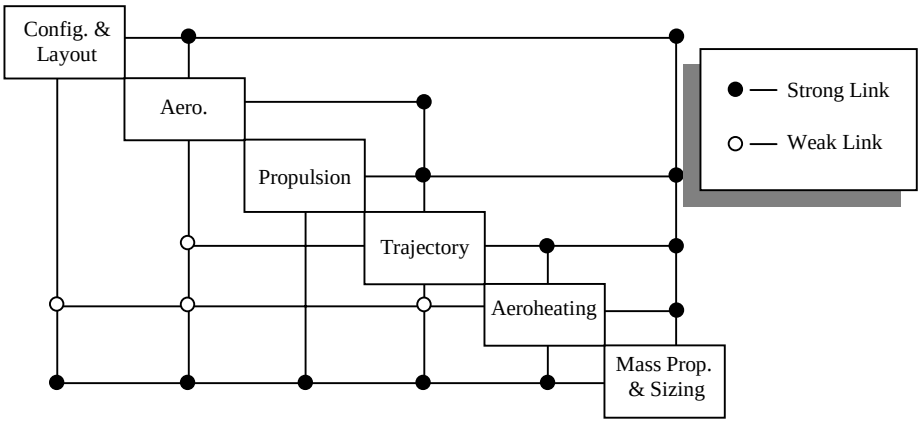

Figure 5 – Design Structure Matrix for RLV

To review, the actual RLV design process traditionally consists of several analyses executed in a highly iterative fashion. A diagram illustrating the data flow is shown in Figure 5. This is known as a Design Structure Matrix (DSM). The boxes are contributing analyses and the square links represent data flows. The links above the diagonal represent feed-forward loops while the links below represent feedback. In order of their typical execution, these analyses and their contributions to the system are:

- Configuration –The geometries and packaging of the vehicle for a reference size are defined.
- Aerodynamics – Aerodynamic force and moment coefficients are calculated and aerodynamic surfaces are defined for a reference size.

- Propulsion – Main ascent propulsion systems are sized and the performance of the engines is calculated.
- Trajectory – The vehicle mission is simulated to generate propellant requirements and acceleration loads.
- Aeroheating – Surface heat rates and temperatures are calculated for a reference entry trajectory and thermal protection system (TPS) panels are sized.
- Mass Properties and Sizing – The vehicle mass is estimated and the vehicle is scaled to provide the needed propellant requirements.

These analyses can consist of different codes depending on the setup and the problem, but there is a standard level of fidelity of each of these that works well for conceptual design. The following is a quantification of this fidelity and a description of the analysis that is behind state of the art launch vehicle conceptual design.

4.1 Configuration

This step usually employs a solid modeling package to determine the geometry of the vehicle, including the areas for subsystems, propellant, payload and load points for aerodynamic surfaces and gear. Here the designer usually defines the outer mold line to balance the aerodynamic and structural needs of the vehicle. An example of the end result of this modeling process is in Figure 6.

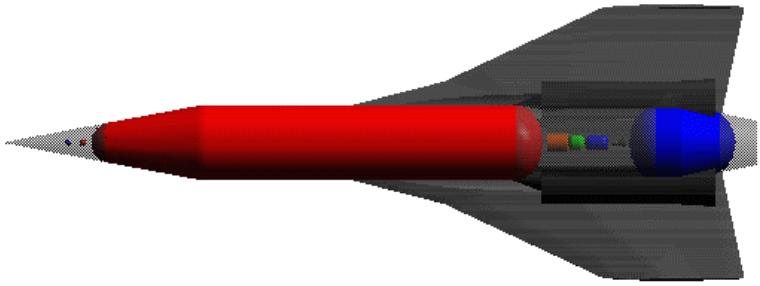

Figure 6 – Example Launch Vehicle Configuration Model

For launch vehicles, one of the primary goals of this analysis is to provide as much volume as is possible for propellants. This goal is measured by packaging efficiency, which is the ratio of propellant volume to total volume. It is also important that these propellants are in containers that reflect their pressurization and support requirements. These two goals are often at odds with each other, and if too much favor is given to fitting more propellant, the process can lead to difficult-to-manufacture propellant tanks [30].

The most general technique for providing scalable packaging information is to fit a parametric curve of packaging efficiency for a range of sizes. The packaging efficiency can vary with length because the constant size of the payload bay changes the percentage of volume available to the propellant as the vehicle size changes. What is typically done is the vehicle is packaged for three reference lengths, then the packaging efficiency is fit using a quadratic polynomial. It is important that these lengths span the range of possible lengths because extrapolating can lead to drastic errors on this type of fit.

The outputs besides packaging efficiency provided by this analysis are the reference lengths, areas and volumes of the components of the vehicle for a specified reference length. These typically include parameters important to the calculation of weights and performance, such as wetted TPS area, engine location and total fuselage volume. All of these terms are then provided for a reference size to the other analyses so that they can be photographically scaled from the given reference scale. Photographic scaling is a method for calculating the dimensions for a parametrically sized vehicle and will be explained in the later in more detail in the section on mass properties and sizing.

4.2 Aerodynamics

For this analysis, the aerodynamic force coefficients are calculated using a combination of preliminary simulation techniques. For the subsonic and supersonic aerodynamics, this usually involves a panel method [82] with fuselage interference. For hypersonic aerodynamics, any combination of modified Newtonian impact, tangent cone or tangent wedge methods are used.

In panel methods, first panels are specified that divide up the wing and fuselage. An example of this can be seen in Figure 7 [82]. Next, some type of singularity distribution is applied to each panel. These can be sources, doublets, vortices, etc. These singularities are constructed in such a way that they may influence the flow through the surface of the wing at some control point, usually in the center of the panel. This flow through the panel control points is then expressed in terms of the singularity strength that when combined with the exterior flow conditions, leads to a set of linear equations. These equations are solved for the singularity strengths that lead to no flow through the control point, thus revealing the pressure differentials on the surface of the vehicle. For example,

vortex-lattice methods use a grid of horseshoe vortices over the wing extending backwards to infinity through the wake.

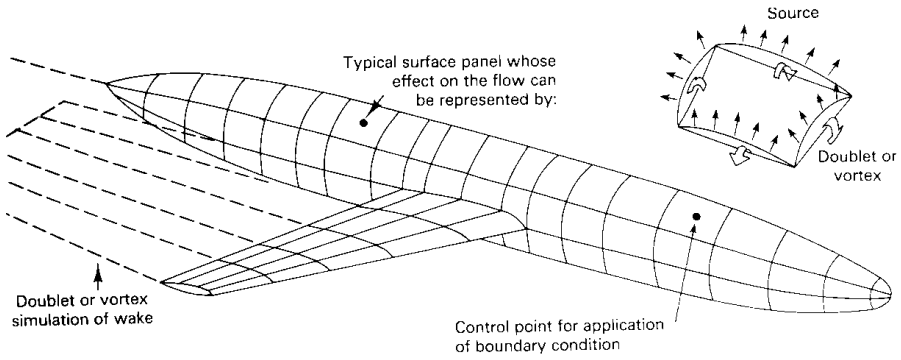

Figure 7 – Diagram of Panel Method Model [82]

The hypersonic methods typically employed either include modified Newton's method, which is effective for blunt body predictions, or tangent cone / wedge methods which are better for slender bodies [83]. None of these methods has a formal derivation, but they seem to provide good engineering results for a number of problems. Newtonian impact theory assumes that the component of the flow momentum perpendicular to the surface is completely transferred to the vehicle. To help this theory agree with experiment, the constant C_{pmax} in front of Eqn. 4.1 is added in place of the constant 2 to turn Newton's theory into modified Newtonian impact theory. Theta is the local incidence angle of the object surface to the flow and C_p is the local pressure coefficient [83].

$$C_p = C_{p\max} \sin^2 \theta \qquad (4.1)$$

$$C_p = \frac{p - p_\infty}{\frac{1}{2}\rho_\infty V_\infty^2} \tag{4.2}$$

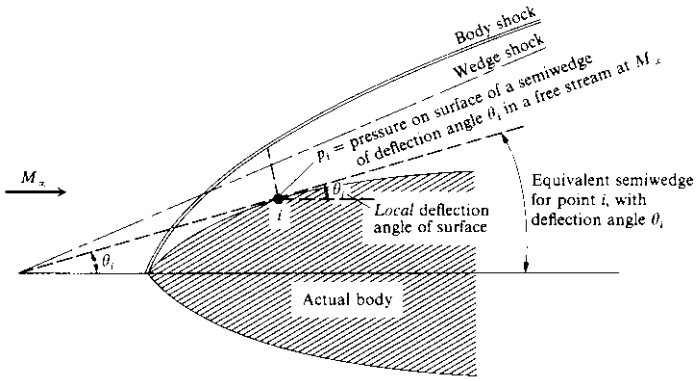

Figure 8 – Application of Tangent Wedge Approximation [83]

Tangent cone/wedge methods [83] are also local incidence methods. Instead of using Newton's equation, these methods assume either a cone or wedge tangent to the body surface, whichever is more appropriate, to estimate the local pressure coefficient. These local pressure coefficients can either come from tables or from closed-form solutions of the hypersonic small disturbance equations. A diagram showing the application of tangent wedge is shown in Figure 8 [83]. All these methods generate non-dimensionalized aerodynamic force coefficient information for the vehicle at a variety of conditions. These values are then fed to the trajectory and aeroheating analyses where they are essential inputs.

4.3 Aeroheating

During this part of the process, the temperatures and heating rates are determined for key parts of the outer surface of the vehicle. These are used to determine the TPS panel thickness and makeup so that the weight per unit area of the TPS can be given to the mass properties analysis.

The first step is the generation of an example trajectory using a 3 degree of freedom (3DOF) simulation. Here the vehicle roll and angle of attack is directly controlled to minimize the maximum heat rate and provide a smooth entry to the desired location on the planet. A lifting entry trajectory traditionally (STS) consists of a pair of unique maneuvers designed to increase the safety of the entry. The first is a bank maneuver at a relatively constant angle of attack early in the trajectory so that a higher angle of attack, which is beneficial for heating, can be held without inducing too much lift and causing a porpoising motion. If the entry must be relatively straight, this bank maneuver must be reversed several times to keep the overall course constant. For maximum cross range on entry, no reversals are performed. These maneuvers are typically done high in the atmosphere. After the vehicle slows down and approaches the runway, a series of S-turns are executed for the purpose of removing the excess energy of the vehicle so it does not overshoot the runway. Designing this extra energy into the trajectory is important, as atmospheric variations may cause the vehicle to have less energy than predicted, causing it to fall short of the runway.

Based on the conditions described by the entry trajectory, heating rates are calculated for various parts of the body by approximating them as cones, spheres, flat plates and cylinders, as well as applying engineering heating equations such as

Chapman's shown in Eqn. 4.3 [84] for stagnation point heating in Earth's atmosphere only.

$$\dot{Q} = \frac{17{,}600}{\sqrt{R_N}} \left(\frac{\rho}{\rho_{SL}} \right)^{1/2} \left(\frac{V_A}{26{,}000} \right)^{3.15} \tag{4.3}$$

In Eqn. 4.3 R_N is the radius of the body in feet, ρ is the air density and V_A is the velocity in feet per second. Once the heat rates are established, there are three common mechanisms for handling the heat. The first is heat sink. This method relies on the total heat load being absorbed by some material as internal energy without the material releasing the energy back into the atmosphere. Materials with high thermal diffusivity and high thermal capacity, such as copper and Beryllium, are good for heat sink protection [16]. Eqn. 4.4 [16] shows the total heat load of a heat sink system, where C_v is the heat capacity of the sink material, m is the mass and ΔT is the temperature change.

$$Q = mC_v \Delta T \tag{4.4}$$

Ablation is the second mechanism for heat absorption. This method relies on the vaporization of a surface material to release the heat transfer from the atmosphere. This method requires materials with a high heat of vaporization. Phenolic compounds and graphite are good choices [16]. The total heat load for an ablative system is given in Eqn. 4.5 [16], where h_v is the heat of vaporization of the heat shield.

$$Q = h_v \Delta m \tag{4.5}$$

The final method of heat handling is radiative. In this technique, the temperature of the heat shield material is allowed rise so that the heat rate from black body radiation balances the heat rate from the atmosphere [16], but not so high that the material melts. High melting temperature materials combined with high emissivity coatings are the ideal choice for this type of TPS. This tends to be the heat-rejection mechanism of choice for lifting-entry vehicles, due to their relatively low heat rates, but high total heat loads when compared to ballistic entries. The equation for blackbody radiation is given in Eqn. 4.6 [85] where ε is the emmissivity of the surface, σ_{sb} the Stephan-Boltzmann constant and T_w is the surface temperature.

$$q = \varepsilon \sigma_{sb} T_w^4 \tag{4.6}$$

Using one or more of these mechanisms, the TPS is sized and its mass per unit area is estimated for different parts of the vehicle. In the case of radiative TPS, a minimum backface temperature must be set and the heat conduction through the material must be calculated to find the equilibrium value of this backface temperature. In this way, the thickness of radiative TPS is calculated [86].

4.4 Propulsion

For conceptual launch vehicle design, the main propulsion analysis generates parameter estimates, usually rubberized, for use by the trajectory and mass properties analyses. Rubberized means that the propulsion variables are parameterized in such a way that the size of the engines can be changed without rerunning the propulsion analysis. Here the performance, weight and thrust of the propulsion unit are defined by

conceptual methods. While many types of engines can be used in reusable launch vehicles, the following explanation pertains primarily to chemical rocket engines.

While the type of engine used can vary widely, the level of fidelity for conceptual design typically includes frozen, one dimension, isentropic flow with historically regressed efficiencies at key stations outside of the combustor, with a chemical equilibrium algorithm inside the combustor to determine the combustion products and heat release. The expansion ratio of the engine nozzle is also sized to preclude the possibility of flow separation along the nozzle, if this is a concern.

Using the calculated results of the combustion process, the thrust and propellant efficiencies are calculated. For a rocket engine assuming isentropic flow, the throat and exit plane conditions determine the thrust according to Eqn. 4.7 [87]. In this equation, $\Im$ is thrust, A^* is the throat area, p_0 is the stagnation pressure in the combustion chamber, γ is the ratio of specific heats for the combustion products, the subscript e denotes exit conditions, a denotes ambient, * denotes throat and 0 denotes stagnation.

$$\frac{\Im}{A^* p_0} = \sqrt{\frac{2\gamma^2}{\gamma-1}\left(\frac{2}{\gamma+1}\right)^{(\gamma+1)/(\gamma-1)}\left[1-\left(\frac{p_e}{p_0}\right)^{(\gamma-1)/\gamma}\right]} + \left(\frac{p_e}{p_0}-\frac{p_a}{p_0}\right)\frac{A_e}{A^*} \tag{4.7}$$

4.5 Trajectory

The trajectory analysis in conceptual launch vehicle design is usually comprised of some type of three degree of freedom ascent (3DOF) simulation. In this simulation, the

equations of motion for three-dimensional translation, along with an equation for mass consumption are integrated for an optimized set of vehicle attitudes to generate the propellant loading and acceleration information for an ascent mission.

The simulation essentially flies the vehicle through its mission by integrating the accelerations on a time-changing vehicle mass due to aerodynamics forces, gravity and thrust. These equations are typically integrated in the Geocentric Equatorial (GCE) coordinate system. The geocentric-equatorial reference plane for the earth is a simple three-dimensional right-handed orthogonal reference frame. The X-axis points in the direction of the vernal equinox. The Z-axis points through the north pole, along the axis of rotation of the Earth. The Y-axis is then defined by the fact that this is a right-handed coordinate system. This frame can be treated as an inertial frame for RLV analysis.

The equations of motion, here described as three second order coupled differential equations, are as described in Eqn. 4.8. [88]. The term ϕ is the gravitational potential of the oblate earth, given by Eqn. 4.9 and a_p is the perturbation acceleration, essentially the thrust and aerodynamic forces divided by the mass.

$$\vec{a} = \frac{\partial \phi}{\partial x}\hat{i} + \frac{\partial \phi}{\partial y}\hat{j} + \frac{\partial \phi}{\partial z}\hat{k} + \vec{a}_p \tag{4.8}$$

$$\phi = \frac{\mu}{r}\left[1 - \sum_{n=2}^{\infty} J_n \left(\frac{r_e}{r}\right)^n P_n\left(\frac{z}{r}\right)\right] \tag{4.9}$$

In Eqn. 4.9, μ is the gravitational parameter of the Earth, J_n is the coefficient corresponding to the nth gravity harmonic of the Earth, r_e is the radius of the Earth, P_n is

the nth Legendre polynomial and z is the corresponding coordinate in the GCE reference frame. The governing equations are then expressed as seven coupled first order differential equations by splitting up the three second order equations and adding the rate of mass consumption. These are given in Eqn. 4.10.

$$\dot{\bar{x}} = \begin{pmatrix} \dot{x} \\ \dot{y} \\ \dot{z} \\ \dot{u} \\ \dot{v} \\ \dot{w} \\ \dot{m}/m_0 \end{pmatrix} = \begin{pmatrix} u \\ v \\ w \\ \frac{\partial \phi}{\partial x} + \frac{a_x}{m} \\ \frac{\partial \phi}{\partial y} + \frac{a_y}{m} \\ \frac{\partial \phi}{\partial z} + \frac{a_z}{m} \\ T/(m_0 g_c I_{sp}) \end{pmatrix} \tag{4.10}$$

These equations are then typically integrated by some manner of predictor-corrector variable time step numerical quadrature. Some examples of these methods are Runge-Kutta-Fehlberg [89, 90] and the Krogh Variable Step-Size, Variable Order Integrator [84]. Parametric user descriptions for the vehicle attitude and throttle settings as a function of time are described and these parameters are used as design variables to optimize the trajectory for repeated simulations. Typically, the propellant consumed is optimized, but the objective function definition can vary depending on the mission, often times with constraints on quantities such as dynamic pressure and axial and longitudinal acceleration. Once the trajectory has been optimized, the solution is analyzed to determine the loads on the vehicle and the propellant required by each of the stages to make orbit.

4.6 Mass Properties and Sizing

Determining the weight and size of the overall system is the job of the mass properties and sizing algorithm. This analysis typically uses historically regressed weight equations for vehicle components to generate a weight breakdown structure (WBS) that tracks the use and disposal of fluids and hardware over the course of the mission. Then, based on this iterative weight estimation algorithm, the vehicle outer mold line (OML) is scaled until the vehicle on-board propellant corresponds to the required mass ratio (MR). All of this is done for a constant payload, so increasing the size leads to more propellant relative to the payload and increases the available mass ratio [16].

The mass properties part of the algorithm typically consists of several interrelated algebraic equations derived from historical values for similar components. Because this set of equations is typically recursive, some sort of root finding algorithm is required. Usually, the root of the system of nonlinear equations is found using simple fixed-point iteration [90], but if there are convergence problems, a relaxation factor can be added. However, fixed-point iteration with no relaxation is the standard technique.

The next part of the algorithm involves sizing. This part is wrapped around the outside of the mass properties algorithm and makes sure that the required mass ratio [16] matches the available mass ratio provided by the vehicle. This is also a root-finding problem, but usually only in one dimension, the vehicle scale.

Photographic scaling is the most common technique for changing the available mass ratio of the vehicle. Here, the vehicle's relative dimensions are left unaltered, but every length scales directly with the scale factor, every area with its square and every

volume with its cube. This scaling technique provides key dimensional information for the mass equations that can then use FPI to find a valid set of component masses.

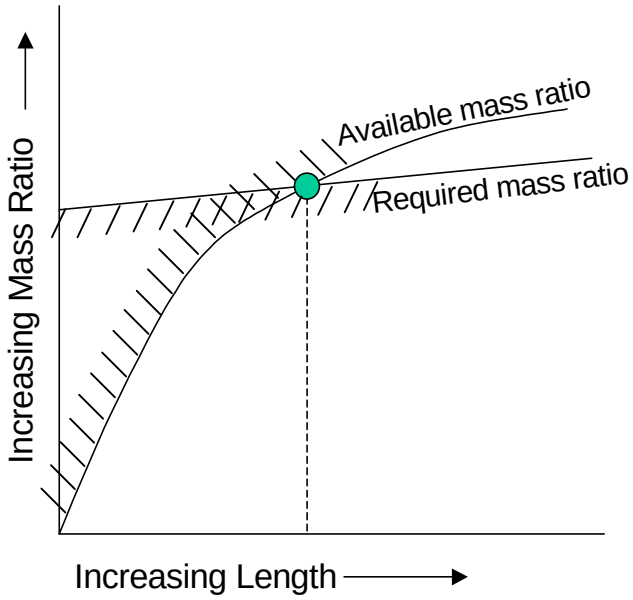

Figure 9 – Sizing Problem Diagram

A more sophisticated numerical root-finding technique than FPI is normally required for the sizing problem. Newton-Rhaphson is a common method. It uses the vehicle scale as the independent variable and the difference in mass ratio requirements as the dependent variable. This is shown in Figure 9. It is possible to encounter a situation where no matter how large the vehicle is grown, the required mass ratio cannot be met. In these cases, changes must be made to the design of the vehicle to either lower the relative structural weight or lower the required mass ratio.

Many disciplines were left out of this review. These include such analyses as Cost, Business and Economics, Operations and Safety/Reliability. While these are quite possibly the most important analyses from a total system standpoint, they are not required to explain the work performed in this thesis. The work here consisted of performance analysis only and did not require these disciplines.

CHAPTER V

BACKGROUND ON UNCERTAINTY AND MDO METHODS

This thesis is an extension of work in both the areas of uncertainty analysis and multidisciplinary design optimization (MDO). To get an idea of the current state of the art in both of these areas, as well as previously observed issues in implementation, the following section provides a synopsis of several previous research efforts.

The first discussion relates to observed implications of implementing probabilistic design optimization. This gives an idea of what kind of information can be generated by these techniques as well as illustrates some of the intuitive benefit. Next is a brief summary of current approximation techniques for probability integrals. These, along with new methods presented in this thesis, will be the options explored for uncertainty analysis in the system contributing analyses. They include both reliability and variance reduction tecnniques and they all have the potential to be useful in a loosely coupled multidisciplinary design optimization framework. It is hoped that this investigation will reveal a suite of methods suitable for conceptual launch vehicle design lower level analyses. Last is a brief overview of some current multidisciplinary design optimization methods.

5.1 Design Uncertainty Implications

Design with uncertainty creates several issues that must be described before effective use of the information generated by these analyses can be utilized. These issues include description of the uncertainties in the design, new categories of design variables depending on when in the design evolution the variables are to be set, new methods of objective function formulation and techniques for evaluating probabilistic constraints.

5.1.1 Sources of Design Uncertainty

There are several types of uncertainty that must be quantified by a conceptual designer. The most commonly encountered source of design uncertainty is that due to error in the simulation of natural phenomena [23, 32-43, 91]. This is the major source of uncertainty in the very early stages of design where faster and more general analyses based on the available design information take place. This type of uncertainty can include model accuracy as well as the required designer estimates of important parameters that rely on later design information.

Most computational models are periodically verified against higher fidelity models or test results. This should give some idea of the typical error present from this source. If this information is not available, then it should either be acquired or the model should not be used, as estimates for model error will more reflect user opinion than reality.

Unknown future conditions also are directly related to the robustness of an engineering product. The ability of a product to successfully operate over a wide range of possible conditions is a common definition of quality. This attribute is something that has been missing from many aerospace products in the past. The identification of this type

uncertainty has been previously presented in [56, 52, 55, 58, 22, 2]. Roth et al. [56] considers four physical unknowns for an unmanned combat air vehicle (UCAV). These are the subsonic and supersonic ranges, load factor during the mission and payload. Mavris et al. [52, 55, 58, 22] identifies economic uncertainties such as load factor, economic range, fuel cost and economic range. Finally, a real-life example of uncertain operating conditions is the failure of Low Earth Orbit (LEO) communications satellite constellations [2]. The business plans for these constellations did not anticipate the exponential growth of terrestrial networks, making them a definite victim of unknown future operating conditions.

5.1.2 Near Term and Far Term Variables

By incorporating uncertainty into the design process, multiple scenarios are analyzed for a single design. It is therefore possible for this design to set certain variables to values that optimize the overall performance of the design, whether that be cost, profitability or effectiveness, etc., while leaving others to be optimized at some future date, when more detailed information is available. An example of this type of design variable is the programming of trajectory control settings for launch vehicles. Because these variables are relatively easy to change, they are altered as late as during flight to ensure an optimal ascent to orbit, taking into account the latest information.

By the same token, no one would suggest changing the size or number of engines on a launch vehicle on the day of the launch, because this change would be difficult to implement and require large scale changes all across the system. It is important to set this type of variable earlier in the design process. This is therefore an inherently different kind of design variable.

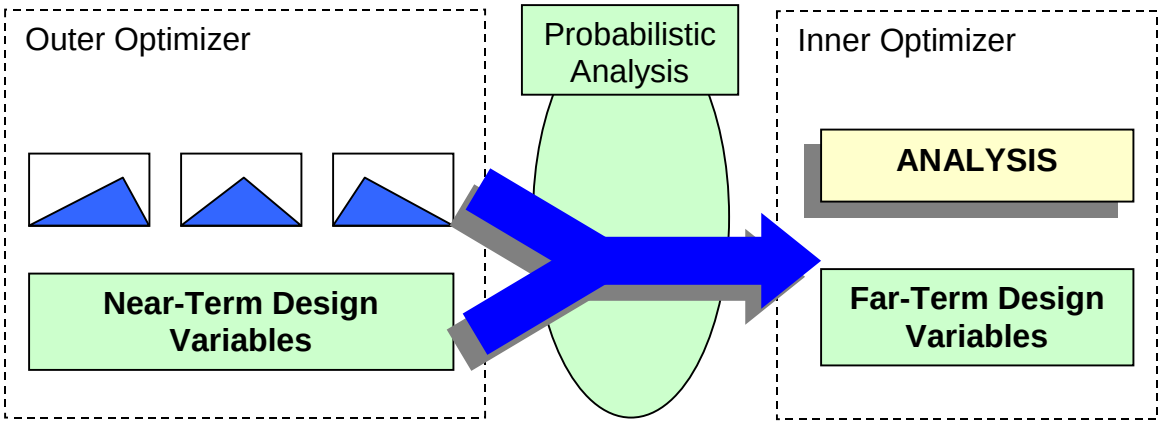

Figure 10 – Idea of Near Term and Far Term Variables

For probabilistic optimization using both of these types of variables, this issue creates a two-level optimization problem. The outside level has traditional control variables as design variables. These variables are those that are to be set for the current optimization. The next level inside is some type of uncertainty analysis like Monte Carlo, where noise variables are added to the design variables set by the outer optimizer. The next level is an optimization of the variables that the designer does not wish to set right now, but would prefer to set at a later date. Even though these variables are not being set right now, it should still be verified that there exists a set of variables for each possible scenario that will optimize a desired objective. This creates categories of design variables that do not exist in deterministic optimization, near and far term variables. Near term variables can be described as those that are set by the current optimization. Far term denotes the variables that are left to float, but must still be optimized within each scenario.

5.1.3 New Options for Objective Formulation

Because the results of a probabilistic analysis are inherently different from those of deterministic analysis, the deterministic idea of an objective function based on a single valued design variable is no longer valid if the objective of interest is a probability distribution. Optimization of a probability distribution for an output design variable or variables can now be accomplished in any number of ways. Some methods that have been proposed are presented in the following sections.

Taylor Series Expansion-Based Criteria

This method by Chen, et al. [20] proposes a response surface approximation to a more complex analysis to estimate the derivative of the response with respect to noise variables for different settings of control variables [20]. In this particular work a design can either be considered robust with respect to both the control variables and noise variables, or just noise variables.

To estimate the mean and variance of an analysis output using this method, a single point and all the corresponding first-order derivatives with respect to noise variables or control variables around that point are generated. Then according to Eqn. 5.1, the variance is estimated. The mean is assumed to be the value of the objective function at the point.

$$\sigma_y^2 = \sum_{all\_noise} \left(\frac{\partial y}{\partial x_i} \right)^2 \sigma_{x_i}^2 \tag{5.1}$$

The accuracy of this estimate depends on two things. First, the analysis in question must have a linear or nearly linear response. This is because Eqn. 5.1 is for a linear model that is tangent to the real model at the given point. Second, these equations

assume an independent normal distribution as the input. Other distributions will react to this linearization with differing levels of accuracy.

This approach is similar to sensitivity minimization in that the minimum derivative value will usually correspond to the most robust solution, depending on the input noise variances. However, this linear assumption should be verified before results from this optimization should be taken as valid, if true variance minimization of the response is desired.

Descriptive Statistics-Based Overall Evaluation Criteria

In previous research, Mavris [22] uses a set of overall evaluation criteria based on the mean and variance of a deterministic objective function. These particular criteria assumed that minimization of the variance of the objective is desirable, then provide multiple options depending whether the objective mean is to be minimized, maximized or set to a specific goal. An example of this OEC set for mean targeting is given in Eqn. 5.2 [22].

$$OEC = \alpha*(Mean - Target) + (1 - \alpha)*Variance \quad (5.2)$$

Linear OEC sums for minimization and maximization are also possible using weighting schemes commonly found in multi-objective deterministic optimization problems, according to this research. This OEC sum method allows the designer to treat variance and mean with separate weightings, depending on the demands of the problem and the desires of the customer.

This flexibility is both the major advantage and major drawback of this type of method. It is an advantage in that it gives the designer flexibility in selecting their objective. The drawback is the lack of a definite objective for comparison between

studies due to this same freedom. Another consideration is that the objective is not easily explained without a detailed reporting of the equations and rationale and/or process for the chosen evaluation criteria weightings.

Cumulative Distribution Function Based Decisions

This type of probabilistic objective function can be stated in two different ways, leading to quite similar results. The first way [23] is to set a goal value for the objective function distribution, then maximize the probability of exceeding that goal value in a favorable way. In this way, the method is said to maximize customer satisfaction, with customer satisfaction being defined as any design result that exceeds expectations.

This method is intuitive, but can run into problems if the goals are set too far away from the starting point of a gradient-based optimization, or if said optimizer strays too far from these goals during the course of optimization and the objective distribution has a finite limit. This possibility of either near 100% probability of customer satisfaction or dissatisfaction can lead to a failure in gradient generation for the objective function.

A similar way to state this optimization problem would be to attempt to minimize a certain percentile value of the objective distribution. This method does not have the gradient generation difficulty that could appear in some design cases that have initial objectives far from the customer satisfaction frontier. Unfortunately, it does not have the intuitive advantage of maximizing the probability of exceeding customer expectations, but it does allow for a confidence level to be set for the estimate of the objective function.

Joint Probabilistic Criteria

This method [18, 19, 52] is similar to the cumulative distribution function (CDF) based decision method, but Mavris and Bandte used a joint probability distribution to meet several goals at once. It uses either a regression fit joint normal distribution or an

empirical distribution directly based on Monte Carlo simulation results. Using one of these methods, a priority-weighted "probability of success" can be obtained and used as an objective function. The positive aspects of this method are similar to the CDF method, with the added advantage of being able to satisfy multiple goals for customer satisfaction. Figure 11 [19] gives an example of this type of goal satisfaction.

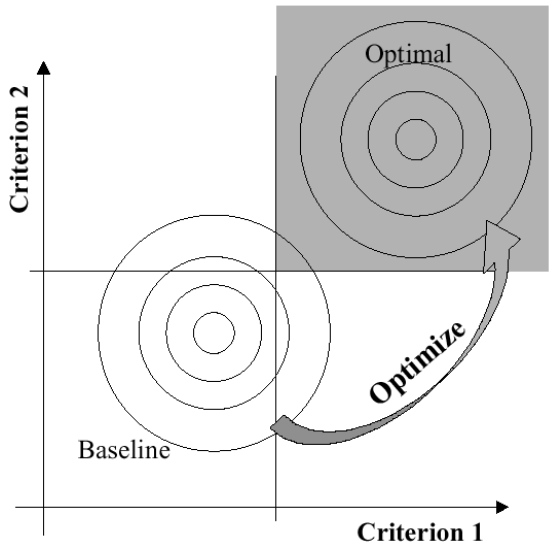

Figure 11 – Optimizing Probability of Success [19]

This is the most advanced method for probabilistic objective function formulation. However, as with the CDF, the empirical distribution option of this method could run into problems when an analysis point is far from the goal settings. An additional requirement of this method above and beyond most of the others listed in this section is knowledge of the correlation coefficients of the output responses that comprise the Joint Probability decision criteria. This requirement made of the distribution

estimating technique eliminates several methods as possibilities, including many most probable point methods [46, 92-106] as they do not provide this correlation information.

All of these objective function formulations require methods to estimate the probabilistic response of an analysis. This shows that there is ample demand for probabilistic design information in the optimization community, and that this information can be utilized in a useful manner.

5.2 Uncertainty Analysis Techniques

To address the performance issues associated with Monte Carlo simulation, many techniques for accelerated uncertainty analysis have been developed over the years. The majority of the work in this area has come from the structural reliability and nuclear engineering communities, but a few methods have come from the operations research and design research communities. The following is a brief description of each, along with the advantages and disadvantages of each. They begin with a review of some historically significant techniques that have, in general, been superceded by newer methods. Next is with a brief overview of Monte Carlo simulation, the most general method. After that, several variance reduction techniques are presented. These are methods closely related to Monte Carlo simulation, but changes made to sampling schemes and estimation techniques to reduce the variance in the simulation estimates. Discrete probability distribution approximations to input distributions are described after that. These methods rely on approximating continuous input distributions as discrete ones to create easily evaluated output distributions. Reliability methods are next. Here, an overview of the general steps and terminology of Most Probable Point methods are presented, along with the areas where different order assumptions can differentiate different reliability methods.

The final technique presented is Response Surface Methodology. This method here represents metamodeling techniques in general.

5.2.1 Historical Methods

One the earliest methods and still quite common methods to guard against system failure was the Worst Case analysis. This method is by far the simplest way to generate a robust design [107]. In general, this method is regarded as a way of "derating" a design since it is usually an extremely conservative way to predict failure. The method, as it sounds, consists of setting all the "demand" input variables to their "worst" value, in this case, their highest possible values. Next, all of the "capacity" input variables should be set to their lowest possible values. Which variables are "demand" and which variables are "capacity" should be determined by user experience. Evaluating the design at these extreme points will ensure that it is not on a failure constraint.

A problem with this method in applying it to complex systems is that it is often impossible to know "demand" from "capacity" variables ahead of time. This makes it impractical for the applications in this research, but important as a historical reference for robust design.

Taguchi robust design [21, 47, 50] is a parametric method for finding designs from a set of designs based on user experience that will have the highest resistance to uncertainty parameters. This methods intends to reduce the "loss to society" of an engineering product. While very practical in its application, it lacks confirmation that the answer determined is in fact an optimum. Some [108, 50] have shown other parametric methods to have superceded Taguchi's Robust Design method. These works point out problems with the method, some of which include biased variability estimates and false

optimum control variable settings due to excess levels of interaction in the system between the noise variables and control variables.

5.2.2 Monte Carlo Simulation

The most general estimation technique is Monte Carlo simulation. As described later, it makes no assumptions approximating the analysis it is simulating nor does it require approximation of input distributions beyond that of random number generation. The major drawback of this technique is computational expense. To reduce this expense, several reduced expense methods have been proposed, some by this research. To verify this cost savings as well as the accuracy of higher order methods, any reduced-expense sampling scheme should be compared to a Monte Carlo analysis in a test case. This means that these higher order methods are primarily useful for either probabilistic optimization, where repeated analyses of a similar solution space are required or on problems that have been proven to be compatible in previous research efforts. The techniques required for Monte Carlo simulation are presented here.

Monte Carlo simulation [109] is a technique where values representing random variables are selected from input distributions and simulated in a deterministic analysis. These analyses are repeated until output distributions of appropriate accuracy are generated. This accuracy is based on the desired probability of constraint satisfaction. If the desired probability is low and closer to the mean, fewer runs are required. Eqn. 5.3 [110] gives a percentage error bound for a generalized Monte Carlo simulation.

$$\%\varepsilon = 100 z_{1-\alpha/2} \sqrt{\frac{P_{constr}}{N(1-P_{constr})}} \tag{5.3}$$

Where $z_{1-\alpha/2}$ is the $(1-\alpha/2)$ percentile of the cumulative standard normal distribution. The value $100(1-\alpha)\%$ is the confidence level for the error estimate. The values P_{constr} and N represent the probability of constraint satisfaction for the simulation and N is the number of trials in the simulation. Eqn. 5.3 shows the trend of higher number of trials for problems with a higher required probability of constraint satisfaction. This indicates the number of trials can grow quite quickly with a higher probability of constraint satisfaction.

The error for mean, standard deviation and correlation coefficient estimates from Monte Carlo simulations are also easily calculable. Assuming a normal response and an unknown variance, the error bound on θ, the mean estimator is given by Eqn. 5.4 [111]. The confidence interval for a normal distribution standard deviation estimate is similarly given in Eqn. 5.5 [111]. The equation for the approximate confidence interval on a correlation coefficient is given in Eqn. 5.6 [111]. In this equation, R is the estimate for correlation coefficient. All equations are for a $100(1-\alpha)\%$ confidence level.

$$Error = \pm t_{\alpha/2}(n-1)\left(\frac{s}{\sqrt{n}}\right) \tag{5.4}$$

$$Std.Dev.CI = \left[\sqrt{\frac{(n-1)}{\chi^2_{\alpha/2}(n-1)}}s, \sqrt{\frac{(n-1)}{\chi^2_{1-\alpha/2}(n-1)}}s\right] \tag{5.5}$$

$$Corr.C.I. = \left[\frac{1+R-(1-R)\exp(2z_{\alpha/2}/\sqrt{n-3})}{1+R+(1-R)\exp(2z_{\alpha/2}/\sqrt{n-3})}, \frac{1+R-(1-R)\exp(-2z_{\alpha/2}/\sqrt{n-3})}{1+R+(1-R)\exp(-2z_{\alpha/2}/\sqrt{n-3})} \right] \quad (5.6)$$

Monte Carlo simulation can be a computational advantage, however. Eqn. 5.3 shows that the error in constraint satisfaction in no way depends on the dimensionality of the problem. This means that for highly dimensional problems, this random technique can be a most efficient way to integrate. This of course is no guarantee of the analysis being cheap, just cheaper.

5.2.3 Control Variables

Control variables [112] are a variance reduction technique that does not change the sampling method, just the calculation of estimates. It uses estimates of variables with either known expectation values or expectation values known to be equal to another variable's expectation value as what are called control variables. As a technique, it is nearly as old as Monte Carlo simulation. It was one of the first attempts to by nuclear scientists to speed up the convergence of random sampling techniques [113].

These control variables are used to modify the unbiased estimator of the parameter of interest into another unbiased parameter with lower variance. For example, assume Y is an estimate of the parameter of interest. The control variable estimator Y(b) using a known expectation value for the control variable estimate C with expectation value μ_c would be given by Eqn. 5.7.

$$Y(b) = Y - b\,(C - \mu_c) \quad (5.7)$$

The variance of the estimate Y(b) is therefore given by Eqn. 5.8. Note that for values corresponding to Eqn. 5.9, the variance of estimate Y(b) is reduced when compared to Y. The minimum variance value corresponds to Eqn. 5.10.

$$Var[Y(b)] = Var[Y] - 2\,b\,Cov[Y,C] + b^2\,Var[C] \tag{5.8}$$

$$2bCov[Y,C] > b^2\,Var[C] \tag{5.9}$$

$$b_{min\_var} = Cov[Y,C] / Var[C] \tag{5.10}$$

Eqn 5.9 reveals an issue with the control variable approach. In order to see any benefit, an accurate b term must be guessed before enough information can be had to determine if it is the minimum variance b. Also, the equations reveal that there is a speed up only for variables that are reasonably correlated to the response of interest. All this points to a need for the user of the method to make a guess of the correlation between the control variable and the output variable. If this guess is accurate, the simulation will converge quickly. If the guess is bad, it can actually hinder convergence.

5.2.4 Importance-Based Sampling

This is a Monte Carlo based approach for determining the failure probabilities of rare events. Estimating the failure probability of systems with a low probability of failure can be expensive using Monte Carlo methods. Therefore, importance-based sampling is a family of methods that uses a surrogate probability density function f' to bias the random samples from the input direction to a tail of the distribution that is of interest. Some techniques [114, 115, 116] use an initial Monte Carlo simulation to determine the proper weighting to find the failure probability. Others [117, 118, 119] use an assumed value

based on an expectation of where the failure boundary will occur, and can therefore use the importance-based sampling methods from the start.

Once the output distribution for θ′ has been obtained using the weighted input distributions, the output distribution is then transformed back based on the type of weighting used for the input distributions, as shown in Eqn. 5.14. This results in the generation of an estimated failure probability that has statistical significance with fewer runs than an unmodified Monte Carlo simulation.

$$\theta = g(x) \tag{5.11}$$

$$E(\theta) = \int g(x) f(x) dx \tag{5.12}$$

$$E(\theta) = \int g(x) \frac{f(x)}{f'(x)} f'(x) dx \tag{5.13}$$

$$\theta' = g(x) \frac{f(x)}{f'(x)} \tag{5.14}$$

It should be noted that this technique is primarily useful for comparing an analysis to a low-probability constraint, and without that kind of target, is no different from Monte Carlo simulation in terms of convergence.

5.2.5 Latin Hypercube Sampling

Latin hypercube sampling [120, 121, 122, 123, 124, 125] is a way of improving the speed of a Monte Carlo simulation, while still using a random sampling technique.

Generally, this is classified as a variance reduction technique [113, 126]. It has been shown to have asymptotically lower result variance for parameter estimates than Monte Carlo simulation [121] and is also an unbiased method [120]. It uses a systematic method of spanning the input distribution space while at the same time maintaining the random element of a Monte Carlo simulation.

A procedure first proposed by McKay, et al. [120] for executing the method to generate an independent, multivariate uniform [0,1) distribution is as follows:

- Select a sample size N for simulation. This should correspond to the estimated computational expense that can be afforded. Let the number of variables be denoted as K.
- Generate K independent random permutations of the vector [1,2, …, N]. The elements of these vectors are denoted as p_{jk} where j goes from 1,…,N and k goes from 1,…,K.
- Next select ε_{jk} (j=1,…, N and k = 1,… K) as NK samples from NK independent uniform(0,1) random variables.
- The sample location, X_{jk} for the independent multivariate uniform distribution, where each j is a sample and each k a dimension, is given by Eqn. 5.15.

$$X_{jk} = N^{-1}(p_{jk} - 1 + \varepsilon_{jk}) \tag{5.15}$$

To adapt this to a simulation without an independent uniform distribution, simply use the results of this algorithm as a probability map. A diagram of a result for five variables and two dimensions is shown in Figure 12. This is done through a cumulative distribution transform of the sample point results X_{jk}.

While this method is better than Monte Carlo simulation as the number of sample points goes to infinity [121], the improvement for smaller sample sizes depends on the problem. McKay et al. [120] have showed that when the output function is monotonic for each of its components, there is a speed-up for smaller than infinite sample sizes. While this cannot generally be assumed, it should be the case for most of the models being tested for this research.

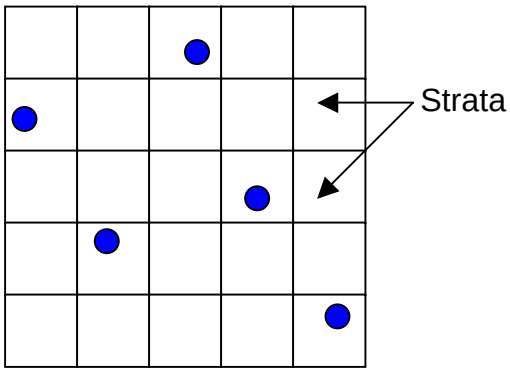

Figure 12 – Latin Hypercube Diagram

5.2.6 Descriptive Sampling

Descriptive Sampling from Saliby [127, 128, 129, 130, 131, 132] is a member of the variance reduction technique family [113, 126]. It is a way to improve the convergence rate of Monte Carlo simulations by imposing more order on the sampling process.

It is very similar to Latin Hypercube sampling [132], as described earlier. As far as the algorithm goes, there is only one small difference. At the final step for generating

the sample location, the uniform random number generation within the strata selected is eliminated. Instead, the point is simply placed at the center of each selected strata on the probability map. This changes Eqn. 5.15 in the section on Latin Hypercube Sampling to Eqn. 5.16 shown here. Notice that the only change is the elimination of the random perturbation and the subsequent placement of the point in the center of the strata.

$$X_{jk} = N^{-1}(p_{jk} - 0.5) \tag{5.16}$$

This technique has been shown to converge more quickly than Latin Hypercube sampling for most problems [132] and in the limit as the number of samples goes to infinity, is equivalent to Latin Hypercube. This is because the difference in sample location is only within each strata, whose dimensions shrink linearly with sample size. So as the strata size goes to zero, so does the difference between the center of the strata and anywhere else in the strata. An example sample set for five samples in two dimensions for a uniform [0,1] distribution is shown in Figure 13.

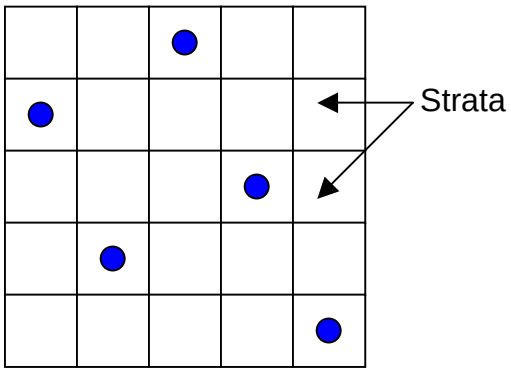

Figure 13 – Descriptive Sampling Diagram

Saliby [130] shows how descriptive sampling can be used with discrete distributions. This does give descriptive sampling an advantage over many of the

techniques here in that can be used with discrete probability input distributions. This makes Descriptive Sampling applicable to a wide range of problems.

5.2.7 Other Variance Reduction Techniques

Other interesting variance reduction techniques include antithetical variables, stratified sampling and common random numbers. Antithetical variables [133, 113] are a method where for every probability that is selected, the complimentary probability is also selected. This creates a negative correlation between the two variable subsets and lowers the variance of parameter estimates. Stratified sampling [134, 113] is similar to Latin Hypercube and Descriptive sampling in that it divides the problem space into strata, but differs in that it does this in the actual problem space, not the probability map. Then, each point in the strata is given a weight corresponding to the probability contained in the area. The method is also sometimes called weighted sampling.

Common random numbers [126] or correlated random numbers is a method for comparing similar distributions that differ in the application of some input parameter. This method essentially states that when comparing the results of two simulations, using the same random number for both simulations creates a strong correlation between the simulation results. This correlation reduces the variance of the comparison estimate drastically. This technique was used for all repeated Monte Carlo simulations performed in this research.

5.2.8 Most Probable Point Methods

MPP methods [46, 92-106, 135, 136] are specifically directed towards comparing a known input probability distribution against some unknown constraint function. Some methods, such as the Advanced Mean Value (AMV) method [92, 55, 94, 51] utilize this

concept to generate cumulative distribution functions for output variables quite efficiently and are therefore a favorite method for structural reliability analysis. Recently, some of these methods have been successfully applied to aircraft systems design problems [55, 57] showing that they have application beyond that of structural analysis.

A suite of techniques for various MPP methods can be found in the software package Nessus and its probability integration routine FPI [96, 98] from the Southwest Research Institute (SwRI) [137]. The computer program has heritage to research sponsored by the former NASA Lewis Research Center (LeRC), the Probabilistic Structural Analysis Program, PSAM [99].

There are many versions of MPP methods proposed by many researchers, far too many to present them all here. Fortunately, there are common elements to all MPP failure estimation techniques. They vary in level of approximation of the constraint function and where these approximations take place. This section will review the common elements of MPP methods.

The first step in most methods is a transform into standard normal space. First used by Hasofer and Lind [138], this transform takes general multivariate normal random variables and transforms them into a space where all the variables are distributed as independent standard normals. This transform is generally only useful when all of the input variables are normally distributed. Other transforms that include Rackwitz-Fiessler [135] have the ability to approximate non-normal distributions with higher accuracy. It does this by fitting a normal distribution to the non-normal CDF around the point of interest. Another fitting technique is the Chen-Lind method [139], which uses a similar three parameter distribution-fitting technique.

Once the space has been transformed, an approximation is made to the constraint function at some point. For most methods, this initial point is the mean of the input distributions. The approximation can be linear or quadratic, but is typically found through some manner of Taylor series approximation [140]. Using this approximation of the constraint function, the value of the constraint that is both equal to zero and is a minimum distance to the mean in standard normal space is found. This is the first design point. For generating a cumulative distribution function, sequential levels of the constraint function are selected instead of zero, then evaluated to generate the most probable point locus (MPPL). As shown in Figure 14 [101], this is a line of design points for different chosen levels of the constraint function. When the design point has been identified, some methods then repeat this process using a new approximation at the design point. Others, such as the advanced mean value first order (AMVFO) method confirm the points found along the MPPL with direct calls to the constraint function, then assume that this locus in close enough to the real MPPL to provide a good approximation.

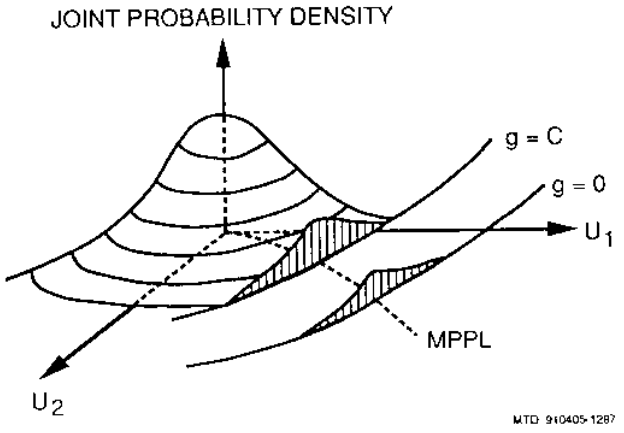

Figure 14 – Diagram of Most Probable Point Locus [101]

Once the design point(s) have been identified, there are several options for evaluating the probability of exceeding the constraint boundary. The first step is to identify the reliability index β. In the case of the Hasofer-Lind reliability index, this is the distance from the design point to the mean of the input random variables in the standard normal space, as is shown in Eqn. 5.17. Using this index, a linear approximation can be made to the constraint function, in which case the probability of failure can be estimated as Eqn. 5.18 [46].

$$\beta_{HL}(\bar{x}_{sns}) = (\bar{x}_{sns}^{T}\bar{x}_{sns})^{1/2} \tag{5.17}$$

$$P_{failure} = 1 - \Phi(\beta_{HL}) \tag{5.18}$$

If the constraint function approximated is highly nonlinear, this can lead to errors in the probability of failure for first order methods. If the constraint boundary curves towards the mean, this can lead to an underestimate of the probability of failure. Likewise curvature away from the mean will cause an overestimate. Figure 15 [46] illustrates this concept. Calculation of this probability is another area where the techniques differentiate. Some rely on the linear estimates, while others attempt more advanced approximations to the constraint function once the design point has been found.

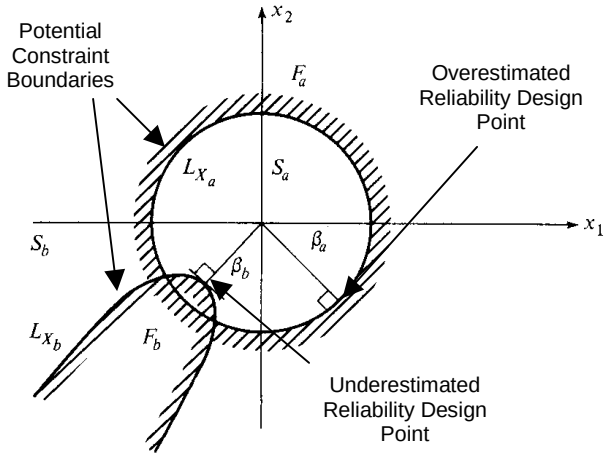

Figure 15 – Example of Potential Inaccuracy in Hasofer-Lind Reliability Index [46]

5.2.9 Discrete Probability Distributions

Discrete probability distribution methods [141, 142, 143, 144, 145] come from the desire of nuclear engineers to perform several sequential, relatively simple probabilistic calculations to solve complex problems. In these papers, the rules for basic mathematical operations are laid out [141, 142, 143] so that a user may perform an analysis with discrete probability distributions at a very basic level. In order to utilize this technique, an algorithm must incorporate this technique from the onset.

This method consists of approximating a continuous distribution as a set of discrete probabilities in a user specified manner. From this assumption, combinatorial rules for addition, multiplication and general function evaluations are laid out. This essentially describes how discrete probability distribution mathematics behave.

After each sequential operation, the problem arises that the output distribution to be used as an input for the next analysis contains an exponentially higher number of points than that of the previous. This problem is overcome by a condensation step. The most common type is vertical condensation [142]. The term vertical refers to dividing the vertical axis of the cumulative probability diagram into a set of equally spaced bins as seen in Figure 16 [142]. This ensures that each bin has the same number of results and the bins are therefore spread out in such a way as to describe the distribution with each point having equal importance.

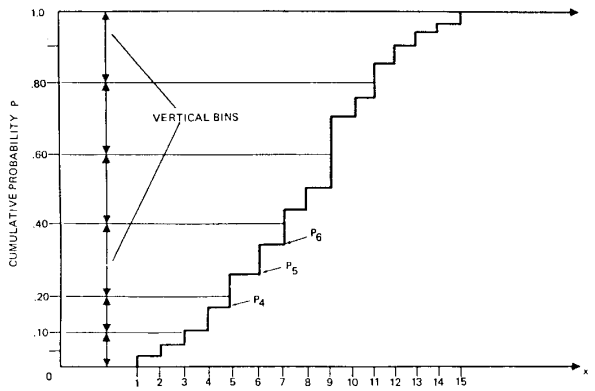

Figure 16 – DPD Vertical Condensation Diagram

5.2.10 Response Surface Methodology

This method [146, 147, 148, 108, 59] consists of creating a polynomial curve fit of the response, then using this meta-model in a Monte Carlo simulation to generate a probabilistic output. These curve fits can be made to any number of Design of Experiments-based or unplanned sampling techniques to allow for varying levels of statistical significance.

A generalized version of the meta-modeling technique is a two step process. The first step is variable screening. This step is done because often the dimensionality of the problem is higher than is practical to sample using higher order models. In this step, the sensitivity of the response to the variables under consideration for modeling are measured. This is typically done through the use of a linear two level model designed to measure the main effects of the variables. The sensitivities of the response to the variables of interest are ranked for cumulative effect. The variables with the most influence are then selected until a certain percentage of the variability of the response is counted. A graphical representation of this process can be seen in Figure 26 on page 103. The bars represent the magnitude of the contribution to the response of each of the variables. The cumulative line shows what percentage of the response variability has been captured. By selecting variables from the top, the maximum amount of variability can be represented with a minimum of variables.

Infinite sampling options for the final model are available, from saturated for minimal computational expense to full-factorial for good fit confirmation and statistical coverage [59]. Once a sampling model is chosen, typically a quadratic polynomial is fit to the data using a least squares technique. For a slightly improved fit, a stepwise regression can be done for each response [149]. This technique performs an F significance test on the terms of the polynomial to determine which ones are essential to the fit and which ones create numerical error. The essential terms of the polynomial are retained and the others are discarded, ignoring the overall fit.

Once the polynomial fit is obtained, a Monte Carlo simulation can be performed on the meta-model for a fraction of the cost of direct simulation. The results are

interpreted just as in Monte Carlo simulation and the required number of trials is also determined the same way. Meta-models are also useful in a more practical sense in that they provide a consistent result, whereas some engineering analyses can have internal convergence problems if appropriate initial guesses are not provided. Providing appropriate initial guesses can prove difficult when such an analysis is running in an automated fashion. This reliability is a major advantage.

5.2.11 DPOMD Methods

What defines a Discrete Probability Optimal Matching Distribution is the idea of approximating the input distributions of a probability problem with discrete distributions that match some number of the expectation value (Eqn. 5.19, [150]) characteristics, beginning with lower order parameters and progressing to higher order. This broad idea allows for several forms of the methods, each using a different numerical technique to match input distribution characteristics. These different methods can handle different types of problems, from low dimensionality analyses with highly skewed input distributions to highly dimensional problems with correlations between the random input variables.

$$E(g(x)) = \sum_i p_i g(x_i) \tag{5.19}$$

To create a matching distribution, any numerical technique has two types of independent variables available, the locations of the point probabilities and the probabilities themselves (Figure 17). Some methods use one or both of these controls,

and they make these techniques very flexible, both in type of implementation and in the degree to which they match the actual input distributions.

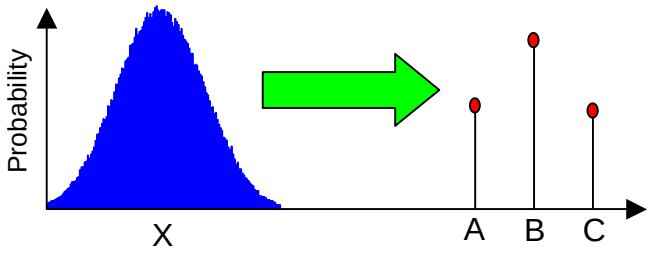

Figure 17 – Discrete Point Representation of Input Distribution

There are several standard numerical techniques that can be used to find good sampling distributions. The methods presented here show three different techniques that were used in the course of this research. They also give a good basis to create new methods that use combinations of these techniques. The independent binomial used a nonlinear Newton-Rhaphson root-finding method to vary both point locations and probabilities for a single variable at a time. This method matches each input distribution to the fourth moment ($E(X^4)$) but it does not account for correlations between the input variables.

The central composite-based used a linear minimization on the point probabilities of a fixed location central composite design. Depending on the number of variables in the problem, this method was used to match both single variable moments and cross-term moments. This means that it could handle input distributions with correlation. An advantage of this technique is that it can reuse sample points to represent different

distributions, as long as the input distributions do not change too much. A disadvantage is that an independent set of moments must be defined for each change in the number of variables.

The fractional factorial method uses a method that is significantly different from the previous two. It starts with a fractional factorial design that matches a standard normal multivariate distribution, then uses a reverse standard normal space variable transform to get sample points for the analysis. This is therefore a variable location technique that matches all moments up to second order including main and cross terms. The major advantage of this technique is that the number of sample points need only rise linearly with number of input variables.

5.2.12 Independent Binomial DPOMD

This technique uses both variable sample point locations and probabilities in its input distribution model. This has an advantage in that the user does not need to arbitrarily set the locations of the sample points. It has another advantage in that additional degrees of freedom are available when minimizing the error to the target input distribution expectation values. This means that more distribution matching accuracy can be carried through the analysis with fewer points when compared to the fixed location method. One drawback is that for repeated analysis with differing input distributions, the deterministic problem must be re-sampled every time.

To make this method computationally tractable, the input distributions are assumed to be independent. This means that each of the sample point settings can be found independently for each variable's input distribution, then combined to form a full-factorial design. This idea is illustrated in Figure 18.

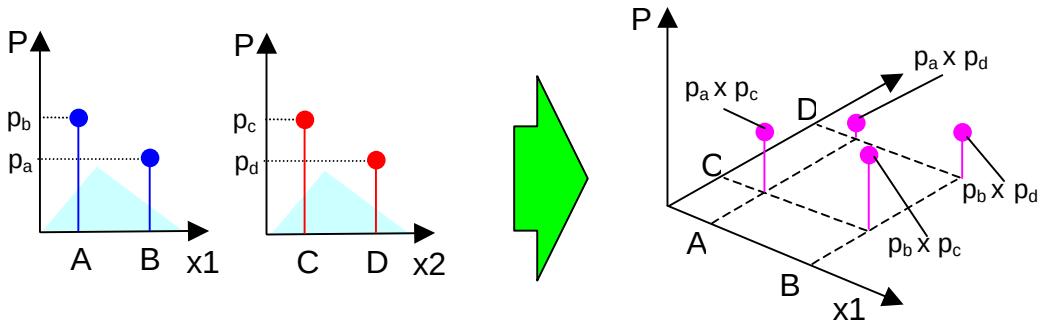

Figure 18 – Variable Location Point Generation

For each of the variable input distributions, the locations and probabilities of the sample points must be determined. In order to maximize the amount of input distribution property information carried through the analysis, this particular method has enough degrees of freedom to drive the error in the selected expectation values to zero for up to third order moments.

For each of the variables, there are four degrees of freedom. That means that all expectation value moments up to cubic can be matched by the method. Consequently, mean, variance and skewness can all be represented. The problem to be solved to find the location and probabilities of the sample points is defined by Equations 5.20 and 5.21.

$$\vec{f} = \begin{pmatrix} p_1 + p_2 - 1 \\ p_1 x_1 + p_2 x_2 - E(x_{inputdist}) \\ p_1 x_1^2 + p_2 x_2^2 - E(x_{inputdist}^2) \\ p_1 x_1^3 + p_2 x_2^3 - E(x_{inputdist}^3) \end{pmatrix} = \vec{0} \qquad (5.20)$$

This is equivalent to:

$$\vec{f} = \begin{pmatrix} p_1 x_1 + (1-p_1)x_2 - E(x_{inputdist}) \\ p_1 x_1^2 + (1-p_1)x_2^2 - E(x_{inputdist}^2) \\ p_1 x_1^3 + (1-p_1)x_2^3 - E(x_{inputdist}^3) \end{pmatrix} = \vec{0} \tag{5.21}$$

From this point, a Newton-Rhaphson multivariate root finding method can be employed to solve the nonlinear set of equations. As a practical note, initial guess is very important. For most cases encountered by this study, an initial guess of the mean plus and minus one standard deviation is sufficient for x_1 and x_2, the high and low sample points. An initial guess of 50% for p_1 is also generally effective when using this approach.

Once the inputs are combined to form a two-level full factorial design (Figure 18), the deterministic analysis finds the response corresponding to each of the sample points. Again the input probabilities are used along with this response to find the output parameters of interest.

The major assumption for this technique is that of input variable independence. This assumption is made so as to simplify the nonlinear root finding step so that the variables can be found individually. This greatly improves the problem convergence so that programs based on this algorithm can run essentially automatically. Relating to convergence, the technique as used in this research assumes an initial guess of mean plus and minus one standard deviation for the location of the two binomial points for root finding purposes. The technique also assumes that the analysis can be characterized by a full factorial sample space. To verify this assumption, any reduced order sampling scheme method should be compared to a Monte Carlo simulation, as discussed in the earlier section on distribution approximation methods.

While the accuracy of this method can be quite high, scalability is a problem. The number of runs required for an analysis goes up factorially with the number of input random variables. This means that a problem with as little as 8-10 random variables (256 – 1024 runs) approaches the range where a Monte Carlo simulation might yield more accurate results.

5.2.13 Central Composite DPOMD

This technique is a fixed-location method. It utilizes a central composite design (CCD) experiment array to determine the sampling point locations for the input distribution model. A three dimensional example of the sampling points is shown in Figure 19. The cube corners form a two level full factorial, while the points radiating from the center are referred to as "star points." These typically extend past the upper and lower bounds of the two-level full factorial. This central composite should span an appropriate amount of the input distribution variables so that a reasonably accurate representation of the distribution is possible.

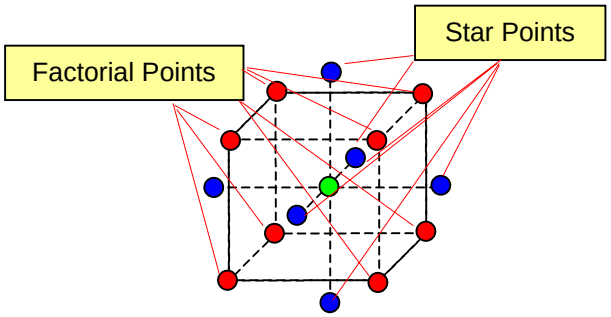

Figure 19 – Three Variable Central Composite Design

The input distribution properties are then matched by varying the probabilities of the individual sampling points in the discrete model. The technique used for this is analogous to least squares curve fit matching. The problem statement for this is given in Eqn. 5.22.

$$\underset{\vec{p}}{Min}\left\|A\vec{p}-\vec{E}\right\|_2 \tag{5.22}$$

The $\vec{E}$ vector contains expectation values for polynomial terms corresponding to different moments of the input distribution. In this way it contains the properties of the input distribution to be matched by the method. It is important that one of the *g* polynomial terms be unity so that the probabilities of the points in the model add up to one. This is in effect matching the zeroth order moment. The matrix *A* contains the locations of the points in the model expressed in rows evaluated using the same polynomial terms expressed in $\vec{E}$. Descriptions of these arrays are found in Eqns. 5.23 and 5.24. The columns of *A* correspond to each of the *m* sample points. The $\vec{p}$ vector contains the probabilities of each of the *m* points in the model to be determined by the minimization.

$$\vec{E}=\begin{bmatrix} E(g_1(\vec{x})) \\ E(g_2(\vec{x})) \\ \vdots \\ E(g_n(\vec{x})) \end{bmatrix} \tag{5.23}$$

$$A=\begin{bmatrix} g_1(\vec{x}_1) & g_1(\vec{x}_2) & \cdots & g_1(\vec{x}_m) \\ g_2(\vec{x}_1) & g_1(\vec{x}_2) & & g_2(\vec{x}_m) \\ \vdots & & \ddots & \vdots \\ g_n(\vec{x}_1) & g_n(\vec{x}_2) & \cdots & g_n(\vec{x}_m) \end{bmatrix} \tag{5.24}$$

The vector $\vec{p}$ can be efficiently found using a QR factorization minimization of the form shown in Eqns. 5.25-5.28.

$$\underset{p}{Min}\left\| A_{mxn}\, p - E \right\|_2 = \underset{p}{Min}\left\| QRp - E \right\|_2 \tag{5.25}$$

$$\underset{p}{Min}\left\| QRp - E \right\|_2 = \underset{p}{Min}\left\| Q(Rp - Q^T E) \right\|_2 \tag{5.26}$$

Because Q is orthogonal, Equation 5.27 is equivalent to Equation 5.28.

$$\underset{\vec{p}}{Min}\left\| \begin{pmatrix} \left(Q^T \vec{E}\right)_{1\ldots n} \\ \left(Q^T \vec{E}\right)_{n+1\ldots m} \end{pmatrix} - \begin{pmatrix} R\vec{p} \\ 0 \end{pmatrix} \right\|_2 \tag{5.27}$$

so

$$R\vec{p} = \left(Q^T \vec{E}\right)_{1\ldots n} \tag{5.28}$$

solves the minimization problem due to the fact that the only variable is the $\vec{p}$ vector and it cannot affect the $(n+1)^{th}$ through m^{th} equations in Eqn. 5.27. Also, to avoid singularity problems, it is important that the polynomial terms chosen for use as expectation values be linearly independent and that sample points are not repeated in the discrete model.

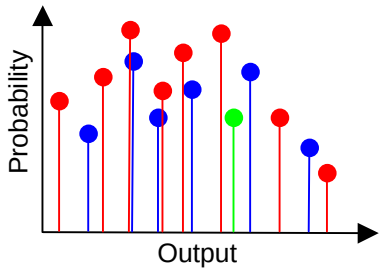

Figure 20 - Final Output Response of a Fixed Location Discrete Probability Method

Once the probabilities are determined, the sample points can be evaluated. This gives the response and each of the corresponding probabilities. For the three dimensional CCD shown in Figure 19, a sample response distribution might resemble Figure 20. Note that each of the input point probability values corresponds to a value for the response.

The central composite-based technique has a flexible assumption base. Whatever polynomial moments are inserted into the matching vector are the ones that are valid for the discrete distribution. Therefore, this technique does not require independence. The technique also assumes that the analysis can be characterized by a central composite experiment design and thus carries the same caveats as the binomial DPOMD.

When using the full central composite design, the number of runs grows about as quickly as the binomial distribution method, so about the same limits apply to the available number of variables. This means that analyses of 8-10 variables are the limits of problems that would benefit from this technique.

5.2.14 Fractional Factorial Based DPOMD

So far, both DPOMD methods have had limited scalability. To remedy this, a method based on a two level fractional factorial experiment design was created. This technique is shown later to have good accuracy for the type of problem considered while only growing linearly with the number of input variables. This means that problems with high dimensionality, such as mass properties and sizing (~40 random input variables), can be modeled using a relatively small number of runs.

This method is based on a linear transform first proposed by Hasofer and Lind [138]. This transform takes joint multinormal variables and transforms them into a

standardized normal space. Here the joint multinormal can be expressed by independent standard normal distributions. The effect of this transform on discrete distributions is that it takes a discrete distribution with a certain mean vector and covariance matrix and expresses the points in a space where they have mean vector zero and an identity covariance matrix. This method takes advantage of this transform by creating a discrete distribution in standardized normal space with zero mean and identity covariance matrix and performing an inverse Hasofer-Lind transform based on a desired mean and covariance matrix to create a discrete distribution in the real problem space with the desired second moment characteristics.

To create a DPOMD using this technique, a discrete distribution with zero mean vector and identity covariance matrix is required. This requirement was satisfied in the form of a fractional factorial two level design of experiments array with high and low levels set to –1 and +1 respectively. Because there are many options for creating fractional factorial arrays, it was assumed that the array with the highest possible resolution number would capture the most useful analysis response. An experiment's design resolution R is one where no n factor effect is confounded with another effect containing fewer than R – n factors [151]. For example, in a resolution IV design, the lowest order effect that can be confounded with a first order (one factor) is a third order (three factor) effect. As further example, second order effects can be confounded with other second order effects.

A Matlab© code was created using the direct generation method [151] that creates maximum resolution fractional factorial designs. The direct generation method uses multiplications of different combinations of the basic factor columns in the design to create runs for factors that are non-basic factors. A basic factor is defined as a factor in a

full factorial design that has size equal to the number of total factors minus the reduction. This smaller, full factorial design of main factors is then used generate additional columns to create a design with more factors. To create a design with the highest possible resolution, the largest combination of basic factors possible should be used to create settings for the new variables as is shown in Table 1.

Table 1 – $2_{IV}^{(4-1)}$ Fractional Factorial Design Using Direct Generation Method

Run #	Basic Factor A	Basic Factor B	Basic Factor C	Factor D = A * B * C
1	-	-	-	-
2	-	-	+	+
3	-	+	-	+
4	-	+	+	-
5	+	-	-	+
6	+	-	+	-
7	+	+	-	-
8	+	+	+	+

This code cycles through all the combinations of basic factors, beginning with the longest (all factors) and progresses until all the columns for the desired non-basic factors have been created. The resultant array therefore has the desired properties of maximum resolution and can be controlled so as to have an appropriate number of runs.

Once the fractional factorial has been generated, an inverse Hasofer-Lind transform must be calculated. The Hasofer-Lind transform and its inverse are shown in Eqns. 5.29 and 5.30 [138, 46].

$$T_{trans}(\bar{x} - \bar{\mu}) = \bar{x}_{sns} \tag{5.29}$$

$$\bar{x} = T_{trans}{}^{-1}\bar{x}_{sns} + \bar{\mu} \tag{5.30}$$

Where x is a vector of positions in the analysis space, x_{sns} is a position vector in the standardized normal space, μ is a vector of means in the analysis space and T_{trans} is a transformation matrix defined by the relation in Eqn 5.31 [138, 46].

$$T_{trans}C_{\sigma}T_{trans}{}^{T} = I \tag{5.31}$$

The matrix T_{trans} is found by way of a Cholesky decomposition [90, 152] of the covariance matrix C_{σ}. Because C_{σ} is positive definite by definition, a Cholesky decomposition will yield the following:

$$\begin{aligned} R^{T}R &= C_{\sigma} \\ &= R^{T}IR \end{aligned} \tag{5.32}$$

so

$$(R^{-1})^{T}C_{\sigma}R^{-1} = I \therefore \tag{5.33}$$

$$T_{trans} = (R^{-1})^{T} \tag{5.34}$$

$$T_{trans}^{-1} = R^T \tag{5.35}$$

Where R is an upper triangular matrix. In the case of fractional factorial DPOMD, the required matrix is T_{trans}^{-1}, so no matrix inversion is required after the Cholesky decomposition.

The fractional factorial method matches the mean vector and covariance matrix of the inputs. It is limited in that it cannot account for higher than second order expectation values. This means that input distributions with high skewness will be missing this characteristic in the fractional factorial discrete probability distribution model. It also has the inherent assumption that the output response can be characterized using a fractional factorial output response.

The primary advantage of this method is its scalability. While the number of sample points can be specified by the user to a degree, the sample point count must be larger than the number of variables if the set is to span all the dimensions of the problem. If the number of sample points is less, not all the variables will be considered. To compound this, the ignored variable has not been determined to be negligible to the response by any kind of screening process.

5.3 MDO Methods

For most advanced aerospace design problems, the amount of design freedom is large. This is especially the case for RLV design, where a standard configuration is not universally accepted. This means that these problems will have a large number of control

variables available for a system level optimization [63, 77, 78, 79]. These systems can also consist of different contributing analyses for different design problems. Tight integration of these problems is often not worth the up front costs involved [62].

A common situation in many design organizations is to have multiple teams in multiple locations provide analysis support for a particular design problem. This creates coordination problems as well as design convergence issues, but allows for disciplinary experts to retain control of their respective analyses. This control also typically means there are specialized optimization methods that work well for each individual analysis, but obviously do not solve the total system problem. A multidisciplinary system setup also provides the opportunity for parallel computation if the problem is properly coordinated between the disciplines.

Because this research deals primarily with multidisciplinary aspects of probabilistic optimization, a background of some multidisciplinary design optimization methods will be presented. The background on this research begins with methods for describing how different disciplines interact [153, 154] and how these interactions can be sequenced to yield maximum efficiency. Then it progresses to more advanced decomposition methods designed to describe new ways for the disciplines to interact. This is typically done to make the system more parallel and object-oriented [63, 77, 78, 79]. The following shows the advantages of advanced multidisciplinary design techniques, as well as gives an idea of the progression of this field over time.

5.3.1 System Sensitivity Analysis

System sensitivity analysis [155, 156, 157, 158, 159, 160] is a calculus-based method for generating system-level total derivatives based on contributing analysis-level partial derivatives. It assumes that the system can be described by a set of analyses

connected by vectors of information flows. How the analysis iterates using fixed-point iteration is not relevant to the calculation of derivatives, as long as the final value for all the states is used to calculate the subsystem derivatives.

These system-level derivatives can then be used in conjunction with a gradient-based optimizer to find optimal settings for certain system level variables that have been taken away from the local optimizations. While this method does not solve the problem of local optimizers conflicting with the system optimizer, it does allow for cheaper calculation of system derivatives.

Applications of this technique to launch vehicle problems similar to that in the current research have shown good results [160] and provided guidance on issues such as noise in contributing analysis gradient generation. Many of the contributing analyses in conceptual launch vehicle design do not often converge to the machine tolerance of the computer system. This means that finite difference steps must be larger in order to account for this heightened level of numerical roundoff error. However, using larger forward difference approximation steps can increase the approximation error in the derivative calculation. According to Olds [160], higher order central difference methods should be used.

A brief summary of the method is demonstrated using the simple Design Structure Matrix (DSM) in Figure 21. The data flows are labeled A1, A2, B, C and O. Following the derivation that can be found in [155-160], this situation leads to the Global Sensitivity Equations. By solving this linear system of equations, the total derivatives for the objective function found in vector O with respect to the system design variables in vector X can be calculated.

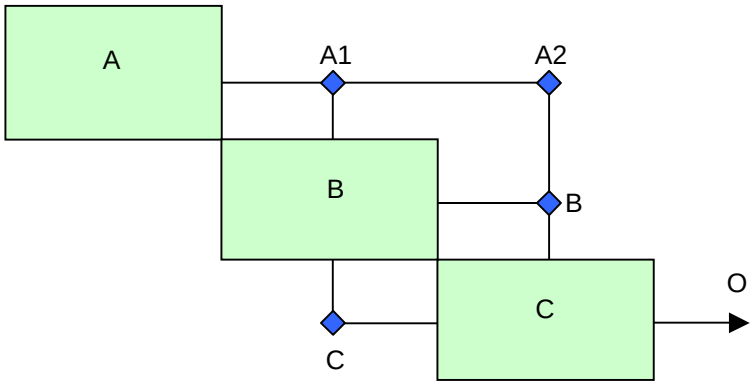

Figure 21 – Sample DSM for Global Sensitivity Equations

$$\begin{bmatrix} I & 0 & 0 & 0 & 0 \\ 0 & I & 0 & 0 & 0 \\ -\frac{\partial B}{\partial A_1} & 0 & I & -\frac{\partial B}{\partial C} & 0 \\ 0 & -\frac{\partial C}{\partial A_2} & -\frac{\partial C}{\partial B} & I & 0 \\ 0 & -\frac{\partial O}{\partial A_2} & -\frac{\partial O}{\partial B} & 0 & I \end{bmatrix} \begin{bmatrix} \frac{dA_1}{dX} \\ \frac{dA_2}{dX} \\ \frac{dB}{dX} \\ \frac{dC}{dX} \\ \frac{dO}{dX} \end{bmatrix} = \begin{bmatrix} \frac{\partial A_1}{\partial X} \\ \frac{\partial A_2}{\partial X} \\ \frac{\partial B}{\partial X} \\ \frac{\partial C}{\partial X} \\ \frac{\partial O}{\partial X} \end{bmatrix} \tag{5.36}$$

5.3.2 Optimal Decomposition

This technique is another that does not seek to change existing methods of contributing analysis interaction, but simply make an existing process more efficient. The idea of optimal decomposition is to change the order in which analyses are run so as to

minimize the amount of “feedback” and make sure that tightly coupled analyses are run close together. The intuitive result of this is that tightly coupled analyses that influence each other a great deal are iterated together before their results are shared with the rest of the contributing analyses. This limits the amount of iteration if fixed-point iteration is used to solve the system.

The primary method of implementing this technique is the computer program DeMaid [153] from the NASA Langley multidisciplinary design optimization branch. It is an Apple Macintosh-based program that given a design structure matrix, relative coupling strengths among the contributing analyses and relative computational expenses for each analysis, will find the optimum order of execution. This code can be quite useful for new and large multidisciplinary engineering analyses.

This does imply a primary drawback of using optimal decomposition. It limits its advantages to those who choose to use fixed-point iteration to solve their system. This technique is also most useful on large problems where the optimum order of analyses is not intuitive. For many established aerospace problems, this order of execution has been determined through experience, thus limiting the improvement yielded by this optimal decomposition.

5.3.3 Optimizer-Based Decomposition

This is a single-level optimization method [71, 62] that eliminates system feedback and/or feedforward loops through use of a system level optimizer and compatibility constraints. These loops are eliminated by the addition of all the input variables for all the analyses as design variables to the system-level optimizer. In addition to the elimination of these loops, conflicts between system level and contributing analysis

optimizers are eliminated by allowing design variables at all levels to be controlled by the system-level optimizer, allowing for a true system optimum to be found.

The compatibility constraints compare the optimizer's version of the coupling variables to the output versions of the variables from the contributing analyses. When these constraints are satisfied, it means that the contributing analyses are consistent with respect to the coupling variables.

The system-level optimizer must then minimize the system objective function while ensuring that the compatibility constraints are satisfied. This is done by simultaneously varying the system-level design variables, the local-level design variables and all the coupling variables. Simultaneously optimizing all these variables can mean that the optimization problem size is proportional to a number of factors, not just the system level optimization design variables.

5.3.4 Collaborative Optimization

Collaborative Optimization (CO) [61-64, 77-79] is an example of a two-level decomposition scheme. Here, the system optimizer is used to coordinate optimizations at the lower levels to seek an overall system objective. As with OBD, the coupling between the contributing analyses is handled by compatibility constraints, but these constraints handle different values.

In CO, the compatibility constraints measure the difference between the targets set by the system-level optimizer and the actual inputs and outputs of the analysis. The system-level optimizer uses the compatibility constraints as constraints to ensure that the coupling variables of the problem are consistent between the analyses. The contributing

analysis optimizer uses its own compatibility constraint as an objective function. This means that the local variables as well as the inputs present in the compatibility constraint can be set to values that best ensure compatibility with the other analyses by the lower level optimizer. This compatibility as defined by the system-level targets.

CO is another way to obtain a true system-level optimum while allowing for parallel operation. The primary advantage of this method when compared to optimizer-based decomposition is its scalability. Because of the distributed optimization of the local design variables, the system-level problem is not typically as large as with OBD.

As the RLV design community stands, there is a conspicuous lack of a counterpart to Collaborative Optimization for probabilistic analysis. The advantages of distributed effort have not been applied in the field of probabilistic simulation-based analysis. Partly due to this, the applications of robust optimization for RLV design are few. Those that have undertaken this problem have done so through either sensitivity or Taguchi methods that have accuracy and optimality problems respectively. The RLV design activity of this thesis intends to demonstrate a method for communicating probabilistic information between flexible contributing analyses utilizing heterogeneous probability analyses in an online launch vehicle design framework on multiple platforms, thus filling a current gap in RLV design methods.

CHAPTER VI

MASS PROPERTIES ANALYSIS TEST

6.1 Distribution Analysis Comparisons

Because the multidisciplinary approach of this paper allows different distribution estimation techniques to be used for different contributing analyses, each of these analyses must be tested using several appropriate techniques to determine which is most suited to characteristics of the particular sub-problem. The three analyses in this example problem, mass properties/sizing, trajectory and propulsion were all analyzed probabilistically using several different methods. The following sections provide the rationale for which method were tested, describes the tests performed on each analysis and presents the results generated by each.

It is hoped that these tests will indicate which of the methods for probability distribution approximation is the best suited for these types of launch vehicle contributing analyses. By using this single point testing approach, a costly Monte Carlo analysis must only be run once as a reference for the other approximation methods. For the sake of practicality, the general techniques tested on each of the contributing analysis will be the same, with variations existing within each of the broad categories that are the methods under consideration. The demands of optimization require methods that can be executed with a reasonable number of samples, depending on the analysis computational requirements. Reasonable for a contributing analysis was considered to be around a

minute. This would allow for optimizations of the system on the order of one day. Next, the method must provide correlations for output variables that are either coupled to other analyses or have a good chance of being used in a probabilistic multiobjective formulation similar to those presented by Bandte, et al. [18, 19, 52] and described in the background chapter.

Advanced methods that can provide this type of information are primarily variance reduction and metamodeling methods. These include among others Monte Carlo simulation, importance-based sampling, Latin hypercube sampling, control variates, discrete probability optimal matching distributions (DPOMD), descriptive sampling and response surface methods from the chapter on uncertainty methods. Importance-based sampling was eliminated from consideration because it is mostly useful for accelerating the calculation of the probability of a low probability event. Because the only constraint comparison for this analysis was one sided and was compared at the 80% confidence level, this method was not expected to provide much benefit. Latin hypercube and stratified sampling were eliminated due to their similarity to descriptive sampling. In addition to this, Saliby [132] has shown descriptive sampling to converge more quickly than Latin hypercube, while stratified sampling is currently not as popular as other methods, as evidenced by the available literature. Control Variates were left out because of the need for user assumptions about the output variables. Antithetical Variates were not studied because of their only slight promised performance benefit when compared to Monte Carlo simulation [113].

This left Monte Carlo simulation, DPOMD, descriptive sampling and response surface methods as the candidate methods. The tests of these methods and the particular

types of each chosen method used is described in the following sections. They are presented in groups defined by the contributing analysis being tested.

6.2 Analysis Test

The Mass Properties and Sizing analysis consists of a set of interrelated nonlinear weight equations. These equations must be iterated to find a consistent set of component weights that can then be displayed in a Weight Breakdown Structure (WBS). An example of this is Table 2. For brevity, only highest-level weight breakdown is shown. There are two more levels of weight statements in this tool. The equations for this analysis are derived from relationships defined by NASA-Langley VAB and recorded by Olds [161]. The sizing portion of the analysis involves scaling up or down the geometry of the vehicle until a desired propellant loading is achieved as shown in Figure 9 on page 43. This is done here using root finding method, such as Newton's method embedded in Excel© Solver.

The sizing analysis for this research assumes advanced material technologies to lower weight. This kind of assumption is well suited to a probabilistic analysis, given the uncertain nature of the final structural form of the components. Among the materials assumed for the vehicle include graphite epoxy propellant tanks as well as Ti-Al SiC metal matrix composite structural elements. The research also assumes advanced thermal protection materials such as Advanced Carbon Carbon (ACC) composite for nose and leading edge surfaces and Toughened Unit-piece Fibrous Insulation (TUFI) for windward surfaces.

For this research, the platform for the mass estimating relationships is a Microsoft Excel© spreadsheet. If this were a deterministic analysis, the difference between the mass

ratio calculated as required by the trajectory and the available mass ratio calculated by the sizing analysis would be driven to zero by the Excel© Solver add-in altering the vehicle size. The corresponding weight breakdown structure would be the output of this analysis.

Table 2 - Example Weight Breakdown Structure

1.0	Wing Group	6,423 lb
2.0	Tail Group	2,150 lb
3.0	Body Group	57,469 lb
4.0	Thermal Protection	20,611 lb
5.0	Landing Gear	5,158 lb
6.0	Propulsion	30,095 lb
7.0	RCS Propulsion	2,283 lb
8.0	OMS Propulsion	4,424 lb
9.0	Primary Power	1,124 lb
10.0	Electrical Conversion & Dist.	6,952 lb
11.0	Hydraulic Systems	0 lb
12.0	Surface Control Actuation	803 lb
13.0	Avionics	1,718 lb
14.0	Environmental Control	2,410 lb
15.0	Personnel Equipment	0 lb
16.0	Dry Weight Margin	0 lb
	Dry Weight	**141,620 lb**
17.0	Crew and Gear	0 lb
18.0	Payload Provisions	0 lb
19.0	Cargo (up and down)	20,000 lb
20.0	Residual Propellants	7,654 lb
21.0	OMS/RCS Reserve Propellants	595 lb
	Landed Weight	**169,868 lb**
22.0	RCS Entry/Landing Propellants	1,168 lb
	Entry Weight	**171,037 lb**
23.0	RCS/OMS Propellants (on-orbit)	5,405 lb
24.0	Cargo Discharged	0 lb
25.0	Ascent Reserve and Unusable Propella	7,690 lb
26.0	Inflight Losses and Vents	1,635 lb
	Insertion Weight	**185,766 lb**
27.0	Ascent Propellants	1,459,786 lb
	Gross Liftoff Weight	**1,645,552 lb**
28.0	Startup Losses	13,946 lb
	Maximum Pre-launch Weight	**1,659,498 lb**

For probabilistic sizing, there are several options for sizing in a probabilistic sense. One method would be to allow the length of the vehicle to float with every trial, ensuring that every predicted scenario is a closed vehicle. This methods presents difficulties for proceeding to detailed design, as there is no single size to which components can be designed. This makes the vehicle size a far term variable as described in the background chapter. To do this would ensure that there were no trials that could not be sized, but it would also prevent a decision on the OML size from being made by the current analysis. This is essentially a probabilistic analysis wrapped around the existing sizing algorithm.

For the current research, a decision on OML size is desired at the conceptual stage. Therefore, this quantity is a near term variable and will be set so that it meets the propellant requirements of all the scenarios, to a certain confidence level. This means that the mass ratio error for a particular size vehicle is not a single value, but an entire distribution of errors. This is the performance constraint that must then be met. This is done by altering the vehicle size until a desired percentage of the mass ratio errors is driven to a positive value. This problem is equivalent to ensuring that the required mass ratio is lower than the available mass ratio to a certain confidence level. Figure 22 illustrates this.

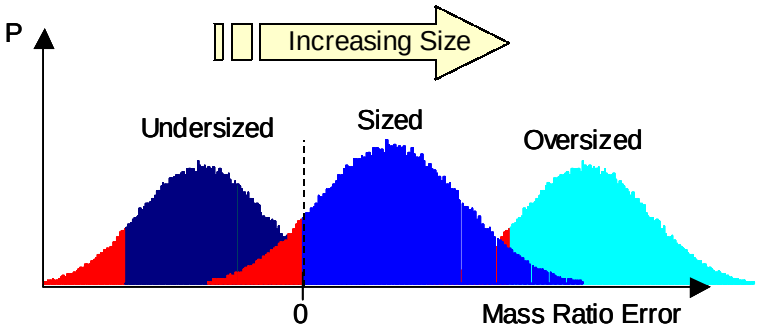

Figure 22 – Probabilistic Sizing Algorithm Used

The inputs and outputs of the mass properties and sizing analysis along with the number of random variables determined the required size of approximation methods that were appropriate. Table 3 shows the number and type of each kind of input and output.

Table 3 – Number and Types of Random Variables in Mass Properties Analysis

Variable Type	Number
Correlated Normal Inputs	3
Independent Triangular Inputs	35
Correlated Outputs	30

A description of the distributions for each random input variable is in Appendix B.

6.3 Test Procedure

To compare different methods for predicting the output distributions of the mass properties analysis, a comparison of several methods on a single analysis was conducted. The goal of this test is to determine the most efficient means of predicting the mass ratio error distribution, along with others, so that this performance constraint can be accurately met in future sizings. To do this, actually meeting the performance constraint is not necessary. It only needs to be shown that an accurate probabilistic function evaluation can be generated.

The first approximation method, response surface methodology, has at its core a response surface of a limited set of variables. This method has as its primary advantage computational speed. Once the experiment design has been evaluated, only simple polynomial evaluations are required. For the mass properties analysis, this saves the time of iterating between the mass equations.

The second method was discrete probability optimal matching distributions (DPOMD). More specifically, the fractional factorial based DPOMD was used. This method created a discrete representation of the entire multivariate input distribution that matched its first and second moment properties. Then the discrete points of the distribution were evaluated and the mean and variances of the outputs were measured. This technique was tested at varying levels of computational expense by varying the reduction level of the fractional factorial experiment design.

The final method tested used a descriptive sampling approach. This method divided the uncorrelated standard normal space input distribution into equal probability areas. Samples were taken at the centers of some of these areas according to the algorithm presented in the background chapter. Because of the high flexibility in sample size for the Descriptive Sampling algorithm, more intuitive sample sizes than the DPOMD method could be selected for the test. These were set to sample sizes of 50, 100 and 200 trials.

The test problem for all of these was a single probabilistic analysis run of the mass properties analysis and was conducted at a vehicle length of 150 ft. For this size, each of the candidate methods were compared on the basis of their accuracy in generating

distributions that would be required for the inclusion of this contributing analysis in the larger launch vehicle optimization problem.

6.4 Outputs of Interest

These included the mean and variances of gross liftoff weight (GLOW) and vehicle dry weight. GLOW is an important output because it is a required coupling variable for the trajectory analysis. Dry weight was selected because it is a rough indicator of vehicle development cost and was to be used as the objective function once the analyses were integrated into the probabilistic framework. Also, because the analysis was run at a single length and only used to generate weight numbers and not actually size the vehicle, another important output was the mass ratio error distribution. Measuring the accuracy of this parameter showed how accurately the analysis would be able to meet its internal performance constraint.

Accuracy in these parameters for a minimal computational expense was the goal of this analysis test. Finding a faster substitute for Monte Carlo simulation for this analysis should definitely make system level optimization easier.

6.5 Monte Carlo Procedure

This analysis is considered to be the most accurate representation of the response distributions. However, its computational expense means that it is being used primarily as a reference for this research. Although a direct analysis would be accurate, the complex nature of weights and sizing analysis makes this impractical.

Monte Carlo analysis consists of randomly selecting sets of inputs from specified input distributions and running a deterministic analysis for several thousand trials, using a pseudo-random number generator to select the sets of inputs.

The random number generation scheme varied depending on the type of input distribution. When multivariate normal samples were required, a previously stored list of independent standard normal samples was transformed using an inverse standard normal space transform [138, 46]. This process is described in the background chapter in the section on fractional factorial DPOMD. The previously stored list was generated using the Matlab function randn(). This saved the computational expense of random number generation and cumulative normal distribution calculations. The only calculation required to generate these samples was a Cholesky factorization [90, 152] to find the transform matrix and then a matrix multiplication and vector addition to actually perform the transform.

A similar technique was used for the independent triangular distributions found in the weight assumption random variables. In this case, a stored list of uniform random samples generated by the Matlab© function rand() was transformed into samples from triangular distributions using an inverse triangular distribution function written for this research. Generation of these numbers took significantly longer than the multivariate normal variables. However, it should be noted that these values will not need to be recalculated during eventual optimization, as they are assumptions internal to the mass properties and sizing analysis, and their parameters do not vary.

The results of each of these trials were then considered as results of a random test and the properties of the output distributions measured. Sample estimates for mean and

standard deviation were used. These are shown in Eqns. 6.1 and 6.2 [150]. Because of the limited number of assumptions and lack of an exact answer available for this type of analysis, the results the Monte Carlo simulation will be considered the baseline for comparison to the other methods.

$$\mu = \frac{1}{N}\sum_{allx} x_i \tag{6.1}$$

$$\sigma = \sqrt{\sum_{allx} \frac{(x_i - \mu)^2}{N-1}} \tag{6.2}$$

The number of trials was chosen to ensure a high confidence of a low error level when measuring an 80% constraint satisfaction probability. The value of 50,000 trials chosen ensures a 95% confidence of a 1.75% maximum error when measuring against a constraint at the 80% level, according to Eqn. 5.3 [110]. This is close enough to the actual answer that it should be able to give an idea of which of the tested approximation methods are also close to the actual answer. This error band should also be considered when comparing answers between the candidate analyses, as a small accuracy advantage may not be significant to prove one analysis superior in accuracy to another.

6.6 Monte Carlo Results

The Monte Carlo simulation generated the means, variances and correlation coefficients required for integration into the probabilistic framework as well as internal constraint satisfaction. The numerical results for these values can be found in Table 4. Confidence intervals for the values below were calculated according to

Table 4 – Table of Mass Properties Monte Carlo Results

	GLOW μ	GLOW σ	G/D corr.	Drywt. μ	Drywt. σ	MR 80% c.l.
Monte Carlo	1,681,950 lb.	34,280 lb.	44.2%	143,630 lb.	3,760 lb.	0.98097
95% c. l.	± 300 lb.	± 210 lb.	± 0.7%	± 33 lb.	± 20 lb.	± 0.03%

The positive MR term in the last cell in Table 4 shows that for this OML size, this vehicle will exceed the required propellant loading to an 80% confidence level. Figure 23 and Figure 24 illustrate the 44.2% correlation coefficient between GLOW and dry weight in both histogram and scatter plots. This property of the output is most easily seen in the skew in the scatter plot. Figure 24 gives a better idea of the normality of the data, as the frequency bars have the familiar bell shaped curve of a Gaussian distribution.

The histogram in Figure 24 along with the normal distribution plot in Figure 25 show clearly that the output distribution for GLOW is in fact normal, except for some small probabilities in the tails of the distribution. This normality is important to the assumptions made by the probabilistic framework and is an important fact to verify.

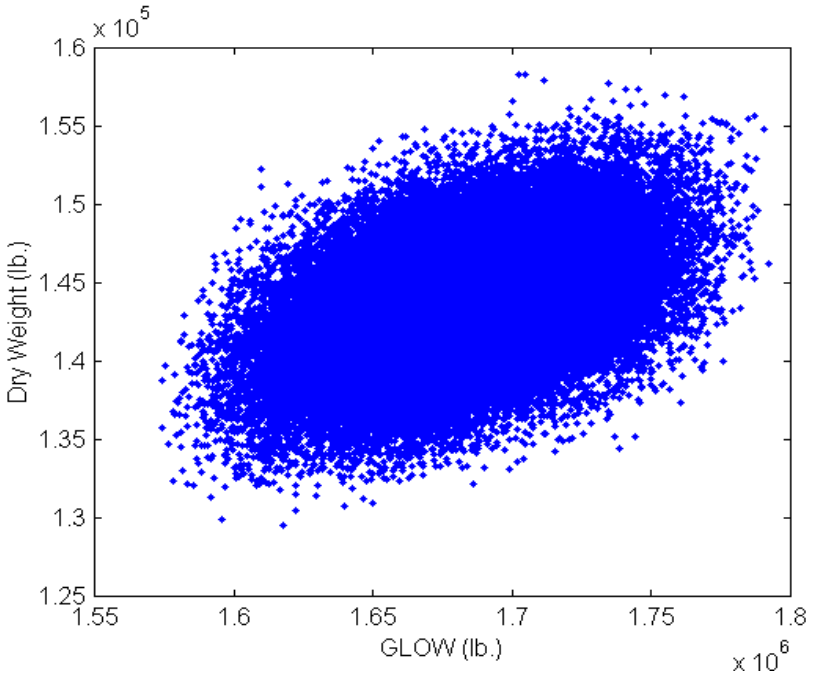

Figure 23 – Monte Carlo Scatter Plot of GLOW and Dry Weight

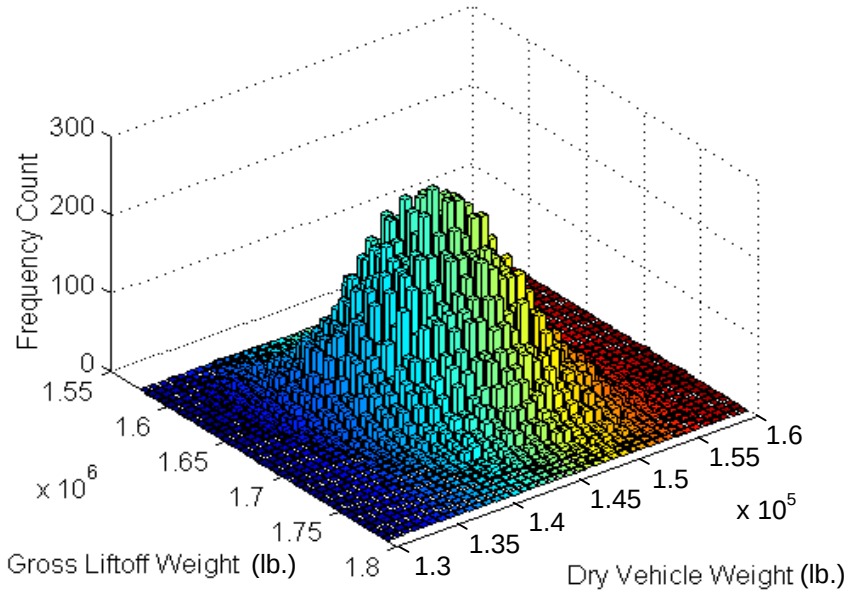

Figure 24 – Monte Carlo Histogram of GLOW and Dry Weight

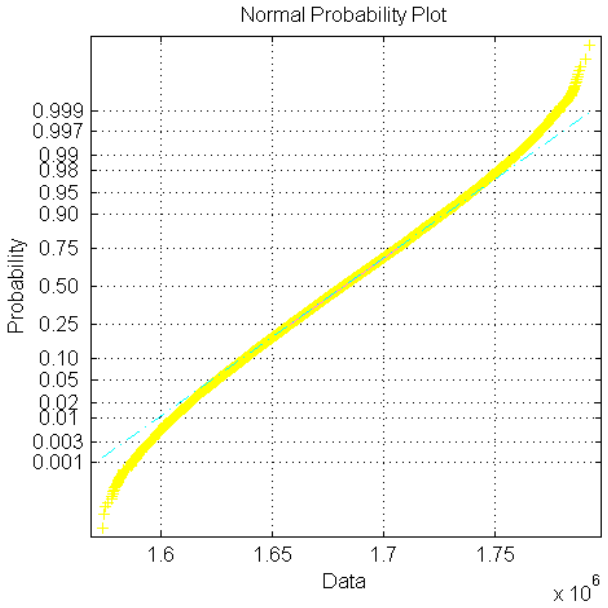

Figure 25 – Normal Probability Plot of GLOW

The results here show that the outputs are in fact correlated and do not violate any of the assumptions made by the probabilistic framework presented earlier. This also means that any of the approximation methods that were able to match the performance of the Monte Carlo simulation should be appropriate for the planned probabilistic framework, as there is no apparent problem with the variables themselves.

6.7 Response Surface Procedure

This method [75, 76, 77, 79, 100] uses a two-level design of experiments arrays to first screen for important factors, then fits a higher order model to the factors contributing most to the response using a second design of experiments array. The design array used for screening was a 64 run, resolution IV fractional factorial design for 38 variables. This

means that the main effects were at most confounded with third order interactions. To design the array, a Matlab© code was created using the direct generation method [151] to create fractional factorial designs with maximum possible resolution. This screening array was then run on the weights and sizing to get the importance of each of the variables.

From this point, the statistical software package JMP© [149] was used to conduct a screening test on the results and generate importance rankings for the main effects for the output variables gross liftoff weight, dry weight and mass ratio error. Ten variables were determined to be the drivers for the three outputs of interest, as is show in the Pareto plots in Figure 26, Figure 27 and Figure 28. Analysis of these plots lead to the selection of the most important variables for the response surface. Variables were considered important to the response if they were one of the top factors in any of the three responses of interest. To be considered a top factor, the variable must be above the 80% cumulative response line on the Pareto plot and therefore be a member of the minimal set of variables that contribute to 80% of the response.

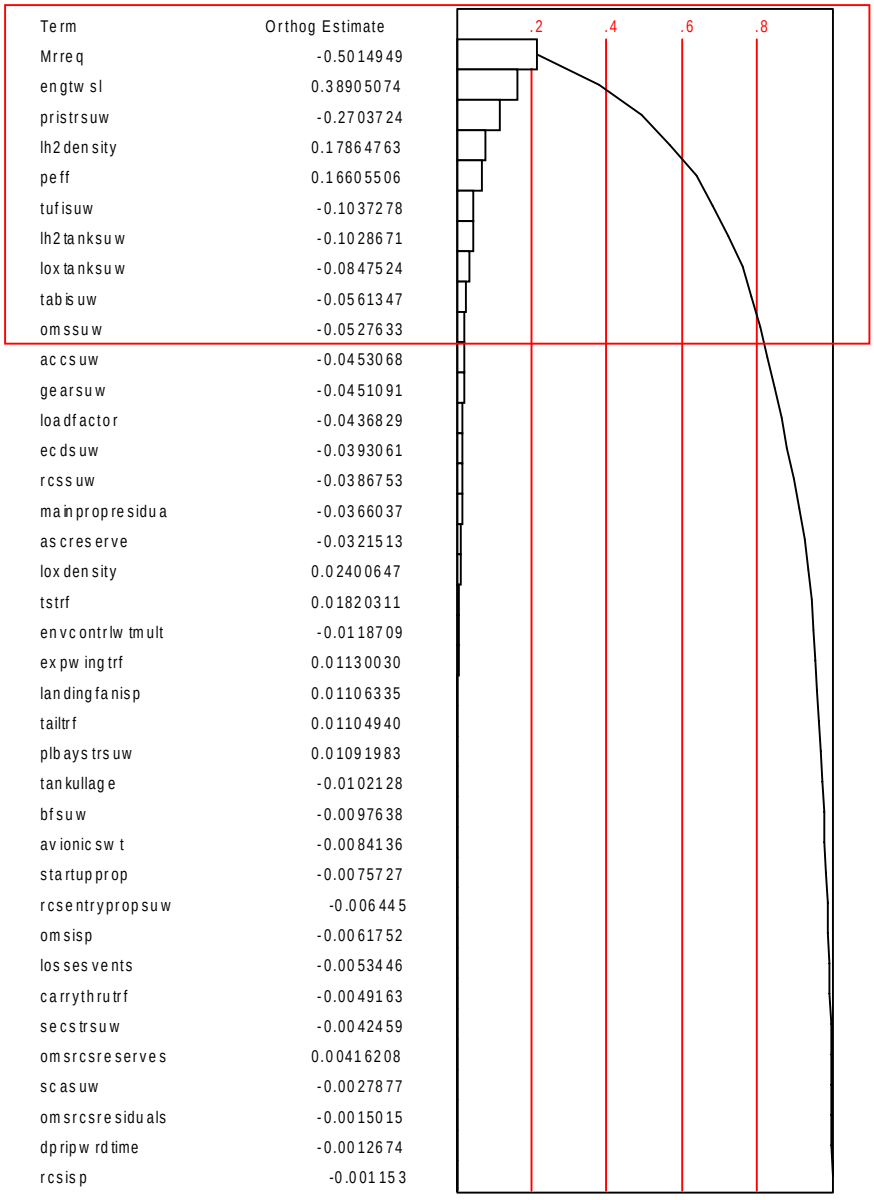

Figure 26 – Pareto Plot for MR Difference Response

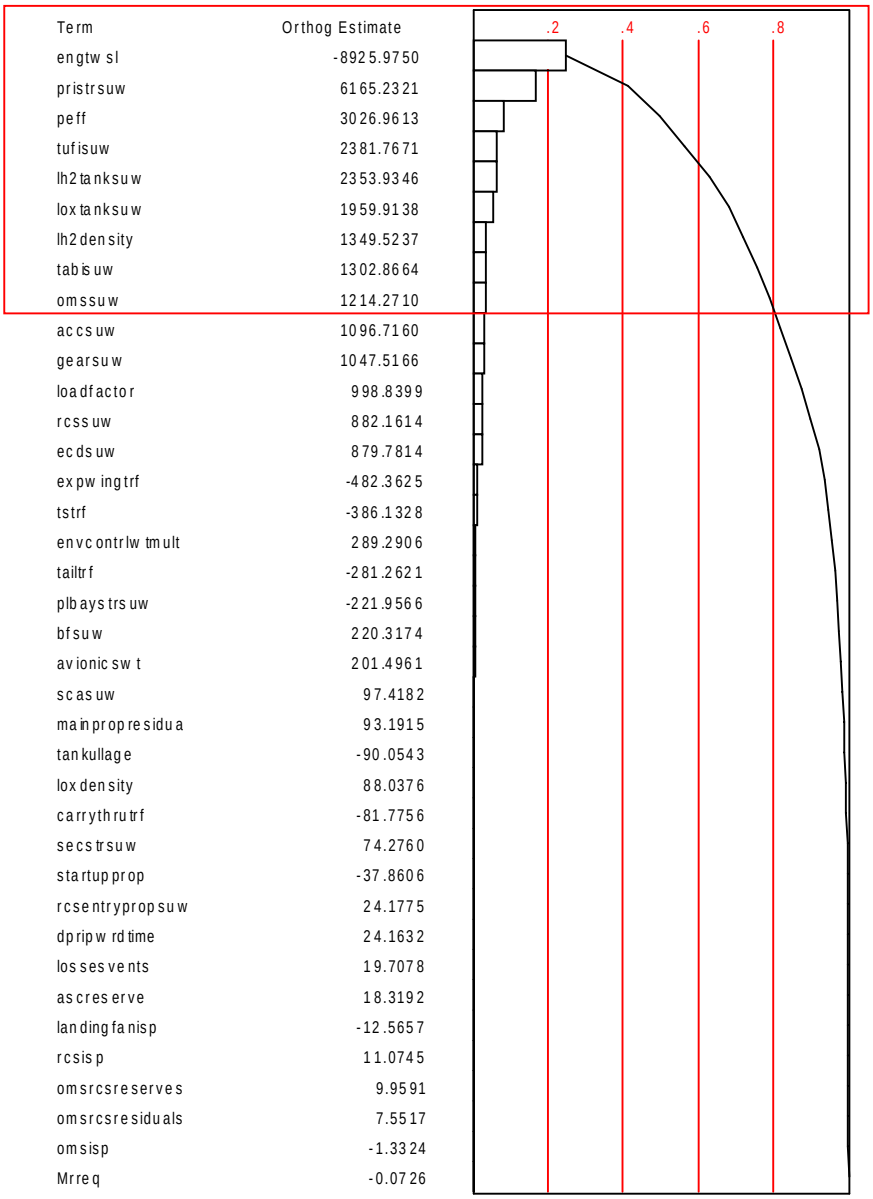

Figure 27 – Pareto Plot for Dry Weight Response

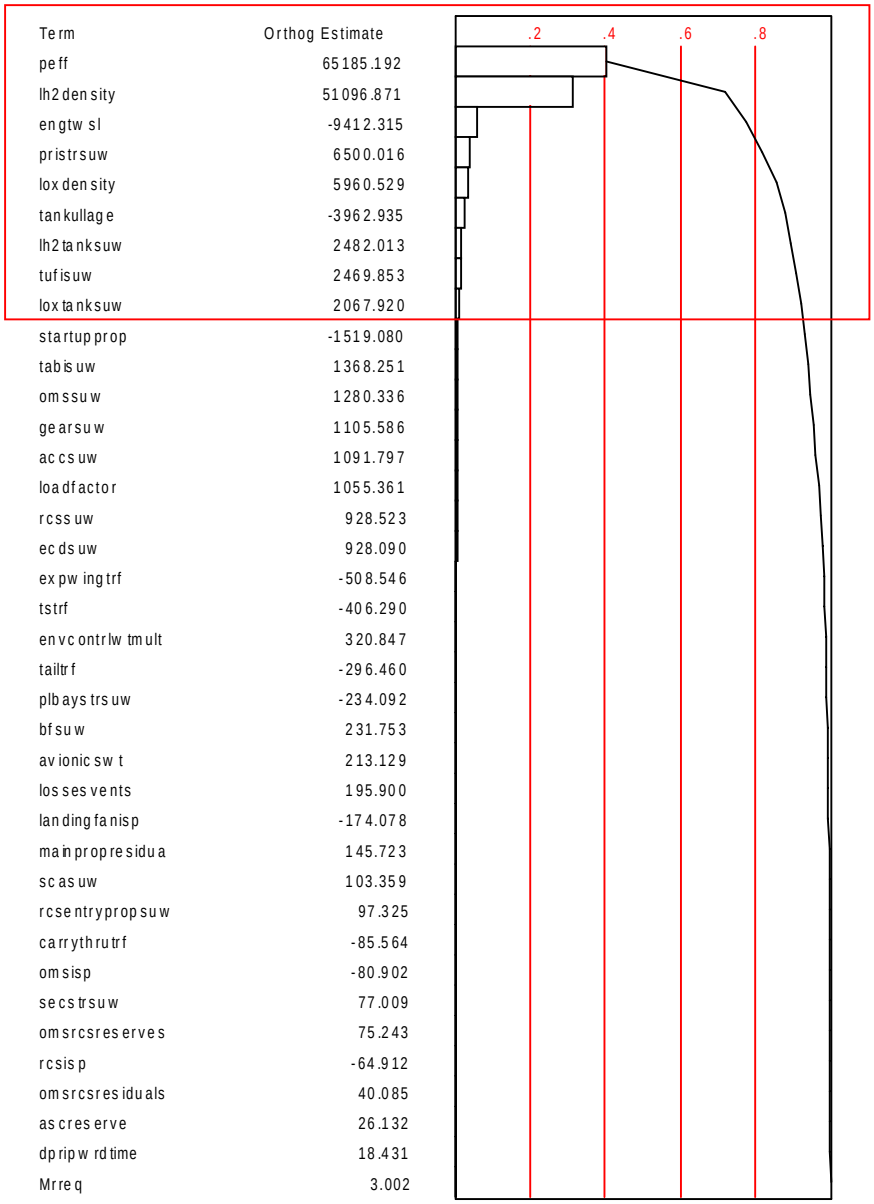

Figure 28 – Pareto Plot for GLOW Response

The Pareto plots presented here revealed ten variables that were important to all of the responses of interest. These ten variables and their corresponding levels are shown in Table 5. It is important to note that some of the variables outside the boxes of the

Pareto plots were actually included in the model. This means that more of the variability in the response than was shown at the cutoff was included in the response surface model.

Table 5 – Important Variable and Their Levels

Variable	Low Setting	High Setting
Mrreq (Mass Ratio Required)	7.3	8.8
engtwsl (Engine Thrust to Weight at S/L)	55	92
pristrsuw (Primary Structure Unit Weight)	2.257 psf.	3.637 psf.
lh2density (Density of LH_2 Fuel)	4.2 lb./ cu. ft.	4.6 lb./ cu. ft.
Peff (packaging efficiency)	70%	76%
loxtanksuw (LOx tank str. unit weight)	0.51 lb./ cu. ft.	0.68 lb./ cu. ft.
Lh2tanksuw (LH_2 fuel tank unit weight)	0.35 lb./ cu. ft.	0.43 lb./ cu. ft.
omssuw (OMS % of entry weight)	1.46%	2.65%
tufisuw (TUFI TPS Structure Unit Weight)	1.17 psf.	1.69 psf.
tabisuw (TABI TPS Structure Unit Weight)	0.72 psf.	1.04 psf.

After this process, commensurate with the expense of the trials, a full factorial experiment design was used to fit a quadratic response surface of the form in Eqn. 6.3. The important variables were set to high, middle and low values corresponding to the ranges over which they were screened. The remaining variables were all set to their most likely value. The regression was done by means of a stepwise process designed to maximize the accuracy of the fit by eliminating parameter estimates that do not contribute to the response. This contribution is determined by a series of F ratio tests as described in the background chapter. The software package JMP© was used to perform this process. Stepwise regression has the effect of eliminating the noise created by the

small coefficient estimates and raising the adjusted R-square of the overall fit. All the response variables were fit using the same process.

$$f(x) = \sum_{alli} \sum_{allj} a_{ij} x_i x_j + \sum_{alli} b_i x_i + c \tag{6.3}$$

Where x represents the input variables and a, b and c are the coefficients of the quadratic polynomial. The adjusted R-Square of all three fits was 1.000. This translates to an extremely good fit, especially considering the number of sample points in the experiment design.

Once the response surface was generated, a Monte Carlo simulation over ten variables was conducted. This analysis was identical to the direct Monte Carlo simulation conducted on the mass properties and sizing model, but this time only the ten variables in the response surface could be varied. The output variables of interest were then analyzed using sample mean and variance calculations.

6.8 Response Surface Results

This simulation generated the same means, variances and correlation coefficients required for integration into the probabilistic framework as well as for internal constraint satisfaction as generated by the Monte Carlo simulation. A comparison of these results to Monte Carlo simulation is in Table 6.

Table 6 – Results of RSE / Monte Carlo Simulation

	GLOW μ	GLOW σ	G/D corr.	Drywt. μ	Drywt. σ	MR 80% c.l.
Monte Carlo	1,681,950 lb.	34,280 lb.	44.2%	143,630 lb.	3,760 lb.	0.98097
95% c. I.	± 300 lb.	± 210 lb.	± 0.7%	± 33 lb.	± 20 lb.	± 0.03%
RSE / Monte Carlo	1,686,275 lb.	34,220 lb.	50.4%	147,000 lb.	3,300 lb.	1.1400
Abs. Rel. error	0.257 %	0.175 %	14.0%	2.35%	12.2%	16.2%

While the GLOW results do not appear to be that inaccurate, the dry weight and mass ratio difference results are quite far away from the direct Monte Carlo results. This was probably due to the lower variability captured by these models when compared to the GLOW model. This can be seen in Figure 26, Figure 27 and Figure 28 in the cumulative variability line to the right of the bars on the plot. The cumulative plots for dry weight and mass ratio difference were near the minimum allowable 80%, while the GLOW effects included in the model were well over 90%.

Figure 29 and Figure 30 illustrate the relationship between the GLOW and dry weight distributions in both histogram and scatter plots. The results show a visual similarity to the Monte Carlo simulation. However, there is a significantly higher correlation coefficient in this distribution than in the direct Monte Carlo result. It is important to note how full the distribution is. While this does not necessarily connote accuracy, it is an important aspect of the method, as cumulative distributions can be calculated without the use of an assumed distribution function. If the nature of the output distribution were not known, this would be a tremendous advantage. In this particular test, the outputs of interest do seem to be quite normal.

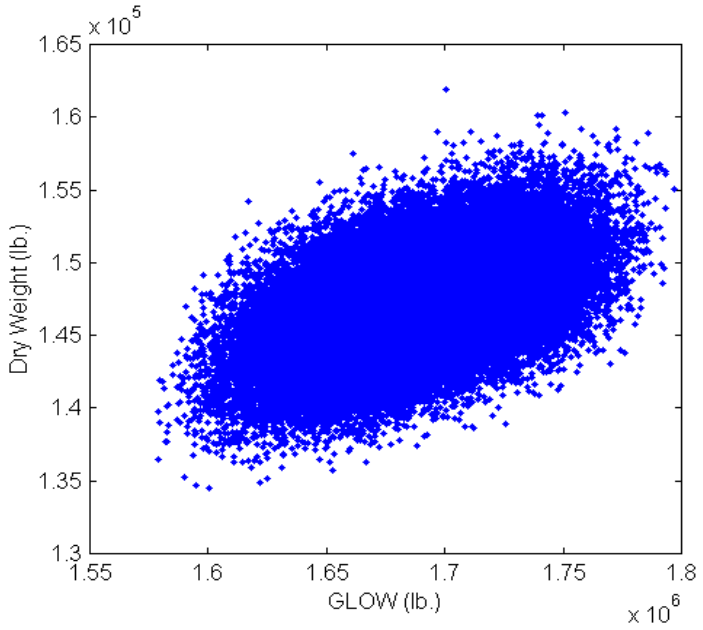

Figure 29 – Scatter Plot of RSE/MC GLOW and Dry Weight

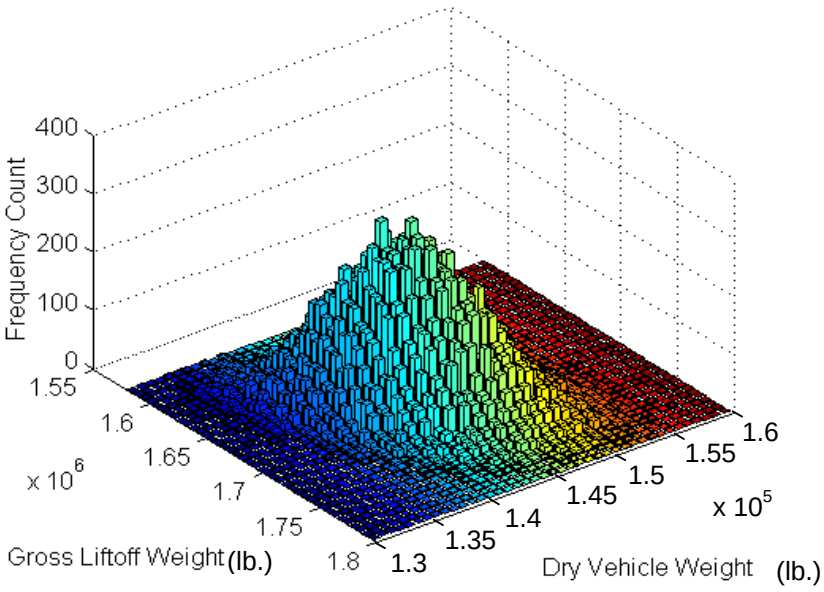

Figure 30 – Histogram of RSE/MC GLOW and Dry Weight

The histogram in Figure 30 along with the normal distribution plot in Figure 31 show clearly that the output distribution for GLOW calculated by the response surface is normal, just as with the Monte Carlo simulation results.

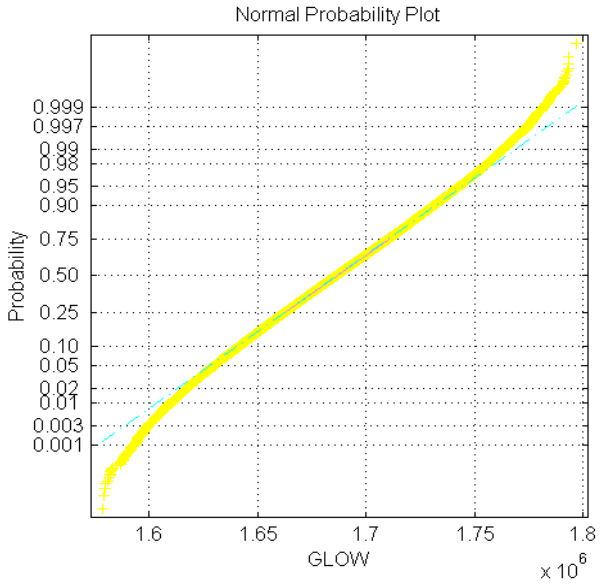

Figure 31 – RSE / MC Normal Probability Plot for GLOW

The results here show that the outputs of the response surface analysis are in fact correlated normals just like the Monte Carlo simulation and therefore do not violate any of the assumptions made by the proposed probabilistic framework. There are issues with accuracy on select variables, however. While neither of the variables of interest with large errors are coupling variables, they are involved with internal constraint satisfaction and objective function formulation. These errors are therefore a serious concern.

6.9 Discrete Probability Optimal Matching Distributions

This group of methods [91] uses a discrete probability distribution as a surrogate for the actual distribution, as described earlier in this paper. Because of the highly dimensional nature of the mass properties problem, none of the methods presented previously by the author [91] were used for this problem. Instead, the fractional factorial method described in the earlier chapter on new uncertainty analysis methods was used. It began with a two level fractional factorial design of experiments array with levels set to –1 and +1 was constructed with each point having equal probability. The settings of the factors in this array are uncorrelated and have means zero and variances of 1. Taking this array and using an inverse standard normal space transform, the desired mean and covariance matrix can be imparted to the set of points. This means that the discrete input distribution matches the means, variances and covariances of the inputs. This process is described in detail in the section in the background chapter on this particular DPOMD method.

In this particular test, several fractional factorial designs were used of varying size. To create these designs, the Matlab© code created for this research used the direct generation method [151] to create a fractional factorial design with the maximum resolution for a given number of random variables and reduction factor. For the test, the reduction factor was varied to gauge the accuracy with respect to discrete input distribution size. Experiment sizes from 64 to 256 runs for 38 variables were considered, with results measured from each and compared here. The resolutions of the experiments are summarized in Table 7.

Table 7 –Fractional Factorial Designs Used

Experiment Type	# Runs	Reduction	Resolution
$2^{(38-32)}$ fractional factorial	64	32	IV
$2^{(38-31)}$ fractional factorial	128	31	V
$2^{(38-30)}$ fractional factorial	256	30	VII

First, the means, variances and covariances of both the triangular and normal input distributions were calculated. This step is necessary to create the inverse standard normal space transform described earlier in the section describing this DPOMD method. Next, the two level fractional factorial experiment design discussed earlier was created with levels at –1 and 1. When expressed in standard normal space, this experiment design has the same mean and covariance matrix as the standard normal distribution.

As a side note, because the DPOMD method chosen only matches the mean and covariance arrays for the input distributions, the skewed triangular distributions in the weight assumptions were not as fully represented as the multivariate normal coupling variables in this particular problem. This was because of their third order moment characteristics. In spite of this, the results for this analysis proved to be quite accurate.

Using the inverse transform found using the mean vector and covariance matrix of the inputs, the experiment design was then transformed from standard normal space into the actual random variable space. This yielded a discrete probability distribution that had the same mean vector and covariance matrix as the set of 38 input variables. This yields a sampling scheme that follows the shape and size of the input distributions.

After evaluating the differently sized sets of points, the results of the analysis were obtained using a distribution mean and covariance calculation. For this analysis, a normal distribution was fit to the results to obtain the desired confidence intervals for the output. This was considered to be a valid assumption due to the fact that the mass properties analysis was mostly additive containing a large number of variables, and was therefore valid under the central limit theorem for normal variables [150]. Also, inspection of the Monte Carlo results for mass properties and sizing showed normal behavior, further bolstering the decision to use an assumed normal distribution to calculate confidence intervals.

6.10 DPOMD Results

The means and standard deviations of GLOW and dry weight were calculated using a moment-based mean and standard deviation calculation. The standard deviation estimator used here differs from the random sampling methods in that the denominator contains the number of points as opposed to number of points minus one. The standard deviation estimator is given in Eqn. 6.4 [150].

$$\sigma = \sqrt{\frac{\sum_{all\_x} (x - \mu)^2}{n_{pts.}}} \tag{6.4}$$

This method was executed for various levels of computational expense using different reduction factor fractional factorial designs. A comparison of these results to the reference Monte Carlo simulation can be found in Table 8.

Table 8 – DPOMD Mass Properties Test Results

	GLOW μ	GLOW σ	G/D corr.	Drywt. μ	Drywt. σ	MR 80% c.l.
Monte Carlo	1,681,950 lb.	34,280 lb.	44.2 %	143,630 lb.	3,760 lb.	0.98097
95% c. l.	± 300 lb.	± 210 lb.	± 0.7%	± 33 lb.	± 20 lb.	± 0.03%
64 run DPOMD	1,681,960 lb.	32,625 lb.	-7.27 %	143,640 lb.	3,290 lb.	0.93730
Abs. Rel. error	0.000860 %	4.84 %	116 %	0.00514 %	12.5 %	4.45 %
128 run DPOMD	1,681,970 lb.	34,275 lb.	44.2 %	143,645 lb.	3,770 lb.	0.98020
Abs. Rel. error	0.00121 %	0.0262 %	0.110 %	0.00875 %	0.392 %	0.0787 %
256 run DPOMD	1,681,970 lb.	34,201 lb.	44.2 %	143,644 lb.	3,750 lb.	0.98171
Abs. Rel. Error	0.00120 %	0.240 %	0.124 %	0.00868 %	0.242 %	0.0753 %

Two scatter plots of dry weight and GLOW can be found in Figure 32 and Figure 33. The first is for 64 runs, while the second is for 256. It is evident from these plots that this method requires the assumption of a type of distribution to go along with the moment information. For these variables, we know from the previous Monte Carlo simulation that they are normal, so an assumed Gaussian distribution was used to calculate confidence intervals for GLOW, dry weight and mass ratio (MR). Despite the lack of a normal appearance, the 256 run scatter plot in Figure 33 does show the correlation between the two variables.

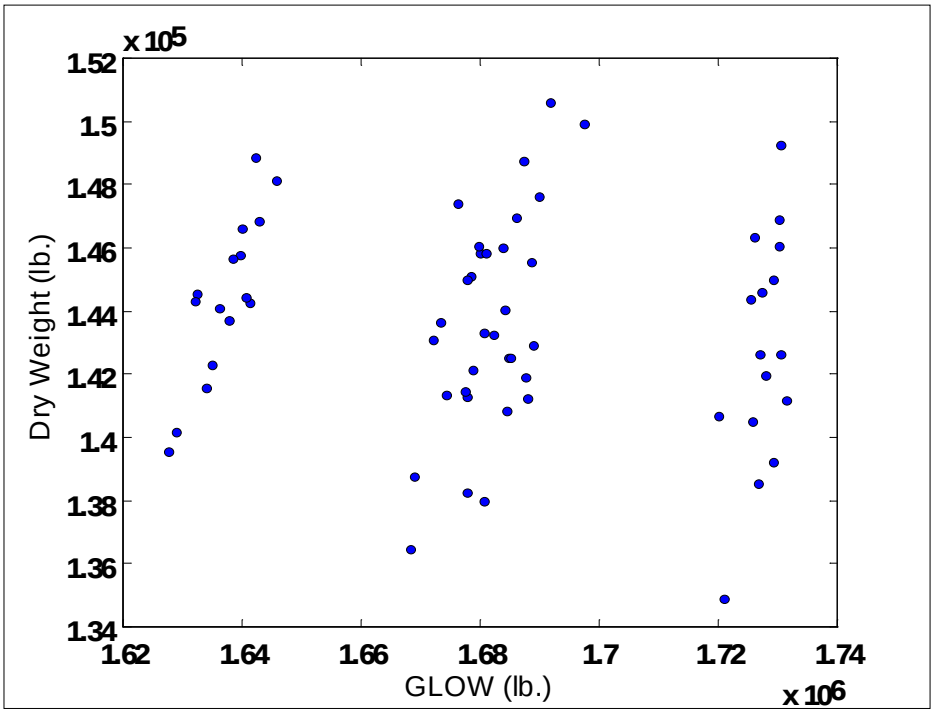

Figure 32 – Scatter Plot for 64 Run DPOMD

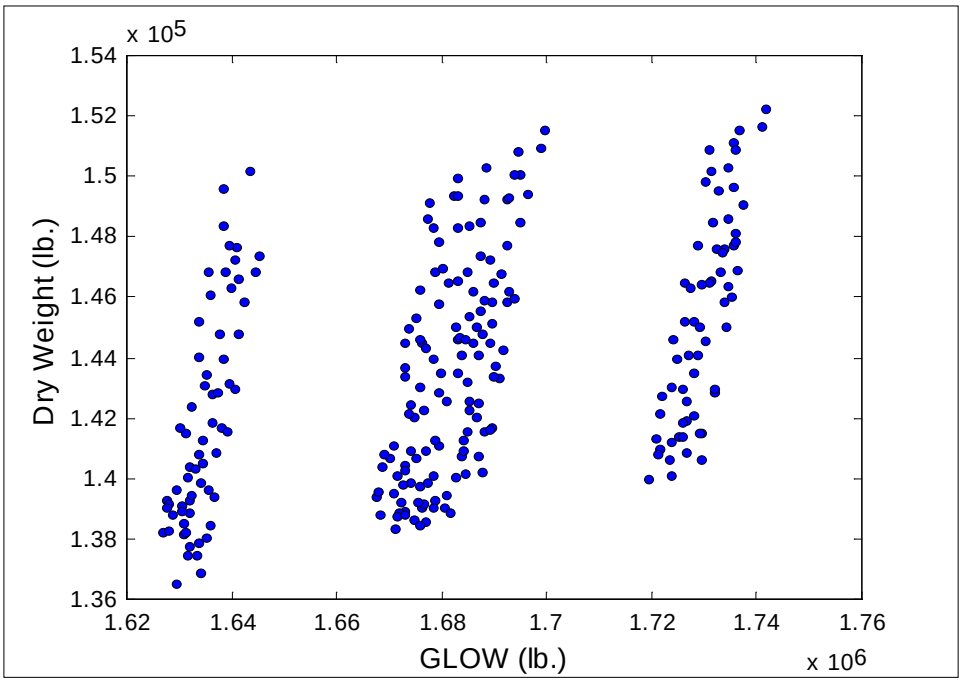

Figure 33 – Scatter Plot for 256 Run DPOMD

The results of the DPOMD testing indicated that while the accuracy of some of the parameters were dependent on sample size, precise results were obtained for the 128 and 256 run models. This would indicate that if tested properly before it is implemented, this DPOMD method is quite useful for probabilistic analysis of this type of problem. The testing caveat pertains to the type of distribution function assumed for the output in order to calculate confidence intervals and verify the accuracy in this particular situation.

6.11 Descriptive Sampling

The descriptive sampling algorithm was used for three selected sample sizes, each of which was chosen on the basis of acceptable execution time. These were selected to be similar in size to the DPOMD runs, but due to the higher sample size flexibility of descriptive sampling, could be at more intuitive values.

The first step was the creation of the probability map. This was done using a custom Matlab© routine designed to generate a descriptive sampling run set for a independent, multivariate uniform distribution. It uses a similar algorithm to the one described by McKay, et al. [120] for Latin hypercube sampling and reviewed in the background chapter, but with the variability within the stratum removed and the point placed at the center of the selected cell. This is an efficient algorithm described by Saliby [132] for generation of efficient descriptive sampling locations. It also means that the Latin hypercube and descriptive sampling techniques are asymptotically similar [132], due to the shrinking of the strata as the sample size grows.

Once the uniform probability map was generated, this was treated just like a table of random numbers for a Monte Carlo simulation. First, for the multivariate normal random variables, sample values in standard normal space [138, 46] from standard normal distributions were calculated based on the probabilities generated by the descriptive sampling algorithm. This was done by way of an inverse cumulative distribution function. Next, the inverse cumulative triangular distribution functions were used to generate the sample locations for the triangular random variables. The triangular variables were calculated directly in the problem space.

Once the locations of the standard normal sample points in standard normal space were identified, this experiment design was transformed into the actual normal random variable space to create a table of trials for the simulation to calculate.

The results of this analysis were analyzed in much the same way as the other weights and sizing tests. For the calculation of confidence intervals, a simple sorted counting technique identical to the method for the Monte Carlo simulation was used. The other parameters were also calculated in the same manner as the Monte Carlo simulation.

6.12 Descriptive Sampling Results

The same output distribution parameters as were presented in the previous section were compared to the Monte Carlo simulation results. The errors for all the parameters except the correlation coefficient are reasonably small for the 200 run version. They are listed in Table 9 along with the results for the variables of interest to the multidisciplinary problem.

Table 9 – Results of Mass Properties Descriptive Sampling Test

	GLOW μ	GLOW σ	G/D corr.	Drywt. μ	Drywt. σ	MR 80% c.l.
Monte Carlo	1,681,950 lb.	34,280 lb.	44.2 %	143,630 lb.	3,760 lb.	0.98097
95% c. l.	± 300 lb.	± 210 lb.	± 0.7%	± 33 lb.	± 20 lb.	± 0.03%
50 run DS	1,681,967 lb.	34,118 lb.	46.8 %	143,648 lb.	3,695 lb.	0.90997
Abs. Rel. error	0.001 %	0.483 %	5.79 %	0.0117 %	1.67 %	7.23 %
100 run DS	1,681,952 lb.	33,698 lb.	51.4 %	143,641 lb.	3,710 lb.	0.93969
Abs. Rel. error	0.0001 %	1.71 %	16.2 %	0.00685 %	1.26 %	4.21 %
200 run DS	1,681,982 lb.	35,086 lb.	53.2 %	143,650 lb.	3,701 lb.	0.96073
Abs. Rel. Error	0.00192 %	2.34 %	20.2 %	0.0111 %	1.50 %	2.06 %

The scatter plot results in Figure 34 for descriptive sampling are similar to those for the DPOMD method. The behavior shown in Figure 35 indicated that an assumed distribution was not necessary for the calculation of confidence intervals. However, this is of minor importance, as the output has already been shown to be normal by the reference Monte Carlo simulation.

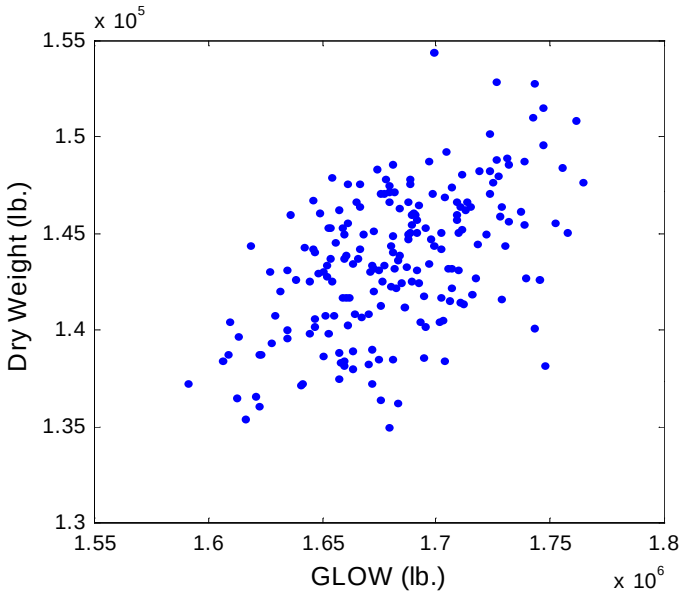

Figure 34 – Scatter Plot of 200 run Descriptive Sampling

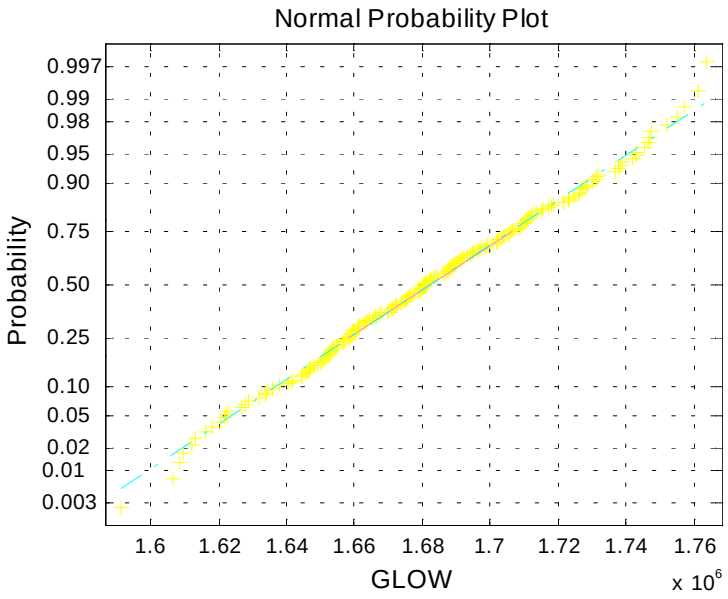

Figure 35 – Normal Probability Plot for DS GLOW Result

6.13 Overall Comparisons

The aim of this test was to determine the characteristics of several methods of uncertainty approximation when applied to a conceptual launch vehicle mass properties analysis and then select a preferred method with which to proceed on to multidisciplinary optimization.

The first goal has been met. The characteristics of this problem has been shown extensively in the previously section with respect to response surface, discrete probability optimal matching distribution and descriptive sampling methods.

Of the techniques tested, the DPOMD method for the two higher sample sizes was able to match the Monte Carlo simulation the best for the output parameters of interest. While the descriptive sampling method was close for some parameters, the DPOMD was clearly the method of choice for this contributing analysis. This can be seen in Figure 36, which shows a trial history of the accuracy of all of the approximation methods. The Monte Carlo simulation accuracy was calculated like the others by comparing it to the final answer generated by the Monte Carlo.

Figure 36 and Figure 37 indicate that the RSE/RSM method was somewhat inaccurate. While some the parameters not shown in Figure 36 and Figure 37 were accurately predicted by the response surface, the errors on the displayed variables were too high to allow the use of this type of simulation. On the Excel© platform, the time to evaluate the RSE for 50,000 trials was 12.8 minutes on a Pentium III 850 MhZ computer. The time to evaluate the same number of Monte Carlo trials was 14.1 minutes. If executed using a custom C++ Monte Carlo RSE evaluation program, this cost is much smaller, taking only 5.5 seconds on an SGI Octane workstation.

The approximation methods that took on the order of one hundred trials were even quicker still. While not as accurate, the 64 trial methods completed in 1.1 seconds, the 128 trial methods in 2.2 and the 256 methods in 4.4 seconds, on the order of the expense of using the RSE on the workstation. A complete listing of the computational expenses can be found in Table 10.

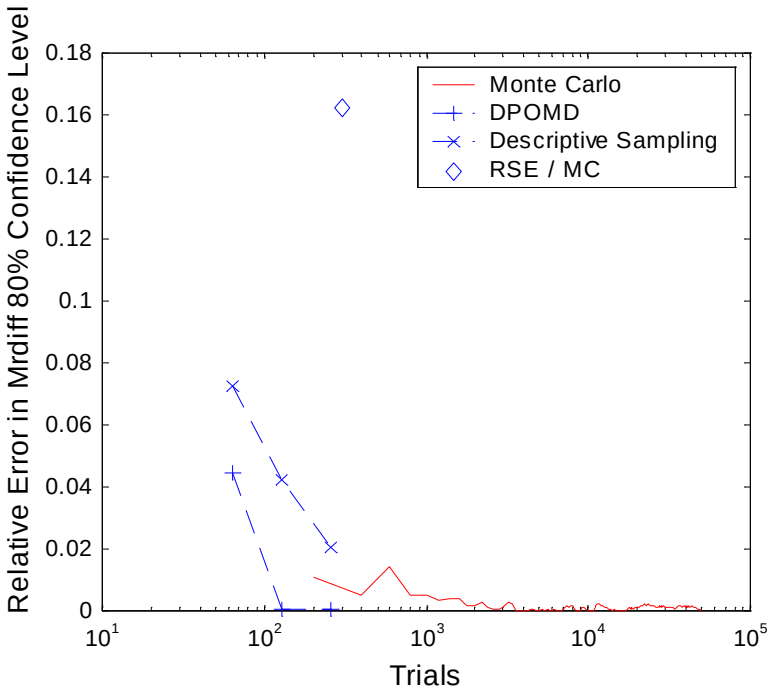

Figure 36 – Trial History of MR C.L. Mass Properties Approximation Tests

Table 10 – Execution Time for Mass Properties Methods

Number of Trials	Platform	Time
50,000 Excel© Analysis Calls	Pentium III PC	14.1 min.
50,000 Excel© RSE	Pentium III PC	12.8 min.
50,000 C++ RSE	SGI Octane	5.5 sec.
256 Excel© Analysis Calls	Pentium III PC	4.3 sec.
200 Excel© Analysis Calls	Pentium III PC	3.4 sec.
128 Excel© Analysis Calls	Pentium III PC	2.2 sec.
100 Excel© Analysis Calls	Pentium III PC	1.7 sec.
64 Excel© Analysis Calls	Pentium III PC	1.1 sec.
50 Excel© Analysis Calls	Pentium III PC	0.85 sec.

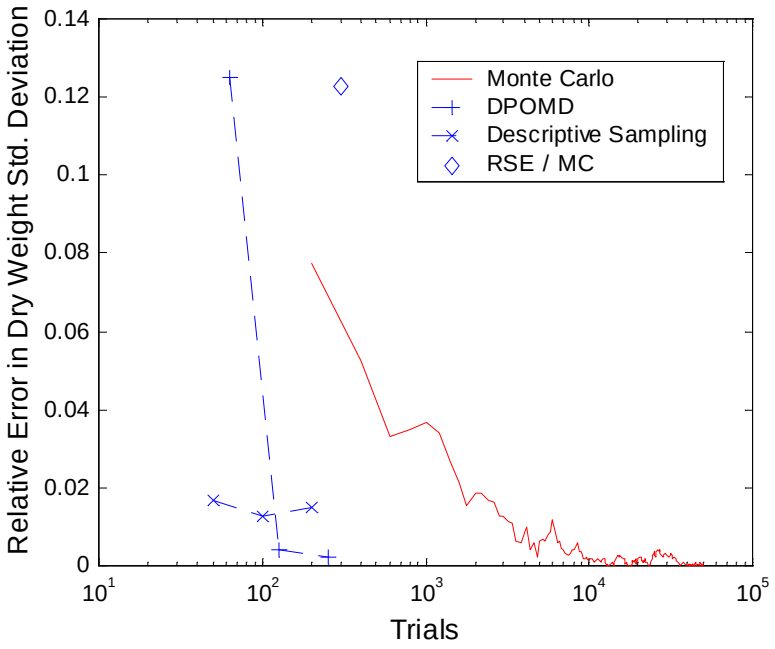

Figure 37 – Trial History of Dry Weight Standard Deviation

Interpretation of the results presented here show that the choice method for this analysis, with this set of inputs and outputs, was the fractional factorial DPOMD. More specifically, the 256 trial version was selected due to the fact that it was accurate for all the selected parameters of interest, and still had one of the lowest computation times. While the descriptive sampling method does not seem to depend as much on sample size, the accuracy of the higher order DPOMD methods is much better.

This meant that the probabilistic multidisciplinary design framework for conceptual launch vehicle design would utilize a 128-run, 38 variable fractional factorial DPOMD method for the calculation of uncertainty information in the mass properties and sizing contributing analysis.

CHAPTER VII

PROPULSION ANALYSIS TEST

The propulsion analysis considered here consisted of a deterministic rocket engine design analysis tool, SCORES [162], with an uncertainty approximation method wrapped around the outside. SCORES was developed in the SSDL by Way to provide quick, conceptual-level estimates of rocket engine performance, taking into account such factors as chemical equilibrium and nozzle type, but not requiring design information about powerhead pump systems.

SCORES consists of two analyses, the first of which calculates the equilibrium chemical state of the propellants in the combustion chamber and the second of which does a frozen flow, converging-diverging nozzle calculation to generate the ideal thrust of the proposed engine. Regressed efficiencies are then placed on the nozzle and combustion chamber depending on the type of engine cycle selected by the user.

To size the rocket, SCORES used a simple scaling [162] algorithm. To create an engine of a specified thrust, first output parameters for a baseline engine with a throat area of one square inch were calculated, then the throat area of the baseline engine was changed linearly with the reference thrust to create a new engine. This allowed for rocket engine performance estimates commensurate with the amount of information available about the engine at this stage in development. It also allows SCORES to generate a sized engine with virtually no computational expense beyond that of a single rocket analysis.

For this particular simulation, four inputs were selected as noise variables. They were the gross liftoff weight, the combustion chamber pressure, the engine power-to-weight ratio and the mass ratio required. The mass ratio required was included in the test because the correlations between it and the propulsion output variables are required by the mass properties and sizing analysis. In addition, there were three deterministic variables used as inputs to the analysis. These were vehicle thrust-to-weight ratio at liftoff, engine nozzle expansion ratio and propellant mixture ratio.

Table 11 – Required Correlations From Propulsion Contributing Analysis

	MR Required	GLOW	Engine Exit Area	Vacuum Thrust	Engine Thrust to Weight @SL	Vacuum Specific Impulse
MR Required	1.0	Input	Req.	Req.	Req.	Not Req.
GLOW		1.0	Req.	Req.	Not Req.	Req.
Engine Exit Area			1.0	Req.	Req.	Req.
Vacuum Thrust				1.0	Req.	Req.
Engine Thrust to Weight @SL					1.0	Not Req.
Vacuum Specific Impulse						1.0

There are 19 output parameters of interest generated by this uncertainty analysis. They include all quantities that are outputs from this contributing analysis and were required as inputs by other analyses. Encompassing the all the normal outputs of the propulsion contributing analysis, there are several other outputs created by the fact that this is part of a probabilistic framework. Information showing the required correlation

coefficients can be seen in Table 11. The correlations that are not required are that way because the two correlated variables are never input to the same analysis. This means that the correlation may exist but it is not important to coupling.

These eleven correlation coefficients, plus the means and variances of the four primary analysis outputs were the criteria for judging the effectiveness of the different uncertainty analysis methods. As described in the goals and objectives section, these quantities were compared to a reference Monte Carlo simulation on the basis of relative error. This gave the propulsion test nineteen comparison parameters, by far the most of any of the three comparisons in this thesis work.

The candidates for the uncertainty analysis are essentially the same methods as the mass properties test. These were selected on the basis of each method's ability to generate multivariate output information, with or without a constraint for comparison. The methods that satisfy these criteria are response surface equation with Monte Carlo simulation, descriptive sampling and discrete probability optimal matching distributions. These methods were all tested at acceptable levels of computational expense for inclusion in an iterative optimization environment.

7.1 Monte Carlo Simulation

The Monte Carlo simulation was conducted by using the same Matlab© random number generation scheme as was described in the mass properties Monte Carlo simulations section to sample from the input distributions listed in Table 12. The trials selected using these input distributions were then run using the rocket sizer [162] mode of SCORES.

Table 12 – Propulsion Monte Carlo Input Distributions

Variable	Distribution Type	Mean	Std. Dev.	Min.	Most Likely	Max.
MR required	Normal corr. = 15%	7.8	0.03	N/A	N/A	N/A
GLOW	Normal	2.1 Mlb.	50 klb.	N/A	N/A	N/A
Chamber Pressure	Normal	206 atm.	4 atm.	N/A	N/A	N/A
Engine Power-to-Weight Ratio	Triangular	N/A	N/A	0.015 MW/lb.	0.017 MW/lb.	0.023 MW/lb.

Because this analysis did not have any constraints compare against, the number of Monte Carlo trials conducted was somewhat arbitrary. It was judged that 10,000 trials was a standard amount and would yield good reference information for the approximation methods without requiring too much computer effort to run after the previous test.

7.2 Monte Carlo Results

These results will be used as reference values for the other distribution approximation methods. The results for the parameters of interest, described earlier in the section can be found in Table 13.

Table 13 – Results of Propulsion Monte Carlo Simulation

Variable	Monte Carlo Result	95% c. l.
Exit Area (Ae) Mean	295 sq. ft.	± 0.2 sq. ft.
Exit Area Std. Dev.	10.1 sq. ft.	± 0.14 sq. ft.
Vacuum Thrust (Tvac) Mean	3.145 Mlbs.	± 1.5 klb.
Vacuum Thrust Std. Dev.	76.86 klbs.	± 1.07 klb.
Engine Thrust-to-Weight (T/We) Mean	54.3	± 0.1
Engine Thrust-to-Weight Std. Dev.	5.05	± 0.07
Vacuum Specific Impulse (Ispvac) Mean	449.4 sec.	± 0.002 sec.
Vacuum Specific Impulse Std. Dev.	0.122 sec.	± 0.0017 sec.
Ae / Tvac Correlation Coefficient	83.0 %	± 0.6%
Ae / T/We Correlation Coefficient	-3.43 %	± 2%
Ae / Ispvac Correlation Coefficient	-71.2 %	± 0.1%
Tvac / T/We Correlation Coefficient	-1.14 %	± 2%
Tvac / Ispvac Correlation Coefficient	-20.1 %	± 1.9%
MRreq / Ae Correlation Coefficient	10.7 %	± 1.9%
Mrreq / Tvac Correlation Coefficient	14.6 %	± 1.9%
Mrreq / T/We Correlation Coefficient	-0.340 %	± 2%
GLOW / Ae Correlation Coefficient	70.5 %	± 1%
GLOW / Tvac Correlation Coefficient	98.0 %	± 0.08%
GLOW / Ispvac Correlation Coefficient	-0.421 %	± 2%

Some of the results in Table 13 are quite interesting. At first glance, the highly negative correlation between vacuum specific impulse and exit area seems incorrect. However, because the area ratio for this test is a constant, an increase in exit area corresponds to an increase in throat area, increasing the mass flow through the engine, lowering the specific impulse for a similar thrust. This exit area correlation also partially causes the negative correlation between vacuum thrust and vacuum specific impulse. For a constant sea-level thrust, a higher vacuum thrust can only be caused by a higher exit area, again leading to the reduction in specific impulse due to the constant area ratio. These changes all seemed to be prompted by changes in engine chamber pressure.

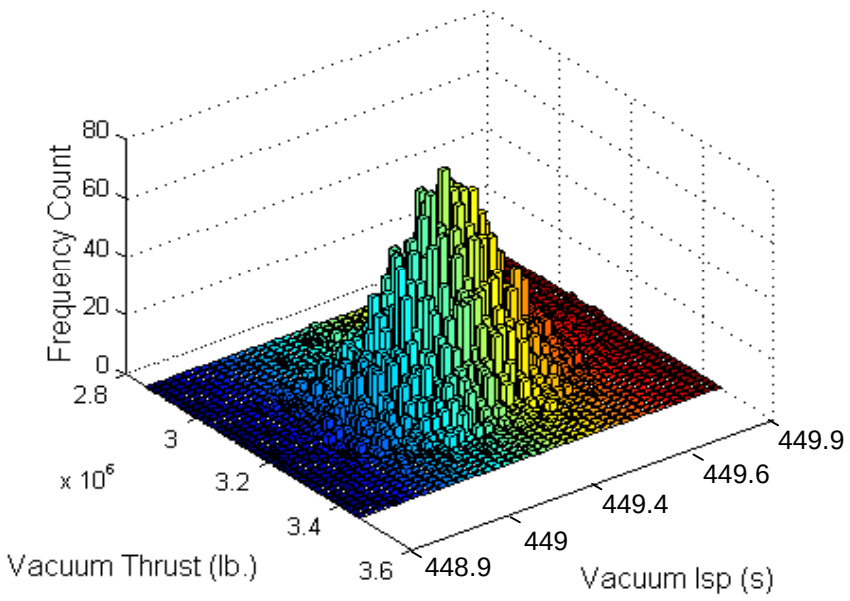

Figure 38 – Histogram of Vacuum Thrust and Isp

Figure 38 shows the slight correlation between the vacuum thrust and specific impulse. Both are apparently normally distributed and fall within a reasonable range of values. The normality of the engine exit area is shown in Figure 39. It does not begin to fall off the line until deep into the tail regions of the distribution.

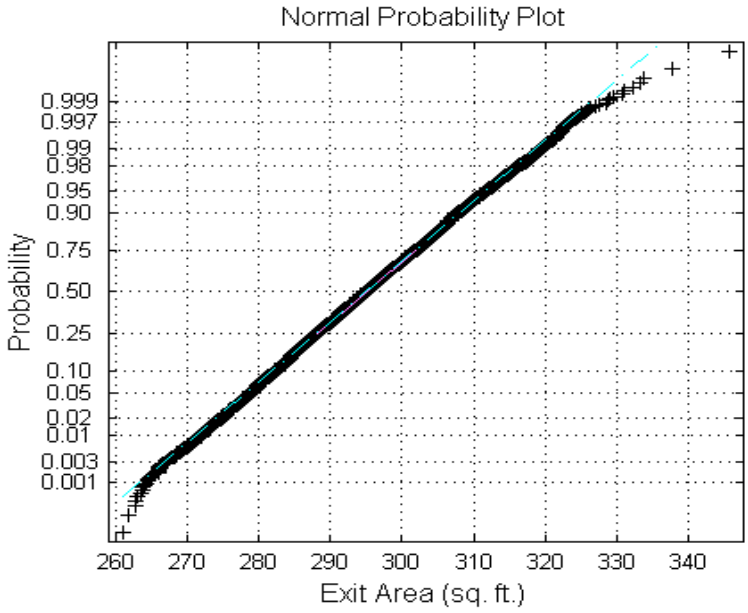

Figure 39 – Normal Probability Plot of Engine Exit Area

7.3 Response Surface Method

The first approximation method tested on the propulsion contributing analysis problem was the response surface / Monte Carlo simulation combination. Usually, the first step in this process is to screen the input variables down to an acceptable number for a quadratic curve fit. However, due to the limited number of input variables, this was not

necessary. The five variables that affected the response could be directly modeled using a using a uniform central composite experiment design.

The central composite design was created by the software package JMP© [149]. The levels for the design are listed in Table 14. These levels were either the bounds of reason for the variables in question or they were the bounds of accuracy for the SCORES tool. Also, an on-face experiment design was used. This was done because when rotatable or orthogonal spacing was used for the star points, some of the variable settings did not make sense (e.g., negative thrust at sea level).

Table 14 – Variable Settings for Propulsion Test RSE

Variable	Low Setting	High Setting
Thrust at Sea Level	1.2 Mlb.	4.8 Mlb.
Chamber Pressure	160 atm.	245 atm.
Power-to-Weight Ratio	0.015 MW/lb.	0.023 MW/lb.
Area Ratio	40	100
Mixture Ratio	4.5	8.0

The experiment corresponding to the levels in Table 14 was then evaluated using the rocket sizing algorithm in SCORES [162]. The responses were then curve fit to a quadratic polynomial of the form in Eqn. 6.3. The fitting process was a stepwise regression analysis, using sequential F-tests to determine whether the contribution of the polynomial term merited its inclusion in the response surface equation. This was done for

all of the output variables. The adjusted R-square values for the four variables are shown in Table 15.

Table 15 – Fit Values for Propulsion Response Surface

Response Surface	R-Square	Adjusted R-Square
Exit Area	1.000	1.000
Vacuum Thrust	0.9990	0.9989
Vacuum Specific Impulse	1.000	1.000
Engine Thrust-to-Weight	0.9997	0.9996

The fit for exit area generated by the stepwise regression initially was not as good as the other values. The adjusted R-Square for this initial fit was 0.9875. To remedy this, the natural log of the response was fit in place of the actual response. When this was done, the adjusted R-Square rose to 1.000. The initial adjusted R-Square value of 0.9875 was therefore had no negative consequences for the test. The Monte Carlo simulation on the response surface was run using this log fit exit area. While not presented, the Monte Carlo simulation was performed on both the initial fit and the log fit. The log fit greatly outperformed the initial fit, so these are the results presented here.

7.4 Response Surface Results

These response surfaces were run 10,000 times using the same random number list as was used for the direct Monte Carlo simulation. The results of the current

simulation were then measured for sample means, standard deviations and correlation coefficients for the output parameters stated earlier in the section.

Table 16 – Results of Propulsion RSE Monte Carlo

Variable	Monte Carlo Result	95% c. l.	RSE / MC Result	Abs. Rel. Error
Exit Area (Ae) Mean	295 sq. ft.	± 0.2 sq. ft.	291 sq. ft.	1.30 %
Exit Area Std. Dev.	10.1 sq. ft.	± 0.14 sq. ft.	10.8 sq. ft.	7.35 %
Vacuum Thrust (Tvac) Mean	3.145 Mlbs.	± 1.5 klb.	3.139 Mlbs.	0.184 %
Vacuum Thrust Std. Dev.	76.86 klbs.	± 1.07 klb.	79.18 Mlbs.	3.02 %
Engine Thrust-to-Weight (T/We) Mean	54.3	± 0.1	54.1	0.401 %
Engine Thrust-to-Weight Std. Dev.	5.05	± 0.07	5.07	0.462 %
Vacuum Specific Impulse (Ispvac) Mean	449.4 sec.	± 0.002 sec.	449.2 sec.	0.029 %
Vacuum Specific Impulse Std. Dev.	0.122 sec.	± 0.0017 sec.	0.102 sec.	16.8 %
Ae / Tvac Correlation Coefficient	83.0 %	± 0.6%	87.0 %	4.83 %
Ae / T/We Correlation Coefficient	-3.43 %	± 2%	-3.44 %	0.269 %
Ae / Ispvac Correlation Coefficient	-71.2 %	± 0.1%	-67.6 %	-5.07 %
Tvac / T/We Correlation Coefficient	-1.14 %	± 2%	-1.31 %	14.8 %
Tvac / Ispvac Correlation Coefficient	-20.1 %	± 1.9%	-22.6%	12.8 %
MRreq / Ae Correlation Coefficient	10.7 %	± 1.9%	11.2 %	4.69 %
Mrreq / Tvac Correlation Coefficient	14.6 %	± 1.9%	14.5 %	0.526 %
Mrreq / T/We Correlation Coefficient	-0.340 %	± 2%	-0.341 %	0.229 %
GLOW / Ae Correlation Coefficient	70.5 %	± 1%	73.9 %	4.92 %
GLOW / Tvac Correlation Coefficient	98.0 %	± 0.08%	97.5 %	0.565 %
GLOW / Ispvac Correlation Coefficient	-0.421 %	± 2%	-0.418 %	0.775%

Table 16 shows that the results of the propulsion response surface Monte Carlo simulation were generally good, with the exception of the vacuum specific impulse standard deviation. While the relative error is quite high, the actual error on this quantity is near the limits of fidelity for the SCORES model. However, specific impulse is a very sensitive variable, and should be as accurate as possible.

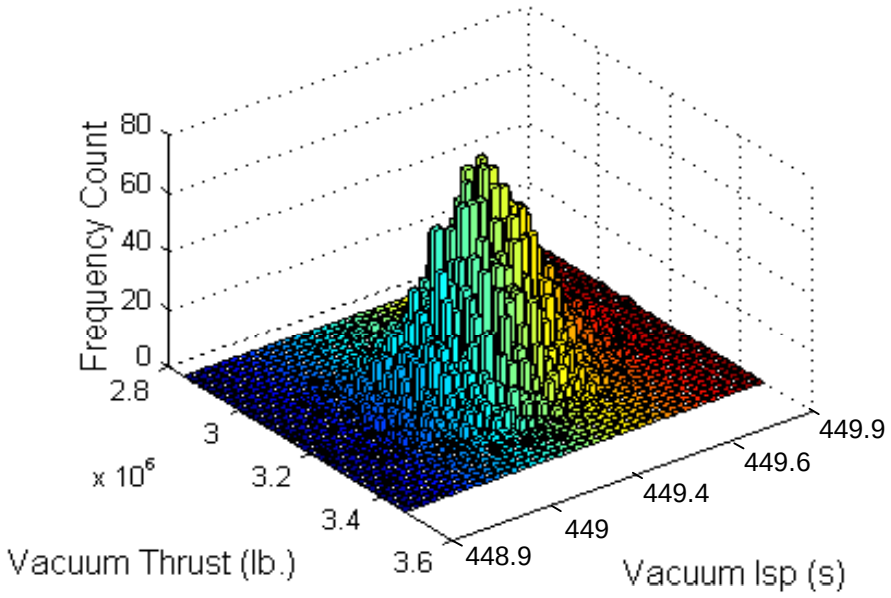

Figure 40 – Histogram of Vacuum Thrust and Isp for Propulsion RSE/MC

Figure 40 and Figure 41 are visually quite similar to the direct Monte Carlo simulation. Overall, the response surface method performed well on this problem and is a viable candidate for inclusion in the system level probabilistic optimization.

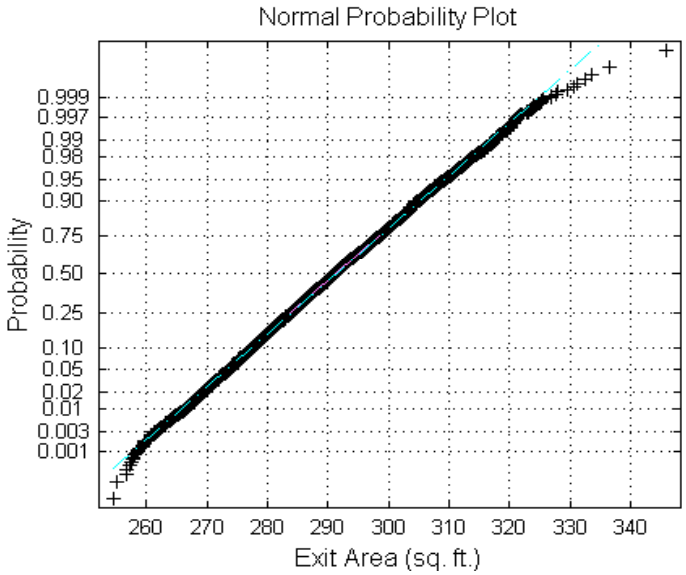

Figure 41 – Normal Probability Plot for Exit Area from Propulsion RSE/MC

7.5 DPOMD Procedure

The procedure for the DPOMD test on propulsion was identical to the other tests except for the reduction in the fractional factorial design in the fractional factorial-based DPOMD. In this case, because of the limited number of input variables, a reduction of zero was selected, creating a full factorial version of this method. The binomial distribution DPOMD method [91] could not be used because the inputs were not independent.

The full factorial design was generated at levels of –1 and +1 for the four uncertainty variables, then an inverse Hasofer-Lind transform [138] based on the mean vector and covariance matrix of the input variables was applied to the variables in the DoE. See section 5.2.14 on DPOMD in the background chapter for details on this

process. The resulting table of runs was then a discrete probability distribution with the same mean vector and covariance matrix as the input random variables. This method did not take into consideration any skewness information, so the skewness in the triangular distribution for power-to-weight ratio was not taken into account.

This table of runs was executed using SCORES [162] and the output parameters of interest were recorded. These parameters were then analyzed using sample estimates for mean, standard deviation and correlation coefficient, similar to those shown in Eqns. 6.1-2. These parameters were compared using relative error to the results of the Monte Carlo simulation. This comparison is shown in Table 17.

The negligible amount of adaptation required to analyze this new problem shows one of the advantages of the DPOMD method. For the types of problems observed in this research, the only user input required was a reduction factor indicating the desired number of runs and the input distribution information

7.6 DPOMD Results

The results of this test in Table 17 show that the DPOMD is accurate again. The only areas for concern with respect to relative error is on a pair of correlation coefficients that are very close to zero. These errors are acceptable given the absolute error values associated with them are quite small.

Table 17 – Results of Propulsion DPOMD Simulation

Variable	Monte Carlo Result	95% c. l.	DPOMD Result	Abs. Rel. Error
Exit Area (Ae) Mean	295 sq. ft.	± 0.2 sq. ft.	295 sq. ft.	3.09e-3 %
Exit Area Std. Dev.	10.1 sq. ft.	± 0.14 sq. ft.	10.4 sq. ft.	2.68 %
Vacuum Thrust (Tvac) Mean	3.145 Mlbs.	± 1.5 klb.	3.144 Mlbs.	0.0260 %
Vacuum Thrust Std. Dev.	76.86 klbs.	± 1.07 klb.	78.9 klbs.	2.65 %
Engine Thrust-to-Weight (T/We) Mean	54.3	± 0.1	54.3	0.0206 %
Engine Thrust-to-Weight Std. Dev.	5.05	± 0.07	5.20	3.10 %
Vacuum Specific Impulse (Ispvac) Mean	449.4 sec.	± 0.002 sec.	449.4 sec.	4.30e-4 %
Vacuum Specific Impulse Std. Dev.	0.122 sec.	± 0.0017 sec.	0.127	3.71 %
Ae / Tvac Correlation Coefficient	83.0 %	± 0.6%	82.8 %	0.300 %
Ae / T/We Correlation Coefficient	-3.43 %	± 2%	3.48 %	1.39 %
Ae / Ispvac Correlation Coefficient	-71.2 %	± 0.1%	-71.4 %	0.233 %
Tvac / T/We Correlation Coefficient	-1.14 %	± 2%	-0.967 %	15.4 %
Tvac / Ispvac Correlation Coefficient	-20.1 %	± 1.9%	-19.9 %	1.10 %
MRreq / Ae Correlation Coefficient	10.7 %	± 1.9%	10.5 %	1.78 %
Mrreq / Tvac Correlation Coefficient	14.6 %	± 1.9%	14.7 %	0.638 %
Mrreq / T/We Correlation Coefficient	-0.340 %	± 2%	2.33e-5 %	100 %
GLOW / Ae Correlation Coefficient	70.5 %	± 1%	70.0 %	0.645 %
GLOW / Tvac Correlation Coefficient	98.0 %	± 0.08%	98.0 %	0.0388 %
GLOW / Ispvac Correlation Coefficient	-0.421 %	± 2%	0.00 %	100 %

The fact that this simulation consists of only sixteen runs does take away from the appearance of the histogram of vacuum thrust and vacuum Isp in Figure 42. If a constraint were to be applied to the engine exit area, a normal curve would also need to be fit, due to the sparseness of the data points. A normal probability plot showing roughly Gaussian behavior is in Figure 43.

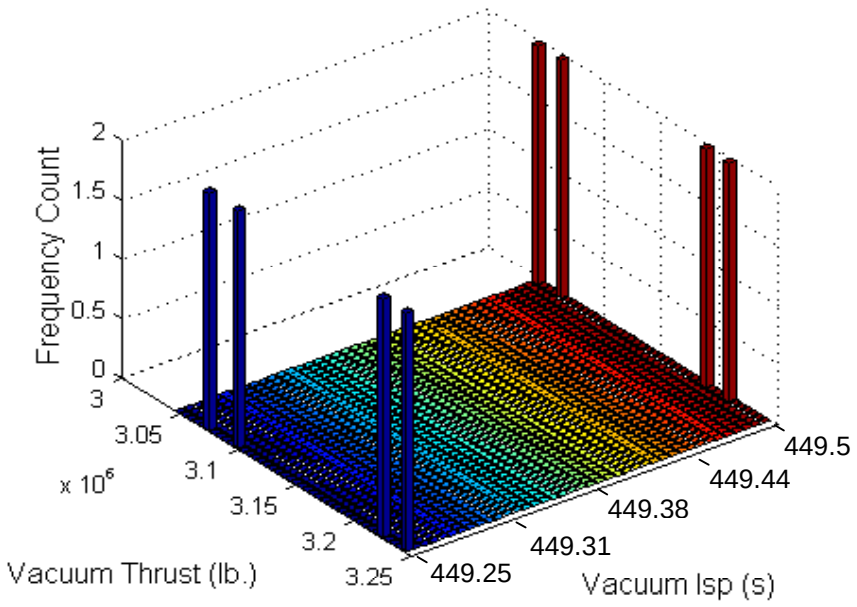

Figure 42 – Histogram of Vacuum Thrust and Isp for Propulsion DPOMD

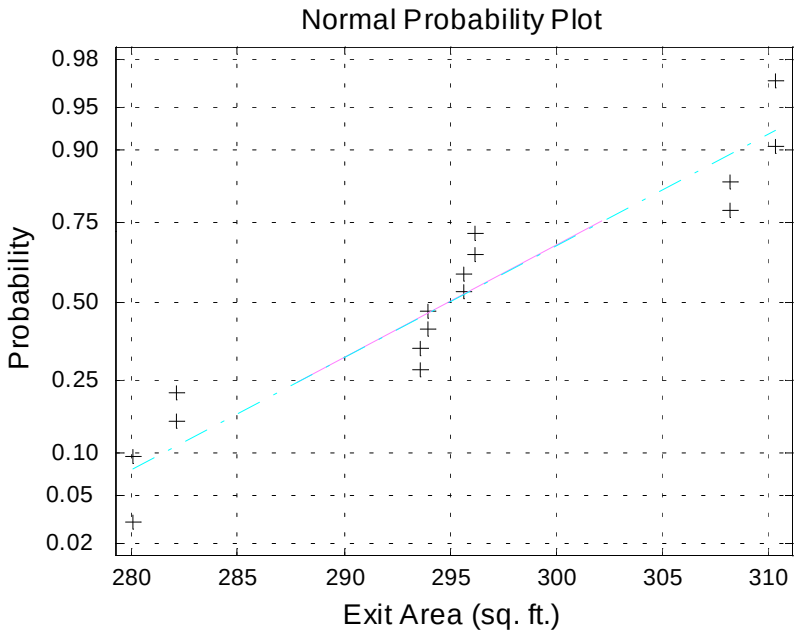

Figure 43 – Normal Probability Plot of Exit Area for Propulsion DPOMD

7.7 Descriptive Sampling

The same routine used to generate the probability map for the mass properties analysis was used for the propulsion analysis for sample sizes of 50 and 100. Once the probability map was generated, it could be conducted treated like any other Monte Carlo simulation using uniform [0,1] pseudo-random numbers. This was done by means of an inverse cumulative probability function transform, as described in detail in the previous section on the mass properties descriptive sampling test.

The distribution variables sampled were identical to that of the Monte Carlo and DPOMD simulations. The extra deterministic variables that were present in the response surface method test were not required, as this method was expected to be run each time a new output distribution was required.

7.8 Descriptive Sampling Results

The results in Table 18 show that the descriptive sampling method works well for predicting the means and standard deviations of the outputs. Many of the errors in correlation coefficient seem to be quite high. However, upon closer inspection, most of these extreme values are all near zero, creating misleading relative errors. Despite this, on some of the correlation coefficients, the method did not seem to be accurate enough. More specifically the mass ratio required and vacuum thrust correlation coefficient error on the 100 run version had both a high absolute and relative error. The same was true for the correlation between the engine exit area and thrust-to-weight at sea level.

Figure 44 shows the similarity in appearance between the descriptive sampling and Monte Carlo simulations. Although over a much more coarse grid than that of the Monte Carlo simulation, the 100 run version of the method is beginning to show a multivariate normal behavior. This is impressive considering the limited number of runs.

The normal probability plot in Figure 45 shows that with descriptive sampling, the output variable exit area retains the normal characteristics of the Monte Carlo simulation result. This was an important consideration for confidence level testing. It meant that a simple counting method could be used in place of an assumed distribution function.

Table 18 – Results for Descriptive Sampling Propulsion Test

Variable	Monte Carlo Result	95% c. l.	50 run DS Result	Abs. Rel. Error	100 run DS Result	Abs. Rel. Error
Exit Area (Ae) Mean	295 sq. ft.	± 0.2 sq. ft.	295 sq. ft.	0.00106 %	295 sq. ft.	0.00322 %
Exit Area Std. Dev.	10.1 sq. ft.	± 0.14 sq. ft.	9.73 sq. ft.	3.32 %	10.2 sq. ft.	0.917 %
Vacuum Thrust (Tvac) Mean	3.145 Mlb.	± 1.5 klb.	3.144 Mlb.	0.0268 %	3.144 Mlb.	0.0259 %
Vacuum Thrust Std. Dev.	76.86 klb.	± 1.07 klb.	75.4 klb.	1.93 %	77.97 klb.	1.45 %
Engine Thrust-to-Weight (T/We) Mean	54.3	± 0.1	54.3	0.0198 %	54.3	0.0241 %
Engine Thrust-to-Weight Std. Dev.	5.05	± 0.07	5.10	1.03 %	5.04	0.0310 %
Vacuum Specific Impulse (Ispvac) Mean	449.4 sec.	± 0.002 sec.	449.4 sec.	4.03e-4 %	449.4 sec.	4.06e-4 %
Vacuum Specific Impulse Std. Dev.	0.122 sec.	± 0.0017 sec.	0.122 sec.	0.322 %	0.123 sec.	0.448 %
Ae / Tvac Correlation Coefficient	83.0 %	± 0.6%	81.6 %	1.69 %	83.4 %	0.480 %
Ae / T/We Correlation Coefficient	-3.43 %	± 2%	-14.9 %	334 %	5.12 %	249 %
Ae / Ispvac Correlation Coefficient	-71.2 %	± 0.1%	- 69.7 %	2.13 %	- 71.3 %	0.120 %
Tvac / T/We Correlation Coefficient	-1.14 %	± 2%	-10.3 %	798 %	5.52 %	583 %
Tvac / Ispvac Correlation Coefficient	-20.1 %	± 1.9%	-15.5 %	22.7 %	- 20.9 %	4.05 %
MRreq / Ae Correlation Coefficient	10.7 %	± 1.9%	11.2 %	5.10 %	13.0 %	22.1 %
Mrreq / Tvac Correlation Coefficient	14.6 %	± 1.9%	14.2 %	2.63 %	26.2 %	79.2 %
Mrreq / T/We Correlation Coefficient	-0.340 %	± 2%	-2.72 %	699 %	2.23 %	754 %
GLOW / Ae Correlation Coefficient	70.5 %	± 1%	68.5 %	2.78 %	71.2 %	1.03 %
GLOW / Tvac Correlation Coefficient	98.0 %	± 0.08%	98.0 %	0.0491 %	98.1 %	0.0618 %
GLOW / Ispvac Correlation Coefficient	-0.421 %	± 2%	4.46 %	1,160 %	-1.56 %	271 %

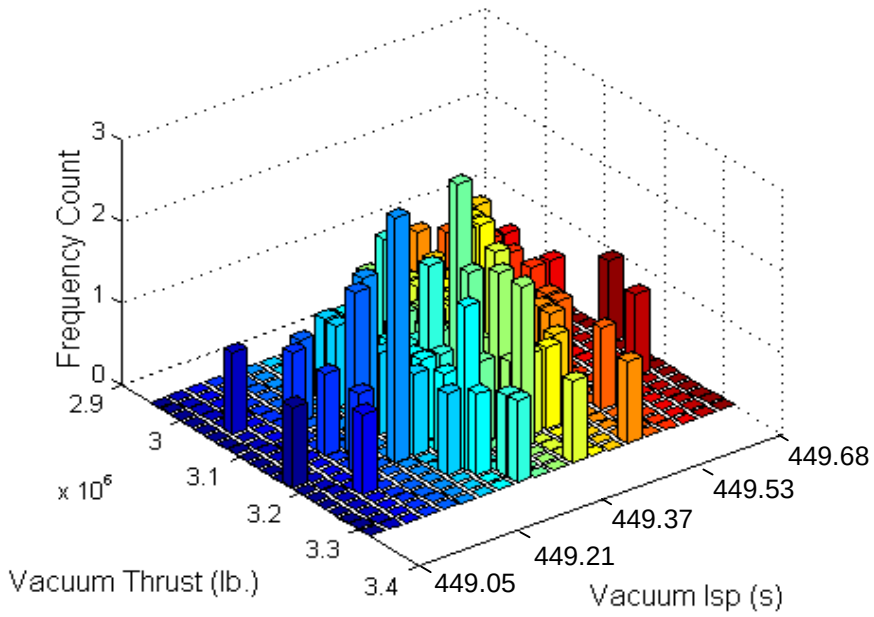

Figure 44 – 100 Run Descriptive Sampling Histogram of Vacuum Thrust and Isp

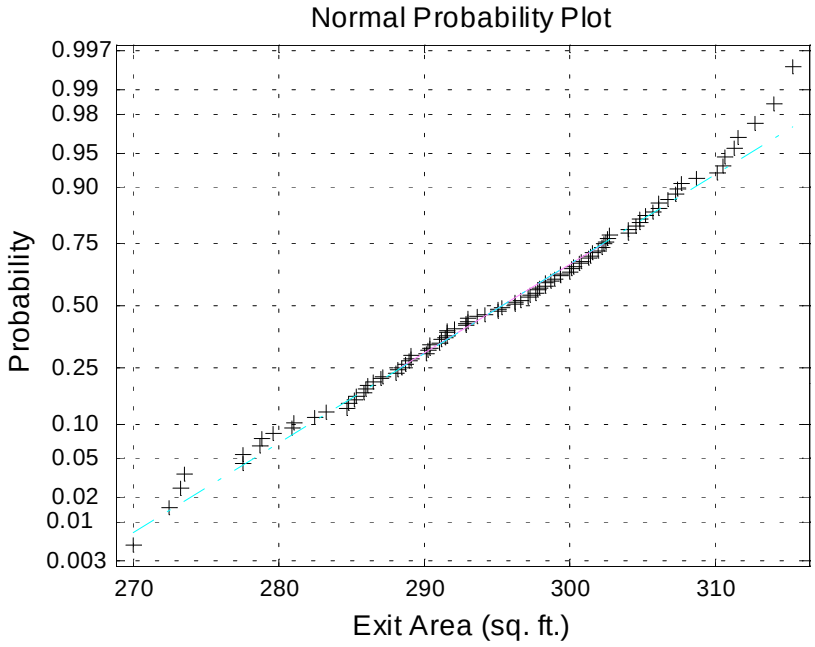

Figure 45 – 100 Run Descriptive Sampling Normal Probability Plot for Exit Area

7.9 Overall Comparisons

The goal of this section was to provide a fast and accurate method for estimating the output distribution information of a rocket engine design simulation. This goal has been met in that several methods showed low error in estimating the probability of several parameters for the propulsion contributing analysis.

Another goal was to measure the error in approximating the probabilistic analysis using the best possible method. The chosen method, DPOMD, showed minimal errors on all the output parameters of interest. There should not be any problems when applying this method to the propulsion contributing analysis.

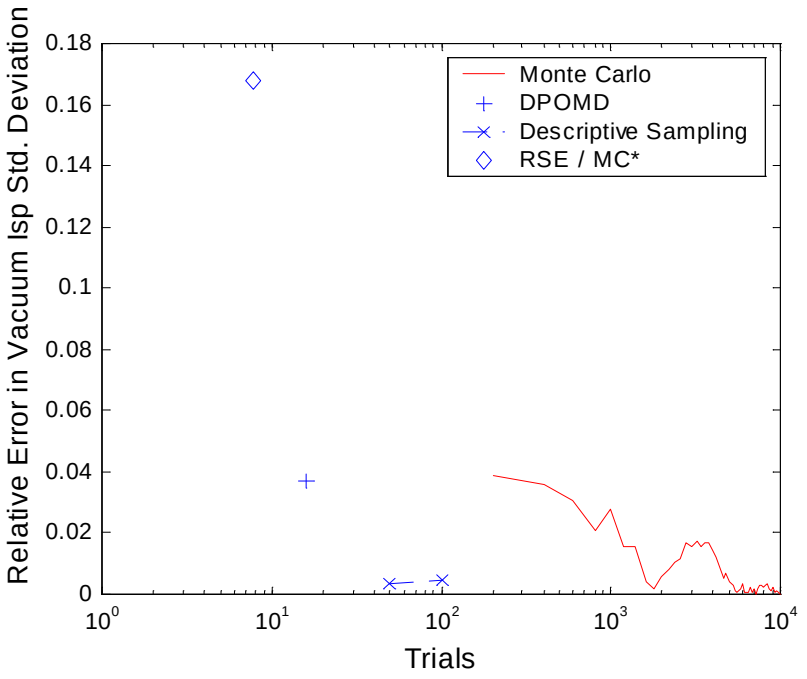

Figure 46 – Relative Errors in Vacuum Isp Std. Deviation

The relative error history in Figure 46 shows why the response surface method was eliminated from contention for use in the full system-level optimization problem. It's error in estimating the very important engine efficiency standard deviation was far too high. The other methods had errors an order of magnitude lower for this parameter. Figure 47 shows a parameter for which all the methods performed reasonably. It is likely a coincidence, but the error in the approximations seems to be decreasing rather exponentially with computational effort for this case.

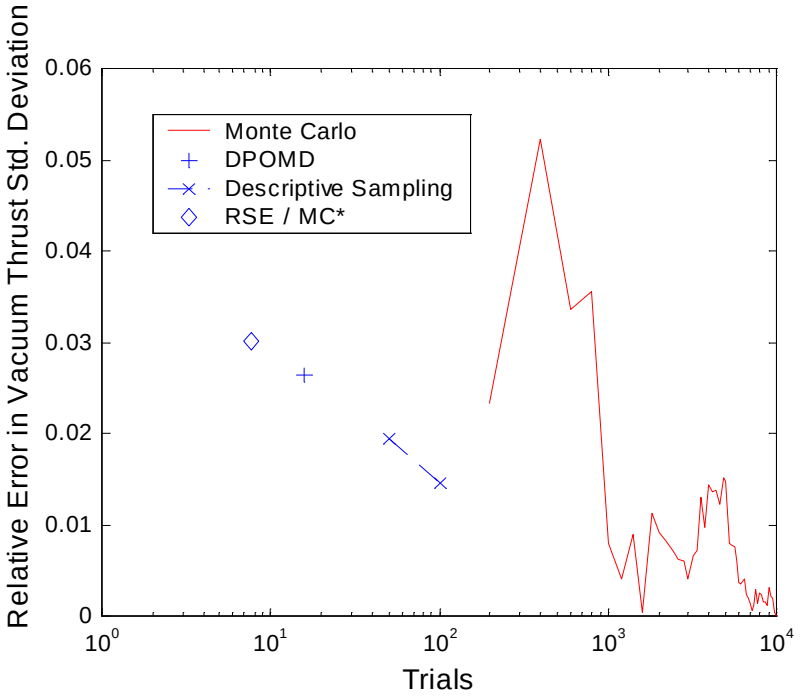

Figure 47 – Relative Errors in Vacuum Thrust Std. Deviation

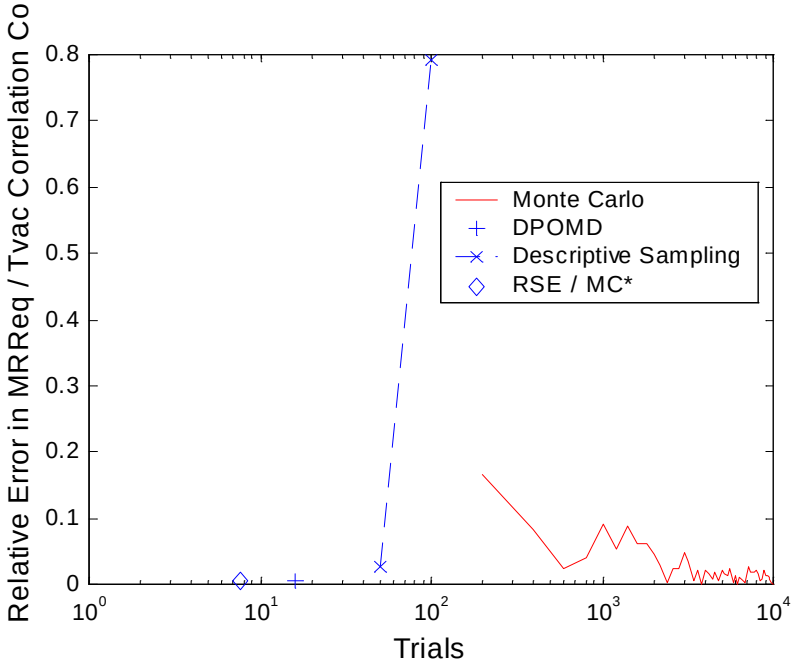

Figure 48 – Relative Errors in MRReq / Tvac Corr. Coeff.

Figure 48 illustrates the difficulty the otherwise accurate and efficient descriptive sampling method had with predicting some of the correlation coefficients in this research. For this particular problem, the most serious error was present in the correlation between mass ratio required and vacuum thrust. The relative error is also not due to any scaling problems, as the baseline value was 14%, sufficiently far from zero to use relative error in a meaningful way.

The execution times of the above methods are hinted at in the previous figures. These times varied greatly from one method to the other, as evidenced by the use of a log scale in the summary figures. The amount of computational time required for the runs for each method is given in Table 19.

Table 19 – Computational Time for Propulsion Uncertainty Methods

Method	Trials	Platform	Time
Monte Carlo	10,000 SCORES calls	SGI Octane	24 min.
Descriptive Sampling	100 SCORES calls	SGI Octane	14 sec.
Descriptive Sampling	50 SCORES calls	SGI Octane	7 sec.
DPOMD	16 SCORES calls	SGI Octane	2.3 sec.
RSE / MC	10,000 C++ RSE calls	SGI Octane	1.1 sec

Taking into account accuracy and time considerations, the best method for estimating the uncertainty of the propulsion contributing analysis appears to be the full factorial DPOMD method. It was reasonably accurate, though not the best, in the mean and standard deviation output parameters. It also had no significant errors in any of the correlation coefficients, which could not be said for any of the other approximation methods.

CHAPTER VIII

TRAJECTORY ANALYSIS TEST

The trajectory analysis for this test was a single stage to orbit (SSTO) trajectory utilizing the POST [163] trajectory optimization program. It takes a set of pitch control variables at selected points along the trajectories and optimizes these for a user specified objective, usually the maximization of burnout weight, while at the same time meeting constraints based on desired burnout conditions, usually a target orbit. This idea is illustrated in Figure 49.

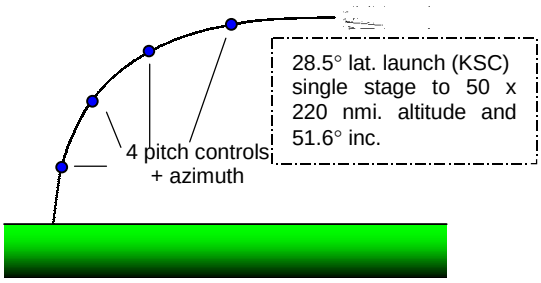

Figure 49 – Trajectory Optimization Diagram

This was a deterministic analysis when taken alone. However, with the inclusion of the GRAM99 [164] atmosphere model, the trajectory analysis included a larger number of noise variables than either of the previous analyses. This model used regressed atmosphere data for selected launch ranges around the world to predict atmospheric conditions given certain known factors. For this Monte Carlo simulation, the known

factors were considered random within a reasonable set of ranges. For the other analyses, because GRAM99 is an inherently stochastic program, the results of a Monte Carlo simulation of just GRAM99 had to be fit at certain key points in the atmosphere in order to use the listed approximation methods. These key points were selected by visual inspection of the mean results for the GRAM99 Monte Carlo for the atmospheric parameters important to the physics of the trajectory simulation.

Once the deterministic version of the stochastic problem was formulated, several candidate methods for probabilistic analysis were tested at acceptable levels of computational expense. These candidate methods were the same as those in the previous tests. They were response surface / Monte Carlo analysis, descriptive sampling and discrete probability optimal matching distributions. These methods were tested for speed and accuracy on selected noise, coupling and output variables based on the goals and objectives stated in the goals and objectives chapter.

While there are many possible outputs from trajectory into other contributing analyses, experience with this contributing analysis for this particular system problem indicates that the only output variable absolutely necessary is the mass ratio required to make the target orbit. However, due to the unique requirements of the probabilistic multidisciplinary design framework, the correlation of one of the outputs to one of the inputs was also required. This is because the input gross liftoff weight (GLOW) and the output mass ratio required are both inputs to the propulsion contributing analysis. Generating these required correlations is one of the important aspects of the proposed probabilistic framework.

The inputs for the analysis include all the information required to perform the analysis and optimization of the trajectory. This translates to information that must be given the GRAM99 [164] in order to generate a random atmosphere deck. Also, for the test, the vehicle outer mold line (OML), including the engine exit area was assumed to be constant. This list of input noise variables is therefore as follows:

- Vehicle gross liftoff weight (GLOW) – This gives the trajectory analysis a necessary initial condition to start its trajectory integration.
- Vehicle thrust at vacuum condition (Tvac) – For a bell nozzle liquid rocket engine, this parameter, combined with total engine exit area gave the trajectory information about the thrust of the engine through a range of altitude conditions.
- Engine Specific Impulse at vacuum condition (Isp_{vac}) – This described the propellant efficiency of the engine.
- Multiplier on C_l (Cl_mult) – This variable changed the overall aerodynamic lift coefficient at all conditions to simulate errors in the aerodynamic modeling.
- Multiplier on C_d (Cd_mult) – This changed the overall aerodynamic drag coefficient at all conditions again to simulate errors in aerodynamic modeling.
- Year of launch (year) – Information required by GRAM99 in order to generate accurate atmospheric condition scenarios.
- Month of launch (month) – Information required by GRAM99 in order to generate accurate atmospheric condition scenarios.
- Day of launch (day) – Information required by GRAM99 in order to generate accurate atmospheric condition scenarios.
- Hour of launch (hour) – Information required by GRAM99 in order to generate accurate atmospheric condition scenarios.

The multipliers on coefficients of drag and lift Cd and Cl were solely to account of errors in the aerodynamic dataset. The program APAS [165] was used to generate the aerodynamic datasets for the OML of the launch vehicle used. It used a vortex panel method for subsonic and supersonic calculations and impact methods for hypersonic aerodynamics. The error for this code has been informally rumored to be about +/- 10%. However, as with any aerodynamic prediction, huge errors are possible from relatively small-scale phenomena. The other noise inputs are either probabilistic coupling variables to other contributing analyses, or inherently unknown quantities, like the time of launch.

It is important to note that these inputs were only used in the direct Monte Carlo trajectory simulation. The other analyses required parameterization of the atmospheric inputs. This yielded a different and much larger set of inputs for the approximation methods. These sets will be described later in more detail in the sections on approximation methods for trajectory uncertainty analysis.

8.1 Monte Carlo Simulation

To calibrate the approximation methods, a Monte Carlo simulation of the combined trajectory / atmosphere problem was conducted. This used the variables listed above using distributions as described in Table 20. It is interesting to note that the simulation could not launch at the end of most months to avoid an error when launching in February. This was done because limitations in the input format for GRAM99.

Table 20 – Monte Carlo Simulation Input Variable Levels

Variable	Distribution Type	Mean	Std. Dev.	X1	X2	X3
GLOW	Normal	2.1 Mlb.	50 klb.	N/A	N/A	N/A
Tvac	Normal	2.9 Mlb.	50 klb.	N/A	N/A	N/A
Ispvac	Normal	451 sec.	0.5 sec.	N/A	N/A	N/A
Clmult	Triangular	N/A	N/A	0.9	1.0	1.1
Cdmult	Triangular	N/A	N/A	0.9	1.0	1.1
Year	Uniform	N/A	N/A	2005	2015	N/A
Month	Uniform	N/A	N/A	1	12	N/A
Day	Uniform	N/A	N/A	1	28	N/A
Hour	Uniform	N/A	N/A	0	24	N/A

The above input variables were used to generate 10,000 trials which were executed using a scripted program that first ran GRAM99 to generate an atmosphere data deck, then ran POST [163] to generate a trajectory optimized for propellant consumed for each given scenario. The atmosphere data deck altitudes were selected to provide thirty evenly spaced altitudes through time for a typical SSTO rocket trajectory. This ensured that atmosphere information was available over the entire course of the trajectory. The random number generation scheme was the built-in Matlab© random number generator function [152].

The simulation consisting of 10,000 trials took approximately 12 hours to complete, with some extra manual interface time required to adjust trajectories that did not optimize. Overall, the process of evaluating the trials took approximately one day.

This was not remotely fast or automated enough to allow for optimization of the probabilistic problem. Therefore, finding a fast approximation method was imperative to incorporating this method into the probabilistic MDO framework. The results in Table 21 will therefore be used as a reference for evaluating these approximation methods, as described in the goals and objectives section of this thesis.

Table 21 – Trajectory Optimization Monte Carlo Simulation Results

	MRreq μ	MRreq σ	Mrreq/GLOW corr.
Monte Carlo	7.8934	0.0328	15.9%
95% c. l.	$\pm$ 0.00064	$\pm$ 0.00045	$\pm$ 1.9%

A histogram of the mass ratio (Figure 50) required from this simulation shows that the response has a very normal behavior. This is important to note, as the proposed probabilistic multidisciplinary framework assumes that the coupling distributions have normal behavior. This fact is confirmed by the normal probability plot of MR required in Figure 51.

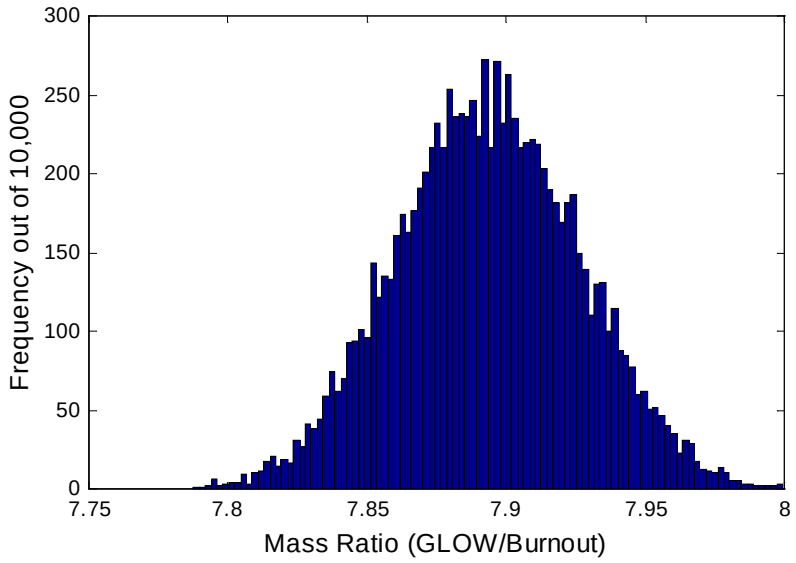

Figure 50 – Histogram of MR Required by Trajectory Monte Carlo Simulation

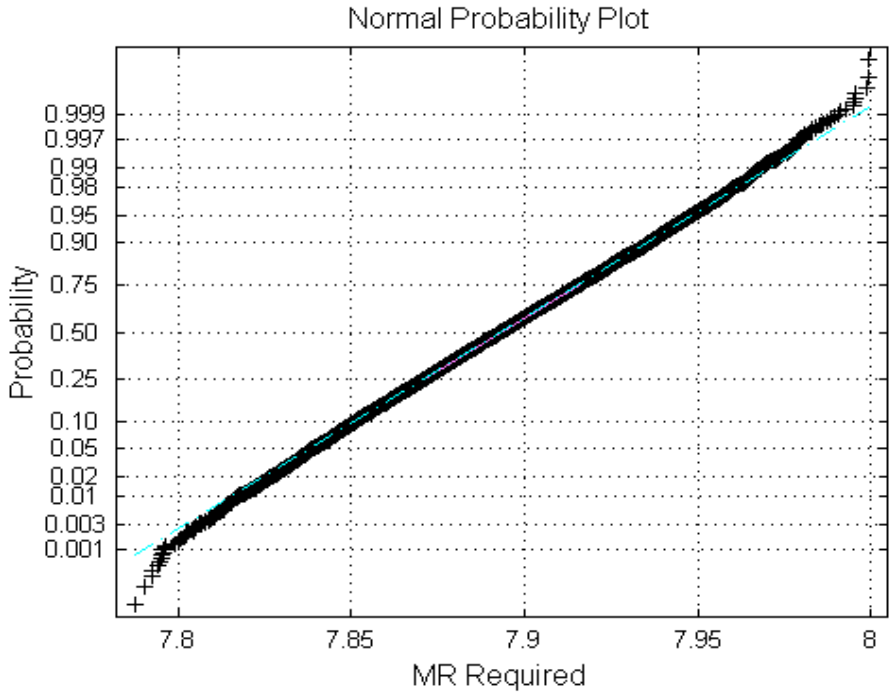

Figure 51 – Normal Probability Plot of MR Required

The goals of this simulation were to provide reference data for the subsequent approximation methods and to confirm that the coupling variables were in fact normal. These goals were achieved, as GLOW was assumed as an input to be normal, and mass ratio required was shown in Figure 50 and Figure 51 to be similarly normal.

8.2 Atmospheric Point Reduction Process

The approximation methods for this analysis could not be used on the same analysis as the Monte Carlo simulation due to the inherent randomness of the GRAM99 atmospheric model. Therefore, a multivariate normal distribution was fit to the data at selected points for each atmospheric parameter. The results were the same points used for the trajectory in the earlier Monte Carlo simulation.

Because the number of atmosphere data points (204) was too high to effectively use an uncertainty approximation method, the number of atmosphere points had to be reduced. The points were reduced by visually inspecting the mean values of the results of a Monte Carlo simulation performed on the GRAM99 atmosphere model. Only the points necessary to satisfy the trends of the mean atmospheric parameters were retained. This section reviews this selection process.

The means of the distributions at each of the points could be used as the criteria because of the relatively small perturbations from the means due to randomness. Figure 52 shows uncertainty bands of plus and minus 5 standard deviations for air density. This is the number of standard deviations required to actually see the bands on the plot.

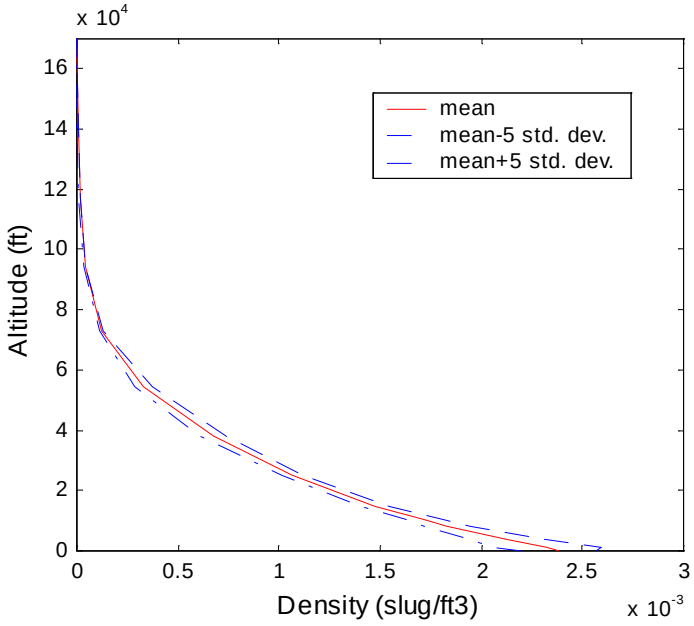

Figure 52 – Density v. Altitude with Uncertainty Bands

The parameters required by the trajectory analysis as a function of altitude were the following:

- Pressure – Ambient atmospheric pressure in lb./ft.^{2}
- Density – Ambient atmospheric density in slug/ft.^{3}
- Temperature – Ambient temperature in °R.
- Northern wind – wind velocity in the northerly direction in fps.
- Eastern wind – wind velocity in the easterly direction in fps.
- Vertical wind – downward wind velocity in fps.

These factors were calculated for 10,000 random trials based on random inputs the same as those used in the combined trajectory / GRAM99 Monte Carlo simulation performed in the previous section. A single multivariate normal distribution was then fit to all 204 output responses. After that, the means of each dimension of this multivariate normal distribution were plotted and points for the reduced atmosphere model selected using these plots.

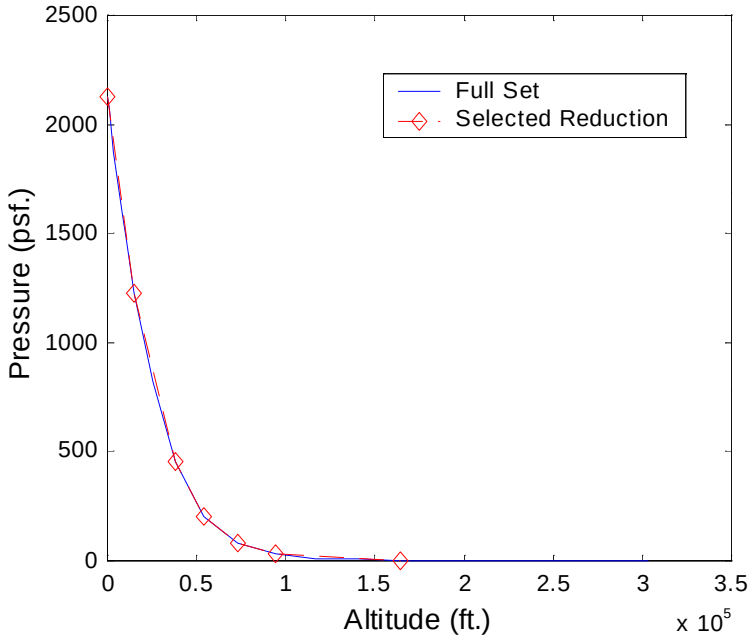

Figure 53 – Pressure Points Selected for Reduced Atmosphere Model

The plot for mean pressure in Figure 53 showed an exponential decay, as was to be expected. The dotted line shows the linear interpolation between the points. This seven point interpolation is nearly indistinguishable from the thirty four point version shown by

the solid line. The final pressure on the interpolation table at an altitude of 210,000 ft. was assumed to be zero.

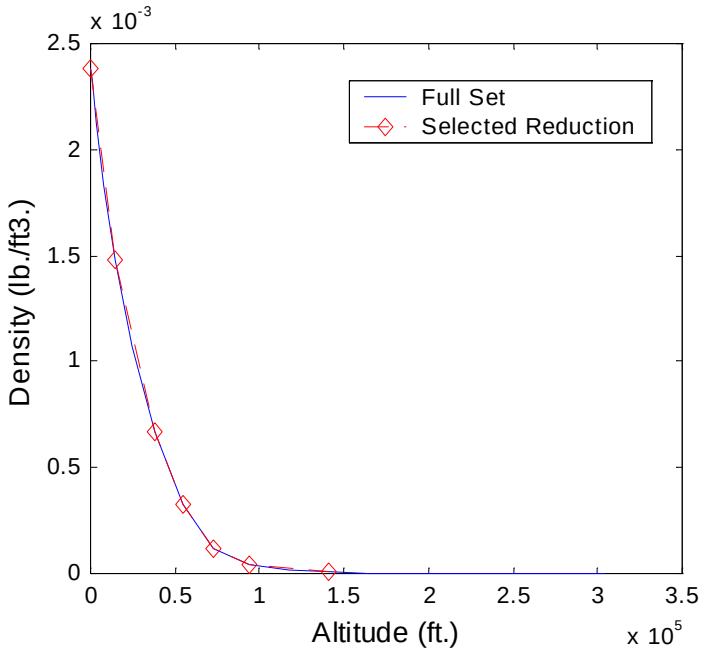

Figure 54 – Density Points Selected for Reduced Atmosphere Model

The plot for density in Figure 54 shows similar behavior to the pressure plot, therefore points were taken at similar altitudes. Again, the seven points approximation is hard to distinguish from the thirty four point version. The final density of zero was also placed at 210,000 ft., just like the pressure table.

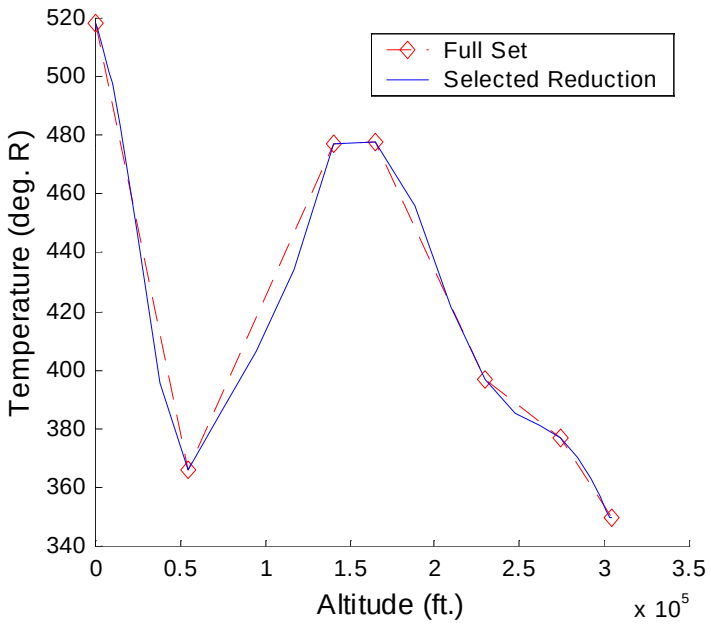

Figure 55 - Temperature Points Selected for Reduced Atmosphere Model

Figure 55 showed that the temperature plot proved slightly more difficult to fit, but still is well represented by the reduced point table. For this table, because the temperature does not ever reach zero, the final value for the table was selected at an altitude of 304,000 ft. and was assumed to have the distribution described by GRAM99. It is important to note that the POST trajectory analysis was set to no extrapolation for all input tables, so this temperature would not be changed above this altitude during any of the trajectory simulation trials.

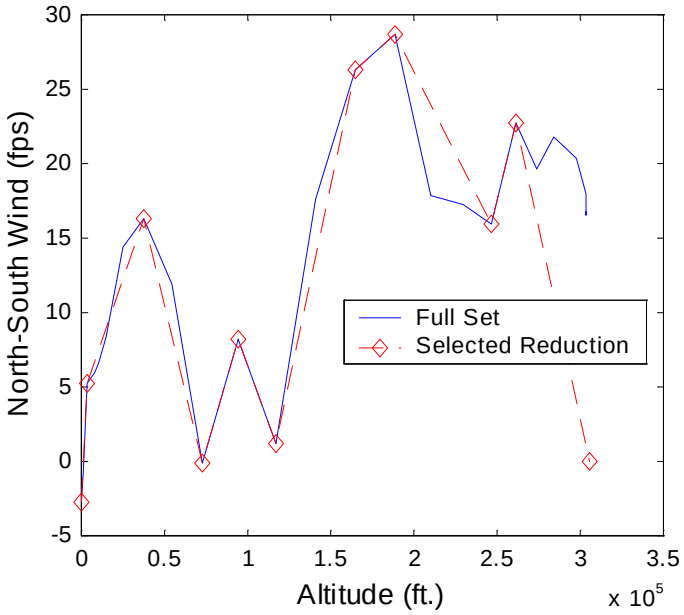

Figure 56 – North Wind Points Selected for Reduced Atmosphere Model

Because the northerly wind (Figure 56) was a little more erratic than the previous parameters, more points were used to reduce the dataset. In this case, eleven points were selected at various altitudes, representing the changes in direction and magnitude for this particular wind component. While the fit of the linear interpolation seemed to fail at higher altitudes, it should be noted that the air density was assumed to be zero above 210,000 ft. This means that these points would not have had any force effect on the vehicle.

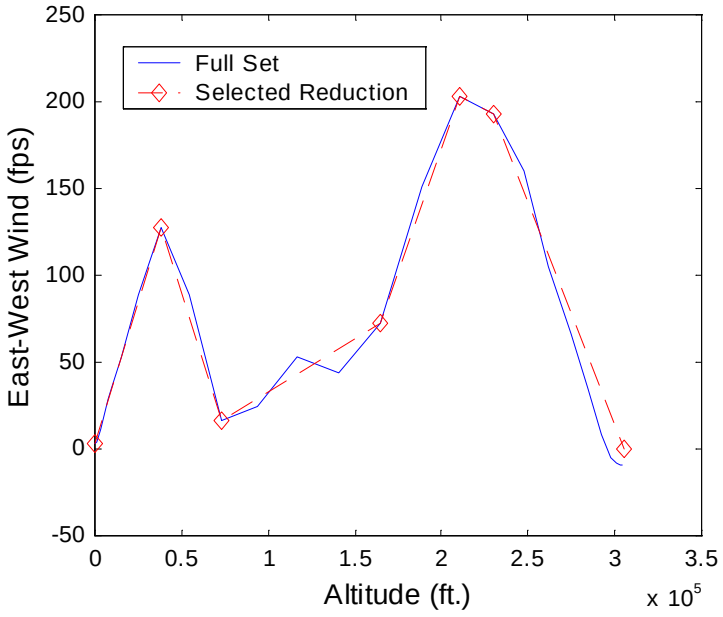

Figure 57 – East Wind Points Selected for Reduced Atmosphere Model

The fit on the east wind component in Figure 57 using the reduced number of points was quite good. This is important as it is expected to be the most influential of the wind components, because of the direction of the launch and the expected magnitude of the wind. Changes in the body axis velocity should have had the biggest effect on the overall trajectory performance, and the screening array results presented later in Table 22 confirm this. Overall, seven points were used to represent this quantity.

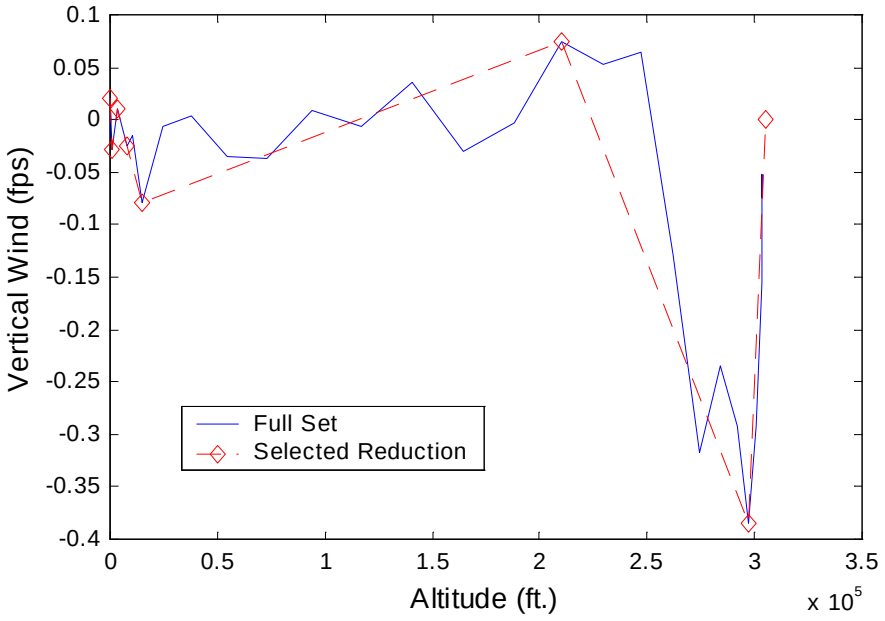

Figure 58 – Vertical Wind Points Selected for Reduced Atmosphere Model

While the vertical wind (Figure 58) was the most erratic and least accurately fit of the parameters, the magnitude of the vertical wind components were small at low altitudes. This where they would have had the best chance to have an effect on the vehicle, so this was the area best represented by the reduced point set. At higher altitudes, there are upward wind components, but these were so high as to be unlikely to have an effect on the trajectory. Eight points were used to represent this quantity.

The selection process presented here left the trajectory contributing analysis with 49 total variables, 5 that go directly into the trajectory analysis and 44 variables used to describe the atmospheric conditions. This means that the trajectory contributing analysis is now ready for the application of uncertainty approximation methods. A listing of the distribution information for the 44 atmospheric variables is available in Appendix A.

8.3 Response Surface Method

Once the atmospheric inputs had been parameterized, the application of response surface methods was possible. This began with the application of a 49 variable screening array. The array was a $2^{(49-43)}_{III}$ fractional factorial array of 64 runs. It could only generate effect estimates for main effects. This screening was therefore based only on the main effects of the 49 variables in question. The screening was also solely based on the contribution to the MR required response. This was the only output required using a response surface model.

The results of the screening array show that the variables that went directly into the trajectory analysis contribute to the vast majority of the response. With the exception of the lift coefficient multiplier, these direct variables were all the top contributors to the response. This can be easily seen in Figure 59. The Pareto plot indicated that the top eight variables contribute to well over 80% of the response and should create an effective response surface representing the entire analysis.

Besides the direct variables, the atmospheric variables that contribute are the sea level ambient pressure (P1) and easterly wind (EW1), along with the air density at 54,000 ft. The importance of these variables makes sense physically. The sea level ambient pressure has a large effect on not only the thrust of the rocket engine, but also its propellant efficiency. The easterly wind makes sense because this is the closest compass heading to the direction of launch, and will effect the velocity of the vehicle when it is moving slowly and its velocity most easily changed. Finally the air density at 54 kft. makes sense because that is where the vehicle passes through transonic into supersonic and is the highest atmospheric drag point in the trajectory.

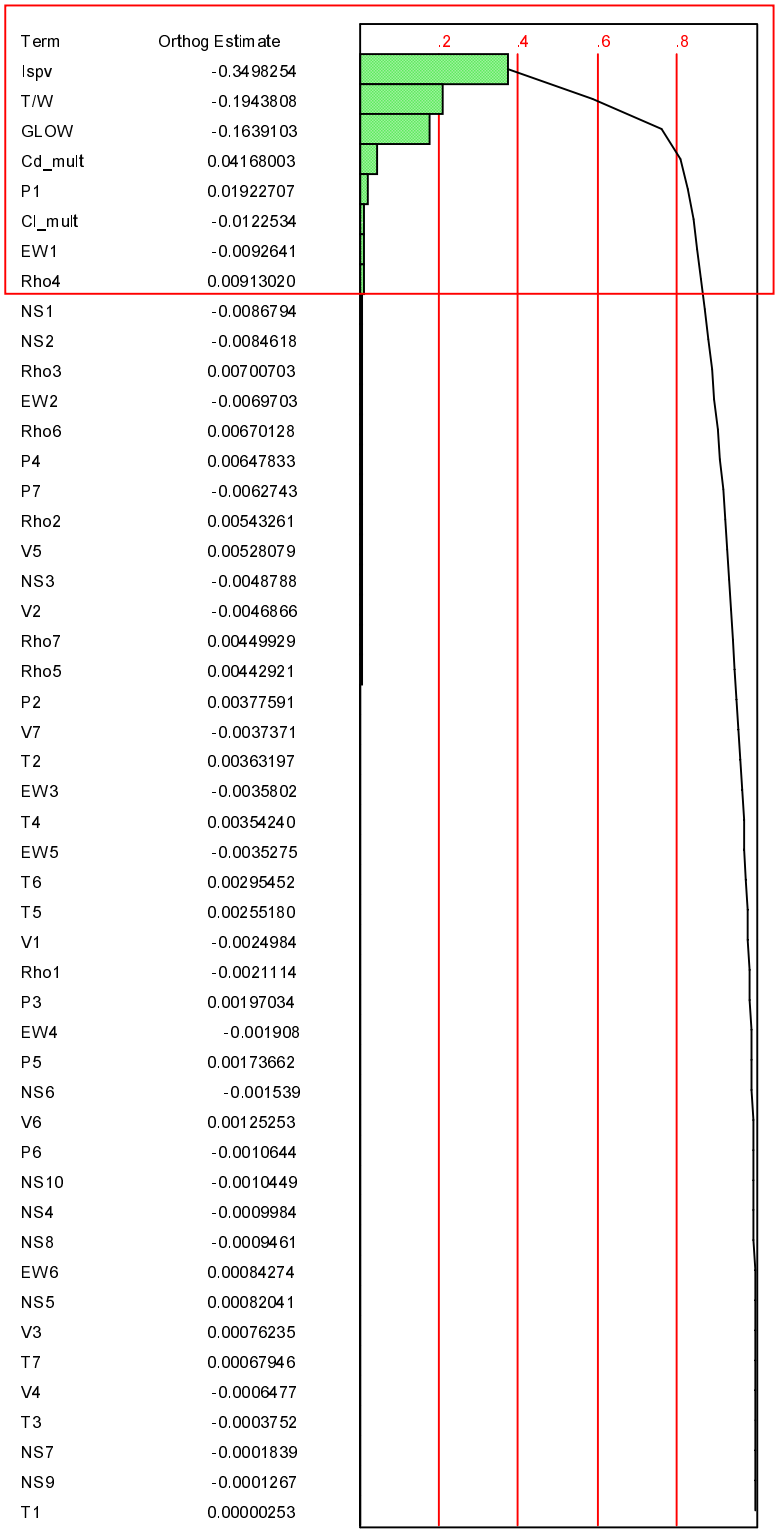

Figure 59 – Pareto Plot for MR Required

In summary for the screening, the variables selected and their levels are listed in Table 22 in order of their contribution to the response.

Table 22 – Selected Variables and Levels for Trajectory RSE

Variable	Low Setting	High Setting
Ispv (engine vacuum specific impulse)	440 sec.	460 sec.
T/W (vehicle liftoff thrust to weight ratio)	1.2	1.5
GLOW (vehicle gross liftoff weight)	1.5 Mlbs.	4.0 Mlbs.
Cd_mult (multiplier for vehicle drag)	0.9	1.1
P1 (Ambient air pressure at sea level)	1980 psf.	2280 psf.
Cl_mult (multiplier for vehicle lift)	0.9	1.1
EW1 (east-direction wind)	-60.1 fps.	65.6 fps.
Rho4 (Air density at 54 kft.)	2.96e-4 slug/ft^3	3.61e-4 slug/ft^3

Once the variables and levels were decided for the trajectory response surface, two different methods for generating the response surface were tested. The first was a uniform central composite design for eight variables comprising 273 runs, not including redundant center points. The second experiment design tested was a D-Optimal design for eight variables. This design contained 236 runs. After the responses for both the arrays were generated, they were both fit to the same quadratic equation of the form in Eqn. 6.3.

The central composite design was created using the JMP© [137] statistical software package. It was evaluated at the same levels, but with the center point defined as the average of the high and low levels. The variables not selected for the RSE were set to their mean values.

The results of the central composite experiment were then fit using stepwise regression, as described in the section on the mass properties test. This was done to minimize the noise created by polynomial coefficients with little influence. The adjusted R-square result of this fitting process was 0.9996. This was quite good. The D-optimal design was also created using the JMP© statistical software package. First, a three level full factorial design was created. This design was then reduced using a D-optimal algorithm [166, 167] with the settings described in Table 23. Once the design was determined, the experiment was evaluated. The results were fit using stepwise regression just as before and the coefficients used to form a response surface equation of the form in Eqn. 6.3. The fit for this regression was also quite good, with an adjusted R-square value of 0.9995.

Table 23 – D-Optimal Settings

Parameter	Value
N Desired	250
N Random	23
K Value	3
Trips	5

8.4 Response Surface Results

The coefficients were then evaluated for 10,000 trials using the same input distributions as the Monte Carlo simulation for the trajectory variables, and the normal fit of the GRAM99 Monte Carlo simulation results as inputs for the atmospheric variables in the equation. The results of this simulation were then compared to the direct Monte Carlo simulation for the mass ratio required distribution as described in the goals and objectives chapter.

The plotted results in Figure 60 and Figure 61 of these analyses showed a great deal of similarity to the direct Monte Carlo simulation. This kind of smooth distribution information is an advantage of the response surface method.

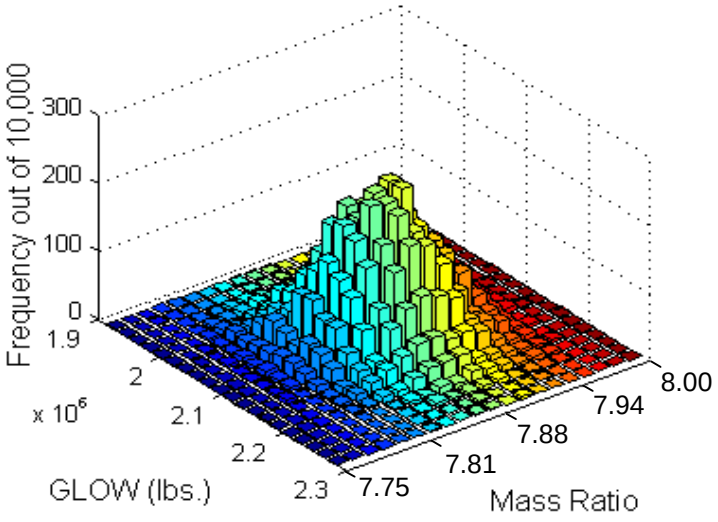

Figure 60 – Histogram of GLOW and MR using CC RSE

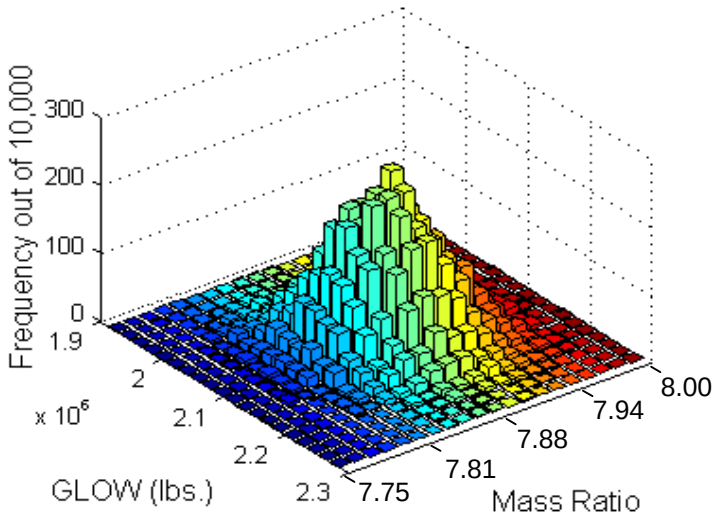

Figure 61 – Histogram of GLOW and MR using D-Optimal RSE

Table 24 – Results of Trajectory Response Surface Monte Carlo Simulation

	MRreq μ	MRreq σ	Mrreq/GLOW corr.
Monte Carlo	7.8934	0.0328	15.9%
95% c. l.	± 0.00064	± 0.00045	± 1.9%
CC RSE / MC	7.9436	0.0343	13.7 %
Abs. Rel. Error	0.637 %	4.54 %	13.7 %
DO RSE / MC	8.0088	0.0350	16.6 %
Abs. Rel. Error	1.46 %	6.78 %	4.47 %

The results for the response surface methods presented in Table 24 show that errors exist, but they are tolerable given their fast evaluation capability during

optimization. This fast calculation capability could very well be the deciding factor, given the slow nature of the trajectory analysis, often taking over one minute to execute. This made nearly all the variance reduction methods look unattractive, when compared to the RSE on the basis of time.

8.5 DPOMD

To measure the effectiveness of DPOMD, a 128 run fractional factorial method was chosen. This method was selected because it can take handle the correlation between variables that goes along with the multivariate normal distribution coupling variables. Also in this case, a great many of the noise variable, namely the atmospheric variables, were distributed as a 44 dimensional multivariate normal distribution. The two triangular variables, multipliers on aerodynamic coefficients, were symmetric meaning that the lack of ability of this particular version of DPOMD to match skewed random input distributions was not as much of an issue.

Because there was no screening process, the first step in the method was to acquire the means, standard deviations and correlation coefficients for all the variables. As described in the chapter on new uncertainty methods, these were used to create a Hasofer-Lind transform [138, 46] by way of Cholesky decomposition [90, 152] of the covariance matrix.

The next step was the creation of a $2_V^{(49-42)}$ fractional factorial experiment design. This design had a distribution mean and variance of zero and one respectively when the levels were set to –1 and +1. This matches the mean and variance a standard normal distribution. The inverse of the Hasofer-Lind transform was then applied to generate a

discrete distribution with the same second order moment characteristics as the input distribution.

Once the discrete distribution was obtained, the points in the distribution were executed using POST [163]. Each point was optimized for minimum propellant consumed (maximum burnout weight) and then recorded along with the appropriate input information.

8.6 DPOMD Results

Once the outputs for the points were obtained, their moment characteristics were measured using the distribution techniques described in the mass properties test section. Eqn. 6.4 was used to calculate second moment information. The outputs were then compared to the Monte Carlo simulation results, as described in the chapter on goals and objectives.

Figure 62 shows a histogram containing the output parameters of interest for this test. The correlation between the mass ratio required and the gross liftoff weight is slightly evident in the change in the MR required distribution between the two levels for GLOW. This plots also illustrates the need to fit a multivariate normal distribution to the results, especially the inputs, if confidence levels were required. For this test, however, none of the parameters of interest were confidence levels.

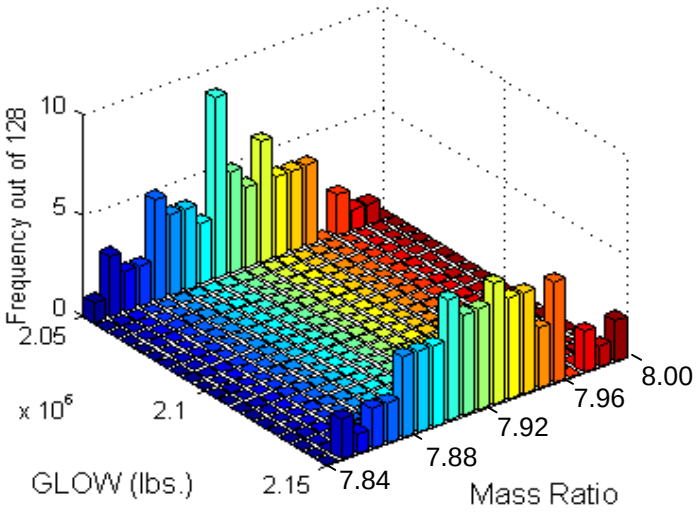

Figure 62 – Histogram of GLOW and Mass Ratio for DPOMD Trajectory Simulation

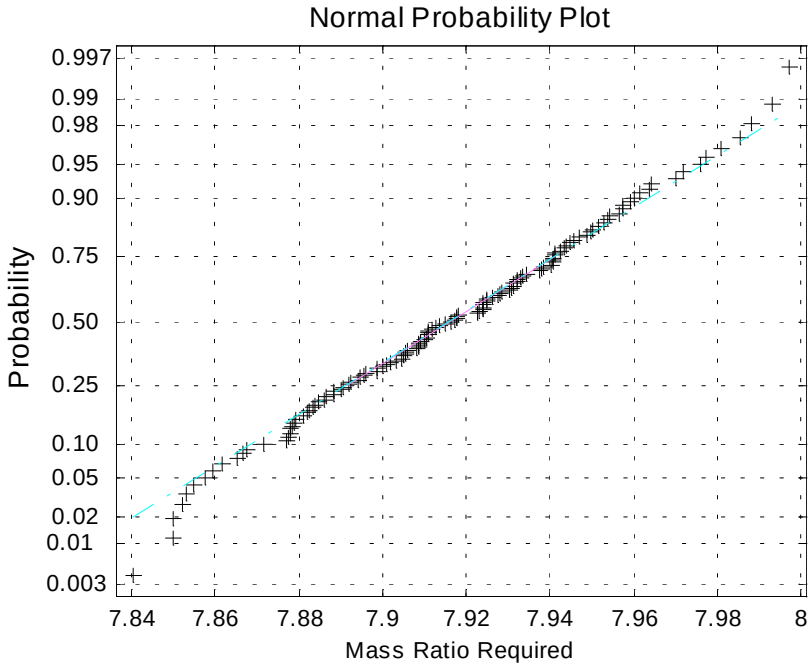

Figure 63 – Normal Probability Plot for DPOMD Trajectory Mass Ratio

The normal probability plot in Figure 63 shows that this DPOMD simulation had a much more normal output than those of the previous tests. This was likely due to the fact that there were many more variables that contributed fairly evenly to the response. This meant that the many discrete levels of the inputs were evenly spaced across the output mass ratio required axis.

Table 25 – Results of DPOMD Trajectory Simulation

	MRreq μ	MRreq σ	Mrreq/GLOW corr.
Monte Carlo	7.8934	0.0328	15.9%
95% c. l.	± 0.00064	± 0.00045	± 1.9%
DPOMD	7.9168	0.0343	15.3 %
Abs. Rel. Error	0.297 %	4.52 %	3.95 %

Table 25 shows that the DPOMD method was again the most accurate method tested for the outputs in question. The results for the mean value of mass ratio required were closer than either of the response surfaces. The mass ratio required standard deviation matched that of the central composite response surface. For the correlation coefficient, this method was by far the closest to the Monte Carlo simulation, with a relative error of 2.41 %.

Computational time was an issue. The POST trials comprising the simulation took approximately three hours to run, depending on the system load of the SGI Octane

workstation. This would be a major drag on an iterative system, and severely hurt the chances of this type of analysis being included in the iteration loop for the proposed probabilistic, multidisciplinary framework for launch vehicle conceptual design optimization.

8.7 Descriptive Sampling

Again, the descriptive sampling algorithm used was the Latin hypercube-based method presented by McKay [120], the same that was used in the previous analysis tests. It generated a map of probabilities for a set of independent random uniform variables that were then put through an inverse cumulative distribution variable corresponding to each input.

The sample points were constructed using inverse cumulative probability functions corresponding to the type of random variable being sampled. For normal distributions, independent standard normal distributions were first sampled, then these results were transformed into the problem space using an inverse Hasofer-Lind transform. Because all the variables were sampled at the same time, the inverse transform for the triangular distributions was identity in the multiplicative matrix and zero for the mean vector, in effect leaving these variable unchanged. This left a table of 100 runs to be evaluated using POST [163].

POST subsequently optimized each table entry to maximize burnout weight. Once the run table optimized results were obtained, they were measured for the previously determined statistical criteria for this test.

8.8 Descriptive Sampling Results

The completed run table was analyzed using sample mean variance calculations. The results were then compared to the Monte Carlo simulation for the selected output parameters as described in the goals and objectives chapter.

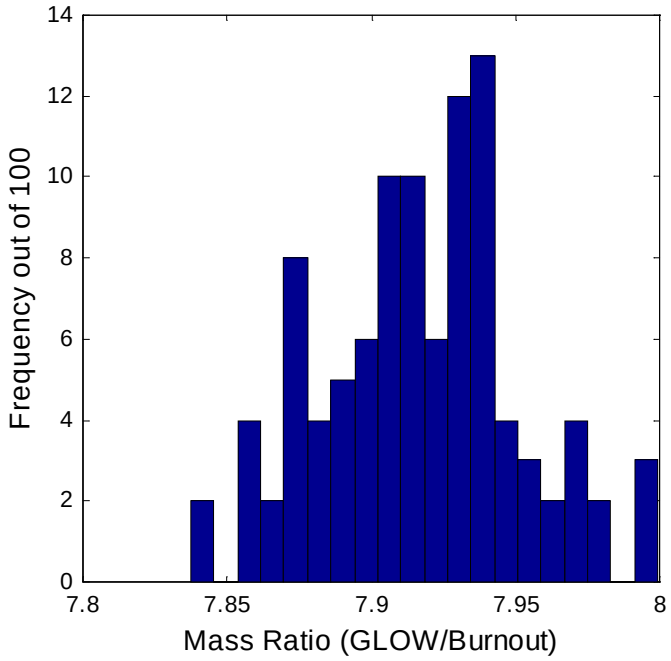

Figure 64 – Histogram of Mass Ratio from DS Trajectory Simulation

As you can see in Figure 64, the histogram of mass ratio showed a developing normal appearance that would most likely be confirmed with more runs. This normality can be seen more easily in the normal probability plot in Figure 65. Other than at the extreme tails, this distribution is fairly normal.

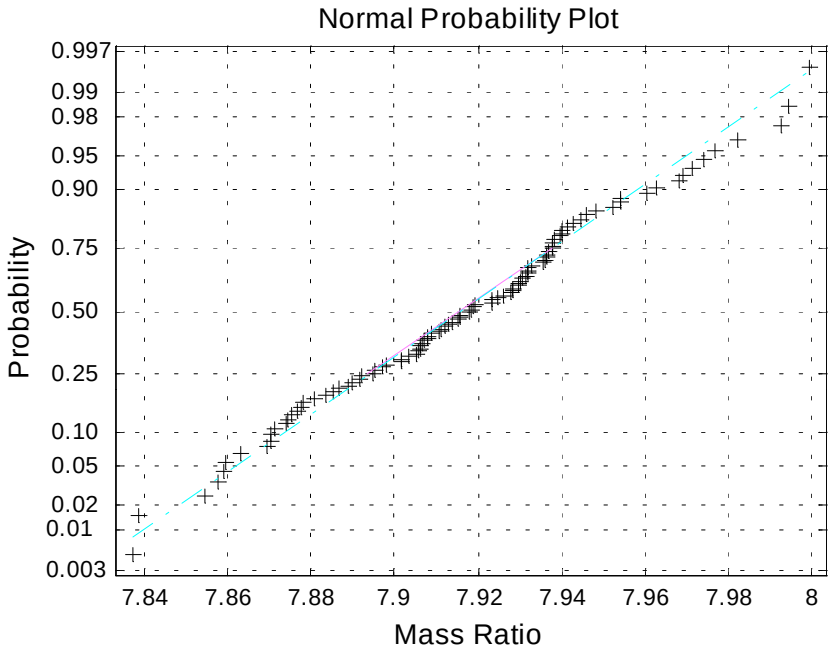

Figure 65 – Normal Probability Plot for Mass Ratio in DS Simulation

Table 26 shows fairly good results for the descriptive sampling simulation. The accuracy is about the same as the other approximation methods tested. Unfortunately for the descriptive sampling and DPOMD methods, this comes at a much higher expense than the response surface method.

The computational effort needed to evaluate this method was a little less that that of the DPOMD. It took about 2.5 hours on an SGI Octane workstation. Coupled with the fact that the response surface methods proved to be just as accurate for this problem, descriptive sampling does not appear to be a standout option for the selected trajectory optimization problem.

Table 26 – Descriptive Sampling Trajectory Test Results

	MRreq μ	MRreq σ	Mrreq/GLOW corr.
Monte Carlo	7.8934	0.0328	15.9%
95% c. l.	± 0.00064	± 0.00045	± 1.9%
Descriptive Sampling	7.9170	0.0342	16.7 %
Abs. Rel. Error	0.299 %	4.25 %	4.89 %

8.9 Overall Comparisons

The primary aim of this analysis test was to find one or more uncertainty analysis techniques for the trajectory optimization contributing analysis that were both fast and accurate. The accuracies of the methods were compared to a Monte Carlo simulation to then determine which candidate method would be used in the full, multidisciplinary optimization problem.

The first goal of testing the accuracies of the methods has been met. All the methods were tested at their most reasonable computational expense and the results were presented in the preceding sections.

Of the methods tested, the descriptive sampling simulation technique proved to be the most accurate. However, the central composite response surface equation methods did not have as large errors during this test as in the previous ones. Combined with the

significant cost savings involved with using this type of analysis as shown in Table 27, this was the method selected for the probabilistic multidisciplinary optimization problem.

The trial histories presented in Figure 66 and Figure 67 surprisingly shows that the Monte Carlo analysis got closer to its final answer sooner than either of the approximate sampling methods. This means that there would be almost no reason to use either of these methods, as the more general Monte Carlo simulation supercedes both the descriptive sampling and the discrete probability optimal matching distributions at their chosen resolutions for every output parameter of interest but MR-GLOW correlation coefficient.

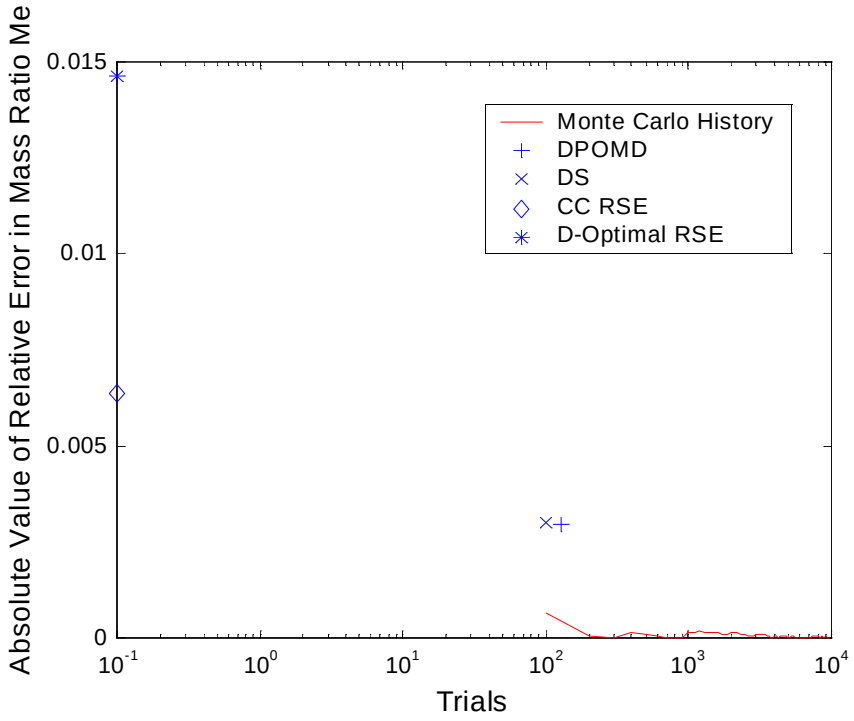

Figure 66 – History of MR Required Mean Error

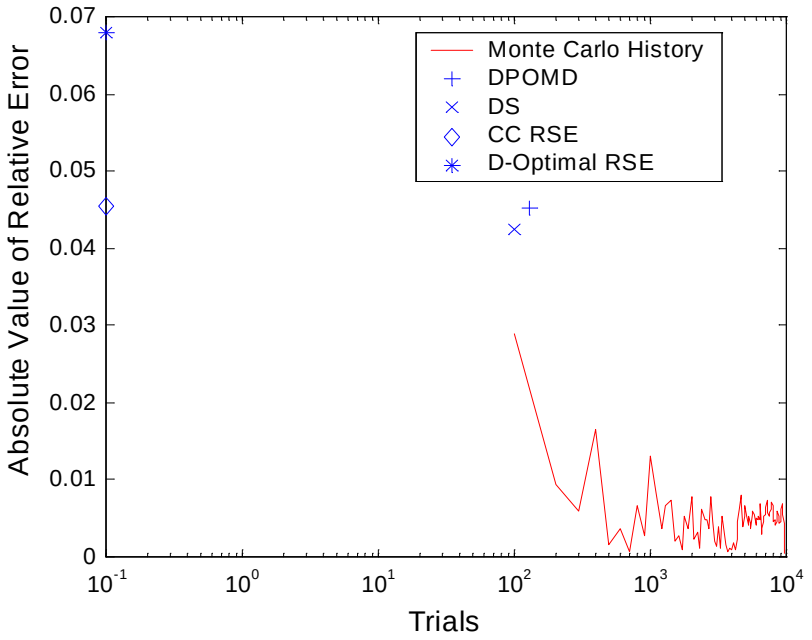

Figure 67 – History of MR Required Standard Deviation Error

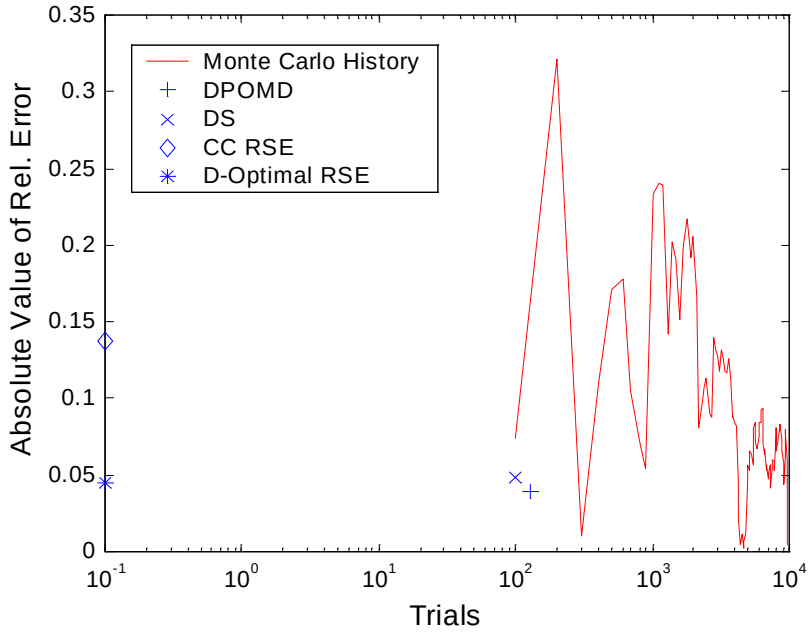

Figure 68 – History of MRReq-GLOW Correlation Coefficient Error

The accuracy of all the approximation methods was slightly lower for this analysis test than in the others. A likely cause of this was the reduction of the atmosphere model described earlier in the section. While necessary due to the program setup of the GRAM99 tool, this nonetheless created an inherent difference in the problem statement for all the approximation methods when compared to the Monte Carlo simulation. The consistent error across all the analyses supports this. Compared to similar tests [22] that neglected atmospheric uncertainty, the accuracy of approximation of this trajectory optimization problem was generally not as good.

Table 27 – Run Times for Trajectory Uncertainty Methods

Method	Trials	Platform	Time
Monte Carlo	10,000 POST Runs	2 SGI Octanes	5 days
DPOMD	128 POST Runs	SGI Octane	3 hrs.
Descriptive Sampling	100 POST Runs	SGI Octane	2.5 hrs.
CC, D-Optimal RSE / MC	10,000 C++ RSE Calls	SGI Octane	1.1 sec.

CHAPTER IX

DISTRIBUTED PROBABILISTIC MULTIDISCIPLINARY OPTIMIZATION

Distributed probabilistic multidisciplinary optimization refers to a loosely coupled architecture of contributing analyses each providing their own techniques of uncertainty analysis. This architecture has certain required capabilities so that it can generate accurate results and be flexible in its implementation. It also has desired characteristics that provide an incentive for its future adaptation in engineering organizations.

9.1 Desired Characteristics

There are several characteristics that distributed probabilistic multidisciplinary design should possess in order to ensure that it retains the advantages of loosely coupled design [67, 63, 61, 77, 78, 79, 64]. These characteristics have to do with ownership of the analyses flexibility of the method over time, as well as accuracy and speed in the aid of optimization.

9.1.1 Flexible Implementation

The first capability desired for this methodology is that it be flexible in its implementation. This means that for each subproblem, widely differing techniques of probabilistic analysis can be employed, depending on the recommendations of

experiences disciplinary experts. This flexibility gives the experts control over the sublevel analysis and allows for improvements to the analysis with minimal impact to the other subproblems. Another advantage is that this will engage the expert and make them more likely to commit to the design process.

9.1.2 Distributed Computational Effort

Another desired characteristic for the method is that it can take advantage of distributed computational effort. This not only creates the possibility of parallel computer operation, but also means that many different people can monitor and provide “sanity checks” on the results. This can also be a way of maintaining responsibility for computational effort. The discipline experts are able to easily see the computational costs of their analyses, so that they can spend a proportional level of cost given the problem accuracy required.

9.1.3 Reduced Computational Effort

A third desired characteristic is that of reduced computational effort when compared to alternative system-level probability analysis. This is because of the possibility of reduced dimensionality of the noise characteristics of each contributing analysis optimization when compared to the whole system level problem. This happens for systems with lower coupling requirements. While this does not lead to any advantages for zeroth order methods such as direct Monte Carlo simulation, higher order methods should see computational cost savings. The assumption here is that direct system-level Monte Carlo simulation is too expensive an option for optimization and that higher order methods are required for the conceptual launch vehicle design problem.

9.2 Required Capabilities

To be a valid multidisciplinary analysis technique, the proposed method must have certain characteristics related to passing accurate information between the disciplines. In addition to accurate data passing, it must also ensure that all the disciplines have all the required inputs for analysis. For deterministic analysis, this is a relatively simple task. When translating this to probabilistic analysis there are some important considerations. Finally, there should exist some capability for handling objective functions from several disciplines. This capability should also exist in deterministic design frameworks, but probabilistic optimization introduces new possibilities, as described in the background chapter, that require more computational effort than most deterministic multi-objective formulations.

9.2.1 Variable Communication

The requirement of accurate variable communication between the contributing analyses meant the transfer of data should include enough distribution information in the coupling variables to give each contributing analysis a good idea of the probability map exiting the other disciplines as they occurred together. This means that at a minimum, second order moments should be transferred. To do this, a set of standard deviations for each variable along with a correlation coefficient for each variable combination that is an input to any contributing analysis. The correlation is required because these variables are not assumptions, they are fits to the multivariate probabilistic solution of another analysis. In many cases, these outputs are highly correlated and ignoring this information would lead to faulty results for subsequent contributing analyses.

This correlation information requirement means that the inputs and outputs of a probabilistic multidisciplinary analysis problem will be slightly different from that of a

deterministic one. In order to generate correlation coefficients required by other analyses, extra variables need to be added to certain contributing analyses that do not require them for deterministic optimization. The DSM in Figure 69 on page 186 illustrates this point. Contributing analyses for propulsion and trajectory both feed multivariate normal distributions into the mass properties analysis, but a correlation between propulsion and trajectory cannot be generated in this situation, yet it exists and is an important input to the mass properties analysis. Therefore, an extra link is created between propulsion and trajectory so that the propulsion analysis can calculate the required correlation between the output of the trajectory contributing analysis and its own outputs.

9.2.2 Correct Distribution Expression

This technique of adding links between disciplines should yield accurate simulation results, assuming that the results of the contributing analyses are in fact normal. This assumption should therefore be tested using a Monte Carlo analysis on each contributing analysis at a typical design point, before optimization begins. The type of output observed by each should then indicate what type of distribution is most appropriate to fit. These variables should still be fit in a multivariate manner, with correlation coefficients recorded and transferred to the other disciplines so that they can be simulated accurately as inputs.

9.2.3 Contributing Analysis Requirements

One of the advantages of this type of loosely coupled formulation is that there are minimal requirements placed on the subsystem probabilistic analysis other than accuracy and the ability to handle its own probabilistic constraints. Besides making sure that confidence levels for constraint satisfaction and the coupling variables are consistent within the system, there is very little else the system level implementation must handle.

The consistency between coupling variables is ensured by requiring the contributing analysis to provide information for its outputs based on updated information about its inputs. This delegation of authority is one of the primary advantages of the loosely coupled approach.

CHAPTER X

LAUNCH VEHICLE EXAMPLE PROBLEM

To test the methods presented in this research, a reusable launch vehicle (RLV) example optimization problem was created. Probabilistic multidisciplinary methods were applied to test the feasibility of generating optimums, then these optimums were confirmed by other optimizations using different starting points. The accuracy of the probabilistic methods was tested using a Monte Carlo simulation for the optimum vehicle. This confirmation was not a sizing process, but simply generated the distributions that were approximated during the optimization to test their accuracy. Finally, the probabilistic optimum was compared to the result of a deterministic optimization process based on the same contributing analyses as the probabilistic test.

These analyses were integrated separately for the purpose of showing that specifically tailored probabilistic approximation methods would be able to execute large problems with accuracy. This was due to the lowering of the dimensionality of the uncertainty subproblems considered, enabling higher order methods with more included noise. This distributed probability analysis also reduces the communication slowdown present when using loosely coupled contributing analyses by greatly reducing data transmission frequency. On top of these benefits, it includes the disciplinary expert in the uncertainty approximation, a process that often makes large assumptions about the behavior of the problem under analysis. Disciplinary experts are extremely important to determining the best approximation method based on the assumptions.

First the example problem models had to be constructed and interfaced. The interfacing was done execution using Phoenix ModelCenter© analysis integration software. This software allows for simple, object-oriented integration of analysis codes that have been wrapped to interface with ModelCenter©. It handled the data flow and the execution scheduling per user instruction, allowing several codes to be interfaced in a loosely coupled manner. This was done across heterogeneous platforms, namely SGI IRIX and Windows NT. The control center for this was based on a Windows NT machine and ran across the local area network. It interfaces with the wrappers set up on local machines through Analysis Server©, also from Phoenix. This allows any models hosted on a local machine to be easily utilized in a system without complicated user-defined communication methods.

ModelCenter© also provided the optimization modules used for both meeting the sizing constraints and optimizing the objective function. The optimizer included a wrapped version of DOT [168], Design Optimization Tool, from Vaderplaat's Research and Development. The chosen method was conjugate gradient in all cases. Custom components were also written to handle system convergence issues, with each variable having a tolerance that must be met before the design is considered converged.

The analyses integrated using ModelCenter© were the trajectory analysis, the mass properties and sizing and the propulsion analysis. The aerodynamics, aeroheating and configuration analyses were done offline before the other models were executed in ModelCenter©. This was possible because both these analyses were only weakly coupled to the rest of the system. They only need to be changed if the vehicle changes a great deal from its reference length, where these analyses were calculated. In this case, the reference

was very close to the actual sized length, so no recalculation of these weakly coupled analyses was required.

The analyses to be calculated online were integrated into ModelCenter© using the probabilistic methods determined for each of them in the chapter on suitability of probabilistic methods. These methods were all applied locally. It allowed each approximation method to be applied in the most effective way possible for each of the analyses. The methods chosen were the fractional factorial DPOMD for the mass properties and sizing analysis, Central Composite RSE / MC method for the trajectory analysis and full factorial DPOMD for the propulsion analysis. These methods provided a maximum of accuracy in the required parameters in a minimum amount of time.

The analysis system as it was applied for optimization can be seen in Figure 69.

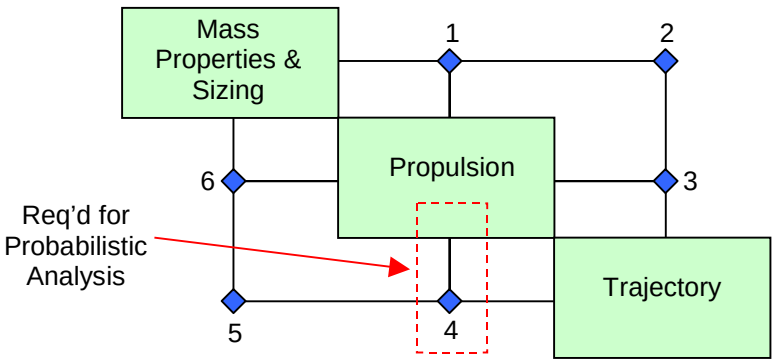

Figure 69 – Design Structure Matrix of Online Probabilistic Design Process

Table 28 – Coupling Variables for Distributed Probabilistic Launch Vehicle Design

Coupling Location	Parameters Passed
Mass Properties and Sizing – Propulsion (1)	GLOW mean, GLOW std. dev.
Mass Properties and Sizing – Trajectory (2)	GLOW mean, GLOW std. dev., Sref
Propulsion – Trajectory (3)	Tvac mean, Tvac std. dev., Ispvac mean, Ispvac std. dev., Ae mean, Ae std. dev., GLOW-Tvac corr., GLOW-Ispvac corr., GLOW-Ae corr., Tvac – Ispvac corr., Ae – Tvac corr., Ae – Ispvac corr.
Trajectory – Propulsion (4)	MR_{req} mean, MR_{req} std. dev., MR_{req} - GLOW corr.
Trajectory – Mass Properties and Sizing (5)	MR_{req} mean, MR_{req} std. dev.
Propulsion – Mass Properties and Sizing (6)	Tvac mean, Tvac std. dev., Ae mean, Ae std. dev., T/W_e mean, T/W_e std. dev., MR_{req} – Ae corr., MR_{req} – Tvac corr., MR_{req} – T/W_e corr., Ae – Tvac corr., Ae – T/W_e corr., Tvac – T/W_e corr.

As you can see, for a deterministic system, it is very nearly fully coupled. When probability distributions are considered, it becomes a fully coupled system due to the feedback from trajectory to propulsion where none existed before. This is because there is a correlation required by mass properties and sizing that is not a standard result of any analysis. To provide this correlation, it is was necessary to introduce a new input into an unrelated analysis, mass ratio required into propulsion in this case. Here, MR_{req} is input into propulsion so that it may calculate the correlation between MR_{req} and T/W_e, which is required by mass properties and sizing. An alternative method to the one presented here would be to introduce T/W_e into the trajectory analysis. The propulsion analysis was considered more flexible, due to its faster execution times and lower initial variable count. A full accounting of the couplings present in the probabilistic system is available

in Table 28. The numbers in the coupling location correspond to the coupling labels in Figure 69.

It is easy to see that the propulsion contributing analysis provides many outputs to the system. This is partially by design, as many of the correlation coefficients can be generated in more than one contributing analysis. For example, the correlation between MR_{req} and Tvac can be generated either by the propulsion analysis, where MR_{req} is an input and Tvac an output or by trajectory analysis where Tvac is an input and GLOW is an output. The propulsion analysis was chosen because it can update these values more easily, as it is the fastest executing contributing analysis in the system. Once these coupling relationships were established, the probabilistic contributing analyses had to be wrapped for automatic execution.

10.1 Mass Properties and Sizing

The mass properties and sizing algorithm was originally constructed using an Excel© spreadsheet. This particular spreadsheet calculated the vehicle weight parameters for a given set of mass estimating relationship (MER) assumptions and a vehicle OML length. Because these MER's were highly interrelated, fixed-point iteration with no relaxation was used. This has proven in this past to be a simple and reliable method for solving these sets of equations. Technically, the analysis performed by the spreadsheet in the probabilistic framework was only mass properties, not sizing.

For this sizing analysis, the vehicle in question had a 20 klb. payload, a 350 fps. orbital maneuvering capability and a five minute powered landing capability provided by a pair of hydrogen turbofans. Also, zero weight growth margin was assumed. This is the

traditional safety factor method for accounting for uncertainty in the MER's and performance estimates. Because this job is now done using more advanced probabilistic methods, this margin was no longer necessary. These assumptions were constant and have a significant impact on the size and weight distribution of the vehicle.

Embedded in the spreadsheet was a Visual Basic (VB) macro that read in a text-based data file of the assumptions and input variables, executed the spreadsheet, then calculated output parameters such as means, standard deviations and confidence levels. These responses include the items in the WBS shown in Table 2 as well as summary variables such as gross liftoff weight (GLOW), vehicle dry weight and mass ratio available (MR_{avail}). These parameters were then sent to cells in the spreadsheet where they would be available to the Analysis Server© wrapper utility.

A compiled Matlab© function generated the DPOMD tables in a format that could be read by the previously described VB script. This function took text file inputs for the mean, standard deviations and correlation coefficients for the input coupling variables and a separate file for triangular distribution information. This information, along with a reduction factor for the fractional factorial DPOMD method described in the chapter on probabilistic methods were the inputs used to generate the run table.

To create the ModelCenter© contributing analysis, two different wrappers were created. The first step was to create a wrapper around the Excel©-based mass properties analysis. This wrapper provided inputs for deterministic variables such as vehicle length, vehicle thrust-to-weight ratio, etc. The output parameters for the probabilistic process were also wrapped during this step, as they were calculated by the VB script in the spreadsheet described in the paragraph above.

The second wrapper provided inputs to the DPOMD analysis in a compiled Matlab© function. This wrapper provided data to the text files for input distribution information. The output from the DPOMD program, however, was not handled by ModelCenter©. DPOMD executable and input files were placed in the same directory as the mass properties spreadsheet so that when the analyses were executed in order, the data was available to the mass properties analysis. This avoided having to send the rather large amounts of data through across the network to the ModelCenter© control panel.

Once both parts of the analyses were wrapped, they were connected together in ModelCenter©. This meant that input distributions could be provided inside ModelCenter, along with a vehicle size and corresponding output parameters could be generated. The next step was to construct the sizing process. This was done using the integrated version of DOT [173]. Using the goal seek method, the 80% confidence level on the difference between the MR_{req} and MR_{avail} by changing the vehicle length. This goal seek was only necessary on the mass properties spreadsheet, as none of the input distributions changed with the vehicle length directly. This added the sizing element to the process and completed the mass properties and sizing contributing analysis as it was incorporated here. This analysis was then inserted into the framework described earlier. A screen shot of the completed set of components in ModelCenter© can be seen in Figure 70.

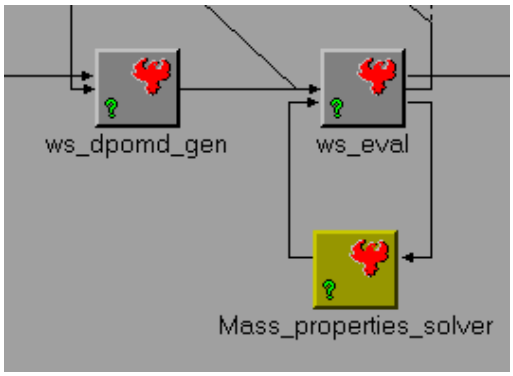

Figure 70 – Probabilistic Weights and Sizing in ModelCenter©

10.2 Propulsion

The propulsion analysis consisted of three layers. The innermost layer was the SCORES analysis, which sized each engine scenario. Wrapped around this analysis was a Perl script that took inputs from a text table, then executed the table for each scenario listed. The outer layer was a Matlab function responsible for generating the DPOMD runs for the propulsion analysis to execute. This is shown in Figure 71.

The input table consisted of the inputs for the propulsion analysis. This meant that variables added for the purpose of generating correlations such as the MR_{req} parameters did not need to be included in the list. The variables that were included in the list were Tsl, Pch, $P/W_{e,}$ AR and r. The last two were deterministic variables, so these did not vary with the runs in the table. For each of the scenarios listed in the table, SCORES [162] constructed an engine with matching sea level thrust and reported the vacuum engine performance and thrust, exit area and whether or not there is a shock in the nozzle.

To generate the table, a Matlab© function producing a full factorial version of the DPOMD method was constructed. This function took distribution information from input

files and then generated a DPOMD table corresponding to those inputs, minus those random variables that were added for the purpose of generating correlation coefficients. Once the script was done generating the table, it executed the Perl script described above. Once the Perl script had run SCORES for the required table of scenarios, the output responses were read from a text file of responses generated by the Perl script. Using these responses, distribution information was calculated and placed in another text file. This final text file would eventually be read by ModelCenter© and used as outputs to other contributing analyses.

The final step of including this analysis in the overall system consisted of first wrapping the correlated normal coupling variable distribution parameters for GLOW and MR_{req}, the uncorrelated normal input P_{ch} and finally the deterministic inputs T/W_v, AR and r. The outputs wrapped were the correlated normal coupling variables parameters for I_{spvac}, T_{vac}, A_e and T/W_e plus correlations to selected input variables as listed in Table 28.

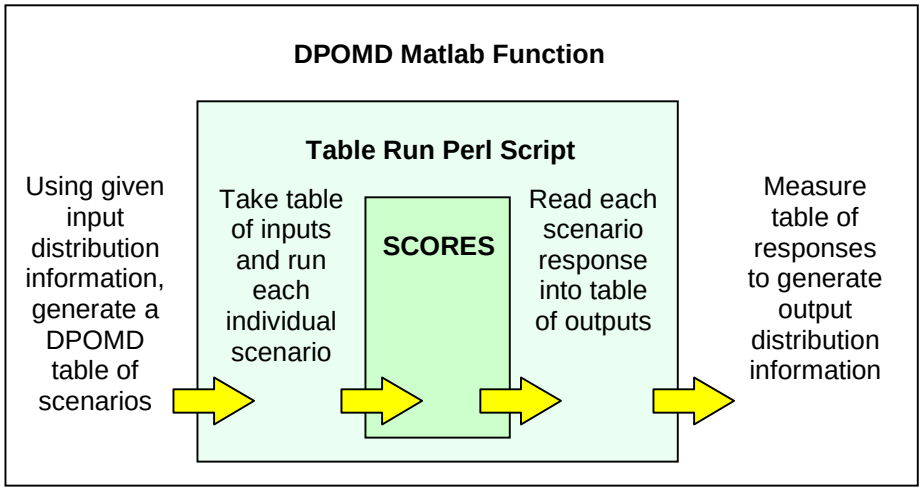

Figure 71 – Overview of Probabilistic Propulsion Analysis

10.3 Trajectory

The trajectory contributing analysis consisted of a Monte Carlo simulation performed on a response surface of propellant-optimized trajectories. This response surface differed slightly from the one presented in Chapter 8 on the trajectory analysis tests, so it is appropriate to discuss those differences here.

The first change made was to the size of the experiment. After the experience gained with the response surface tests in the chapter on suitability, it was easier to generate responses for experiment designs with more runs. Because of this, and the necessary addition of the deterministic variables S_{ref} and T/W_v, a ten variable on-face central composite experiment with full factorial box points was used. This design had 1,045 runs that took approximately two days evaluate.

Once the responses to the experiment were generated, a quadratic function of the form in Eqn. 6.3. was fit in a least squares sense using the software package JMP©. A stepwise regression technique used sequential F-tests as described in the probabilistic methods chapter on response surface methods. These tests determined which terms of the equation would be used. This process improves the fit of the equation by eliminating terms that only slightly contributed to the response. The fit parameters resulting from this process are given in Table 29.

Table 29 – Results of Stepwise Regression for Trajectory RSE

Fit Parameter	Value
R-Square Value	0.9995
Adjusted R-Square Value	0.9995
Number of Terms Selected	33
Number of Terms Eliminated	33

Once the coefficients of the equation were determined, they were put into a text file that was read by a C++ program designed to evaluate a response surface for a text file list of inputs. Now the probabilistic analysis was ready to be run using Monte Carlo simulation. Because of the inherent batch nature of the RSE evaluation program, this process did not require a Perl script step like the propulsion test. Instead, a Matlab© function that generated a list of inputs from a previously created list of pseudo-random numbers was wrapped directly around the RSE executable.

The random number generation process used a table of random numbers generated offline, then relied on a transform to give the trials the proper distribution characteristics. First, for the normal distributions, samples from independent standard normal distributions were generated offline. This saved the expense of having to perform a costly inverse cumulative probability function call for each variable in each trial. For each subsequent Monte Carlo simulation, this list of standard normal samples was transformed into the required multivariate normal distribution by means of an inverse Hasofer-Lind [138, 46] transform.

For the triangular distributions, a more standard approach was taken. Here, a list of uniform [0,1) samples was generated offline. Then, for each different Monte Carlo simulation, an inverse triangular cumulative probability function was used to determine the samples from each of the triangular random variables. This was more time consuming than the normal distribution generation, but there were only two triangular random variables, so this extra expense was not noticeable. In addition, the distribution parameters for triangular distributions did not lend themselves to a simple transform like the normals.

Once the table of random inputs for the RSE program was ready, the program was run and the responses recorded to a separate file. These responses were then read in by the outer Matlab function and the parameters for the output distributions calculated. In this case, the sole output distribution was the MR_{req}, but the correlation of this variable with GLOW was also calculated. These parameters were then written to a text file where they would be easily accessible to ModelCenter©. This process is illustrated in Figure 72.

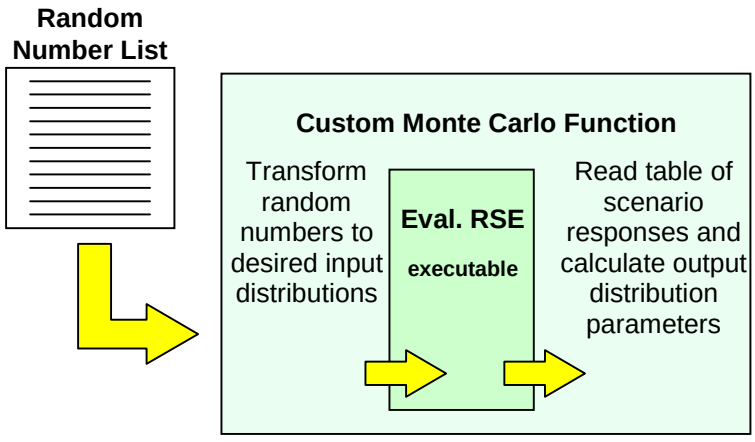

Figure 72 – Overview of Probabilistic Trajectory Analysis

10.4 Optimization

To test the feasibility of these distributed probability methods to generate a probabilistically optimum launch vehicle, an optimization of the launch vehicle design system described in the previous section was undertaken. This optimization altered four design variables traditionally known to have a large effect on all-rocket SSTO RLV's. These were:

- Engine Mixture Ratio (r) – This variable is the ratio of oxidizer mass to fuel mass burned in the engine. This variable primarily affects engine efficiency and propellant bulk density. For optimization, the value of this variable was limited to values from 5 to 7.
- Engine Area Ratio (AR) – This is the ratio of the engine exit area to the engine throat area. It primarily affects how the engine performs with changing altitude. For the system optimization, the value of this variable was constrained to be from 40 to 85.
- Vehicle Liftoff Thrust to Weight (T/W_v) – This ratio determines how much vehicle thrust is present at liftoff. It primarily affects the relative weight of the engines on the vehicle, the trajectory gravity losses and required throttle level on ascent. The limits on this variable were set to be from 1.2 to 1.6. 1.2 was the minimum to ensure safety while clearing the launch tower, while 1.6 was chosen because of throttling concerns near burnout.
- Mean Engine Combustion Chamber Pressure (Pch) – This variable was assumed to be a somewhat controllable noise. The mean value was varied while the standard deviation around that mean was assumed to be a constant 4 atm. This parameter primarily affects engine weight and performance. It was limited to values from 150 atm. to 210 atm.

Each time these values were altered, the resulting vehicle was sized according to the rules and techniques laid out in the previous section. When this sizing was completed, the objective function, the 95th percentile dry weight, was returned to the optimizer. The particular optimizer used for this process was the DOT [168] package using conjugate gradient unconstrained optimization method.

Because numerical noise from the sizing process was a concern, a finite difference derivative test was undertaken at a particularly difficult point. This point was identified by launching the optimizer using the default settings for finite difference gradients and observing the area where the optimizer could not generate a viable search direction. The defaults for this preliminary search were forward difference gradients with a relative step size of 0.001. This point around which the derivative test was conducted can be seen in Table 30.

Table 30 – Testing Point for Finite Difference Derivatives

Design Variable	Value
Mixture Ratio (r)	5
Area Ratio (AR)	40
Vehicle Thrust to Weight (T/W_v)	1.2
Engine Chamber Pressure (Pch)	210 atm.

Once a trouble point was located, several step sizes using both forward and central differences were taken. These were used to calculate both forward and central difference partial derivative estimates. A sweep of step size can be seen in Figure 73.

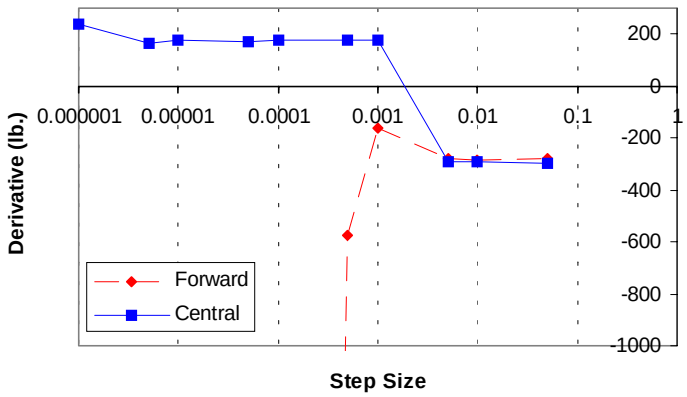

Figure 73 – Step Size Sweep for Derivatives with Respect to Area Ratio

The sweep in Figure 73 illustrates how the decision on step size was made. The general direction of the large step sizes was considered to be correct. This was assumed because the error here is in the finite difference approximation, which is unlikely to reverse the direction of the estimate for reasonably large derivative values. However, the magnitude of these large step sizes was assumed to be faulty. At the other extreme, the numerical noise in the sizing process can create huge errors in the derivative estimate. So to minimize the error due to both the finite difference approximation and numerical noise, the smallest step size that did not have obvious numerical noise was taken. Because the other three derivative sweeps exhibited similar behavior to the one shown in Figure 73, a relative step size of 0.005 was chosen. Because this was a rather large step size, central

difference gradient estimates were used in place of forward difference. This change made sure that the gradients supplied to the optimizer were as accurate as was possible. It will be shown later that this step size enabled the system optimizer to consistently find the optimum design.

Once the derivative test was complete, the optimization process was started at several points, each one with its own rationale. The baseline point was an SSTO starting out with an engine design similar to the Space Shuttle Main Engine (SSME). This baseline optimization data can be found in Table 31. This baseline point optimized quickly, taking about six hours to find the best solution. An iteration history of the objective function, the 95% confidence level of dry weight, can be seen in Figure 74.

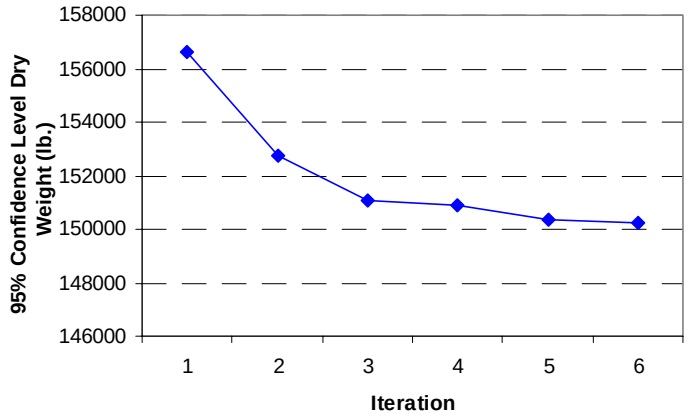

Figure 74 – Objective Function History for Initial Probabilistic Optimization

The design variables in this case went to optimum settings common for this type of problem. The area ratio went to a lower value, from 77.5 to 53. This is to be expected,

since the engines must provide the entire vehicle thrust from the pad to orbit. This differs from the Shuttle Transportation System (STS) in that the STS delivers the majority of its main engine impulse at higher altitudes. The lower mixture ratio also shows indicated the high demand for engine performance provided by this variable. The other variables did not change very much, instead going to their constraints for this problem.

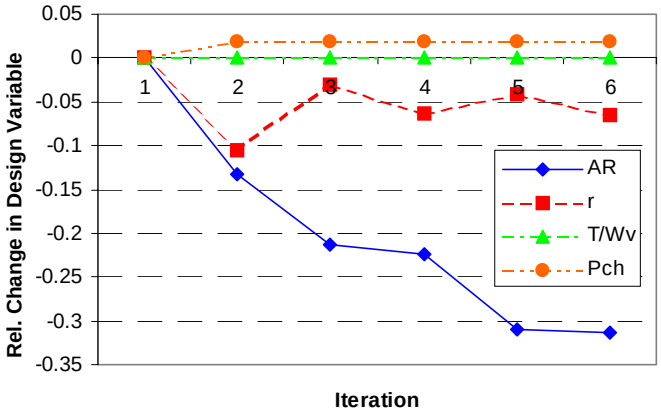

Figure 75 – Design Variable History for Initial Optimization

To confirm that in fact this was the true optimum, two other starting points were run. The first re-optimization began from the engine manufacturer's dream design. This point maximized area ratio for the best vacuum performance, minimized mixture ratio for the highest propellant efficiency, maximized chamber pressure in order to push the limits of power head technology and maximized vehicle thrust to weight in order to sell more engines. This set of design variables then proceeded to the system optimum found in the

initial optimization in about the same amount of time, even though it started further away. The overall comparison of start and end points can be seen in Table 31.

The next point to be optimized came from the standpoint of using a slightly lower propellant performance, but also try to take advantage of a higher bulk density and higher thrust, lower gravity loss trajectory. This corresponded to a low engine chamber pressure, a high mixture ratio, a high area ratio and mid-level vehicle thrust to weight. This optimization also traveled to the same optimum as the others. This fact can be seen in Table 31. Each of these system-level optimizations took six hours to complete on a combination of Windows NT© and SGI Octane© workstations.

Table 31 – Optimum Confirmation Run Results

Design Variable	Start Pt. 1	Opt. Pt. 1	Start Pt. 2	Opt Pt. 2	Start Pt. 3	Opt. Pt. 3
Mixture Ratio (r)	6	5.61	5	5.60	7	5.62
Area Ratio (AR)	77.5	53.2	85	52.1	85	51.3
Vehicle Thrust to Weight (T/W_v)	1.2	1.2	1.6	1.2	1.4	1.2
Engine Chamber Pressure (Pch)	206 atm.	210 atm.	210 atm.	210 atm.	150 atm.	210 atm.
Objective: 95% C.L. Dry Weight	156.7 klb.	150.2 klb.	237.2 klb.	150.2 klb.	286.1 klb.	150.1 klb.

The two design variables that were not limited by constraints generally fell to the same value. While there are slight differences in the optimum results, these all resulted in

negligible differences in the 95% confidence level value for dry weight, so they can be considered the same result. To further illustrate the convergence of these two variables, Figure 76 shows a path iteration history of mixture ratio versus area ratio.

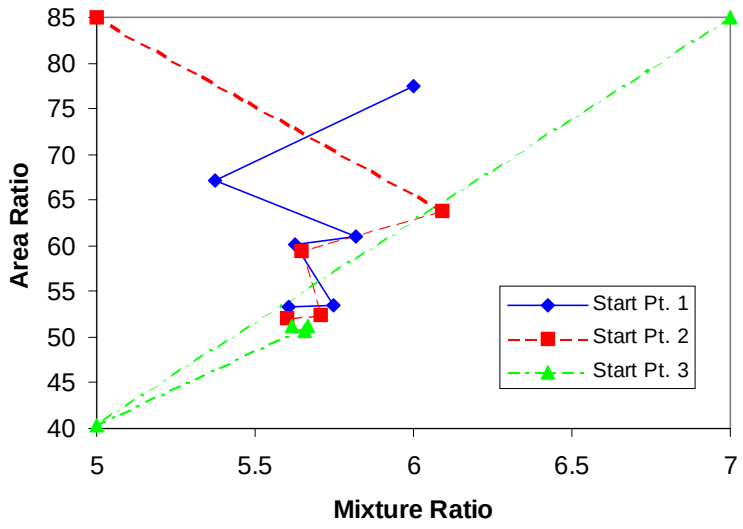

Figure 76 – Design Variable Paths for Area Ratio and Mixture Ratio

The results above show that consistent probabilistic optimums can be generated using this distributed probabilistic technique in a reasonable amount of time. This was one of the key goals of the research and the objectives relating to this goal have been met.

10.5 Monte Carlo Confirmation

To confirm that the generated probabilistic optimum has been accurately approximated, a Monte Carlo simulation of the optimum point was executed. This involved removing authority over the local noise variables and bringing them into

ModelCenter© and applying a central Monte Carlo simulation. This tested the accuracy of the overall process, including all of the approximations made. This simulation consisted of 1,000 trials, all of which had to be run on the heterogeneous framework.

The process for each trial consisted of iteratively sizing the propulsion system with the mass properties analysis, then feeding the resultant scenario to the combination of POST/GRAM99. This system therefore tested the atmospheric approximation GRAM99 as well as the probabilistic methods. A design structure matrix and coupling table illustrating the confirmation process data flow are shown in Figure 77 and Table 32.

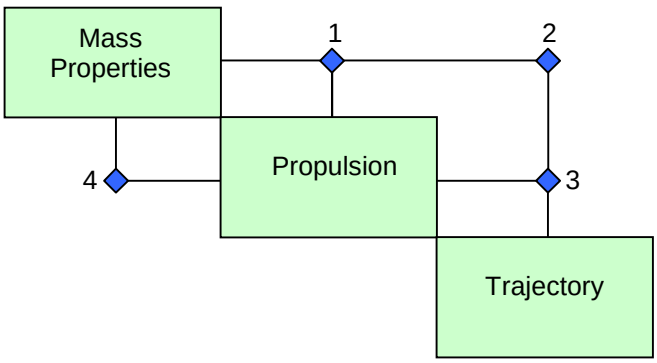

Figure 77 – Design Structure Matrix for Monte Carlo Confirmation

The coupling variables in Table 32 were all deterministic, since the probabilistic analysis would be handled at the system level. The DSM above was only responsible for evaluating the scenarios given to it by the top-level Monte Carlo simulation.

Table 32 – Table of Coupling Variables for Monte Carlo Confirmation

Coupling Location	Parameters Passed
Mass Properties – Propulsion (1)	GLOW
Mass Properties – Trajectory (2)	GLOW, Sref
Propulsion – Trajectory (3)	Tvac, Ae, Ispvac
Propulsion – Mass Properties	T/W_e

The mass properties algorithm was different from the previous probabilistic optimization in two ways. First, there was no sizing step. This meant that the analysis took place for a single length vehicle, the same length that was the solution to the probabilistic optimization. Second, the probabilistic analysis does not take place at the contributing analysis level, so the functions to generate runs and pass them to the mass properties spreadsheets were eliminated. The steps taken to implement this were to eliminate the VB script to run several scenarios for mass properties and then wrap all of the assumptions corresponding to random variables into ModelCenter© as inputs, and all of the responses corresponding to output variables required by other analyses and output distributions.

The propulsion contributing analysis in this case was a simple wrapping of the SCORES analysis, with no run generating function or Perl wrapper. Inputs were taken for Tsl (generated by T/W_v and GLOW) and the settings of the design variables at the optimum point, and a sized engine was sent back to the mass properties. These analyses were iterated until the engine size was consistent, then the propulsion data for the chosen scenario was sent to the trajectory analysis.

The Monte Carlo trial ended with a call to the trajectory contributing analysis. Because there was no sizing involved, a feedback to mass properties was not necessary. The trajectory contributing analysis here consisted of the original call to POST using a random atmosphere generated by the GRAM99 range model. This was not the parameterized atmosphere used by the approximation methods.

This system of contributing analyses was run 1,000 times for random scenarios picked from the POST / GRAM99, SCORES and mass properties random inputs. For the POST analysis, the random variables that were required for input were the aerodynamic multipliers and the random atmosphere. The atmosphere generation required a different random seed each time, along with a random date and time of launch. SCORES required random values for the engine chamber pressure and power-to-weight ratio while the mass properties took random parameters corresponding the assumptions in the MER's. The settings for these random variables were identical to those in the respective analysis test baseline Monte Carlo simulations. The simulation took approximately 24 hours running on a combination of Windows NT and SGI Octane workstations. This makes it far too slow to even use in a sizing process, much less an optimization.

The table of results in Table 33 reveals some important facts about the approximations used for optimization in this research. Because there was no feedback from the trajectory optimization, inaccuracies in the results of this analysis must either come from an inaccurate input or a bias in the analysis approximation itself. In converse, inaccuracies in the trajectory outputs had no effect on the results from the other contributing analyses. Keeping this in mind, Table 33 seems to show that the propulsion and mass properties analyses matched well with the Monte Carlo simulation, while the

trajectory analysis output parameters had values outside the error bands for the Monte Carlo. Most likely due to a problem modeling the trajectory during optimization, this fortunately only lead to a slight underestimate of the probability of success with regards to meeting propellant requirements in the sizing process. This meant that the size of the vehicle was slightly overestimated when compared to the confidence level indicated by the result of the Monte Carlo simulation. However, this error was small enough that it was still well within the 95% confidence level error bands calculated for the Monte Carlo simulation.

Table 33 – Results of Full Monte Carlo Confirmation of Optimum

System Parameter	Approx. Estimate	Monte Carlo Estimate	95% C.I.	Rel. Error
Dry Weight μ	142,190 lb.	142,190 lb.	$\pm$ 300 lb.	0 %
Dry Weight σ	4,880 lb.	4,840 lb.	$\pm$ 213 lb.	0.826 %
P(Dry > 150,200 lb.)	95 %	94.7 %	$\pm$ 11 %	0.317 %
MRReq μ	8.0496	8.0400	$\pm$ 0.0016	0.119 %
MRReq σ	0.0309	0.0261	$\pm$ 0.0011	18.4 %
MRavail μ	8.2331	8.2446	$\pm$ 0.013	0.139 %
MRavail σ	0.217	0.215	$\pm$ 0.010	0.930 %
P(MRReq - MRavail > 0)	80 %	82.4 %	$\pm$ 5 %	2.91 %

To show the accuracy of the propulsion and mass properties approximations, Figure 78 shows a plot of the approximate dry weight for the fixed OML optimum vehicle generated using the approximation compared to the Monte Carlo result for the same random variable. As is shown in Table 33, the result here has negligible error. The probability density values for the Gaussian plot were scaled to match the frequency plot for the Monte Carlo simulation.

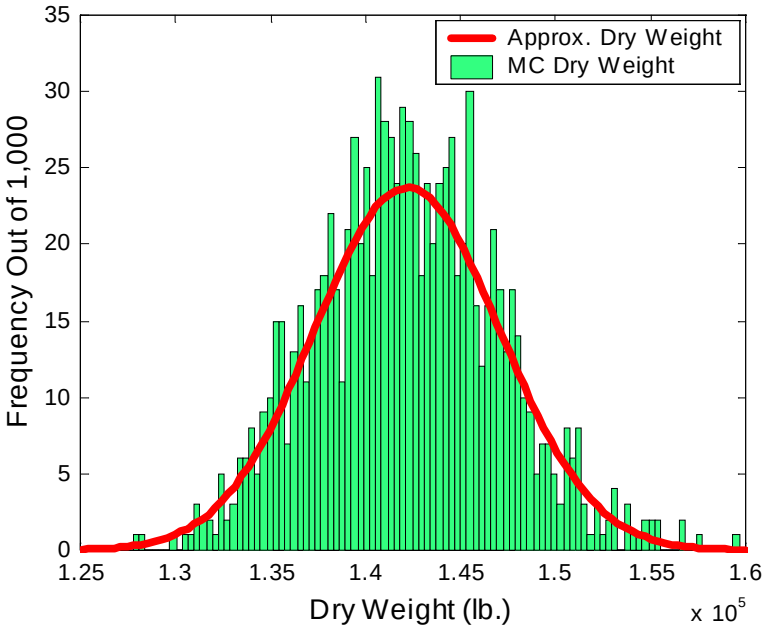

Figure 78 – Dry Weight Approximation and Monte Carlo Confirmation

Figure 79 shows the error in mass ratio required and the impact it had on the overall system. While the errors are significant to the estimate for required mass ratio, the large spread of the mass ratio available probability minimizes the impact of the error and puts the mass ratio difference error back in the confidence level for the Monte Carlo

simulation. For the Gaussian line plots, the probability density was scaled to match the frequency axis of the Monte Carlo simulation results.

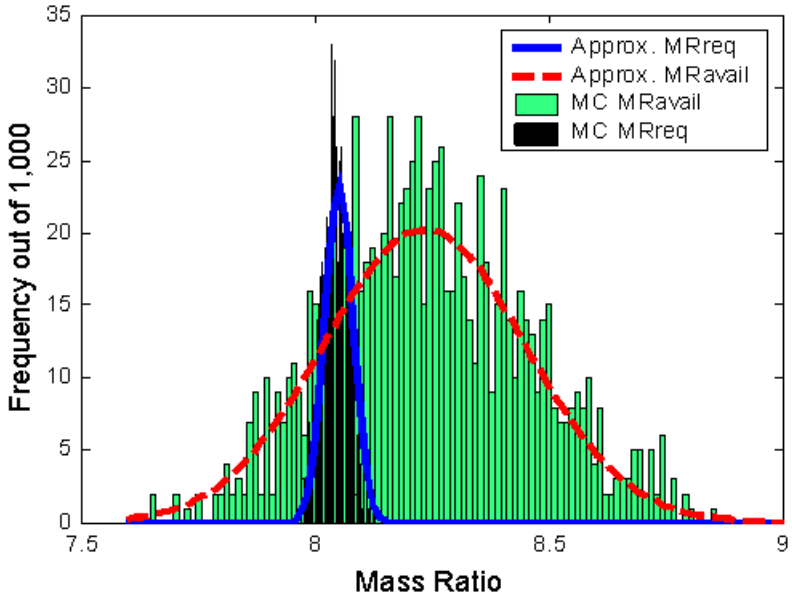

Figure 79 – Sizing Histogram for Full Monte Carlo Confirmation

While the cause of this small error does lie in the trajectory analysis, the cause could be any number of approximations made by this algorithm. Because the error was not a problem to the overall synthesis estimates, this was still a good method for probabilistic optimization. However, it is clear where room for improvement in accuracy in terms of contributing analysis probability estimation lies.

10.6 Deterministic Optimization Comparison

To see if there was any difference between the deterministic optimum and the probabilistic optimum solution, a deterministic optimization using the same models and design variables was conducted. The models used were the direct versions of the propulsion and mass properties/sizing algorithms and the response surface version of the trajectory analysis. The results of this were compared to the probabilistic optimum for 95% confidence level dry weight to determine their differences.

These results were compared using two criteria. First, it was determined if the settings of the design variables were any different from the probabilistic optimization. This should give relative information about which design variables are related to robustness in weight growth. Second, the difference will be shown in the results of the two optimizations, such as the reported dry weight value and OML size. This will show how using probabilistic information can tailor the reported results to the desired risk level of the program. If a high risk is tolerable, the confidence levels can be reduced and more optimistic results can be reported. If it is not tolerable, the confidence levels can be raised and correspondingly less optimistic results reported. The key is that the risk is expressed in easy to translate terms, such as the probability of not having enough propellant for the mission, or the probability of a dry weight value larger than 150,000 lb. It is easier to quantify this risk than the risk associated with changing dry weight margins.

The results in Table 34 show a decided similarity between the design variable settings for the probabilistic and deterministic optimizations. The one small difference that is consistent is the difference in mixture ratio. The optimizations found that a slightly lower mixture ratio was favorable for the probabilistic optimum. This is surprising because most of the uncertainty in sizing is due to the mass properties algorithm, an

analysis that usually favors higher bulk density for system robustness [37]. The shift in mass ratio required due to the slightly higher engine specific impulse seems to have offset this effect.

Table 34 – Results of Deterministic Optimization Comparison

Design Variable	Start Pt. 1	Opt. Pt. 1 (Prob./Det.)	Start Pt. 2	Opt Pt. 2 (Prob./Det.)	Start Pt. 3	Opt. Pt. 3 (Prob./Det.)
Mixture Ratio (r)	6	5.61 / 5.65	5	5.60 / 5.65	7	5.62 / 5.66
Area Ratio (AR)	77.5	53.2 / 52.3	85	52.1 / 52.7	85	51.3 / 54.0
Vehicle Thrust to Weight (T/W_v)	1.2	1.2 / 1.2	1.6	1.2 / 1.2	1.4	1.2 / 1.2
Engine Chamber Pressure (Pch)	206 atm.	210 / 210 atm.	210 atm.	210 / 210 atm.	150 atm.	210 / 210 atm.
95% C.L. Dry Weight / Dry Weight	158.3 / 138.4 klb.	151.0 / 133.8 klb.	186.4 / 163.5 klb.	151.0 / 133.8 klb.	250.4 / 213.7 klb.	151.1 / 133.9 klb.
Prob. Length / Det. Length	147 / 142 ft.	147 / 142 ft.	152 / 147 ft.	147 / 142 ft.	168 / 161 ft.	147 / 142 ft.

These optimizations took around 10 minutes each to complete. While this was a very short amount of time, it took only 40 times longer (~6 hrs.) to optimize the probabilistic system. Considering the number of noise variables (84), this is a below linear real-time cost scale-up to use the distributed probabilistic system. This was a major cost savings over existing methods.

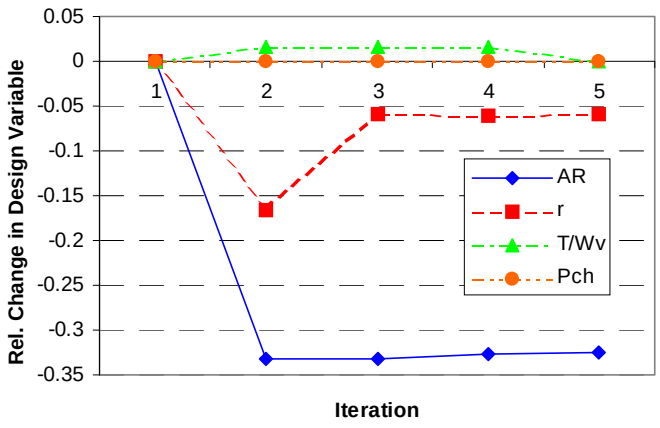

Figure 80 – Design Variable History for Initial Deterministic Optimization

The convergence of the deterministic optimization was slightly better than that of the probabilistic optimization. This was most likely due to the more accurate gradients, since a smaller step size was possible for finite difference estimates. It is clear from a comparison of Figure 75 and Figure 80 that the deterministic optimization process was close to the optimum much sooner than the probabilistic process. The results here show that there is a small difference in the optimum variable settings for the two optimizations, but a large difference in the conservatism of the final answer.

To determine to which confidence levels the deterministic optimum corresponded, a Monte Carlo simulation of the final deterministic optimum was conducted. This simulation was similar to the confirmation of the probabilistic optimum except that it was conducted at a smaller length for slightly different settings of the design variables. The results of this simulation show that the probability of the reported dry weight being equal to or lower than 133.8 klbs. was only 53%. In addition, the confidence level associated

with having enough propellant to perform the mission was only 54%. When compared to the error associated with a 1,000 trial Monte Carlo simulation, these can be both considered around 50%. These values are much lower than the 95% and 80% confidence levels reported for the probabilistic optimum. Histograms of mass ratio required and mass ratio available for the deterministic optimum can be seen in Figure 81. The curves represent the predictions for the probabilistic optimum. As can be seen in Figure 81, the probabilistically sized vehicle has a much higher probability of the mass ratio available exceeding the mass ratio required.

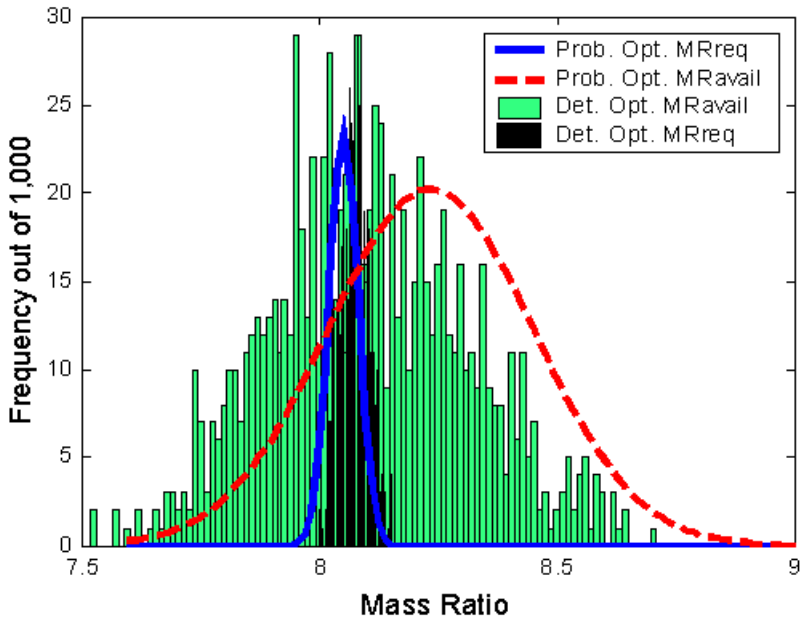

Figure 81 – Sizing Histogram of Deterministic Optimum

Apparently, the deterministic assumption of 15% dry weight margin corresponds to a fairly high risk level when compared to what was considered acceptable for the

probabilistic phases of this study. The acceptable probability of success with regards to meeting propellant requirements for orbit was only 80%, and the probability of coming in under dry mass budget was 95%. These probabilities were not outrageously high, and in the case of the propellant requirement constraint, actually quite low. These results combined with the results of the Monte Carlo simulation of the deterministic optimum suggested that a 15% margin was very risky with respect to the assumptions made here about noise variables.

CHAPTER XI

CONCLUSIONS AND RECOMMENDATIONS

11.1 Conclusions

In conclusion, the goals set for this research have been met as they pertained to aspects of the problem formulation, the distributed probabilistic launch vehicle design framework and the new methods for output distribution estimation. The contribution of the distributed probability method has been demonstrated and confirmed as accurate. Also, new methods for uncertainty analysis, and the inclusion of previously unconsidered uncertainties in the conceptual launch vehicle design process were demonstrated. When combined together, these contributions greatly enhance loosely coupled conceptual launch vehicle design.

The specific goals attained were as follows:

- A new distributed probabilistic framework for launch vehicle conceptual design was demonstrated.

This was evidenced by the detailed process account given in this research. Also, now that the technique has been demonstrated, it should allow for this process to be re-implemented in less than two man-weeks. This implementation can also be done in

parallel by individual disciplinary experts and as a result improve the overall process setup time. Finally, all of the uncertainty analysis was conducted at the contributing analysis level. This was important to retaining the advantages of distributed analysis.

- The utilization of heterogeneous computing platforms in a distributed probabilistic framework was demonstrated by the inclusion of executable programs, Perl scripts, Matlab scripts and Excel worksheets in a single automated framework.

These codes were based on both SGI workstations and Windows NT PC's. While this was done using the ModelCenter© commercial analysis integration package, the compatibility of this package with the distributed probabilistic launch vehicle design problem was a key to the utility of the technique.

- The goal of a multiple order of magnitude improvement in speed over a Monte Carlo simulation method was demonstrated.

This was shown in the fact that an entire probabilistic vehicle sizing process could be accomplished in about thirty minutes using the distributed approximations, while just a single length evaluation process took around 16 hours using a non-distributed Monte Carlo simulation. Accounting for the repeated simulations that would be required for a sizing process, this is a three order of magnitude improvement over a direct, system-level Monte Carlo process.

- Optimization utilizing the distributed probability analysis method was shown to be fast.

The goal of overnight optimization was met by the fact that the demonstration optimizations took between 6 and 8 hours each. Considering the amount of time that the non-distributed Monte Carlo simulation took for just a single length analysis, this is a huge savings.

- The test optimization was confirmed, showing that the problem formulation was sound and that the noise in the sizing process was not so great as to interfere with accurate gradient generation. This was shown by the optimization finding the same point from three separate starting locations.

- The accuracy of the distributed approximation was also found to be quite good.

It exceeded the objective of 5% accuracy set for constraint satisfaction by a comfortable margin for both the propellant required and dry weight confidence level calculations. This was determined by comparison of the found optimum to a single length Monte Carlo simulation. In addition to this, all of the critical output parameters, along with the majority of all parameters were well within the error bounds calculated for the Monte Carlo simulation.

- A new method of engineering uncertainty analysis, DPOMD, was demonstrated and tested. This was evidenced by a detailed description of the procedure, and a series of applications in the analysis testing section of this research. This method is separate from the distributed framework and can be applied to a single discipline problem.

- This new method was shown to have ease of setup, as the only inputs to the process were the moment information and the reduction factor for the fractional factorial

design. This demonstration also showed that the technique could be easily applied once the underlying algorithm had been programmed.

- Several techniques for uncertainty analysis on the conceptual launch vehicle design contributing analyses were tested and preferred methods were identified.

The tests revealed several things about the methods that were tested with respect to each of the contributing analyses. First, it is important that all of the output parameters were accurately represented by the methods. Some of the eliminated techniques were excellent on the main output parameters, but were far away from the reference for many of the correlations.

- More than one type of uncertainty analysis was chosen for the final optimization problem.

This confirms the hypothesis that different methods are better suited for different contributing analyses. This is one of the major motivating factors behind using distributed probability analysis.

- Several sources for uncertainty were identified and incorporated into the reusable launch vehicle conceptual design process.

These sources included weight, engine performance and atmospheric uncertainties. For the distributions available in the open literature, historical values were set. Otherwise, reasonable assumptions were made based on deltas around deterministic

values. All major assumptions for this launch vehicle problem were expressed as noise distributions.

- While the deterministic and probabilistic optimum design variable settings were not very different, the reported vehicle size by the two processes was vastly different. This means that the reported size of the analysis corresponds to a specific user confidence level, not just an arbitrary growth safety factor.

All in all, a new fast and efficient method for probabilistic optimization of conceptual launch vehicle designs was presented, along with test results verifying its speed and accuracy. This new architecture has the potential to allow for the practical probabilistic optimization of reusable launch vehicles in inherently distributed environments where it was impractical before.

11.2 Recommendations

There are several recommendations related to future application of this work. These relate to areas for improvement of the existing system, as well as advice about the application of more advanced multidisciplinary design optimization (MDO) methods such as collaborative optimization and optimization-based decomposition. This advice should be a useful guide for future research in this area, as well as identify specific areas where technological advancement is need in optimization, analysis and meta-modeling techniques.

11.2.1 Trajectory Contributing Analysis

The trajectory contributing analysis poses some unique obstacles to efficient conceptual design. An industry-standard tool used in this research, POST [163], is universally accepted as accurate, but has some robustness problems. This makes it difficult to use in an automated framework. To overcome this, there are several options.

One option is to use a meta-modeling technique. This allows the code to be run offline, where failed runs can be fixed by user intervention. Once the meta-model is complete, the reliability of the original analysis no longer matters. Future work in this area should concentrate on finding meta-models that are more accurate for probabilistic analysis. While the response surface equations used in this research were acceptable, there is room for improvement in this area. This improvement could come from either alternative modeling techniques such as neural networks and Kriging, or methods that allow inherent uncertainties to represented by the model without variable assumptions. This would allow for higher numbers of noise variables to be considered without lowering the number of input variables in the model.

Another way to improve the analysis would be to improve the speed and reliability of the trajectory analysis itself. Collocation methods could be one way to do this, but these are not yet as universally accepted as the integration methods of POST [190]. In any event, a several order of magnitude improvement in the optimization time would be required to make any of the accelerated sampling schemes such as Descriptive Sampling or DPOMD practical. This may be possible in the future, but right now it is impractical for even moderate levels of noise.

All considered, the trajectory problem with atmospheric uncertainty is a difficult analysis to incorporate into a conceptual design optimization. While it was done successfully here, future attempts could benefit from the advice in this section.

11.2.2 Application of Advanced MDO Techniques

There are many issues pertaining to the application of advanced MDO techniques to problems containing uncertainty. Primarily, these issues relate to the idea of near-term and far-term design variables, and how these are handled by the system.

It may be possible to apply Collaborative Optimization (CO) to this problem, but the bi-level optimization of the standard CO application would have to become a tri-level scheme. This is because the near and far term variables at the contributing analysis level would have to be optimized separately.

The system level optimization would coordinate the probabilistic analyses in much the same way a deterministic system would be optimized using CO. Here the coupling variables would be the distribution parameters and the compatibility constraints would be set up to ensure compatibility among these couplings.

At the second level, the optimizer minimizes the compatibility constraint from the system, but for each analysis, selects randomly from its own version of the input and output coupling distributions. Based on each scenario selected from these distributions, a new compatibility constraint is constructed for each trial.

The third-level optimizer minimizes this new compatibility constraint using its own version of the scenario variables, along with any far-term variables that may exist.

Back at the second level, this leads to a distribution of the lower level compatibility constraints that represents each scenario's viability. This distribution is therefore a constraint at the second level that must be satisfied probabilistically, to some confidence level. This system would ensure an entire system optimum for a probabilistic objective function even with respect to variables that are not determined in the current analysis.

Because bi-level optimization is only in the early stages of becoming practical, and usually leads to slower systems that generally find an answer similar to traditional methods, tri-level optimization was deemed not practical to include in this work. It had the disadvantage of being even more unintuitive than collaborative optimization and therefore even less likely to be applied in a real-world engineering environment. The above observations are offered solely out of academic interest.

On another note, Optimization-Based Decomposition (OBD) is not very compatible with this idea of probability analysis, as the near-term and far-term variables would all have to be controlled by the same optimizer. This means that there would have to be a set of far-term variables for each scenario in the probabilistic analysis, potentially leading to millions of control variables for the system-level optimizer to handle, depending on the size of the probabilistic analysis. This also does not seem practical and is therefore not a recommended advanced method.

APPENDIX A

ATMOSPHERIC ASSUMPTIONS

The following tables are the result of the GRAM99 Monte Carlo multivariate normal distribution fit for the reduced number of points.

.

Atmospheric Variable	Alias	Mean	Std. Dev.	Corr. to P1	Corr. to P2	Corr. to P3	Corr. to P4
Pressure @ S/L (psf.)	P1	2.129E+03	3.649E+01	1.0000	0.7186	0.9671	-0.6247
Pressure @ 14,880 ft. (psf.)	P2	1.226E+03	1.330E+01	0.7186	1.0000	0.7845	0.0591
Pressure @ 38,060 ft. (psf.)	P3	4.571E+02	8.079E+00	0.9671	0.7845	1.0000	-0.5376
Pressure @ 54,240 ft. (psf.)	P4	2.063E+02	3.155E+00	-0.6247	0.0591	-0.5376	1.0000
Pressure @ 73,200 ft. (psf.)	P5	7.984E+01	1.030E+00	0.3921	-0.2083	0.2715	-0.7168
Pressure @ 94,290 ft. (psf.)	P6	2.972E+01	6.137E-01	-0.0838	0.5232	0.0576	0.6456
Pressure @ 164,770 ft. (psf.)	P7	1.639E+00	6.759E-02	0.8893	0.5775	0.9085	-0.6919
Density @ S/L (slug/ft3.)	ρ1	2.382E-03	3.767E-05	0.1090	-0.3463	-0.0423	-0.4314
Density @ 14,880 ft. (slug/ft3.)	ρ2	1.477E-03	1.379E-05	0.5512	0.0023	0.4769	-0.7676
Density @ 38,060 ft. (slug/ft3.)	ρ3	6.728E-04	1.311E-05	0.1190	-0.3757	0.0452	-0.4887
Density @ 54,240 ft. (slug/ft3.)	ρ4	3.287E-04	8.154E-06	0.3817	0.5716	0.4842	0.0902
Density @ 73,200 ft. (slug/ft3.)	ρ5	1.208E-04	1.857E-06	-0.6929	-0.5584	-0.7340	0.4651
Density @ 94,290 ft. (slug/ft3.)	ρ6	4.259E-05	7.344E-07	0.7236	0.4565	0.7383	-0.5730
Density @ 140,660 ft. (slug/ft3.)	ρ7	5.036E-06	1.822E-07	0.5142	0.6112	0.5964	-0.1351
Temperature @ S/L (°R)	T1	5.183E+02	7.119E+00	0.7120	0.8333	0.7854	-0.1508
Temperature @ 54,240 ft. (°R)	T2	3.657E+02	5.083E+00	-0.6259	-0.4247	-0.6672	0.4328
Temperature @ 140,660 ft. (°R)	T3	4.773E+02	1.083E+01	-0.7425	-0.3811	-0.7342	0.6868
Temperature @ 164,770 ft. (°R)	T4	4.776E+02	9.264E+00	0.5021	0.6041	0.5864	-0.1212
Temperature @ 229,720 ft. (°R)	T5	3.966E+02	1.307E+01	-0.5548	0.0018	-0.4753	0.7861
Temperature @ 274,320 ft. (°R)	T6	3.769E+02	1.526E+01	0.6701	0.2846	0.6486	-0.6729
Temperature @ 303,800 ft. (°R)	T7	3.496E+02	2.470E+01	-0.3831	-0.5291	-0.4651	0.0292
Northerly Wind @ S/L (fps.)	N1	2.770E+00	1.572E+01	-0.8555	-0.3823	-0.8298	0.8370
Northerly Wind @ 38,060 ft. (fps.)	N2	1.278E+02	4.650E+01	-0.8569	-0.4703	-0.8555	0.7544
Northerly Wind @ 73,200 ft. (fps.)	N3	1.681E+01	2.498E+01	-0.2035	0.3842	-0.0765	0.6575
Northerly Wind @ 164,770 ft. (fps.)	N4	7.264E+01	7.982E+01	-0.8228	-0.4388	-0.8171	0.7370
Northerly Wind @ 210,080 ft. (fps.)	N5	2.030E+02	1.027E+02	0.7330	0.2816	0.7027	-0.7632
Northerly Wind @ 229,720 ft. (fps.)	N6	1.928E+02	1.215E+02	0.0350	-0.4548	-0.0861	-0.4899
Easterly Wind @ S/L (fps.)	E1	-2.788E+00	1.591E+01	-0.6809	-0.4320	-0.6948	0.5424
Easterly Wind @ 3,550 ft. (fps.)	E2	5.186E+00	2.171E+01	-0.2229	0.2603	-0.1216	0.5631
Easterly Wind @ 38,060 ft. (fps.)	E3	1.626E+01	4.412E+01	-0.6567	-0.4685	-0.6833	0.4719
Easterly Wind @ 73,200 ft. (fps.)	E4	-1.005E-01	1.130E+01	-0.2935	0.1829	-0.2040	0.5860
Easterly Wind @ 94,290 ft. (fps.)	E5	8.268E+00	1.781E+01	0.1558	-0.3066	0.0531	-0.5178
Easterly Wind @ 116,950 ft. (fps.)	E6	1.203E+00	2.600E+01	-0.2319	0.2494	-0.1360	0.5667
Easterly Wind @ 164,770 ft. (fps.)	E7	2.633E+01	4.552E+01	-0.6312	-0.3788	-0.6388	0.5222
Easterly Wind @ 188,260 ft. (fps.)	E8	2.875E+01	4.618E+01	0.1342	0.4582	0.2304	0.2524
Easterly Wind @ 247,020 ft. (fps.)	E9	1.595E+01	8.840E+01	-0.6626	-0.6329	-0.7298	0.3244
Easterly Wind @ 261,900 ft. (fps.)	E10	2.269E+01	9.251E+01	-0.7571	-0.2830	-0.7213	0.7951
Downward Wind @ S/L (fps.)	D1	2.034E-02	3.066E+00	0.0051	-0.0089	-0.0006	-0.0127
Downward Wind @ 844 ft. (fps.)	D2	-2.860E-02	4.988E+00	0.0048	-0.0003	0.0003	-0.0069
Downward Wind @ 3,550 ft. (fps.)	D3	9.852E-03	5.050E+00	-0.0021	-0.0103	-0.0066	-0.0083
Downward Wind @ 8,150 ft. (fps.)	D4	-2.450E-02	4.582E+00	0.0117	0.0034	0.0110	-0.0137
Downward Wind @ 14,880 ft. (fps.)	D5	-7.831E-02	3.785E+00	-0.0092	-0.0037	-0.0094	0.0099
Downward Wind @ 210,080 ft. (fps.)	D6	7.499E-02	5.149E+00	0.0018	-0.0033	0.0022	-0.0077
Downward Wind @ 297,520 ft. (fps.)	D7	-3.853E-01	1.626E+01	0.0119	0.0131	0.0127	-0.0027

Atmospheric Variable	Alias	Corr. to P5	Corr. to P6	Corr. to P7	Corr. to ρ1	Corr. to ρ2	Corr. to ρ3
Pressure @ S/L (psf.)	P1	0.3921	-0.0838	0.8893	0.1090	0.5512	0.1190
Pressure @ 14,880 ft. (psf.)	P2	-0.2083	0.5232	0.5775	-0.3463	0.0023	-0.3757
Pressure @ 38,060 ft. (psf.)	P3	0.2715	0.0576	0.9085	-0.0423	0.4769	0.0452
Pressure @ 54,240 ft. (psf.)	P4	-0.7168	0.6456	-0.6919	-0.4314	-0.7676	-0.4887
Pressure @ 73,200 ft. (psf.)	P5	1.0000	-0.9047	0.2327	0.8837	0.7330	0.8145
Pressure @ 94,290 ft. (psf.)	P6	-0.9047	1.0000	0.0259	-0.8965	-0.6179	-0.7984
Pressure @ 164,770 ft. (psf.)	P7	0.2327	0.0259	1.0000	-0.1345	0.5081	0.0072
Density @ S/L (slug/ft3.)	ρ1	0.8837	-0.8965	-0.1345	1.0000	0.5248	0.7696
Density @ 14,880 ft. (slug/ft3.)	ρ2	0.7330	-0.6179	0.5081	0.5248	1.0000	0.5586
Density @ 38,060 ft. (slug/ft3.)	ρ3	0.8145	-0.7984	0.0072	0.7696	0.5586	1.0000
Density @ 54,240 ft. (slug/ft3.)	ρ4	-0.3933	0.6293	0.5141	-0.6211	-0.1088	-0.4072
Density @ 73,200 ft. (slug/ft3.)	ρ5	0.0520	-0.1786	-0.7828	0.3038	-0.2789	0.1976
Density @ 94,290 ft. (slug/ft3.)	ρ6	0.2067	0.0628	0.8089	-0.1033	0.4244	0.0219
Density @ 140,660 ft. (slug/ft3.)	ρ7	-0.3286	0.5146	0.6941	-0.5578	0.0086	-0.4143
Temperature @ S/L (°R)	T1	-0.3031	0.5617	0.7609	-0.6078	0.0523	-0.4406
Temperature @ 54,240 ft. (°R)	T2	-0.0427	-0.1971	-0.7835	0.3041	-0.3029	0.0784
Temperature @ 140,660 ft. (°R)	T3	-0.3315	0.1464	-0.8479	-0.0281	-0.5184	-0.1300
Temperature @ 164,770 ft. (°R)	T4	-0.3282	0.5141	0.5497	-0.5558	-0.0006	-0.4079
Temperature @ 229,720 ft. (°R)	T5	-0.7389	0.6327	-0.5117	-0.5322	-0.6862	-0.5396
Temperature @ 274,320 ft. (°R)	T6	0.4123	-0.2403	0.7033	0.1373	0.5402	0.2137
Temperature @ 303,800 ft. (°R)	T7	0.3705	-0.5176	-0.4976	0.5493	0.0693	0.4214
Northerly Wind @ S/L (fps.)	N1	-0.4989	0.2812	-0.8920	-0.1555	-0.6630	-0.2545
Northerly Wind @ 38,060 ft. (fps.)	N2	-0.3545	0.1237	-0.9196	-0.0021	-0.5774	-0.1297
Northerly Wind @ 73,200 ft. (fps.)	N3	-0.9111	0.9180	-0.0867	-0.8550	-0.6410	-0.7803
Northerly Wind @ 164,770 ft. (fps.)	N4	-0.3562	0.1387	-0.8850	-0.0215	-0.5608	-0.1369
Northerly Wind @ 210,080 ft. (fps.)	N5	0.4986	-0.3164	0.7575	0.2011	0.6110	0.2877
Northerly Wind @ 229,720 ft. (fps.)	N6	0.7972	-0.8508	-0.0876	0.8111	0.5059	0.7115
Easterly Wind @ S/L (fps.)	E1	-0.1845	-0.0078	-0.7469	0.1010	-0.3971	-0.0127
Easterly Wind @ 3,550 ft. (fps.)	E2	-0.7270	0.7162	-0.1357	-0.6620	-0.5441	-0.6092
Easterly Wind @ 38,060 ft. (fps.)	E3	-0.0957	-0.0968	-0.7324	0.1800	-0.3312	0.0520
Easterly Wind @ 73,200 ft. (fps.)	E4	-0.7014	0.6606	-0.2193	-0.5981	-0.5523	-0.5694
Easterly Wind @ 94,290 ft. (fps.)	E5	0.7146	-0.7314	0.0616	0.6784	0.5022	0.6086
Easterly Wind @ 116,950 ft. (fps.)	E6	-0.7215	0.7073	-0.1496	-0.6490	-0.5434	-0.6042
Easterly Wind @ 164,770 ft. (fps.)	E7	-0.2036	0.0279	-0.6930	0.0596	-0.3920	-0.0379
Easterly Wind @ 188,260 ft. (fps.)	E8	-0.5819	0.6607	0.2380	-0.6545	-0.3031	-0.5570
Easterly Wind @ 247,020 ft. (fps.)	E9	0.1781	-0.3896	-0.7855	0.4644	-0.1620	0.3161
Easterly Wind @ 261,900 ft. (fps.)	E10	-0.5313	0.3466	-0.7778	-0.2309	-0.6421	-0.3080
Downward Wind @ S/L (fps.)	D1	0.0248	-0.0251	-0.0038	0.0300	0.0173	0.0234
Downward Wind @ 844 ft. (fps.)	D2	0.0123	-0.0164	-0.0035	0.0143	0.0015	0.0103
Downward Wind @ 3,550 ft. (fps.)	D3	0.0193	-0.0224	-0.0049	0.0199	0.0161	0.0156
Downward Wind @ 8,150 ft. (fps.)	D4	0.0114	-0.0091	0.0105	0.0074	0.0172	-0.0039
Downward Wind @ 14,880 ft. (fps.)	D5	-0.0015	-0.0020	-0.0152	0.0018	0.0054	-0.0032
Downward Wind @ 210,080 ft. (fps.)	D6	0.0047	-0.0034	0.0054	-0.0028	0.0069	0.0089
Downward Wind @ 297,520 ft. (fps.)	D7	0.0052	-0.0002	0.0132	0.0054	0.0081	0.0028

Atmospheric Variable	Alias	Corr. to ρ4	Corr. to ρ5	Corr. to ρ6	Corr. to ρ7	Corr. to T1	Corr. to T2
Pressure @ S/L (psf.)	P1	0.3817	-0.6929	0.7236	0.5142	0.7120	-0.6259
Pressure @ 14,880 ft. (psf.)	P2	0.5716	-0.5584	0.4565	0.6112	0.8333	-0.4247
Pressure @ 38,060 ft. (psf.)	P3	0.4842	-0.7340	0.7383	0.5964	0.7854	-0.6672
Pressure @ 54,240 ft. (psf.)	P4	0.0902	0.4651	-0.5730	-0.1351	-0.1508	0.4328
Pressure @ 73,200 ft. (psf.)	P5	-0.3933	0.0520	0.2067	-0.3286	-0.3031	-0.0427
Pressure @ 94,290 ft. (psf.)	P6	0.6293	-0.1786	0.0628	0.5146	0.5617	-0.1971
Pressure @ 164,770 ft. (psf.)	P7	0.5141	-0.7828	0.8089	0.6941	0.7609	-0.7835
Density @ S/L (slug/ft3.)	ρ1	-0.6211	0.3038	-0.1033	-0.5578	-0.6078	0.3041
Density @ 14,880 ft. (slug/ft3.)	ρ2	-0.1088	-0.2789	0.4244	0.0086	0.0523	-0.3029
Density @ 38,060 ft. (slug/ft3.)	ρ3	-0.4072	0.1976	0.0219	-0.4143	-0.4406	0.0784
Density @ 54,240 ft. (slug/ft3.)	ρ4	1.0000	-0.4029	0.4361	0.6321	0.7134	-0.8541
Density @ 73,200 ft. (slug/ft3.)	ρ5	-0.4029	1.0000	-0.5706	-0.6161	-0.7301	0.5512
Density @ 94,290 ft. (slug/ft3.)	ρ6	0.4361	-0.5706	1.0000	0.5360	0.6135	-0.6617
Density @ 140,660 ft. (slug/ft3.)	ρ7	0.6321	-0.6161	0.5360	1.0000	0.7704	-0.5958
Temperature @ S/L (°R)	T1	0.7134	-0.7301	0.6135	0.7704	1.0000	-0.6650
Temperature @ 54,240 ft. (°R)	T2	-0.8541	0.5512	-0.6617	-0.5958	-0.6650	1.0000
Temperature @ 140,660 ft. (°R)	T3	-0.3104	0.6285	-0.6513	-0.7587	-0.5358	0.6089
Temperature @ 164,770 ft. (°R)	T4	0.6307	-0.6022	0.5174	0.6146	0.7612	-0.5884
Temperature @ 229,720 ft. (°R)	T5	0.1240	0.2896	-0.4235	-0.0006	-0.0485	0.2980
Temperature @ 274,320 ft. (°R)	T6	0.2162	-0.5148	0.5846	0.3356	0.4072	-0.5257
Temperature @ 303,800 ft. (°R)	T7	-0.5707	0.5105	-0.3980	-0.5870	-0.6662	0.4915
Northerly Wind @ S/L (fps.)	N1	-0.2842	0.6664	-0.7349	-0.4338	-0.5346	0.6651
Northerly Wind @ 38,060 ft. (fps.)	N2	-0.3972	0.7222	-0.7552	-0.5304	-0.6413	0.7177
Northerly Wind @ 73,200 ft. (fps.)	N3	0.5042	-0.1306	-0.0823	0.4149	0.4368	-0.0827
Northerly Wind @ 164,770 ft. (fps.)	N4	-0.3663	0.6857	-0.7271	-0.5044	-0.6018	0.6829
Northerly Wind @ 210,080 ft. (fps.)	N5	0.1964	-0.5474	0.6253	0.3270	0.4107	-0.5546
Northerly Wind @ 229,720 ft. (fps.)	N6	-0.5621	0.2449	-0.0606	-0.4952	-0.5336	0.2185
Easterly Wind @ S/L (fps.)	E1	-0.3935	0.6047	-0.6140	-0.4869	-0.5802	0.6068
Easterly Wind @ 3,550 ft. (fps.)	E2	0.3608	-0.0414	-0.1172	0.2755	0.2897	-0.0121
Easterly Wind @ 38,060 ft. (fps.)	E3	-0.4391	0.6110	-0.6005	-0.5211	-0.6167	0.6089
Easterly Wind @ 73,200 ft. (fps.)	E4	0.2767	0.0263	-0.1865	0.2003	0.1906	0.0711
Easterly Wind @ 94,290 ft. (fps.)	E5	-0.4170	0.0976	0.0276	-0.3318	-0.3509	0.0843
Easterly Wind @ 116,950 ft. (fps.)	E6	0.3507	-0.0188	-0.1389	0.2660	0.2732	-0.0021
Easterly Wind @ 164,770 ft. (fps.)	E7	-0.3404	0.5553	-0.5623	-0.4353	-0.5141	0.5522
Easterly Wind @ 188,260 ft. (fps.)	E8	0.5196	-0.3442	0.1799	0.4956	0.5526	-0.3031
Easterly Wind @ 247,020 ft. (fps.)	E9	-0.6331	0.7182	-0.6363	-0.7128	-0.8159	0.6934
Easterly Wind @ 261,900 ft. (fps.)	E10	-0.1844	0.5573	-0.6379	-0.3228	-0.4074	0.5599
Downward Wind @ S/L (fps.)	D1	-0.0251	0.0062	0.0041	-0.0209	-0.0163	0.0159
Downward Wind @ 844 ft. (fps.)	D2	-0.0237	-0.0082	-0.0183	-0.0166	-0.0040	0.0188
Downward Wind @ 3,550 ft. (fps.)	D3	-0.0137	0.0142	-0.0068	-0.0152	-0.0140	0.0065
Downward Wind @ 8,150 ft. (fps.)	D4	-0.0013	-0.0079	0.0137	0.0070	0.0034	-0.0056
Downward Wind @ 14,880 ft. (fps.)	D5	-0.0079	-0.0050	-0.0184	-0.0192	-0.0066	0.0118
Downward Wind @ 210,080 ft. (fps.)	D6	-0.0002	0.0067	0.0062	0.0016	0.0034	-0.0036
Downward Wind @ 297,520 ft. (fps.)	D7	0.0067	0.0028	0.0085	0.0121	0.0055	-0.0073

Atmospheric Variable	Alias	Corr. to T3	Corr. to T4	Corr. to T5	Corr. to T6	Corr. to T7	Corr. to N1
Pressure @ S/L (psf.)	P1	-0.7425	0.5021	-0.5548	0.6701	-0.3831	-0.8555
Pressure @ 14,880 ft. (psf.)	P2	-0.3811	0.6041	0.0018	0.2846	-0.5291	-0.3823
Pressure @ 38,060 ft. (psf.)	P3	-0.7342	0.5864	-0.4753	0.6486	-0.4651	-0.8298
Pressure @ 54,240 ft. (psf.)	P4	0.6868	-0.1212	0.7861	-0.6729	0.0292	0.8370
Pressure @ 73,200 ft. (psf.)	P5	-0.3315	-0.3282	-0.7389	0.4123	0.3705	-0.4989
Pressure @ 94,290 ft. (psf.)	P6	0.1464	0.5141	0.6327	-0.2403	-0.5176	0.2812
Pressure @ 164,770 ft. (psf.)	P7	-0.8479	0.5497	-0.5117	0.7033	-0.4976	-0.8920
Density @ S/L (slug/ft3.)	ρ1	-0.0281	-0.5558	-0.5322	0.1373	0.5493	-0.1555
Density @ 14,880 ft. (slug/ft3.)	ρ2	-0.5184	-0.0006	-0.6862	0.5402	0.0693	-0.6630
Density @ 38,060 ft. (slug/ft3.)	ρ3	-0.1300	-0.4079	-0.5396	0.2137	0.4214	-0.2545
Density @ 54,240 ft. (slug/ft3.)	ρ4	-0.3104	0.6307	0.1240	0.2162	-0.5707	-0.2842
Density @ 73,200 ft. (slug/ft3.)	ρ5	0.6285	-0.6022	0.2896	-0.5148	0.5105	0.6664
Density @ 94,290 ft. (slug/ft3.)	ρ6	-0.6513	0.5174	-0.4235	0.5846	-0.3980	-0.7349
Density @ 140,660 ft. (slug/ft3.)	ρ7	-0.7587	0.6146	-0.0006	0.3356	-0.5870	-0.4338
Temperature @ S/L (°R)	T1	-0.5358	0.7612	-0.0485	0.4072	-0.6662	-0.5346
Temperature @ 54,240 ft. (°R)	T2	0.6089	-0.5884	0.2980	-0.5257	0.4915	0.6651
Temperature @ 140,660 ft. (°R)	T3	1.0000	-0.3784	0.5210	-0.6247	0.3288	0.7859
Temperature @ 164,770 ft. (°R)	T4	-0.3784	1.0000	0.0022	0.3164	-0.5792	-0.4227
Temperature @ 229,720 ft. (°R)	T5	0.5210	0.0022	1.0000	-0.5286	-0.0711	0.6698
Temperature @ 274,320 ft. (°R)	T6	-0.6247	0.3164	-0.5286	1.0000	-0.2009	-0.7235
Temperature @ 303,800 ft. (°R)	T7	0.3288	-0.5792	-0.0711	-0.2009	1.0000	0.3003
Northerly Wind @ S/L (fps.)	N1	0.7859	-0.4227	0.6698	-0.7235	0.3003	1.0000
Northerly Wind @ 38,060 ft. (fps.)	N2	0.7817	-0.5202	0.5828	-0.7039	0.3951	0.8907
Northerly Wind @ 73,200 ft. (fps.)	N3	0.2193	0.4164	0.6545	-0.3067	-0.4351	0.3619
Northerly Wind @ 164,770 ft. (fps.)	N4	0.7580	-0.4691	0.5675	-0.6818	0.3701	0.8584
Northerly Wind @ 210,080 ft. (fps.)	N5	-0.6784	0.3243	-0.6173	0.6389	-0.2113	-0.8013
Northerly Wind @ 229,720 ft. (fps.)	N6	-0.0613	-0.4876	-0.5007	0.1627	0.4894	-0.1824
Easterly Wind @ S/L (fps.)	E1	0.6183	-0.4790	0.4064	-0.5346	0.3816	0.6923
Easterly Wind @ 3,550 ft. (fps.)	E2	0.2322	0.2853	0.5431	-0.2833	-0.3102	0.3485
Easterly Wind @ 38,060 ft. (fps.)	E3	0.5884	-0.5133	0.3363	-0.5104	0.4148	0.6477
Easterly Wind @ 73,200 ft. (fps.)	E4	0.2852	0.2016	0.5640	-0.3399	-0.2344	0.4062
Easterly Wind @ 94,290 ft. (fps.)	E5	-0.1715	-0.3462	-0.5114	0.2349	0.3554	-0.2802
Easterly Wind @ 116,950 ft. (fps.)	E6	0.2372	0.2732	0.5555	-0.2999	-0.2914	0.3516
Easterly Wind @ 164,770 ft. (fps.)	E7	0.5802	-0.3998	0.3995	-0.5188	0.3346	0.6451
Easterly Wind @ 188,260 ft. (fps.)	E8	-0.0929	0.5139	0.3166	-0.0046	-0.4713	-0.0226
Easterly Wind @ 247,020 ft. (fps.)	E9	0.5932	-0.6933	0.1844	-0.4700	0.5921	0.6061
Easterly Wind @ 261,900 ft. (fps.)	E10	0.6975	-0.3143	0.6600	-0.6510	0.2091	0.8262
Downward Wind @ S/L (fps.)	D1	0.0048	-0.0125	-0.0107	0.0081	0.0166	-0.0034
Downward Wind @ 844 ft. (fps.)	D2	0.0071	-0.0131	-0.0096	0.0102	0.0108	0.0000
Downward Wind @ 3,550 ft. (fps.)	D3	0.0025	-0.0257	-0.0179	0.0010	0.0205	-0.0021
Downward Wind @ 8,150 ft. (fps.)	D4	-0.0133	0.0131	-0.0016	0.0005	-0.0107	-0.0135
Downward Wind @ 14,880 ft. (fps.)	D5	0.0196	-0.0081	-0.0028	-0.0053	0.0133	0.0108
Downward Wind @ 210,080 ft. (fps.)	D6	-0.0056	0.0018	-0.0043	0.0074	-0.0089	-0.0065
Downward Wind @ 297,520 ft. (fps.)	D7	-0.0134	-0.0149	0.0047	0.0041	-0.0138	-0.0069

Atmospheric Variable	Alias	Corr. to N2	Corr. to N3	Corr. to N4	Corr. to N5	Corr. to N6	Corr. to E1
Pressure @ S/L (psf.)	P1	-0.8569	-0.2035	-0.8228	0.7330	0.0350	-0.6809
Pressure @ 14,880 ft. (psf.)	P2	-0.4703	0.3842	-0.4388	0.2816	-0.4548	-0.4320
Pressure @ 38,060 ft. (psf.)	P3	-0.8555	-0.0765	-0.8171	0.7027	-0.0861	-0.6948
Pressure @ 54,240 ft. (psf.)	P4	0.7544	0.6575	0.7370	-0.7632	-0.4899	0.5424
Pressure @ 73,200 ft. (psf.)	P5	-0.3545	-0.9111	-0.3562	0.4986	0.7972	-0.1845
Pressure @ 94,290 ft. (psf.)	P6	0.1237	0.9180	0.1387	-0.3164	-0.8508	-0.0078
Pressure @ 164,770 ft. (psf.)	P7	-0.9196	-0.0867	-0.8850	0.7575	-0.0876	-0.7469
Density @ S/L (slug/ft3.)	ρ1	-0.0021	-0.8550	-0.0215	0.2011	0.8111	0.1010
Density @ 14,880 ft. (slug/ft3.)	ρ2	-0.5774	-0.6410	-0.5608	0.6110	0.5059	-0.3971
Density @ 38,060 ft. (slug/ft3.)	ρ3	-0.1297	-0.7803	-0.1369	0.2877	0.7115	-0.0127
Density @ 54,240 ft. (slug/ft3.)	ρ4	-0.3972	0.5042	-0.3663	0.1964	-0.5621	-0.3935
Density @ 73,200 ft. (slug/ft3.)	ρ5	0.7222	-0.1306	0.6857	-0.5474	0.2449	0.6047
Density @ 94,290 ft. (slug/ft3.)	ρ6	-0.7552	-0.0823	-0.7271	0.6253	-0.0606	-0.6140
Density @ 140,660 ft. (slug/ft3.)	ρ7	-0.5304	0.4149	-0.5044	0.3270	-0.4952	-0.4869
Temperature @ S/L (°R)	T1	-0.6413	0.4368	-0.6018	0.4107	-0.5336	-0.5802
Temperature @ 54,240 ft. (°R)	T2	0.7177	-0.0827	0.6829	-0.5546	0.2185	0.6068
Temperature @ 140,660 ft. (°R)	T3	0.7817	0.2193	0.7580	-0.6784	-0.0613	0.6183
Temperature @ 164,770 ft. (°R)	T4	-0.5202	0.4164	-0.4691	0.3243	-0.4876	-0.4790
Temperature @ 229,720 ft. (°R)	T5	0.5828	0.6545	0.5675	-0.6173	-0.5007	0.4064
Temperature @ 274,320 ft. (°R)	T6	-0.7039	-0.3067	-0.6818	0.6389	0.1627	-0.5346
Temperature @ 303,800 ft. (°R)	T7	0.3951	-0.4351	0.3701	-0.2113	0.4894	0.3816
Northerly Wind @ S/L (fps.)	N1	0.8907	0.3619	0.8584	-0.8013	-0.1824	0.6923
Northerly Wind @ 38,060 ft. (fps.)	N2	1.0000	0.2262	0.8578	-0.7721	-0.0454	0.7123
Northerly Wind @ 73,200 ft. (fps.)	N3	0.2262	1.0000	0.2271	-0.3835	-0.7982	0.0759
Northerly Wind @ 164,770 ft. (fps.)	N4	0.8578	0.2271	1.0000	-0.7164	-0.0451	0.6810
Northerly Wind @ 210,080 ft. (fps.)	N5	-0.7721	-0.3835	-0.7164	1.0000	0.3382	-0.5878
Northerly Wind @ 229,720 ft. (fps.)	N6	-0.0454	-0.7982	-0.0451	0.3382	1.0000	0.0607
Easterly Wind @ S/L (fps.)	E1	0.7123	0.0759	0.6810	-0.5878	0.0607	1.0000
Easterly Wind @ 3,550 ft. (fps.)	E2	0.2355	0.6921	0.2432	-0.3432	-0.6131	0.2099
Easterly Wind @ 38,060 ft. (fps.)	E3	0.6813	-0.0146	0.6539	-0.5460	0.1345	0.5641
Easterly Wind @ 73,200 ft. (fps.)	E4	0.3059	0.6539	0.3040	-0.3995	-0.5618	0.1776
Easterly Wind @ 94,290 ft. (fps.)	E5	-0.1648	-0.6971	-0.1753	0.3019	0.6391	-0.0518
Easterly Wind @ 116,950 ft. (fps.)	E6	0.2426	0.6846	0.2451	-0.3583	-0.6022	0.1191
Easterly Wind @ 164,770 ft. (fps.)	E7	0.6603	0.1005	0.6373	-0.5512	0.0252	0.5291
Easterly Wind @ 188,260 ft. (fps.)	E8	-0.1338	0.6076	-0.1119	-0.0402	-0.6038	-0.1732
Easterly Wind @ 247,020 ft. (fps.)	E9	0.6913	-0.2856	0.6559	-0.4868	0.4042	0.6063
Easterly Wind @ 261,900 ft. (fps.)	E10	0.7918	0.4129	0.7639	-0.7328	-0.2432	0.6092
Downward Wind @ S/L (fps.)	D1	0.0006	-0.0217	0.0014	0.0149	0.0345	0.0031
Downward Wind @ 844 ft. (fps.)	D2	-0.0003	-0.0098	-0.0005	0.0086	0.0099	0.0051
Downward Wind @ 3,550 ft. (fps.)	D3	0.0007	-0.0168	0.0018	-0.0017	0.0173	0.0042
Downward Wind @ 8,150 ft. (fps.)	D4	-0.0094	-0.0116	-0.0135	0.0057	0.0099	-0.0104
Downward Wind @ 14,880 ft. (fps.)	D5	0.0067	-0.0030	0.0137	-0.0119	0.0079	0.0048
Downward Wind @ 210,080 ft. (fps.)	D6	0.0044	-0.0013	-0.0089	-0.0014	-0.0020	-0.0140
Downward Wind @ 297,520 ft. (fps.)	D7	-0.0051	0.0023	-0.0065	0.0067	0.0004	-0.0181

Atmospheric Variable	Alias	Corr. to E2	Corr. to E3	Corr. to E4	Corr. to E5	Corr. to E6	Corr. to E7
Pressure @ S/L (psf.)	P1	-0.2229	-0.6567	-0.2935	0.1558	-0.2319	-0.6312
Pressure @ 14,880 ft. (psf.)	P2	0.2603	-0.4685	0.1829	-0.3066	0.2494	-0.3788
Pressure @ 38,060 ft. (psf.)	P3	-0.1216	-0.6833	-0.2040	0.0531	-0.1360	-0.6388
Pressure @ 54,240 ft. (psf.)	P4	0.5631	0.4719	0.5860	-0.5178	0.5667	0.5222
Pressure @ 73,200 ft. (psf.)	P5	-0.7270	-0.0957	-0.7014	0.7146	-0.7215	-0.2036
Pressure @ 94,290 ft. (psf.)	P6	0.7162	-0.0968	0.6606	-0.7314	0.7073	0.0279
Pressure @ 164,770 ft. (psf.)	P7	-0.1357	-0.7324	-0.2193	0.0616	-0.1496	-0.6930
Density @ S/L (slug/ft3.)	ρ1	-0.6620	0.1800	-0.5981	0.6784	-0.6490	0.0596
Density @ 14,880 ft. (slug/ft3.)	ρ2	-0.5441	-0.3312	-0.5523	0.5022	-0.5434	-0.3920
Density @ 38,060 ft. (slug/ft3.)	ρ3	-0.6092	0.0520	-0.5694	0.6086	-0.6042	-0.0379
Density @ 54,240 ft. (slug/ft3.)	ρ4	0.3608	-0.4391	0.2767	-0.4170	0.3507	-0.3404
Density @ 73,200 ft. (slug/ft3.)	ρ5	-0.0414	0.6110	0.0263	0.0976	-0.0188	0.5553
Density @ 94,290 ft. (slug/ft3.)	ρ6	-0.1172	-0.6005	-0.1865	0.0276	-0.1389	-0.5623
Density @ 140,660 ft. (slug/ft3.)	ρ7	0.2755	-0.5211	0.2003	-0.3318	0.2660	-0.4353
Temperature @ S/L (°R)	T1	0.2897	-0.6167	0.1906	-0.3509	0.2732	-0.5141
Temperature @ 54,240 ft. (°R)	T2	-0.0121	0.6089	0.0711	0.0843	-0.0021	0.5522
Temperature @ 140,660 ft. (°R)	T3	0.2322	0.5884	0.2852	-0.1715	0.2372	0.5802
Temperature @ 164,770 ft. (°R)	T4	0.2853	-0.5133	0.2016	-0.3462	0.2732	-0.3998
Temperature @ 229,720 ft. (°R)	T5	0.5431	0.3363	0.5640	-0.5114	0.5555	0.3995
Temperature @ 274,320 ft. (°R)	T6	-0.2833	-0.5104	-0.3399	0.2349	-0.2999	-0.5188
Temperature @ 303,800 ft. (°R)	T7	-0.3102	0.4148	-0.2344	0.3554	-0.2914	0.3346
Northerly Wind @ S/L (fps.)	N1	0.3485	0.6477	0.4062	-0.2802	0.3516	0.6451
Northerly Wind @ 38,060 ft. (fps.)	N2	0.2355	0.6813	0.3059	-0.1648	0.2426	0.6603
Northerly Wind @ 73,200 ft. (fps.)	N3	0.6921	-0.0146	0.6539	-0.6971	0.6846	0.1005
Northerly Wind @ 164,770 ft. (fps.)	N4	0.2432	0.6539	0.3040	-0.1753	0.2451	0.6373
Northerly Wind @ 210,080 ft. (fps.)	N5	-0.3432	-0.5460	-0.3995	0.3019	-0.3583	-0.5512
Northerly Wind @ 229,720 ft. (fps.)	N6	-0.6131	0.1345	-0.5618	0.6391	-0.6022	0.0252
Easterly Wind @ S/L (fps.)	E1	0.2099	0.5641	0.1776	-0.0518	0.1191	0.5291
Easterly Wind @ 3,550 ft. (fps.)	E2	1.0000	0.0383	0.5320	-0.5482	0.5496	0.1312
Easterly Wind @ 38,060 ft. (fps.)	E3	0.0383	1.0000	0.2102	0.0342	0.0535	0.5234
Easterly Wind @ 73,200 ft. (fps.)	E4	0.5320	0.2102	1.0000	-0.3961	0.5505	0.1963
Easterly Wind @ 94,290 ft. (fps.)	E5	-0.5482	0.0342	-0.3961	1.0000	-0.4347	-0.0660
Easterly Wind @ 116,950 ft. (fps.)	E6	0.5496	0.0535	0.5505	-0.4347	1.0000	0.1690
Easterly Wind @ 164,770 ft. (fps.)	E7	0.1312	0.5234	0.1963	-0.0660	0.1690	1.0000
Easterly Wind @ 188,260 ft. (fps.)	E8	0.4543	-0.2368	0.4103	-0.4712	0.4633	0.0229
Easterly Wind @ 247,020 ft. (fps.)	E9	-0.1630	0.6256	-0.0835	0.2312	-0.1549	0.5464
Easterly Wind @ 261,900 ft. (fps.)	E10	0.3821	0.5565	0.4218	-0.3150	0.3863	0.5686
Downward Wind @ S/L (fps.)	D1	-0.0142	0.0021	-0.0083	0.0070	-0.0266	-0.0116
Downward Wind @ 844 ft. (fps.)	D2	-0.0182	0.0125	-0.0062	0.0028	-0.0164	-0.0100
Downward Wind @ 3,550 ft. (fps.)	D3	-0.0243	0.0250	-0.0044	0.0168	-0.0111	0.0005
Downward Wind @ 8,150 ft. (fps.)	D4	-0.0054	-0.0068	-0.0054	0.0025	-0.0071	-0.0251
Downward Wind @ 14,880 ft. (fps.)	D5	0.0058	0.0119	0.0169	0.0079	0.0010	0.0100
Downward Wind @ 210,080 ft. (fps.)	D6	-0.0030	-0.0093	0.0005	0.0063	-0.0031	-0.0110
Downward Wind @ 297,520 ft. (fps.)	D7	0.0038	-0.0089	-0.0066	-0.0052	-0.0047	0.0033

Atmospheric Variable	Alias	Corr. to E8	Corr. to E9	Corr. to E10	Corr. to D1	Corr. to D2	Corr. to D3
Pressure @ S/L (psf.)	P1	0.1342	-0.6626	-0.7571	0.0051	0.0048	-0.0021
Pressure @ 14,880 ft. (psf.)	P2	0.4582	-0.6329	-0.2830	-0.0089	-0.0003	-0.0103
Pressure @ 38,060 ft. (psf.)	P3	0.2304	-0.7298	-0.7213	-0.0006	0.0003	-0.0066
Pressure @ 54,240 ft. (psf.)	P4	0.2524	0.3244	0.7951	-0.0127	-0.0069	-0.0083
Pressure @ 73,200 ft. (psf.)	P5	-0.5819	0.1781	-0.5313	0.0248	0.0123	0.0193
Pressure @ 94,290 ft. (psf.)	P6	0.6607	-0.3896	0.3466	-0.0251	-0.0164	-0.0224
Pressure @ 164,770 ft. (psf.)	P7	0.2380	-0.7855	-0.7778	-0.0038	-0.0035	-0.0049
Density @ S/L (slug/ft3.)	ρ1	-0.6545	0.4644	-0.2309	0.0300	0.0143	0.0199
Density @ 14,880 ft. (slug/ft3.)	ρ2	-0.3031	-0.1620	-0.6421	0.0173	0.0015	0.0161
Density @ 38,060 ft. (slug/ft3.)	ρ3	-0.5570	0.3161	-0.3080	0.0234	0.0103	0.0156
Density @ 54,240 ft. (slug/ft3.)	ρ4	0.5196	-0.6331	-0.1844	-0.0251	-0.0237	-0.0137
Density @ 73,200 ft. (slug/ft3.)	ρ5	-0.3442	0.7182	0.5573	0.0062	-0.0082	0.0142
Density @ 94,290 ft. (slug/ft3.)	ρ6	0.1799	-0.6363	-0.6379	0.0041	-0.0183	-0.0068
Density @ 140,660 ft. (slug/ft3.)	ρ7	0.4956	-0.7128	-0.3228	-0.0209	-0.0166	-0.0152
Temperature @ S/L (°R)	T1	0.5526	-0.8159	-0.4074	-0.0163	-0.0040	-0.0140
Temperature @ 54,240 ft. (°R)	T2	-0.3031	0.6934	0.5599	0.0159	0.0188	0.0065
Temperature @ 140,660 ft. (°R)	T3	-0.0929	0.5932	0.6975	0.0048	0.0071	0.0025
Temperature @ 164,770 ft. (°R)	T4	0.5139	-0.6933	-0.3143	-0.0125	-0.0131	-0.0257
Temperature @ 229,720 ft. (°R)	T5	0.3166	0.1844	0.6600	-0.0107	-0.0096	-0.0179
Temperature @ 274,320 ft. (°R)	T6	-0.0046	-0.4700	-0.6510	0.0081	0.0102	0.0010
Temperature @ 303,800 ft. (°R)	T7	-0.4713	0.5921	0.2091	0.0166	0.0108	0.0205
Northerly Wind @ S/L (fps.)	N1	-0.0226	0.6061	0.8262	-0.0034	0.0000	-0.0021
Northerly Wind @ 38,060 ft. (fps.)	N2	-0.1338	0.6913	0.7918	0.0006	-0.0003	0.0007
Northerly Wind @ 73,200 ft. (fps.)	N3	0.6076	-0.2856	0.4129	-0.0217	-0.0098	-0.0168
Northerly Wind @ 164,770 ft. (fps.)	N4	-0.1119	0.6559	0.7639	0.0014	-0.0005	0.0018
Northerly Wind @ 210,080 ft. (fps.)	N5	-0.0402	-0.4868	-0.7328	0.0149	0.0086	-0.0017
Northerly Wind @ 229,720 ft. (fps.)	N6	-0.6038	0.4042	-0.2432	0.0345	0.0099	0.0173
Easterly Wind @ S/L (fps.)	E1	-0.1732	0.6063	0.6092	0.0031	0.0051	0.0042
Easterly Wind @ 3,550 ft. (fps.)	E2	0.4543	-0.1630	0.3821	-0.0142	-0.0182	-0.0243
Easterly Wind @ 38,060 ft. (fps.)	E3	-0.2368	0.6256	0.5565	0.0021	0.0125	0.0250
Easterly Wind @ 73,200 ft. (fps.)	E4	0.4103	-0.0835	0.4218	-0.0083	-0.0062	-0.0044
Easterly Wind @ 94,290 ft. (fps.)	E5	-0.4712	0.2312	-0.3150	0.0070	0.0028	0.0168
Easterly Wind @ 116,950 ft. (fps.)	E6	0.4633	-0.1549	0.3863	-0.0266	-0.0164	-0.0111
Easterly Wind @ 164,770 ft. (fps.)	E7	0.0229	0.5464	0.5686	-0.0116	-0.0100	0.0005
Easterly Wind @ 188,260 ft. (fps.)	E8	1.0000	-0.4270	0.0614	-0.0334	-0.0285	-0.0185
Easterly Wind @ 247,020 ft. (fps.)	E9	-0.4270	1.0000	0.6070	0.0114	0.0071	0.0134
Easterly Wind @ 261,900 ft. (fps.)	E10	0.0614	0.6070	1.0000	-0.0148	-0.0069	-0.0059
Downward Wind @ S/L (fps.)	D1	-0.0334	0.0114	-0.0148	1.0000	0.3453	0.1086
Downward Wind @ 844 ft. (fps.)	D2	-0.0285	0.0071	-0.0069	0.3453	1.0000	0.1382
Downward Wind @ 3,550 ft. (fps.)	D3	-0.0185	0.0134	-0.0059	0.1086	0.1382	1.0000
Downward Wind @ 8,150 ft. (fps.)	D4	-0.0116	-0.0041	-0.0207	0.0482	0.0711	0.1081
Downward Wind @ 14,880 ft. (fps.)	D5	-0.0118	0.0140	0.0024	0.0169	0.0263	0.0485
Downward Wind @ 210,080 ft. (fps.)	D6	-0.0099	-0.0071	-0.0032	-0.0228	0.0024	0.0019
Downward Wind @ 297,520 ft. (fps.)	D7	-0.0012	-0.0052	-0.0047	-0.0101	-0.0095	-0.0086

Atmospheric Variable	Alias	Corr. to D4	Corr. to D5	Corr. to D6	Corr. to D7
Pressure @ S/L (psf.)	P1	0.0117	-0.0092	0.0018	0.0119
Pressure @ 14,880 ft. (psf.)	P2	0.0034	-0.0037	-0.0033	0.0131
Pressure @ 38,060 ft. (psf.)	P3	0.0110	-0.0094	0.0022	0.0127
Pressure @ 54,240 ft. (psf.)	P4	-0.0137	0.0099	-0.0077	-0.0027
Pressure @ 73,200 ft. (psf.)	P5	0.0114	-0.0015	0.0047	0.0052
Pressure @ 94,290 ft. (psf.)	P6	-0.0091	-0.0020	-0.0034	-0.0002
Pressure @ 164,770 ft. (psf.)	P7	0.0105	-0.0152	0.0054	0.0132
Density @ S/L (slug/ft3.)	ρ1	0.0074	0.0018	-0.0028	0.0054
Density @ 14,880 ft. (slug/ft3.)	ρ2	0.0172	0.0054	0.0069	0.0081
Density @ 38,060 ft. (slug/ft3.)	ρ3	-0.0039	-0.0032	0.0089	0.0028
Density @ 54,240 ft. (slug/ft3.)	ρ4	-0.0013	-0.0079	-0.0002	0.0067
Density @ 73,200 ft. (slug/ft3.)	ρ5	-0.0079	-0.0050	0.0067	0.0028
Density @ 94,290 ft. (slug/ft3.)	ρ6	0.0137	-0.0184	0.0062	0.0085
Density @ 140,660 ft. (slug/ft3.)	ρ7	0.0070	-0.0192	0.0016	0.0121
Temperature @ S/L (°R)	T1	0.0034	-0.0066	0.0034	0.0055
Temperature @ 54,240 ft. (°R)	T2	-0.0056	0.0118	-0.0036	-0.0073
Temperature @ 140,660 ft. (°R)	T3	-0.0133	0.0196	-0.0056	-0.0134
Temperature @ 164,770 ft. (°R)	T4	0.0131	-0.0081	0.0018	-0.0149
Temperature @ 229,720 ft. (°R)	T5	-0.0016	-0.0028	-0.0043	0.0047
Temperature @ 274,320 ft. (°R)	T6	0.0005	-0.0053	0.0074	0.0041
Temperature @ 303,800 ft. (°R)	T7	-0.0107	0.0133	-0.0089	-0.0138
Northerly Wind @ S/L (fps.)	N1	-0.0135	0.0108	-0.0065	-0.0069
Northerly Wind @ 38,060 ft. (fps.)	N2	-0.0094	0.0067	0.0044	-0.0051
Northerly Wind @ 73,200 ft. (fps.)	N3	-0.0116	-0.0030	-0.0013	0.0023
Northerly Wind @ 164,770 ft. (fps.)	N4	-0.0135	0.0137	-0.0089	-0.0065
Northerly Wind @ 210,080 ft. (fps.)	N5	0.0057	-0.0119	-0.0014	0.0067
Northerly Wind @ 229,720 ft. (fps.)	N6	0.0099	0.0079	-0.0020	0.0004
Easterly Wind @ S/L (fps.)	E1	-0.0104	0.0048	-0.0140	-0.0181
Easterly Wind @ 3,550 ft. (fps.)	E2	-0.0054	0.0058	-0.0030	0.0038
Easterly Wind @ 38,060 ft. (fps.)	E3	-0.0068	0.0119	-0.0093	-0.0089
Easterly Wind @ 73,200 ft. (fps.)	E4	-0.0054	0.0169	0.0005	-0.0066
Easterly Wind @ 94,290 ft. (fps.)	E5	0.0025	0.0079	0.0063	-0.0052
Easterly Wind @ 116,950 ft. (fps.)	E6	-0.0071	0.0010	-0.0031	-0.0047
Easterly Wind @ 164,770 ft. (fps.)	E7	-0.0251	0.0100	-0.0110	0.0033
Easterly Wind @ 188,260 ft. (fps.)	E8	-0.0116	-0.0118	-0.0099	-0.0012
Easterly Wind @ 247,020 ft. (fps.)	E9	-0.0041	0.0140	-0.0071	-0.0052
Easterly Wind @ 261,900 ft. (fps.)	E10	-0.0207	0.0024	-0.0032	-0.0047
Downward Wind @ S/L (fps.)	D1	0.0482	0.0169	-0.0228	-0.0101
Downward Wind @ 844 ft. (fps.)	D2	0.0711	0.0263	0.0024	-0.0095
Downward Wind @ 3,550 ft. (fps.)	D3	0.1081	0.0485	0.0019	-0.0086
Downward Wind @ 8,150 ft. (fps.)	D4	1.0000	0.0881	0.0047	-0.0041
Downward Wind @ 14,880 ft. (fps.)	D5	0.0881	1.0000	0.0068	0.0009
Downward Wind @ 210,080 ft. (fps.)	D6	0.0047	0.0068	1.0000	0.0218
Downward Wind @ 297,520 ft. (fps.)	D7	-0.0041	0.0009	0.0218	1.0000

APPENDIX B

WEIGHT ASSUMPTIONS

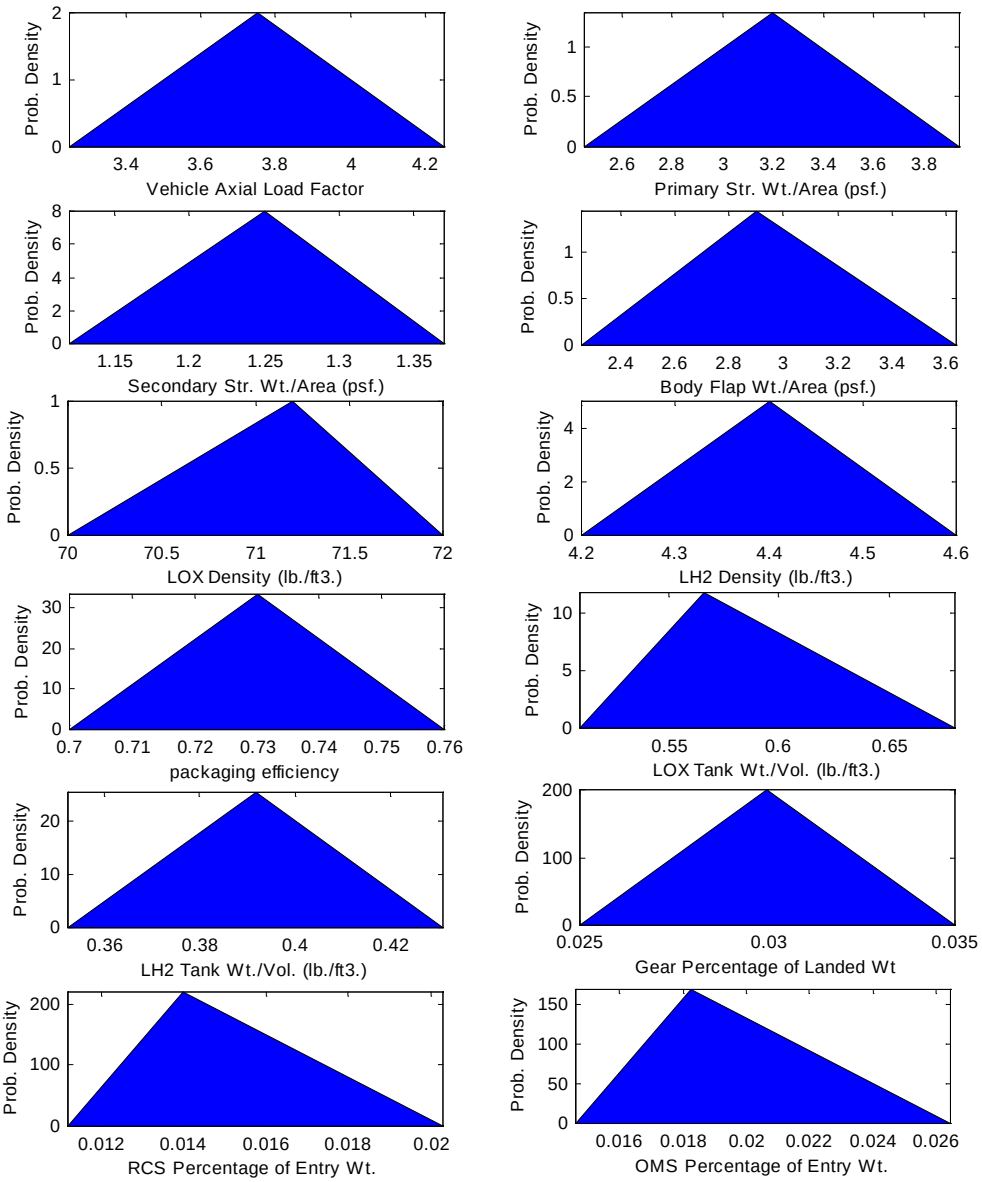
Prob. Density
Vehicle Axial Load Factor
Primary Str. Wt./Area (psf.)
Secondary Str. Wt./Area (psf.)
Body Flap Wt./Area (psf.)
LOX Density (lb./ft3.)
LH2 Density (lb./ft3.)
packaging efficiency
LOX Tank Wt./Vol. (lb./ft3.)
LH2 Tank Wt./Vol. (lb./ft3.)
Gear Percentage of Landed Wt
RCS Percentage of Entry Wt.
OMS Percentage of Entry Wt.

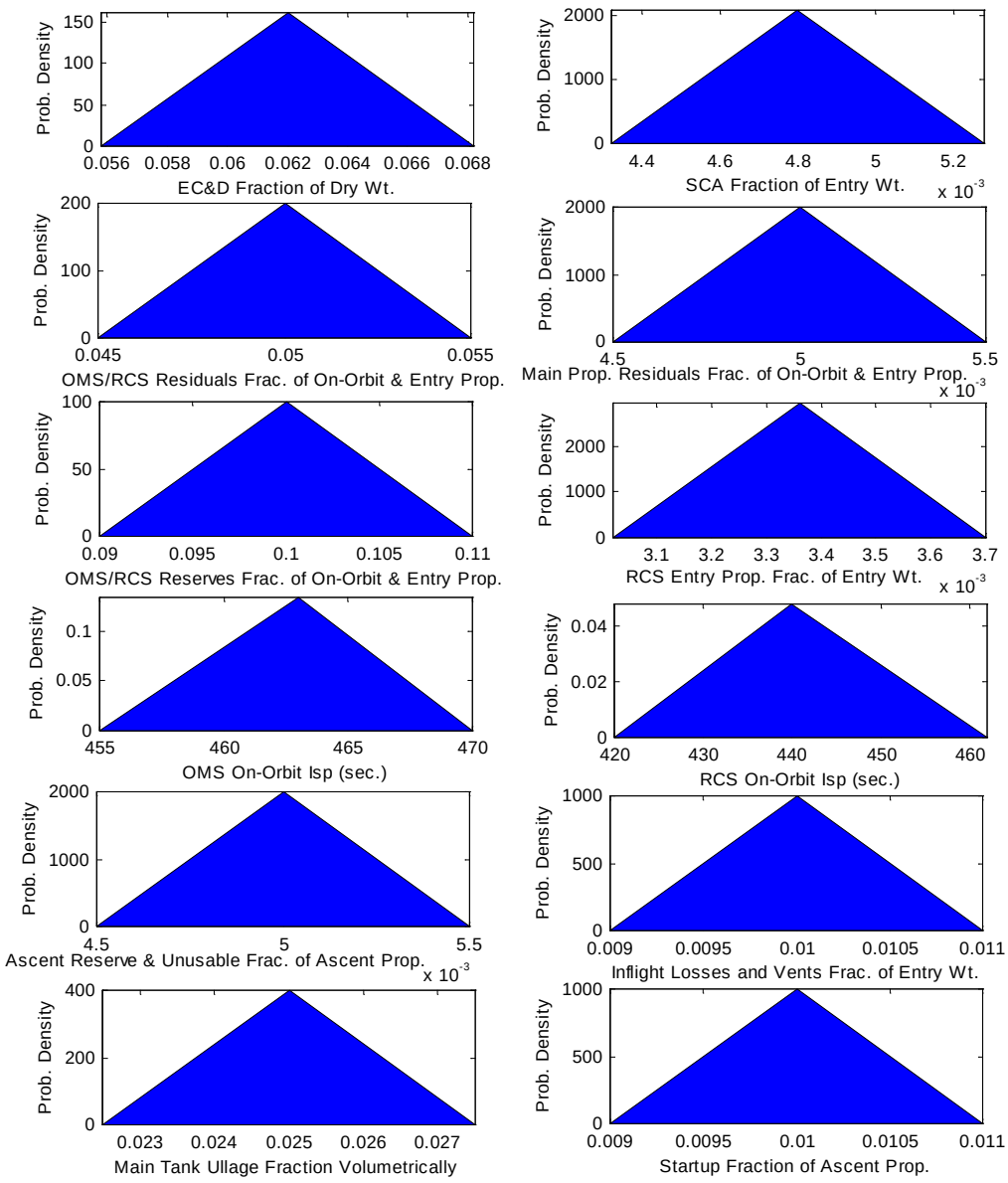
Prob. Density
150
100
50
0
0.056 0.058 0.06 0.062 0.064 0.066 0.068
EC&D Fraction of Dry Wt.
2000
1000
0
4.4 4.6 4.8 5 5.2
x 10-3
SCA Fraction of Entry Wt.
200
100
0
0.045 0.05 0.055
OMS/RCS Residuals Frac. of On-Orbit & Entry Prop.
4.5 5 5.5
Main Prop. Residuals Frac. of On-Orbit & Entry Prop.
100
50
0.09 0.095 0.1 0.105 0.11
OMS/RCS Reserves Frac. of On-Orbit & Entry Prop.
3.1 3.2 3.3 3.4 3.5 3.6 3.7
RCS Entry Prop. Frac. of Entry Wt.
0.1
0.05
455 460 465 470
OMS On-Orbit Isp (sec.)
0.04
0.02
420 430 440 450 460
RCS On-Orbit Isp (sec.)
4.5 5 5.5
Ascent Reserve & Unusable Frac. of Ascent Prop.
1000
500
0.009 0.0095 0.01 0.0105 0.011
Inflight Losses and Vents Frac. of Entry Wt.
400
200
0.023 0.024 0.025 0.026 0.027
Main Tank Ullage Fraction Volumetrically
0.009 0.0095 0.01 0.0105 0.011
Startup Fraction of Ascent Prop.

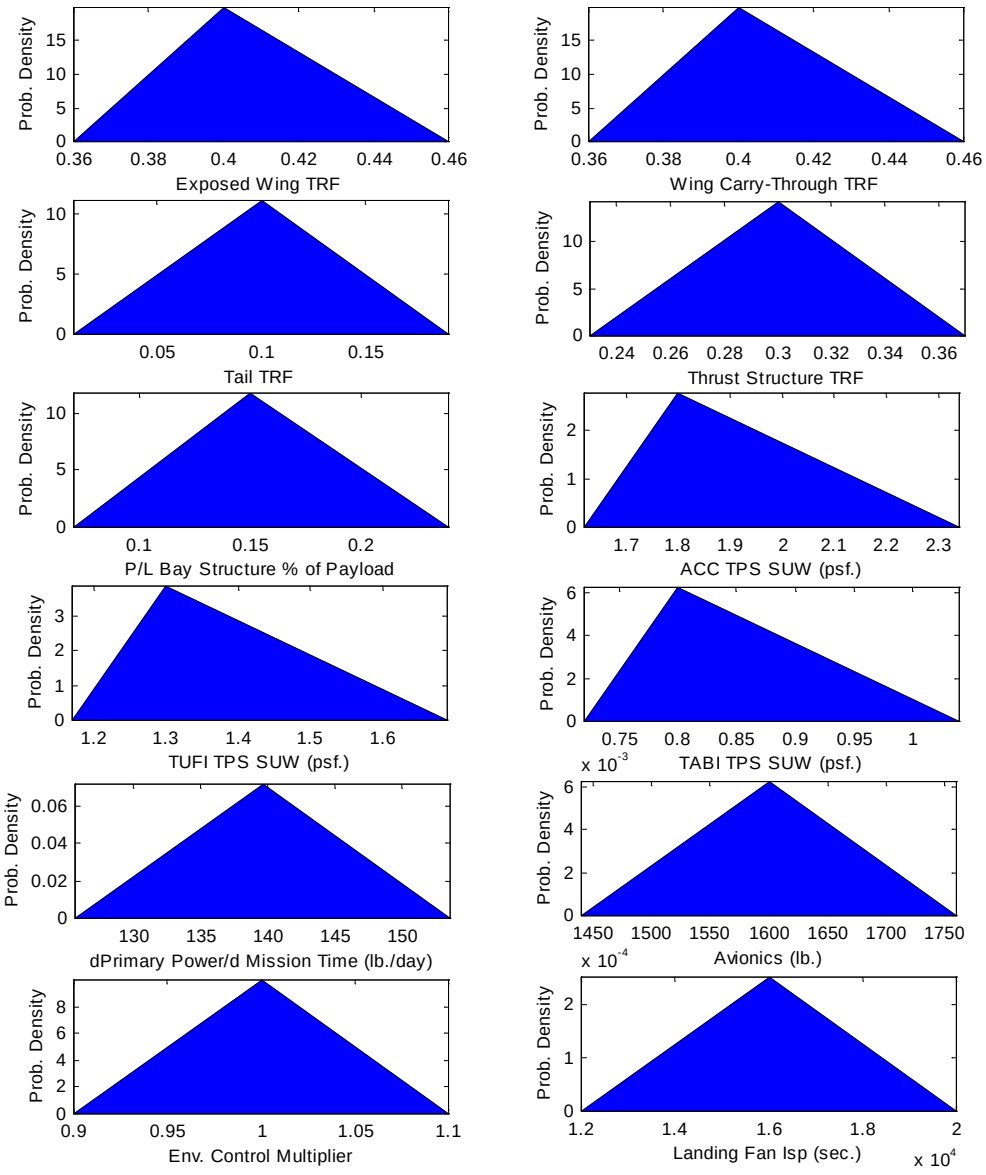
Prob. Density
Exposed Wing TRF
Wing Carry-Through TRF
Tail TRF
Thrust Structure TRF
P/L Bay Structure % of Payload
ACC TPS SUW (psf.)
TUFI TPS SUW (psf.)
TABI TPS SUW (psf.)
x 10^-3
dPrimary Power/d Mission Time (lb./day)
Avionics (lb.)
x 10^-4
Env. Control Multiplier
Landing Fan Isp (sec.)
x 10^4

APPENDIX C

SELECTED SOURCE CODE

This appendix lists source code written for this research that might be useful in future applications. They are all written as Matlab© functions.

File: ds_genprob.m

Matlab© function ds_genprob.m generates a Descriptive Sampling probability map for a given number of variables and runs.

```
function prob = ds_genprob(nvars, nruns);

%%%%%%%%%%%%%%%%%%%%%%%%%%%%%%%%%%%%%%%%%%%%%%%
%% Written by David McCormick in support of
%% Ph.D. thesis work.


%%%%%%%%%%%%%%%%%%%%%%%%%%%%%%%%%%%%%%%%%%%%%%%
%% Descriptive Sampling algorithm using
%% combination of procedures from Saliby and McKay.


%%%%%%%%%%%%%%%%%%%%%%%%%%%%%%%%%%%%%%%%%%%%%%%
%% Algorithm described in detail in background
%% section of dissertation.



%%%%%%%%%%%%%%%%%%%%%%%%%%%%%%%%%%%%%%%%%%%%%%%
%% P contains the vectors to permute.

p = zeros(nruns, nvars);

k = 0;

while (k<nvars)

   check = 0;

   temp = randperm(nruns)';

%%%%%%%%%%%%%%%%%%%%%%%%%%%%%%%%%%%%%%%%%%%%%%%
%% Check to make sure permutation is
%% independent of previous permutations.


   for i = 1:k-1,

      if temp == p(:,i)
```

```
         check = 1

      end

   end

%%%%%%%%%%%%%%%%%%%%%%%%%%%%%%%%%%%%%%%%%%%%%%%%


%%%%%%%%%%%%%%%%%%%%%%%%%%%%%%%%%%%%%%%%%%%%%%%%
%% Add permutation to matrix if it is
%% independent.

if check == 0,

      k = k+1;

      p(:,k) = temp;

   end

end

%%%%%%%%%%%%%%%%%%%%%%%%%%%%%%%%%%%%%%%%%%%%%%%%



%%%%%%%%%%%%%%%%%%%%%%%%%%%%%%%%%%%%%%%%%%%%%%%%
%% Transform matrix to probabilities by moving
%% to center of stratum and dividing by the
%% number of runs.

for j = 1:nruns,

   for k = 1:nvars,

      prob(j,k) = 1/nruns * (p(j,k)-0.5);

   end

end



%%%%%%%%%%%%%%%%%%%%%%%%%%%%%%%%%%%%%%%%%%%%%%%%
%% Report matrix prob.
```

File: DPOMD_frf.m

This Matlab© function generates a fractional factorial DPOMD run list based an input mean vector, covariance matrix and reduction factor.

```
function [x, template] = DPOMD_frf(mu, sig, reduction)

%%%%%%%%%%%%%%%%%%%%%%%%%%%%%%%%%%%%%%%%%%%%%%%%%%%%
%% Written by David McCormick in support of
%% Ph.D. thesis work.

%%%%%%%%%%%%%%%%%%%%%%%%%%%%%%%%%%%%%%%%%%%%%%%%%%%%%%%%
%% Generate inverse linear transform matrix for
%% Hasofer-Lind

[transform, p] = chol(sig);

%%%%%%%%%%%%%%%%%%%%%%%%%%%%%%%%%%%%%%%%%%%%%%%%%%%%%%%%

n = size(mu,1);

%%%%%%%%%%%%%%%%%%%%%%%%%%%%%%%%%%%%%%%%%%%%%%%%%%%%%%%%
%% Generate a -1, +1 fractional factorial design.

[x, template] = frf2n(n, reduction);


runs = size(x,1);


%%%%%%%%%%%%%%%%%%%%%%%%%%%%%%%%%%%%%%%%%%%%%%%%%%%%%%%%
%% Perform inverse transform on DOE.

temp = mu';

mu = temp(ones(runs,1),:);


x = x * transform + mu;


%%%%%%%%%%%%%%%%%%%%%%%%%%%%%%%%%%%%%%%%%%%%%%%%%%%%%%%%
%% Report run list and template for DOE generation.
```

File: frf2n.m

Matlab© function that given the number of factors and reduction parameter, will find a maximum resolution two-level fractional factorial experiment design.

```
function [Exp, template] = frf2n(nvars, reduction)

%%%%%%%%%%%%%%%%%%%%%%%%%%%%%%%%%%%%%%%%%%%%%%%
%% Written by David McCormick in support of
%% Ph.D. thesis work.

%%%%%%%%%%%%%%%%%%%%%%%%%%%%%%%%%%%%%%%%%%%%%%%
%% Calculate the number of basic factors

nbasic = nvars - reduction;

table = ones(2^nbasic,1);


%%%%%%%%%%%%%%%%%%%%%%%%%%%%%%%%%%%%%%%%%%%%%%%
%% Generate a full-factorial desgin for basic
%% factors.

table(:,2:nbasic+1) = ff2n(nbasic);

nforsat = 0;

%%%%%%%%%%%%%%%%%%%%%%%%%%%%%%%%%%%%%%%%%%%%%%%
%% Remap the zeros to be -1.

for i = 1:2^nbasic

   for j = 2:nbasic+1

      if table(i,j) == 0

         table(i,j) = -1;

      end

   end

end


for i = 1:nbasic
```

```
   nforsat = nforsat + nchoosek(nbasic,i);

end

%%%%%%%%%%%%%%%%%%%%%%%%%%%%%%%%%%%%%%%%%%%%%%%
%% Generate a saturated design template and
%% then grab the columns starting from the
%% right so that the resolution is as high
%% as possible.

template = zeros( nbasic, nforsat-nbasic );

current_pos = 0;
v = linspace(1,nbasic,nbasic);


for i = 2:nbasic

   nforthisblock = nchoosek(nbasic,i);

   template(1:i,current_pos+1:current_pos+nforthisblock) =
nchoosek(v,i)';

   current_pos = current_pos + nforthisblock;

end

%%%%%%%%%%%%%%%%%%%%%%%%%%%%%%%%%%%%%%%%%%%%%%%
%% Now step backwards through the template and
%% generate enough rows to fill in the table.
%% The template contains the position of the
%% ordinate in one of the basic variables to
%% use in the running product used in the direct
%% method of table generation.

%%%%%%%%%%%%%%%%%%%%%%%%%%%%%%%%%%%%%%%%%%%%%%%
%% Produces an error if resolution is below 3.

for i = nvars+1:-1:nbasic+2,

   table(:,i) = ones(2^nbasic,1);

   for j = 1:2^nbasic,

      for k = 1:nbasic,

         table(j,i) = table(j,i) * table(j, template( k, (nforsat -
nbasic) - (nvars+1) + i)+1 );

      end

   end
```

```
end


%%%%%%%%%%%%%%%%%%%%%%%%%%%%%%%%%%%%%%%%%%%%%%%%
%% Report experiment design and template for
%% generation.

Exp = table(:,2:nvars+1);

template = template(:,nforsat-nvars+1:nforsat-nbasic);
```

File: inverse_tri.m

This Matlab© function calculates the inverse cumulative distribution function for a triangular distribution given a single probability.

```
function x = inverse_tri( prob, x1, x2, x3 );

%%%%%%%%%%%%%%%%%%%%%%%%%%%%%%%%%%%%%%%%%%%%%%%%
%% Written by David McCormick in support of
%% Ph.D. thesis work.

%%%%%%%%%%%%%%%%%%%%%%%%%%%%%%%%%%%%%%%%%%%%%%%%
%% transform so x starts at zero.

   xa = x2 - x1 ;
   xb = x3 - x1 ;
   h = 2./xb;

%%%%%%%%%%%%%%%%%%%%%%%%%%%%%%%%%%%%%%%%%%%%%%%%
%% Find probability at discontinuity.

   pa = xa .* h ./2;

%%%%%%%%%%%%%%%%%%%%%%%%%%%%%%%%%%%%%%%%%%%%%%%%
%% if the prob. is before the break, calculate
%% x.

   if prob <= pa

      x = sqrt( 2.0 .* xa ./ h .* prob );

   else


%%%%%%%%%%%%%%%%%%%%%%%%%%%%%%%%%%%%%%%%%%%%%%%%
%% Find probability on second half of distrbution.
```

```
      C = 1.0/2.0 .* xa .* h - h .* xa .* xb./( xb-xa ) + h .* xa .* xa
./ (xb-xa) ./ 2 - prob ;


      B = h.* xb./(xb-xa);


      A =  -h./(xb-xa)./2;


      x = (-1.*B + sqrt(B.*B - 4.*A.*C))./(2.*A) ;


      xp = (-1.*B - sqrt(B.*B - 4.*A.*C))./(2.*A) ;

%%%%%%%%%%%%%%%%%%%%%%%%%%%%%%%%%%%%%%%%%%%%%%%
%% Confirm that the calculated value is on the
%% right interval.

      if (xp >= xa) & (xp <= xb )

         x = xp;

      end;

   end


%%%%%%%%%%%%%%%%%%%%%%%%%%%%%%%%%%%%%%%%%%%%%%%
%% transform back and report.

   x = x + x1 ;
```

REFERENCES

1. "Growing Pains," *Aviation Week and Space Technology*, Vol. 147, No. 15, October 13, 1997.

2. "Wounded birds," *The Economist*, May 12, 2001.

3. "Medicine Sales Forecast at $1 Billion," *Aviation Week and Space Technology*, June 25, 1984.

4. Savage, P., Hines, M., Barnes, R., "An Inflight Refill Unit for Replenishing Research Animal Drinking Water," NASA Technical Memorandum TM-4684, May, 1995.

5. "Nearly 900 Projects Vying for ISS Research," *Aviation Week & Space Technology*, Vol. 154, No. 7, February 12, 2001.

6. Howell, J., Mankins, J., "Preliminary Results from NASA's Space Solar Power Exploratory Research and Technology Program," IAF Paper IAA-00-R.1.02, October 2000.

7. Charania, A., Olds, J., "A Unified Economic View of Space Solar Power (SSP)," IAF IAA-00-R.1.06, 2000.

8. Olds, J., Way, D., Charania, A., Budianto, I., and Marcus, L., "In-Space Deployment Options for Large Space Solar Power Satellites," IAF Paper IAA-00-R.2.02, October, 2000.

9. Collins, P., "Public Choice Economics and Space Policy: Realising Space Tourism," IAF IAA-00-IAA.1.3.03, Oct. 2000.

10. *Commercial Space Transportation Study Final Report*, May 1994.

11. Olds, J., McCormick, D., Charania, A., and Marcus, L., "Space Tourism: Making It Work for Fun and Profit," IAF Paper IAA-00-IAA.1.3.05, October 2000.

12. Grier, P., "NRO Needs Cash, Attention, Effort," *Air Force Magazine*, Jan. 2001.

13. "Missile Defense: Still Mad," *National Review*, Vol. LIII, No. 10, May 2001.

14. Simpson, S., "Deeper Impact: Was Yet Another Mass Extinction the Work of an Asteroid?" *Scientific American*, Vol. 284, No. 5, pp. 18-19, May 2001.

15. lannotta, B. "China's Divine Craft," *Aerospace America*, April 2001, pg. 36.

16. Hale, Francis J., *Introduction to Space Flight,* Englewood Cliffs, NJ*:* Prentice Hall, Inc., 1994.

17. Raymer, D., *Aircraft Design: A Conceptual Approach*, Washington, DC: AIAA, 1989.

18. Bandte, O., "A Probabilistic Multi-Criteria Decision Making Technique for Conceptual and Preliminary Aerospace Systems Design," Ph.D. Thesis, Georgia Institute of Technology, 2000.

19. Bandte, O., Mavris, D., and DeLaurentis, D., "Viable Designs Through a Joint Probabilistic Estimation Technique," SAE paper 1999-01-5623, 1999.

20. Chen, W., Allen, J., Tsui, K. L., Mistree, F., "A Procedure for Robust Design: Minimizing Variations caused by Noise Factor and Control Factors," ASME *Journal of Mechanical Design*, Vol. 118, No. 4, 1996.

21. Myers, R. H., Khuri, A. I., and Vining, G., "Response Surface Alternatives to the Taguchi Robust Parameter Design Approach," *The American Statistician*, Vol. 46, No. 2, May 1992.

22. Mavris, D. N., Bandte, O., and Schrage, D. P., "Effect of Mission Requirements on the Economic Robustness of an HSCT Concept," 18th Annual Conference of the International Society of Parametric Analysts, Cannes, France, June 1996.

23. Mavris, D.N., Bandte, O., and Schrage, D. P., "Application of Probabilistic Methods for the Determination of an Economically Robust HSCT Configuration," AIAA paper 96-4090, Oct. 1996.

24. DeLaurentis, D. A., Mavris, D. N., and Schrage, D. P., "System Synthesis in Preliminary Aircraft Design Using Statistical Methods," 20th International Council of the Aeronautical Sciences (ICAS) Congress, Sorrento, Italy, September 8-13, 1996.

25. "2nd Generation RLV Systems Engineering and Risk Reduction," NASA Research Announcement NRA8-30, October, 2000.

26. "The Year in Review: Space Systems," *Aerospace America*, December 2000.

27. Smith, B., "MCO Board Probes Deeper Into Flaws," *Aviation Week and Space Technology*, Vol. 152, No. 12, pg. 38, March 20, 2000.

28. Oberg, J., "Houston, We Have a Problem," *New Scientist*, pg. 26, April 15, 2000.

29. Guterl, F., "The Space Siren," *Newsweek*, March 26, 2001.

30. Morring, F., "NASA Kills X-33, X-34, Trims Space Station," *Aviation Week and Space Technology*, Vol. 154, No. 10, pg. 24, March 5, 2001.

31. *Research Opportunities in Engineering Design*, NSF Strategic Planning Workshop Final Report, April 1996.

32. DeLaurentis, D., "A Probabilistic Approach to Aircraft Desgin Emphasizing Stability and Control Uncertainties," Ph.D. Thesis, Georgia Institute of Technology, 1999.

33. Zhao, K., Glover, K. and Doyle, J. C., *Robust and Optimal Control*, Englewood Cliffs, N.J.: Prentice Hall, 1996.

34. Hazelrigg, G. A., *Systems Engineering: An Approach to Information-Based Design*, Upper Saddle River, NJ: Prentice Hall, 1996.

35. Siddall, J. N., *Probabilistic Engineering Design*, New York, NY: Marcel Dekker, Inc., 1983.

36. Yen, B. C. and Tung, Y. (ed.) *Reliability and Uncertainty Analyses in Hydraulic Design*, New York, NY*:* ASCE, 1993.

37. McCormick, D. and Olds, J., "System Robustness Comparison of Advanced Space Launch Concepts," AIAA paper 98-5209, Oct. 1998.

38. Mavris, D. N., Bandte, O., and DeLaurentis, D. A., "Robust Design Simulation: A Probabilistic Approach to Multidisciplinary Design", *Journal of Aircraft*, Vol. 36, No. 1, pp. 298-307, 1999.

39. DeLaurentis, D., Mavris, D.N., "Uncertainty Modeling and Management in Multidisciplinary Analysis and Synthesis," AIAA paper 2000-0422, 2000.

40. DeLaurentis, D. A., Mavris, D. N., Calise, A. C., and Schrage, D. P., "Generating Dynamic Models Including Uncertainty for Use in Aircraft Conceptual Design," AIAA paper 97-3590, Aug. 1997.

41. Mavris, D.N., DeLaurentis, D.A., and Soban, D.S., "Probabilistic Assessment of Handling Qualities Constraints in Aircraft Preliminary Design," AIAA paper 98-0492, Jan. 1998.

42. Mavris, D.N., DeLaurentis, D.A., Bandte, O., and Hale, M.A., "A Stochastic Approach to Multi-disciplinary Aircraft Analysis and Design," AIAA paper 98-0912, Jan. 1998.

43. Mavris, D., DeLaurentis, D., Hale, M., and Tai, J., "Elements of an Emerging Virtual Stochastic Life Cycle Environment," World Aviation Congress, San Francisco, CA, paper 1999-01-5638, October 1999.

44. Koch, P. N., Wujek, B. and Golovidov, O., "A Multi-Stage, Parallel Implementation of Probabilistic Design Optimization in an MDO Framework," AIAA paper 2000-4805, September 2000.

45. Cagan, J., and Williams, B.C. , "First-Order Necessary Conditions for Robust Optimality," *Advances in Design Automation,* ASME DE-Vol. 65-1, 1993.

46. Madsen, H. O., Krenk, S., and Lind, N. C., *Methods of Structural Safety*, Englewood Cliffs, NJ: Prentice-Hall, 1986.

47. Taguchi, G., Wu, Y., "Introduction to Offline Quality Control," Central Japan Quality Control Association (available from the American Supplier Insititute, 32100 Detroit Industrial Expressway, Romulus, MI, 48174)

48. Phadke, Madhav S., "A Review of Taguchi and Related Approaches," Proceedings of the Annual Reliability and Maintainability Symposium, 1993.

49. Ross, P. J., *Taguchi Techniques for Quality Engineering*, New York, NY: McGraw-Hill, 1988.

50. Tsui, K. L., "Taguchi's Robust Design and Some Alternatives", *Ch. 8 in Statistics of Quality*, New York, NY: Marcel Dekker, 1996.

51. Du, X. and Chen, W., "An Efficient Approach to Probabilistic Uncertainty Analysis in Simulation-Based Multidisciplinary Design," AIAA paper 2000-0423, January 2000.

52. Mavris, D.N., Bandte, O., and DeLaurentis, D.A., "Determination of System Feasibility and Viability Employing a Joint Probabilistic Formulation," AIAA paper 99-0183, Jan. 1999.

53. Zink, P.S., Mavris, D.N., Love, M., and Karpel, M., "Robust Design for Aeroelastically Tailored/Active Aeroelastic Wing," AIAA paper 98-4781, Sept. 1998.

54. Mavris, D. N., Nottingham, C. R., and Bandte, O., "The Impact of Supportability on the Economic Viability of a High Speed Civil Transport", 1st

Joint International Conference of the International Society of Parametric Analysts and the Society of Cost Estimating and Analysis, Toronto, Canada, June 1998.

55. Mavris, D.N., and Bandte, O., "A Probabilistic Approach to Multivariate Constrained Robust Design Simulation," AIAA paper 97-5508, Oct. 1997.

56. Roth, B., Mavris, D., and Elliott, D., "A Probabilistic Approach to UCAV Engine Sizing," AIAA paper 98-3264, July 1998.

57. Mavris, D. N., Mantis, G., and Kirby, M. R. "Demonstration of a Probabilistic Technique for the Determination of Economic Viability," SAE paper 97-5585, Oct. 1997.

58. Mavris, D. N., and Bandte, O., "Comparison of Two Probabilistic Techniques for the Assessment of Economic Uncertainty," 19th Annual Conference of the International Society of Parametric Analysts, New Orleans, LA, May, 1997.

59. Chen, W., Allen, J. K., Schrage, D. P., and Mistree, F., "Statistical Experimentation Methods for Achieving Affordable Concurrent Systems Design," *AIAA Journal*, Vol. 35, No. 5, May 1997.

60. Koch, P. N., Simpson, T. W., Allen, J. K., and Mistree, F., "Statistical Approximations for Multidisciplinary Design Optimization: The Problem of Size," *Journal of Aircraft*, Vol. 36, No. 1, pp. 275-286, Jan.-Feb. 1999.

61. Cormier, T., Scott, A., Ledsinger, L., McCormick, D., Way, D., and Olds, J., "Comparison of Collaborative Optimization to Conventional Design Techniques for a Conceptual RLV," AIAA paper 2000-4885, Sept. 2000.

62. Ledsinger, L., "Solutions to Decomposed Branching Trajectories with Powered Flyback Using Multidisciplinary Desgin Optimization," Ph.D. Thesis, Georgia Institute of Technology, July 2000.

63. Braun, R. D., Kroo, I. M., "Development and Application of the Collaborative Optimization Architecture in a Multidisciplinary Design Environment," International Congress on Industrial and Applied Mathematics, August 1995.

64. Budianto, I., "A Collaborative Optimization Approach to Inprove the Design and Deployment of Satellite Constellations," Ph.D. Thesis, Georgia Institute of Technology, 2000.

65. Brady, H., Acting Head of Advanced Concepts, NASA-MSFC, *Personal Correspondence*, June 14, 2001.

66. Stanley, T., Alexander, R., and Landrum, D. B., "A Collaborative Analysis Tool for Integrating Hypersonic Aerodynamics, Thermal Protection Systems, and RBCC Engine Performance for Single Stage to Orbit Launch Vehicles," AIAA paper 99-4808, Nov. 1999.

67. Acton, D. and Olds, J., "Computational Frameworks for Collaborative Multidisciplinary Design of Complex Systems," AIAA 98-4942, Sept. 1998.

68. Sobieszanski-Sobieski, J., "Optimization by Decomposition: A Step from Hierarchic to Non-Hierarchic Systems," NASA CP-3031, Sept. 1989.

69. Himmelblau, D. M. ed., *Decomposition of Large-Scale Problems,* Amsterdam: North Holland Publishing, 1973.

70. Wagner, T. C. "A General Decomposition Methodology for Optimal System Design," Ph.D. Dissertation, University of Michigan, 9319649, 1993.

71. Balling, R. J., and Sobiezanski-Sobieski, J., "An Algorithm for Solving the System-Level Problem in Multilevel Optimization," AIAA paper 94-4333, Sept. 1994.

72. Barthelemy, J.M., and Riley, M. F., "Improved Multilevel Optimization Approach for the Design of Complex Engineering Systems," *AIAA Journal*, Vol. 26, No. 3, March 1988.

73. Beltracchi, T. J., "Decomposition Approach to Solving the All-Up Trajectory Optimization Problem," *Journal of Guidance, Control and Dynamics*, Vol. 15, No. 3, May-June 1992.

74. Peterson, F.M., Cornick, D. E., Brauer, G. L., and Rehder, J. J., "A Two-Level Trajectory Decomposition Algorithm Featuring Optimal Intermediate Target Selection," *Journal of Spacecraft and Rockets*, Vol. 14, No. 11, pp. 676-682, Nov. 1977.

75. Sobieszanski-Sobieski, J., "Two Alternative Ways for Solving the Coordination Problem in Multilevel Optimization," *Structural Optimization*, Vol. 6, pp. 205-215, Dec. 1993.

76. Walsh, J. L., Young, K. C., Pritchard, J. I., Adelman, H. M., and Mantay, W. R., "Integrated Aerodynamic/Dynamic/Structural Optimization of Heliocopter Rotor Blades Using Multilevel Decomposition," NASA TP-3465, Jan. 1995.

77. Braun, R., "Collaborative Optimization: An Architecture for Large-Scale Distributed Design," Ph.D. Thesis, Stanford University, June 1996.

78. Braun, R., Gage, P., Kroo, I., and Sobieski, I., "Implementation and Performance Issues in Collaborative Optimization," AIAA Paper 96-4017, 1996.

79. Braun, R., Moore, A., Kroo, I, "Use of the Collaborative Optimization Architecture for Launch Vehicle Design." AIAA paper 96-4018, 1996.

80. Whitfield, J. and Olds, J., "Economic Uncertainty of Weight and Market Parameters for Advanced Space Launch Vehicles," AIAA Paper 98-5179, October 1998.

81. Engler, V., Coors, D., Jacob, D., "Optimization of a Space Transportation System Including Design Sensitivities," AIAA Paper 98-1553, April 1998.

82. Bertin, J. and Smith, M., *Aerodynamics for Engineers*, Prentice Hall, NJ, 1989.

83. Anderson, J., *Hypersonic and High Temperature Gas Dynamics*, Boston, MA: McGraw-Hill, Inc., 1989.

84. Brauer, G. L., Cornick D. E., Olson, D., Peterson, F., and Stevenson, R., “Program to Optimize Simulated Trajectories (POST) Formulation Manual," NAS1-18147, September 1990.

85. Thornton, S. and Rex, A., *Modern Physics for Scientists and Engineers*, Orlando, FL: Saunders College Publishing, 1993.

86. Cowart, K. and Olds, J., "TCAT - A Tool for Automated Thermal Protection System Design," AIAA 2000-5265, 2000.

87. Hill, P. and Peterson, R., *Mechanics and Thermodynamics of Propulsion*, Boston, MA: Addison-Wesley, 1992.

88. Bate, R., Mueller, D., and White, J., *Fundamentals of Astrodynamics*, New York, NY: Dover Publications Inc., 1971.

89. Fehlberg, E., "Klassiche Runge-Kutta-Formeln vierter und niedrigerer Ordnumg mit Schrittweiten-Kontrolle und ihre Anwendung auf Warmeleitungsprobleme," *Computing* Vol. 6, 1970.

90. Atkinson, K., *An Introduction To Numerical Analysis*, New York, NY: John Wiley & Sons, 1989.

91. McCormick, D. and Olds, J., “Approximation of Probabilistic Distributions Using Selected Discrete Simulations,” AIAA paper 2000-4863, Sept. 2000.

92. Wu, Y.-T., "Structural Reliability Analysis Methods for Implicit Performance Functions," Probabilistic Mechanics and Structural and Geotechnical Reliability Proceedings of the Special Conference, New York, NY: ASCE, pp. 483-486, 1992.

93. Wirsching, Paul H. Martin, Warren S., "Fracture Mechanics Fatigue Reliability Assessment Employing the Most Probable Point Locus Method," Probabilistic

Methods in Civil Engineering, Proceedings of the 5th ASCE Special Conference, New York, NY, pp. 78-81.

94. Wu, Y. T., Millwater, H. R., and Cruse, T. A., "An Advanced Probabilistic Structural Analysis Method for Implicit Performance Functions," *AIAA Journal*, Vol. 28, No. 9, pp. 1663-1669, 1990.

95. Wu, Y. T., Burnside, O. H., Cruse, T. A., "Probabilistic Methods for Structural Response Analysis," *Ch. 7 of Computational Mechanics of Reliability Analysis*, W. K. Liu and T. Belytschko (ed.), Lauseanne, WA: Elmepress International, 1989.

96. Wu, Y. T., "Demonstration of a Fast, New Probability Integration Method for Reliability Analysis," *ASME Journal of Engineering for Industry*, Vol. 109, pp. 24-28, 1987.

97. Wu, Y.-T. and Wirsching, P.H., "Advanced Reliability Methods for Probabilistic Structural Analysis," *Structural Safety and Reliability, Vol. III*, New York, NY: ASCE pp. 2275-2281, 1989.

98. Wu, Y. T. and Wirsching, P. H., "New Algorithm for Structural Reliability Estimation," *ASCE Journal of Engineering Mechanics*, Vol. 113, No. 9, Sept. 1987.

99. Cruse, T. A., Chamis, C. C., and Millwater, H. R., "An Overview of the NASA (LeRC) - SwRI Probabilistic Structural Analysis (PSAM) Program." *5th International Conference on Structural Safety and Reliability*, 1989.

100. Du, X. and Chen, W., “A Most Probable Point Based Method for Uncertainty Analysis,” ASME paper DETC2000/DAC-14263, September 2000.

101. Khalessi, M.R. Wu, Y.-T. and Torng, T.Y., "Most-Probable-Point-Locus Reliability Method in Standard Normal Space," ASME Design Engineering Division, Vol. 30, pp. 15-20, 1991.

102. Mahadevan, Sankaran Cruse, Thomas A., "Advanced First-Order Method for System Reliability," ASCE Probabilistic Mechanics and Structural and Geotechnical Reliabiability Special Conference Proceedings, New York, NY pp. 487-490, 1992.

103. Lin, H.-Z. Khalessi, M.R., "Calculation of Failure Probability by Using X-Space Most-Probable-Point," *Collection of Technical Papers from the AIAA ASME Structures, Structural Dynamics and Materials Conference, pt. 5*, Washington, DC: AIAA, pp. 2801-2808, 1993.

104. Lin, H.-Z. Khalessi, M.R., "Identification of the Most-Probable-Point in Original Space - Applications to Structural Reliability," Collection of Technical Papers from the AIAA ASME Structures, Structural Dynamics and Materials Conference, Pt. 5, Washington, DC: AIAA, pp. 2791-2800, 1993.

105. Grandhi, R. V. and Wang, L., "Higher-order Failure Probability Calculation Using Nonlinear Approximations," *Computer Methods in Applied Mechanics and Engineering*, Vol. 168, No. 1-4, Jan. 1999.

106. Thacker, B. H., and Wu, Y. T., "A New Response Surface Approach for Structural Reliability Analysis," Proceedings of the AIAA 33rd Structural Dynamics and Materials Conference, Washington, DC: AIAA, 1992.

107. Dieter, G. E., *Engineering Design, A Materials Processing Approach , 2nd Edition*, New York, NY: McGraw Hill Inc., 1971.

108. Unal, R. Stanley, D., Engelund, W. and Lepsch, R., "Design for Quality Using Response Surface Methods: An Alternative to Taguchi's Parameter Design Approach," *Engineering Management Journal*, Vol. 6, No. 3, Sept. 1994.

109. Hammersley, J. M. and Handscomb, D. C., *Monte Carlo Methods*, London: Chapman and Hall, 1964.

110. Law, A. M. and Kelton, W. D., *Simulation Modeling and Analysis*, New York, NY: McGraw-Hill, 1982.

111. Hogg, R. V., and Tanis, E. A., *Probability and Statistical Inference, 4th Ed.*, Englewood Cliffs, NJ: Prentice-Hall, Inc., 1993.

112. Lavenberg, S., and Welch, P., "A Perspective on the Use of Control Variables to Increase the Efficiency of Monte Carlo Simulations," *Management Science*, Vol. 27, 1981, pp. 322-335.

113. James, B., "Variance Reduction Techniques," *Journal of the Operational Research Society*, Vol. 36, pp. 525-530, 1985.

114. Ang, G. L., Ang, A. H-S., and Tang W. H., "Optimal Importance-Sampling Density Function," *Journal of Engineering Mechanics*, Vol. 118, No. 6, 1992.

115. Ang, G. L., Ang, A. H-S., and Tang W. H., "Kernel Method in Importance Sampling Density Function," *Structural Safety and Reliability, Vol. II.* New York, NY: ASCE, 1989.

116. Karamchandari, A. , "New Methods in System Reliability," Report No. RMS-7, Reliability of Marine Structures Program, Department of Civil Engineering, Stanford University, Stanford, CA, 1990.

117. Bourgund, U. and Bucher, C. G., "Importance Sampling Procedure Using Design Points (ISPUD) - A User's Manual," Report No. 8, Institute of Engineering Mechanics, University of Innsbruck, Austria, 1986.

118. Harbitz, A., "An Efficient Sampling Method for Probability of Failure Calculation." *Structural Safety*, Vol. 3, No. 2, 1986.

119. Schueller, G. I., and Stix, R. "A Critical Appraisal of Methods to Determine Failure Probabilities," *Structural Safety*, Vol. 4, No. 4, pp. 293-309, 1987.

120. McKay, M. D., Beckman, R. J., and Conover, W. J., "A Comparison of Three Methods for Selecting Values of Input Variables in the Analysis of Output from a Computer Code." *Technometrics*, Vol. 21, pp. 239-245, 1979.

121. Stein, M., "Large Sample Properties of Simulations Using Latin Hypercube Sampling," *Technometrics*, Vol. 29, pp. 143-151, 1985.

122. Iman, R. and Conover, W., "A Distribution-Free Approach to Inducing Rank Correlation Among Input Variables," *Communications in Statistics*, Ser. B 11, pp. 311-334, 1982.

123. Iman, R. and Helton, J., "The Repeatability of Uncertainty and Sensitivity Analyses for Complex Probabilistic Risk Assesments," *Risk Analysis*, Vol. 11, pp. 591-606, 1991.

124. Loh, W., "On Latin Hypercube Sampling," *The Annals of Statistics*, Vol. 24, pp. 2058-2080, 1996.

125. Owen, A., "A Central Limit Theorum for Latin Hypercube Sampling," *Journal of the Royal Statistical Society* Ser. B 54, pp. 541-551, 1992.

126. Kleijnen, J., *Statistical Techniques in Simulation, Part 1*, New York: Marcel Dekker, 1974.

127. Saliby, E., "Descriptive Sampling: A Better Approach to Monte Carlo Simulation," *Journal of the Operational Research Society*, Vol. 41, No. 12, pp. 113-114, 1990.

128. Paul, R. J. and Doudkis, G. I., "Artificial Intelligence and Expert Systems in Simulation Modeling," *Artificial Intelligence in Operational Research*, pp. 229-238, 1992.

129. Ziha, K., "Descriptive Sampling in Structural Safety," *Structural Safety*, Vol. 17, pp. 33-41, 1995.

130. Jonsson, H. S., and Edward A., "Some Insights Regarding Selecting Sets of Scenarios in Combinatorial Stochastic Problems," *International Journal of Production Economics*, Vol. 45, No. 1-3, pp. 463-472, 1996.

131. Saliby, E., and Paul, R., "Implementing Descriptive Sampling in Three-Phase Discrete Event Simulation Models," Journal of the Operational Research Society, Vol. 44, No. 2, pp. 147-160, Feb. 1993.

132. Saliby, E., "Descriptive Sampling: An Improvement over Latin Hypercube Sampling," IEEE Cat. No. 97CB36141, 1997.

133. Tocher, K., *The Art of Simulation*, London: English University Press, 1963.

134. Clark, C., "The Utility of Statistics of Random Numbers," *Operations Research*, Vol. 8, 1960.

135. Rackwitz, R. and Fiessler, B., "Structural Stability Under Combined Random Load Sequences," *Computers and Structures*, Vol. 9, pp. 489-494, 1978.

136. Y.-T. Wu and Chen, K., "Characterization of Input Uncertainties Using Random Variables for Reliability Analysis," AIAA Paper 99-1606, April, 1999.

137. *FPI User's and Theoretical Manual*, San Antonio, TX: Southwest Research Institute, 1995.

138. Hasofer, A. M. and Lind, N. C., "Exact and Invariant Second Moment Code Format," *Journal of Engineering Mechanics*, ASCE, Vol. 100, No. EM1, February, 1974.

139. Chen, X., and Lind, N. C., "Fast Probability Integration by Three Parameter Normal Tail Approximation," *Structural Safety*, Vol. 1, pp. 269-276, 1983.

140. Kreyszig, E., *Advanced Engineering Mathematics*, New York, NY: John Wiley & Sons, 1993.

141. Kaplan, S., “On the Method of Discrete Probability Distributions in Risk and Reliability Calculations - Application to Seismic Risk Assesments,” *Risk Analysis*, Vol. 1, pp. 189-196, 1981.

142. Kaplan, S., and James C., “Improved Condensation Procedure In Discrete Probability Distribution Calculations.” *Risk Analysis* Vol. 7, No. 1, pp. 15-19, Mar 1987.

143. Kurth, Robert E. Cox, David C., “Random Sampling Discrete Probability Algorithm with Condensation for Probabilistic Analysis,” *Nuclear Technology*, Vol. 92, No. 2, pp. 186-193, Nov. 1990.

144. Moghadam, A. and Theofanous, T. G., “On the Use of Discrete Probability Distributions in Failure Analysis-Numerical Aspects,” *Reliabiality and Engineering System Safety*, Vol. 23, No. 2, pp. 81-107, 1988.

145. Kurth, R. E. and Cox, D. C., “Discrete Probability Distributions For Probabilistic Fracture Mechanics,” Risk Analysis Vol. 5, No. 3, pp. 235-240, Sept. 1985.

146. Kleijnen, J. P., *Statistical Tools for Simulation Practitioners*, New York, NY: Marcel Dekker, 1987.

147. Chen, W., Tsui, K-L., Allen, J. K., and Mistree, F., "Integration of Respnse Surface Method with the Compromise Decision Support Problem in Developing a General Robust Design Procedure," *Advances in Design Automation* , ASME DE - Vol. 82, No. 2, 1995.

148. Mavris, D.N., and Bandte, O., "Economic Uncertainty Assessment Using a Combined Design of Experiments/Monte Carlo Simulation Approach with Application to an HSCT," 17th Annual Conference of the International Society of Parametric Analysts, San Diego, CA, May, 1995.

149. *JMP Statistics and Graphics Guide*, Cary, NC: SAS Institute, Inc., 1995.

150. Hayter, A. J., *Probability and Statistics for Engineers and Scientists*, Boston, MA: PWS Publishing, 1996.

151. Box, G. E. P., Hunter, W. G., and Hunter, J. S., *Statistics for Experimenters*, New York, NY: John Wiley and Sons, 1978.

152. MATLAB - *User's Guide*, Natick, MS: The Math Works, Inc., January 1995.

153. Rogers, J. L., “DeMaid – A Design Manager’s Aid for Intelligent Decomposition – User’s Guide,” NASA Technical Memorandum TM-101575, March 1989.

154. Braun, R. D., Powell, R. W., Lepsch, R. A., Stanley, D. O., and Kroo, I. M., "Multidisciplinary Optimization Strategies for Launch Vehicle Design," AIAA paper 94-4341, Sept. 1994.

155. Hajela, P., Bloebaum, C., and SobieszczanskiSobieski, J., "Application of Global Sensitivity Equations in Multidisciplinary Aircraft Synthesis." *Journal of Aircraft*, Vol. 27, No. 12, December, 1990.

156. Sobieszczanski-Sobieski, J. "Sensitivity Analysis and Multidisciplinary Optimization for Aircraft Design: Recent Advances and Results." *Journal of Aircraft*, Vol. 27, No. 12, December, 1990.

157. Sobieszczanski-Sobieski, J. "A System Approach to Aircraft Optimization." NASA TM104074, March, 1991.

158. Sobieszczanski-Sobieski, J. "Sensitivity of Complex, Internally Coupled Systems," AIAA Journal, Vol. 28, No. 1, January, 1990.

159. Sobieszczanski-Sobieski, J. "On the Sensitivity of Complex, Internally Coupled Systems," AIAA paper 882378, April 1988.

160. Olds, J., "System Sensitivity Analysis Applied to the Conceptual Design of a Dual Fuel Rocket SSTO," AIAA paper 94-4339, Sept. 1994.

161. Olds, J., "Multidisciplinary Design Techniques Applied to Conceptual Aerospace Vehicle Design," Ph.D. Thesis, North Carolina State University, 1993.

162. Way, D. W., Olds, J. R., "SCORES: Web-Based Rocket Propulsion Analysis Tool for Space Transportation System Design," AIAA paper 99-2353, June 1999.

163. Brauer, G. L., Cornick D. E., and Stevenson, R., “Capabilities and Applications of the Program to Optimize Simulated Trajectories,” NASA CR-2770, Feb. 1977.

164. Justus, C. G., Johnson, D. L., "The NASA/MSFC Global Reference Atmospheric Model - 1999 Version (GRAM-99)," NASA Technical Memorandum TM-1999-209630, May 1999.

165. Sova, G., and Divan, P., "Aerodynamic Preliminary Analysis System II, Part II - User's Manual," NASA CR-182077, April, 1991.

166. Mitchell, T., "An Algorithm for the Construction of "D-optimal" Experimental Designs," *Technometrics,* Vol. 42, No. 1, pp. 48-54, Feb. 2000.

167. Khuri, A., "A Note on D-optimal Designs for Partially Nonlinear Regression Models," *Technometrics,* Vol. 26, pp. 59-61, Feb. 1984.

168. *DOT™ User's Manual, Version 4.20.*, Vanderplaats Research & Development, Inc., Colorado Springs, CO, 1995.

VITA

David Jeremy McCormick was born on January 15, 1974 in Jamestown, New York. After moving to Florida at an early age, he graduated from Lake Brantley High School in Altamonte Springs, Florida in 1992. In August of that same year, he enrolled at the University of Florida for his undergraduate studies in Aerospace Engineering. During this time, David was an undergraduate researcher in the Florida Space Grant Consortium Program studying computational fluid dynamics. He received his Bachelor of Science degree, with Highest Honor, in May of 1996.

The following October, David began his graduate studies by enrolling at the Georgia Institute of Technology. Upon arrival, he began work for Dr. John Olds studying advanced concepts for reusable launch vehicles. During this time, he worked on the *Argus* and *Hyperion* concepts. He also spent a summer working on Rocket-Based Combined Cycle engine weight estimation at the Kaiser-Marquardt Corporation of Van Nuys, CA. He earned his Master of Science degree in Aerospace Engineering in December of 1997, but stayed to continue his studies. While continuing to work on concept vehicles for Dr. Olds, he subsequently spent summers working at the NASA-Langley Vehicle Analysis Branch in Hampton, VA and Lockheed-Martin Reusable Space Transportation Systems in Denver, CO. During this time, David began research into probabilistic methods for conceptual launch vehicle design, the culmination of which is the thesis entitled “Distributed Uncertainty Analysis Techniques for Conceptual Launch Vehicle Design.” David is a member of the American Institute of Aeronautics and Astronautics.